

**Climate change mitigation potential of green roofs:**  
Exploring urban heat island indicators and a green roof's capacity to sequester carbon  
in the Flint Hills Ecoregion

by

M. M. Lekhon Alam

B. Arch., Khulna University, 2014  
MS. Arch., Kansas State University, 2018

AN ABSTRACT OF A DISSERTATION

submitted in partial fulfillment of the requirements for the degree

DOCTOR OF PHILOSOPHY

Department of Environmental Design and Planning  
College of Architecture, Planning and Design

KANSAS STATE UNIVERSITY  
Manhattan, Kansas

2022

## Abstract

Green roofs have evolved as an important part of “sustainable development” initiatives around the world. With increasing global warming, many tools are needed, including living roof ecosystems, to reduce urban heat island and climate change impacts. Rooftop green infrastructure can enhance sustainable urban development by reducing atmospheric CO<sub>2</sub> due to its ability to reduce the energy consumption of a building and sequester carbon in plants and substrates. Green roof research indicates that temperature regulation atop buildings is quantifiable and demonstrates a crucial role in reducing the energy demand of a building. Additional environmental benefits of green roofs include improved air quality by removing pollutants from the air and reducing ambient CO<sub>2</sub> concentrations. Given different climates, researchers are uncertain as to what substrate types, depths, and plant combinations sequester the greatest amounts of carbon in green roofs across different ecoregions. Additional research is needed to understand the benefits and limitations of green roofs in specific locations such as the U.S. Great Plains.

A two-growing-season-long study evaluated the carbon sequestration and thermal loading performance of two experimental green roof beds with different depths ~20 cm and ~10 cm and two substrate types in Manhattan, Kansas. Three plant mixes consist of *Sedum* only (A), *Sedum* + native grass mix (B), and native grasses + forbs (C). This study also makes connections to building energy performance. Soil samples were collected at depths of ~8-inch or ~20 cm and ~4-inch or ~10 cm in 2019 and 2020. The soil was analyzed for microbial community composition by PLFA (phospholipid fatty acids), Total Organic Carbon and Nitrogen, and microbial respiration. Root biomass was also determined. Three-way and four-way analysis of variance (ANOVA) and Tukey’s HSD post-hoc analyses were conducted using R version 4.2.0 and SPSS Statistics 29. New methods have been proposed in this study to use data from in-situ measurements of temperatures on building envelopes to estimate the rate of change in heat storage within the soil layer (*Q-value*).

The research was inspired by the summation technique as this calculation procedure allowed the researcher to analyze the accumulation of data on soil moisture content and differences in green roof surface and sub-surface temperatures over time. In-situ sensors were used to measure soil moisture content and surface and sub-surface temperatures so that thermal

properties crucial to understanding heat transfer could be examined. Soil (substrate) types (Kansas BuildEx® [K] and rooflite® extensive mc [R]) and substrate depth were the independent variables for this study, where the primary focus was on determining the significance of soil moisture of a green roof system in building energy performance. All APD-EGR beds were provided supplemental irrigation on an as-need basis.

This two-year (2019 and 2020) analysis found that beds with the R substrate (with its lower bulk density, higher pore space, and lower water-holding capacity than substrate K) likely sequester a greater amount of C per substrate volume. Analysis of temperature data showed that the 4-inch bed at the APD-EGR with R substrate seems to work more efficiently during the building cooling season (with summertime HVAC use) considering both day and night times than the 4-inch bed with K substrate. Interestingly, substrate types do not seem to play a significant role in influencing Q-values in the wintertime and the deeper substrate (8-inch bed) appeared to have more positive Q-values that could improve building performance. Considering depth, the study finds that the thermal performance of two different depths (4-inch and 8-inch) are not similar in two time periods (summertime vs. wintertime). Therefore, suggesting a depth (shallower or deeper) that will improve the energy performance of a building for both time periods in the Flint Hills Ecoregion needs more long-time research and proper instrumentations to determine the approximate R-value (thermal resistance). The soil moisture content is very likely an important factor related to green roof system-induced building energy performance.

The study concludes that in both cases of carbon sequestration and thermal performance, a shallower bed with R substrate may work better as a climate change mitigation strategy in the context of the Flint Hills Ecoregion. However, more research is needed to confirm this. From both studies (thermal and C sequestration), the moisture-holding capacity of different substrate types at different depths appeared to be the key factor in determining green roofs' climate change mitigation potential. A more precise understanding of these dynamic processes and systems is essential to improve design, implementation, and management of green roof ecosystems in support of sustainable building design and climate change mitigation.

**Key Words:** Experimental Green Roof Systems, Climate Change Mitigation, Carbon Sequestration, Building Energy Performance, Sustainability

**Climate change mitigation potential of green roofs:**  
Exploring urban heat island indicators and a green roof's capacity to sequester carbon  
in the Flint Hills Ecoregion

by

M. M. Lekhon Alam

B. Arch., Khulna University, 2014  
MS. Arch., Kansas State University, 2018

A DISSERTATION

submitted in partial fulfillment of the requirements for the degree

DOCTOR OF PHILOSOPHY

Department of Environmental Design and Planning  
College of Architecture, Planning and Design

KANSAS STATE UNIVERSITY  
Manhattan, Kansas

2022

Approved by:

Major Professor  
Lee R. Skabelund

# **Copyright**

© M. M. Lekhon Alam 2022.

## Abstract

Green roofs have evolved as an important part of “sustainable development” initiatives around the world. With increasing global warming, many tools are needed, including living roof ecosystems, to reduce urban heat island and climate change impacts. Rooftop green infrastructure can enhance sustainable urban development by reducing atmospheric CO<sub>2</sub> due to its ability to reduce the energy consumption of a building and sequester carbon in plants and substrates. Green roof research indicates that temperature regulation atop buildings is quantifiable and demonstrates a crucial role in reducing the energy demand of a building. Additional environmental benefits of green roofs include improved air quality by removing pollutants from the air and reducing ambient CO<sub>2</sub> concentrations. Given different climates, researchers are uncertain as to what substrate types, depths, and plant combinations sequester the greatest amounts of carbon in green roofs across different ecoregions. Additional research is needed to understand the benefits and limitations of green roofs in specific locations such as the U.S. Great Plains.

A two-growing-season-long study evaluated the carbon sequestration and thermal loading performance of two experimental green roof beds with different depths ~20 cm and ~10 cm and two substrate types in Manhattan, Kansas. Three plant mixes consist of *Sedum* only (A), *Sedum* + native grass mix (B), and native grasses + forbs (C). This study also makes connections to building energy performance. Soil samples were collected at depths of ~8-inch or ~20 cm and ~4-inch or ~10 cm in 2019 and 2020. The soil was analyzed for microbial community composition by PLFA (phospholipid fatty acids), Total Organic Carbon and Nitrogen, and microbial respiration. Root biomass was also determined. Three-way and four-way analysis of variance (ANOVA) and Tukey’s HSD post-hoc analyses were conducted using R version 4.2.0 and SPSS Statistics 29. New methods have been proposed in this study to use data from in-situ measurements of temperatures on building envelopes to estimate the rate of change in heat storage within the soil layer (*Q-value*).

The research was inspired by the summation technique as this calculation procedure allowed the researcher to analyze the accumulation of data on soil moisture content and differences in green roof surface and sub-surface temperatures over time. In-situ sensors were used to measure soil moisture content and surface and sub-surface temperatures so that thermal

properties crucial to understanding heat transfer could be examined. Soil (substrate) types (Kansas BuildEx® [K] and rooflite® extensive mc [R]) and substrate depth were the independent variables for this study, where the primary focus was on determining the significance of soil moisture of a green roof system in building energy performance. All APD-EGR beds were provided supplemental irrigation on an as-need basis.

This two-year (2019 and 2020) analysis found that beds with the R substrate (with its lower bulk density, higher pore space, and lower water-holding capacity than substrate K) likely sequester a greater amount of C per substrate volume. Analysis of temperature data showed that the 4-inch bed at the APD-EGR with R substrate seems to work more efficiently during the building cooling season (with summertime HVAC use) considering both day and night times than the 4-inch bed with K substrate. Interestingly, substrate types do not seem to play a significant role in influencing Q-values in the wintertime and the deeper substrate (8-inch bed) appeared to have more positive Q-values that could improve building performance. Considering depth, the study finds that the thermal performance of two different depths (4-inch and 8-inch) are not similar in two time periods (summertime vs. wintertime). Therefore, suggesting a depth (shallower or deeper) that will improve the energy performance of a building for both time periods in the Flint Hills Ecoregion needs more long-time research and proper instrumentations to determine the approximate R-value (thermal resistance). The soil moisture content is very likely an important factor related to green roof system-induced building energy performance.

The study concludes that in both cases of carbon sequestration and thermal performance, a shallower bed with R substrate may work better as a climate change mitigation strategy in the context of the Flint Hills Ecoregion. However, more research is needed to confirm this. From both studies (thermal and C sequestration), the moisture-holding capacity of different substrate types at different depths appeared to be the key factor in determining green roofs' climate change mitigation potential. A more precise understanding of these dynamic processes and systems is essential to improve design, implementation, and management of green roof ecosystems in support of sustainable building design and climate change mitigation.

**Key Words:** Experimental Green Roof Systems, Climate Change Mitigation, Carbon Sequestration, Building Energy Performance, Sustainability

# Table of Contents

List of Figures .....	xiii
List of Tables .....	xviii
Acknowledgements .....	xx
Dedication .....	xxi
Chapter 1 - Introduction.....	1
Background and Statement of the Problem .....	4
Scope of the study .....	7
Goals of the study .....	8
Research questions.....	8
Overarching research question:.....	9
Primary research questions: .....	9
Project objectives .....	9
1) Explore indicators of carbon sequestration in the green roof substrates: .....	10
2) Measure and track the building’s energy performance: .....	10
Chapter 2 - Literature Review.....	12
Carbon sequestration by green roofs.....	15
Reduced energy consumption of buildings with green roofs: .....	20
Comprehensive approach reported by (Jaffal et al., 2012) .....	24
The Importance of Green-Roof Substrates and Living Vegetation .....	26
Green roofs as a climate change mitigation policy: .....	27
Policies and Arguments (Adaptation and Mitigation) .....	27
Understanding Total Organic Carbon (TOC) and Total Nitrogen (TN) in Soil .....	30
Origin and factors affecting SOC .....	30
Biological effects .....	31
Physical effects .....	31
Functions of SOC.....	31
SOM stores C for climate change mitigation.....	31
Relationship between Soil Heat Storage and Building Energy Performance .....	33
Heat Transfer .....	33

Thermal Conductivity ( $\lambda$ ) .....	34
Thermal Resistance (R-Value).....	35
Specific Heat Capacity.....	36
Volumetric Heat Capacity.....	36
Volumetric Water Content, $\theta_v$ .....	36
U-value .....	36
Thermal Energy Storage .....	37
Thermal Energy Storage and its Effect on Building Energy Performance .....	37
Application of Thermal Energy Storage Solutions in APD-EGR Research Settings...	38
Chapter 3 - Research Context and Methods .....	42
Research Setting .....	42
Substrate constituents and characteristics .....	47
Substrate chemical characteristics .....	47
APD-EGR substrates, K and R, affect soil moisture .....	48
The Flint Hills Ecoregion and Regional-Scale Green Roof Studies.....	50
Research approach .....	53
Variables related to the research hypotheses: .....	53
Hypotheses:.....	53
Methodology and methods.....	54
a) Methods For Estimating Soil C Sequestration.....	55
PLFA analysis.....	56
Soil sampling protocols for PLFA analysis (Protocol 1).....	57
Root biomass.....	59
Procedure for root biomass analysis .....	59
Soil respiration analysis .....	61
Soil sampling protocols for soil respiration analysis (outdoor portion) .....	62
TOC and N analyses .....	63
Soil sampling protocols for TOC and N analysis .....	64
Statistical data analysis .....	64
Soil-sampling timeline .....	65

(b) Methods for Investigating the Role of Green Roof Systems in Improved Building Energy Performance .....	67
Sensor Map of the APD-EGR and Installation Timeline.....	68
Instrumentation at the APD-EGR for the Research.....	71
Rationale for the Use of Only Plant Mix C Type (Native Grasses and Forbs) Plots....	72
Proposed Methods for Thermal Analysis .....	73
In situ observations .....	74
The Summation Technique of in-situ Measurements .....	74
Perpendicular Heat Flow.....	75
Necessary Equations to Determine Heat Flux (q) from In-Situ Measurement.....	75
Conduction of Heat in Soil .....	76
Other Constant Values Required for Calculating $C_v$ .....	80
Estimating $\phi$ , the Fractional Volume of Substrate Organic Matter .....	81
Converting Mass Percentage of Soil OM to Fractional Volumes of soil OM .....	81
Determining $C_v$ with the Volumetric Water Content (primary variable $\theta_v$ ) .....	82
Possibility of Determining $R_e$ in the Context of the APD-EGR .....	83
Possible Solutions for this Research Setting.....	85
Duration of Test .....	86
Calculation of Mean Soil Heat Storage and Mean Temperature .....	86
Sensors Associated with Equal Areas of the Plots at APD-EGR).....	86
Special Considerations in Determining Net Heat Change (Q) .....	90
Case 1 .....	91
Case 2.....	91
Case 3, particular to the conditions at APD-EGR: .....	92
Research Time Period / In-situ Data Collection Duration .....	94
Average Temperature in Manhattan, Kansas, United States .....	94
Chapter 4 - Results.....	97
(a) Soil C Sequestration .....	97
Factors studied for the APD-EGR at KSU .....	97
Statistical analysis procedures for separate bed analysis.....	97
Repeated-measures analysis.....	99

Repeated-measures ANOVA .....	99
Total Organic Carbon (TOC) (derived from soil samples collected in 2019 and 2020)	100
Total Nitrogen (TN) (derived from soil samples collected in 2019 and 2020) .....	103
Microbial Biomass (MB) (derived from soil samples collected in 2019 and 2020).....	106
Summary of the statistical results from the repeated-measures ANOVA .....	111
Root biomass (samples collected in 2020).....	112
Soil respiration (samples collected in 2020).....	114
Results from the two-way ANOVA.....	115
Summary of statistical results from soil-respiration data .....	118
(b) Thermal analysis of the APD-EGR’s Beds.....	119
Chapter 5 - Discussion and Conclusions .....	125
Soil C Sequestration.....	125
Role of TOC.....	125
Fundamentals of SOC.....	130
Research Findings from C Sequestration Analysis.....	138
Leaf Area Index (LAI) Value Examples.....	141
Research Findings from Thermal Analysis.....	143
Conclusion .....	143
Limitations of the study .....	144
References.....	146
Appendix A - Climate of Manhattan Kansas .....	157
Appendix B - Substrate Analysis and Testing Procedures by the KSU Soil Testing Lab and Turf and Soil Diagnostics .....	161
Appendix C - Protocols of the PLFA Analysis in the Lab (Indoor Portion) .....	164
Appendix D - Protocols of the Total Organic Carbon & Nitrogen as well as Organic Matter Analysis in the Lab (Indoor Portion).....	171
Appendix E - Protocols of the Soil Respiration Analysis in the Lab (Indoor Portion) .....	177
Appendix F - The SAS output for the TOC analyses by different bed (both 4-inch and 8-inch- deep bed) and year (year as repeated measure) .....	200
Appendix G - The SAS output for the TN analyses by different bed (both 4-inch and 8-inch-deep bed) and year (year as repeated measure).....	188

Appendix H - The SAS output for the MB analyses by different bed (both 4-inch and 8-inch-deep bed) and year (year as repeated measure) ..... 194

## List of Figures

Figure 1.1. Basic research model for this study .....	3
Figure 1.2. Photo of the APD-EGR at KSU showing the 4-, 6-, and 8-inch deep APD-EGR beds (the 4-inch bed is closest to the camera).....	4
Figure 1.3. Photos of the three APD-EGR beds (4-, 6-, and 8-inch deep, shown from left to right, respectively) APD-EGR.....	5
Figure 1.4. Basic layout of the KSU APD-EGR research site illustrating the plots and beds.....	6
Figure 1.5. Irrigating the APD-EGR and its plants in summer 2021.....	9
Figure 1.6. APD-EGR substrate-plant interactions during the summer of 2020.....	11
Figure 2.1. Basic components of green roof .....	13
Figure 2.2. APD-EGR green roof literature review diagram.....	14
Figure 2.3. Field measurement setup of Li et al. (2010).....	19
Figure 2.4. Energy balance for a green roof, including latent heat flux (L), sensible heat flux (H), shortwave radiation ( $I_s$ ), and incoming longwave radiation ( $I_{ir}$ ). Conduction into the soil and the complicated exchange of long-wave (LW) radiation within the canopy are also shown (Sailor, 2008). (diagram and text borrowed from Sailor).....	22
Figure 2.5. Coupling of green roof model with building thermal model (Jaffal et al., 2012) (diagram and text borrowed from Jaffal et al.) .....	24
Figure 2.6. Studied parameters for conventional and green roofs (Jaffal et al., 2012).....	25
Figure 2.7. Cooking stove illustration demonstrating heat transfer through radiation, convection, and conduction (Selker and Or, 2021) .....	34
Figure 2.8. Thermal conductivity of a specimen .....	35
Figure 2.9. Thermal test sites assemblies (simplified) at APD-EGR. ....	41
Figure 3.1. Illustration of the APD-EGR site at KSU showing the positions of the three beds, with the 4-in bed situated closest to the camera (i.e., on the north side). ....	42
Figure 3.2. A roughly 4 x 4-ft/1.2 x 1.2-m plot on the APD-EGR, with a surface temperature sensor cover visible.....	43
Figure 3.3. Section of the APD-EGR showing the green roof components. ....	44

Figure 3.4. Layouts of the beds containing plant mix types A, B, and C in the K (gray boxes) and R substrates in the 4- and 8-in-deep beds, with the plots in each bed numbered from 1 to 24. ....	46
Figure 3.5 Plant layouts for plant mix types A, B, and C (after Shrestha, 2019). ....	46
Figure 3.6. Substrate types K (left) and R (right) planted with native grass + forbs (mix type C) on the APD-EGR. ....	47
Figure 3.7. Flint Hills Ecoregion in Kansas. ....	50
Figure 3.8. Concept map for the research project. ....	52
Figure 3.9. Research design for estimating soil C sequestration. ....	55
Figure 3.10. Collecting soil samples for the soil PLFA, TOC and N analyses from the APD-EGR in 2019. ....	56
Figure 3.11. Lekhon and Tonima collecting soil samples for PLFA, TOC, and N analyses from the APD-EGR in 2020 (outdoor portion). ....	58
Figure 3.12. Collecting soil samples for respiration analysis from the APD-EGR’s 4- and 8-in-deep beds in 2020 (outdoor portion). ....	58
Figure 3.13. Collecting and analyzing root biomass samples from the 4-inch-/10-cm- and 8-inch-/20-cm-deep beds. ....	61
Figure 3.14. Soil laboratory activities (indoor portion)—preparing soil samples for PLFA analysis. ....	62
Figure 3.15. Soil laboratory activities (indoor portion)—preparing soil samples for respiration analysis. ....	63
Figure 3.16. Experimental design and data analysis procedures for comparing the soil C sequestration potential of different APD-EGR beds. ....	66
Figure 3.17. Installing temperature sensors, checking sensor readings, and an assortment of temperature and soil moisture sensors at APD-EGR. ....	67
Figure 3.18. Sensor map of the APD-EGR, Kansas State University. Sub-surface sensors were placed in the eight C plots in mid-March 2018. ....	69
Figure 3.19. The latest sensor map of the APD-EGR, marking surface temperature RT-1 sensors in 4-inch & 8-inch-deep beds, lasting until June 11, 2020 ....	69
Figure 3.20. Sensor map of the in 4-inch & 8-inch-deep beds, including the plot IDs, with RT-1 & 5TM surface temperature sensors marked in yellow ....	71

Figure 3.21. APD-EGR heat transfer model.....	73
Figure 3.22. Illustration of heat flow in soils, emphasizing the role of mineral composition, porosity, and water content (Stephens et al., 2018; Selker and Or, 2021).....	77
Figure 3.23. Diagram depicting thermal energy loss and gain through the soil layer at the APD- EGR with volumetric heat capacity, $C_v$ .....	92
Figure 3.24. Average (1972 - 2021) high and low temperatures in Manhattan, Kansas, USA (Weatherspark, 2020-2021) .....	95
Figure 3.25. Average (1972 - 2021) daily chance of precipitation in Manhattan, Kansas, USA (Weatherspark, 2020-2021) .....	95
Figure 4.1. Four blocks (NE, NW, SE, SW) in the 4-inch- and 8-inch-deep beds, as allocated by the strip-plot design.....	98
Figure 4.2 Descriptive statistics, with box-and-whisker plots showing the data distribution for TOC from the two substrates (K and R) of the 4-inch-deep bed (comparing TOC with year). .....	100
Figure 4.3 Descriptive statistics, with box-and-whisker plots showing the data distribution for TOC from the two substrates (K and R) of the 8-inch-deep bed (comparing TOC with year). .....	101
Figure 4.4. TOC means and standard errors from the 8-in-deep bed (comparing means of TOC from the two substrates (K and R) with year). **Significant effect of TOC in two years ( $\alpha =$ 0.05). Vertical bars denote upper and lower standard errors. ....	102
Figure 4.5. Descriptive statistics, with box-and-whisker plots showing the data distribution for TN from the two substrates (K and R) of the 4-inch-deep bed (comparing TN with year).103	
Figure 4.6. Descriptive statistics, with box-and-whisker plots showing the data distribution for TN from the two substrates (K and R) of the 8-inch-deep bed (comparing TN with year).104	
Figure 4.7. TN means and standard errors from the 8-inch-deep bed (comparing the means of TN from the two substrates (K and R) with year). *Significant effect of TN in two years ( $\alpha =$ 0.05). Vertical bars denote upper and lower standard errors. ....	105
Figure 4.8. Descriptive statistics, with box-and-whisker plots showing the data distribution for MB from the three plant mixes (A, B, and C) of the 4-inch-deep bed (comparing MB with year). (0— <i>Sedum</i> only, plant mix type A; 1— <i>Sedum</i> + native grass mix, plant mix type B; 2—native grasses + forbs, plant mix type C).....	106

Figure 4.9. Descriptive statistics, with box-and-whisker plots showing the data distribution for MB from the two substrates (K and R) of the 4-inch-deep bed (comparing MB with year). .....	107
Figure 4.10. Descriptive statistics, with box-and-whisker plots showing the data distribution for MB from the three plant mix types (A, B, and C) of the 8-in-deep bed (comparing MB with year). (0— <i>Sedum</i> only, plant mix type A; 1— <i>Sedum</i> + native grass mix, plant mix type B; 2—native grasses + forbs, plant mix type C). .....	108
Figure 4.11. MB means and standard errors from the 8-inch-deep bed, comparing the means of MB from the two substrates (K and R) with year. **Significant effect of MB in two years ( $\alpha = 0.05$ ). Vertical bars denote upper and lower standard errors. ....	109
Figure 4.12. MB means and standard errors from the 8-inch-deep bed, comparing means of MB from the three plant mixes (A, B, and C) within the year. **Significant effect of MB in the two years ( $\alpha = 0.05$ ). Vertical bars denote upper and lower standard errors. (0— <i>Sedum</i> only, plant mix type A; 1— <i>Sedum</i> + native grass mix, plant mix type B; 2—native grasses + forbs, plant mix type C). ....	110
Figure 4.13. Average root density at two depths (4-inch and 8 inch) in the belowground biomass of plant mix types A, B, and C and the two substrates (K and R). ....	113
Figure 4.14. Soil respiration at two depths (4 and 8 in) in belowground biomass samples from three plant mix types (A, B, and C) and two substrates (K and R). ....	115
Figure 4.15. Soil respiration in belowground biomass samples of three plant mix types (A, B, and C) and two substrates (K and R). ....	116
Figure 4.16. Soil respiration at two depths (4 and 8 in) and in three belowground biomass samples (A, B, and C). ....	118
Figure 4.17. The rate of change in heat storage within the soil layer ( <i>Q-value</i> ) of all KC plots from 4-inch-deep beds at APD-EGR during the summertime. ....	119
Figure 4.18. The rate of change in heat storage within the soil layer ( <i>Q-value</i> ) of all RC plots from 4-inch-deep beds at APD-EGR during the summertime. ....	119
Figure 4.19. The rate of change in heat storage within the soil layer ( <i>Q-value</i> ) of all KC plots from 8-inch-deep beds at APD-EGR during the summertime. ....	120
Figure 4.20. The rate of change in heat storage within the soil layer ( <i>Q-value</i> ) of all RC plots from 8-inch deep beds at APD-EGR during the summertime. ....	120

Figure 4.21. The rate of change in heat storage within the soil layer ( <i>Q-value</i> ) of all KC plots from 4-inch deep beds at APD-EGR during the wintertime.....	122
Figure 4.22. The rate of change in heat storage within the soil layer ( <i>Q-value</i> ) of all RC plots from 4-inch deep beds at APD-EGR during the wintertime.....	122
Figure 4.23 The rate of change in heat storage within the soil layer ( <i>Q-value</i> ) of all KC plots from 8-in deep beds at APD-EGR during the wintertime.....	123
Figure 4.24 The rate of change in heat storage within the soil layer ( <i>Q-value</i> ) of all RC plots from 8-inch deep beds at APD-EGR during the wintertime.....	124
Figure 5.1. Relative aerobic (respiration, ammonification, and nitrification) and anaerobic (denitrification) microbial activity related to water-filled pore space in soil (after Linn and Doran, 1984; Parkin et al., 1997).....	132
Figure 5.2. Relationship between porosity and SOC (after Franzluebbers, 2011). .....	134
Figure 5.3 Summertime vs. Wintertime moisture content comparison of K and R.....	135
Figure 5.4. All the box-and-whisker plots together, showing the data distribution for TOC, TN, and MB from the two substrates (K and R). .....	137
Figure 5.5. The research focused only on the substrate layer of the APD-EGR (Confluence, 2019). .....	140

## List of Tables

Table 3.1. Plant mixes planted on the ARD–EGR.....	44
Table 3.2. Research settings for the APD-EGR considering two substrate types, three vegetative plant mixes, two bed depths, and four plots sampled for each plot type (a combination of depth, substrate type, and plant mix) .....	45
Table 3.3. Soil test results for substrate types K and R from the 4-in-deep APD-EGR bed (the tests were conducted by the KSU Soil Testing Lab in April 2018).....	48
Table 3.4. Type K and R substrate properties tested at the Turf and Soil Diagnostics Laboratory in Linwood, Kansas in 2018 .....	48
Table 3.5. Green-roof porosity, pH, EC, and OM test results for substrate types K and R (tests conducted by Turf and Soil Diagnostics, Linwood, Kansas, in March 2019) .....	49
Table 3.5(a). Average water holding capacity for K and R for 4-inch and 8-inch beds .....	70
Table 3.6. Soil sampling details for the APD-EGR for 2019 and 2020.....	65
Table 3.7 KSU APD-EGR data logger information .....	70
Table 3.8 Dry bulk density and porosity of the two APD-EGR substrates, K and R per (Decker, 2021). .....	80
Table 3.9 Mass percentage of substrate Organic Matter (OM) for the selected twelve plots.....	81
Table 3.10 Properties of soil components at 293 K (Brutsaert, 1982).....	82
Table 3.11 Fractional volume of soil Organic Matter (OM) for the selected twelve plots.....	82
Table 3.12 Sensor site groupings for the overall mean of mQ and m(Moi) calculations .....	88
Table 3.13 Various symbols used in the thermal analyses .....	89
Table 3.14 Total Data Collection Points and Duration.....	96
Table 4.1. Test of fixed effects on TOC of the 4-inch-deep bed (SAS output).....	100
Table 4.2. Test of fixed effects on TOC of the 8-in-deep bed (SAS output).....	101
Table 4.3. Test of fixed effects on TN of the 4-inch-deep bed (SAS output).....	103
Table 4.4. Test of fixed effects on TN of the 8-in-deep bed (SAS output) .....	104
Table 4.5. Test of fixed effects on MB of the 4-inch-deep bed (SAS output).....	106
Table 4.6. Test of fixed effects on MB of the 8-in-deep bed (SAS output).....	108
Table 4.7. Descriptive statistics of the root density data .....	112

Table 4.8. Three-way ANOVA results of the root density data for the 4- and 8-in-deep beds (SPSS).....	113
Table 4.9. Descriptive statistics for soil respiration.....	114
Table 4.10. Three-way ANOVA results for soil respiration (SPSS outputs) .....	114
Table 4.11. Descriptive statistics of soil respiration from the two-way ANOVA.....	116
Table 4.12. Two-way ANOVA results for soil respiration (SPSS outputs) .....	116
Table 4.13. Descriptive statistics of soil respiration.....	117
Table 4.14. Two-way ANOVA results of respiration.....	117
Table 5.1. Average SOC and TN values, and their correlation coefficients (after Wibowo and Kasno, 2021).....	127

## **Acknowledgements**

I would like to express my profound gratitude to my advisor, Professor Lee R. Skabelund (Landscape Architecture and Regional & Community Planning), for his generous guidance and mentorship during my time at Kansas State University. He always had time for me, offered his counsel on any problem I was facing, and aided me with infinite goodwill. I can still remember my struggle in 2019 when suddenly my previous advisor Dr. David Sachs retired, and I was without a mentor. Professor Skabelund accepted me as his PhD student. It is because of his kindness and guidance I was able to continue my scholarly journey at Kansas State University.

I am also thankful to Dr. Charles Rice (soil scientist in the Department of Agronomy), Professor Michael Gibson (Department of Architecture), and statistician and instructor Tim Todd (Department of Plant Pathology). As members of my dissertation committee, they counseled me at every stage of the research, offered valuable perspectives and data analysis support, and gave me many tips to improve my research. I am also grateful to James Lin, who helped me throughout my PhD journey (he truly went the extra mile to support my data collection). Without these four individuals, the dissertation would not be complete.

The College of Architecture, Planning, and Design (APDesign) at Kansas State University also deserves special thanks for supporting my PhD journey. Those leading and supporting the Environmental Design and Planning (EDP) PhD Program have provided me with consistent funding and healthcare during my studies, which allowed me to concentrate on my research without distraction. Those working for APDesign have always been very efficient in handling my paperwork, and I am incredibly thankful to Dr. Anne Beamish (Director of the EDP PhD Program), Professor Stephanie Rolley (Department Head of Landscape Architecture and Regional & Community Planning through June 2022), and Dean Tim de Noble.

Finally, I am especially thankful to my parents; without whom, I would certainly not be where I am today. And to my sister and brother, Shimul and Siraji, who are my lifelong friends; their support has been invaluable to me. Lastly, I express my sincere gratitude to my dear wife, Tasmeen Tonima, who has always encouraged me to achieve more than I ever could imagine.

## **Dedication**

To my parents:

**Md. Zahangir Alam and Rabeya Alam**

## Chapter 1 - Introduction

Green roofs can be traced back as far as the gardens of Babylon and the Roman Empire, in that trees or other types of vegetation have been grown on top of built structures since that time (Peck, 2002). During the 19th and 20th centuries, rooftops in major cities of the United States (US) were greened in order to mitigate the rising cost of land for building parks on in the inner city (Herman, 2003). Currently, the world leader in green roof technologies is Germany, where more than 10% of houses have installed green roofs (Köhler, 2006). Several authors have noted that the first wave of constructing green roofs in Germany came at the end of the 19th century (Köhler, 2006; Li and Yeung, 2014; Jim, 2017). This roof technology was later modernized in the 1960s, when people started to seek improvements in the greening aspects (Jim, 2017). Green roofs, having been established for many years, have become important elements in urban areas during the last few decades. Many scientific studies have been undertaken to assess their qualities, including their cooling performance, energy efficiency, and plant survival rates (Li and Yeung, 2014).

Green roofs are sometimes called “anthropogenic patches” (Sutton, 2015) because they have a vegetative layer that is planted and grown on the rooftop (Davis, 2015). As such, these created structures serve as bio-retention systems consisting of soils or substrates, typically planted with hardy perennial plants (sometimes native) and, ideally (if the owner is concerned about operations and management cost savings), not requiring much tending (Jaffal et al., 2012). Unlike traditional black tar roofs, green roofs reduce energy costs by reducing potential heat via evapotranspiration instead of absorbing heat, and by providing natural insulation for the buildings they are placed on (Wong et al., 2003; Davis, 2015). This innovative application can have a substantive positive impact on stormwater management by reducing rooftop runoff and improving water quality. According to the US National Park Service (NPS), there are significant benefits to green roofs, including economic benefits, improved stormwater management, reduced urban heat-island effect, improved air quality, building insulation, improved efficiency of mechanical equipment, reduced greenhouse gas (GHG) emissions, extended waterproofing life of the roof, and the provision of urban amenities for people to enjoy (NPS Technical Preservation Services, 2018).

The installation of a green roof on any building allows the sequestration of the primary GHG, carbon dioxide (CO<sub>2</sub>) (Getter et al., 2009a; Kuronuma et al., 2018), from the atmosphere. Recent research has indicated that the importance of green roofs to the temperature regulation of buildings is quantifiable and plays a crucial role in reducing the energy demand of a building (Islands, 2008; Sailor, 2008; Foster et al., 2011; Price et al., 2015).

In recent years, with the increasing global-warming phenomenon, it has been recognized that green roofs can contribute to climate-change mitigation by reducing electricity usage, shrinking a building's carbon footprint, and improving the building's energy performance (Garrison et al., 2012; Refahi and Talkhabi, 2015). With the increase in global-warming phenomena, it is not enough to concentrate on either adaptation or mitigation policies to combat climate change; a combination of these is essential. Since global warming is driven, in large part, by the increase in atmospheric temperatures caused by burning fossil fuels and releasing GHGs (including CO<sub>2</sub>), dramatically reducing GHG emissions is very important in order to mitigate negative climate change impacts (Fioretti et al., 2010). Green roofs may be helpful in this mitigation effort. However, more investigation is needed into different types of systems in different locations around the world (Laukkonen et al., 2009). Because of different climates, plant materials, substrate types and depths, and a wide variety of construction materials and methods, many studies have concluded that regional research is needed to demonstrate the benefits of green roofs in specific locations (Lin et al., 2013).

To understand the research importance, one must understand climate-change mitigation and adaptation policies and strategies. Since the beginning of the 21st Century, adaptation to climate change has required an appraisal of future climate-change scenarios and the development of strategies and plans to modify current practices in ways that enable future human co-existence with changed environmental conditions (Cooper and Lemckert, 2012). Although many policy responses are being developed at local and regional levels, Hamin and Gurrán (2009) argued that very few attempts are being made to ensure those strategies are implemented so that society can adapt to the inevitable impacts of enhanced climate change (hotter temperatures, longer and more intense dry periods, and very heavy rainfall). We should also bear in mind that adaptation is basically a supporting feature of many ongoing policies that are intended to mitigate local contributions to climate change (Hamin and Gurrán, 2009). In some cases, mitigation and

adaptation are complementary, but in other cases, these policy goals may conflict (Hamin and Gurran, 2009; Laukkonen et al., 2009).

Therefore, it is crucial to consider sustainability in terms of climate change adaptation and mitigation, supported by evidence-based environmental design. According to Demuzere et al. (2014), several opportunities exist for developing climate-resilient urban areas and reducing GHG emissions, starting with wise planning and the design of green (and blue) spaces in these landscapes. Green urban infrastructure (including green roofs) has been regarded as beneficial, involving, for example, balancing water flows and providing thermal comfort. In this study, the author explored the evidence on the contribution of green roofs to climate-change mitigation and adaptation by examining an experimental green roof in north-central Kansas.

The study was conducted with three essential elements in mind: 1) the environment, exemplified by the northern United States Midwest; 2) green roofing, specifically, the Architecture, Planning, and Design Experimental Green Roof (APD-EGR) at Kansas State University (KSU); and 3) an existing building—KSU’s Regnier Hall—where the primary purpose is to analyze a green roof’s potential to mitigate climate change by focusing on the potential of the APD-EGR to sequester carbon and reduce heat load on this new building. A simple framework for this study is shown in Figure 1.1.

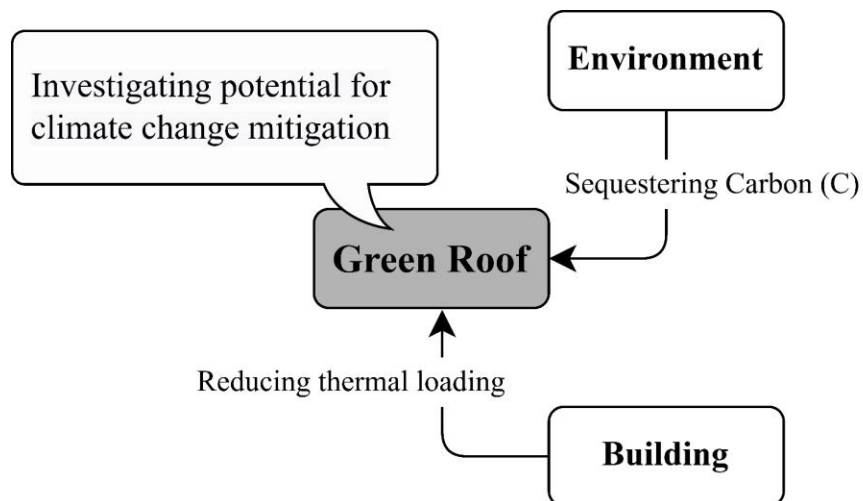


Figure 1.1. Basic research model for this study.

## Background and Statement of the Problem

Green roof research is a relatively new field of interest, having taken hold in the 1990s (Jim, 2017). A wide range of factors affect the performance of green roofs, and each of these created ecosystems provides different benefits (Sutton, 2015). Currently, factors such as depths, substrate characteristics and plant dynamics have not yet been investigated in terms of quantifying a green roof's urban heat-island indicators and the ability to sequester carbon in specific ecoregions across the world, including green roofs implemented in the Flint Hills Ecoregion in north-central Kansas.

Between 2015 and 2016, an experimental green roof was designed in Manhattan, Kansas by Lee Skabelund, working with other researchers at KSU and members of the Ennead–BNIM–Confluence design team. Landscape architects at Confluence were tasked with completing detailed design and construction documents for KSU's APD-EGR, which was constructed and planted between July 2017 and June 2018. One of the primary purposes of establishing the APD-EGR was to study native prairie grasses and forbs in the continental climate zone. Multi-year observations (Skabelund et al., 2014) and findings (Skabelund et al., 2015, 2017) were published by the research team, where they identified the need to expand the scale of the research to explore the impact of green roofs in a more systematic way. This was made possible with completion of the APD-EGR (see figures 1.2 and 1.3).



**Figure 1.2.** Photo of the APD-EGR at KSU showing the 4-, 6-, and 8-inch deep APD-EGR beds (the 4-inch bed is closest to the camera).

(Image taken by M. M. Lekhon Alam in late May 2020.)



**Figure 1.3.** Photos of the three APD-EGR beds (4-, 6-, and 8-inch deep, shown from left to right, respectively) APD-EGR.

(Image taken by M. M. Lekhon Alam in May 2020.)

The substrate is one of the most critical parts of a green roof system because most of the water-holding capacity is dependent on the substrate type and depth. The substrate also accounts for much of the saturated and dry dead loads on a green roof (Sutton et al., 2012). Best et al. (2015) asserted that the success of green-roof plants is mostly affected by the substrate's capacity for water retention, adequate drainage, and appropriate nutrient availability. Substrate characteristics, such as texture and organic matter (OM) content, are essential for growing and maintaining healthy green-roof plants (Best et al., 2015). In addition, organic and inorganic substrate components and their combinations affect plant survival, growth, and success on green roofs (Graceson et al., 2014). Vegetation and substrates combine to sequester carbon (C) (Graceson et al., 2014).

A review of the significant literature on the performance and benefits of green roofs has been published in Ismail and Abdullah (2016), in which they asserted that green roofs have the proven potential to reduce problems related to climate change. The depth of a green roof's substrate is a key factor that can optimize its potential benefits discussed in detail in Chapter 2 (Ismail and Abdullah, 2016).

At the beginning of this study, it was unknown what substrate components, depths, and plant combinations would best support climate-change mitigation strategies that could help sequester carbon by sinking the highest amount of CO<sub>2</sub> from the environment into green roof vegetation growing within the continental climate of Manhattan, Kansas. Hence, in this study, we sought to explore the APD-EGR's urban heat load capacity and carbon sequestration rates through observation of the soil moisture content and surface and subsurface temperature dynamics and through laboratory analysis of the soil phospholipid fatty acid (PLFA) content, respiration, root biomass, total organic C (TOC) and total nitrogen (TN). We performed the study on the two engineered substrate types that are used on the APD-EGR—Kansas BuildEx® (K) and rooflite® extensive mc (R). This quantitative observational study was conducted on beds with depths of ~4 in/~10 cm and ~8 in/~20 cm, each bed consisting of 24 plots (see Figure 1.4).

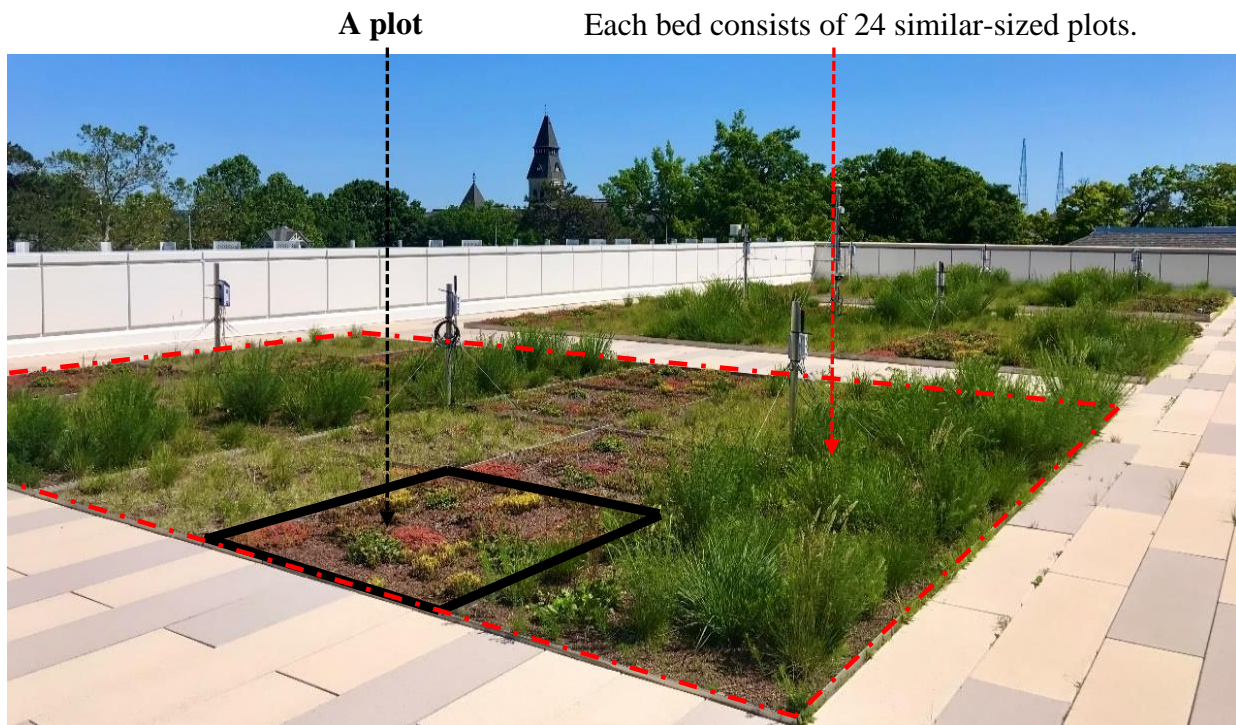


**Figure 1.4.** Basic layout of the KSU APD-EGR research site illustrating the plots and beds.

(Image taken by M. M. Lekhon Alam in May 2020.)

Considering the perspective of climate change mitigation, Getter et al. (2009a) and Whittinghill et al. (2014) both indicated that green roofs can sequester C in vegetative biomass and substrates. In addition, a green roof can reduce the energy consumption of a building (Fioretti et al., 2010; Jaffal et al., 2012), thus helping to reduce global-warming impacts. The primary research objective was to examine the connections between building energy use reductions and carbon sequestration by exploring the climate-change-mitigation potential of the APD-EGR over a two-year period.

Through this study, answers were sought to two fundamental questions: 1) To what degree can a green roof substrate or soil contribute to climate change mitigation (i.e., atmospheric CO<sub>2</sub> reduction) in Manhattan, Kansas? 2) To what degree can the substrates in the APD-EGR systems reduce the heat-island effect? Underpinning these questions was the idea that, together with the water held in soil pores, the mineral soil can store heat acquired from solar radiation in the daytime and gradually release some or much of this heat over an extended duration (Wei et al., 2020), depending on air temperature dynamics, precipitation, and other climatic and building, location, and context related variables.

### **Scope of the study**

A portion of this study complements ongoing research by Lee Skabelund on the APD-EGR at KSU regarding the performance (survival and health) of the selected plant materials used in the different substrate types and depths. Given this context, this doctoral dissertation presents research aimed at understanding the fundamental links between specific climate change mitigation strategies and the performance of a green roof related to carbon sequestration and building energy use/demand.

The intent of this study was to evaluate the climate change mitigation potential of the APD-EGR in response to different substrates, depths, and engineered growing media. This research focused on the ~4-inch (~10-cm) and ~8-inch (~20-cm) substrate depths since these two substrate depths are deemed to be the most appropriate for comparing climate effectiveness (Faaij et al., 2013, p. 207) of green roofs. For example, sustainable adaptation or climate effectiveness can be measured through “measures that reduce vulnerability and promote long-term resilience in a changing climate” (Leichenko & O’Brien, 2008, p. 01). During the study, observations were made over two growing seasons (in 2019 and 2020). The data collected was

intended to set a baseline and an important reference for longer-term studies. The desire is that this study will provide a useful reference and source materials for similar studies, especially for studies to be performed under similar and different climatic regimes by green-roof researchers worldwide.

## **Goals of the study**

The primary goals of this study were to:

- 1) **Provide scientific evidence for the APD-EGR's contribution to sequestering CO<sub>2</sub> from the atmosphere by examining two substrate types and depths and measuring the soil biological properties, root biomass, and the age of the roof (as a measure of time).** The roof's performance was addressed by measuring the root biomass, microbial biomass, TOC, TN (C:N ratio), and soil respiration to determine the possible indicators and the amount of soil C sequestered.
- 2) **Obtain a better understanding of how the two APD-EGR green-roof substrate types and depths enhanced or limited climate-change mitigation by quantifying the bulk heat flows through the green roof system over time using in-situ measurements.** In the study, two different temperature values were evaluated for the APD-EGR—substrate surface temperature and substrate subsurface temperature—in response to the two substrate types and depths, and their characteristics. Additionally, moisture data from the substrate was used to explain how the water content in the green roof system affected thermal functions.

## **Research questions**

The research questions posed of this study included three essential elements—unique green roof characteristics, carbon sequestration, and building energy performance. The focus was on how green roofs could help reduce CO<sub>2</sub> emissions in the Flint Hills Ecoregion in Kansas, both directly and indirectly. The hope was to provide useful scientific evidence that might support the adoption of green roofs in building construction projects as an effective climate mitigation strategy.

***Overarching research question:***

**What are the factors and indicators that could explain the climate-change mitigation potential of green roofs in the context of the Flint Hills Ecoregion?**

***Primary research questions:***

- 1) How do the K and R substrates, microbial communities, two green roof substrate depths (~8- and ~4-inch), and the age of the green roof (time since implementation) impact the carbon sequestration capability of the APD-EGR?
- 2) How do the two different substrate depths (~8- and ~4-inch), two substrate types (K and R), substrate moisture levels, and time (summer vs. winter) influence CO<sub>2</sub> drawdown related to building energy performance (in this instance, the magnitude of the green roof system as a building insulator) at the APD-EGR?



**Figure 1.5.** Irrigating the APD-EGR and its plants in summer 2021.

(Images taken by Lekhon Alam in May 2021.)

**Project objectives in greater detail**

This study sought to address the effect of the APD-EGR on (C) sequestration in order to assess the benefits of this urban-greening project, including its connections to building energy performance. More detailed objectives were to:

**1) Explore indicators of carbon sequestration in the green roof substrates:**

- a) Gather data on the different indicators of the carbon sequestration potential of the two APD-EGR substrates. Measure the microbial biomass, TOC, TN, respiration, and root biomass of two different substrates—K and R—during two growing seasons and compare these substrate types at two depths (~4-inch and ~8-inch).
- b) Exclude aboveground ground-plant types from the research variables. “Different plant mixes” focused only on the three different belowground biomass samples for the plant mixes: *Sedum* only (**A**), *Sedum* + native grass mix (**B**), and native grasses + forbs (**C**).
- c) Include the age of the root (time), two different depths (~4-inch and ~8 inch), two substrate types (K and R), microbial biomass, and root biomass as the primary variables responding to the Flint Hill Ecoregion’s climate.

**2) Measure and track the building’s energy performance:**

- a) Compare the relative thermal effectiveness of the 8-inch and 4-inch beds on the APD-EGR, excluding different plant mixes as variables. This thermal study was designed to be conducted on plot type C (native grasses + forbs), based on the assumption that the belowground biomass would have the highest root density for the two study years (2019 and 2020).
- b) Examine the performance of the two substrate types—K and R—recognizing that there are variations in their respective water-holding capacities.
- c) Compare the relative thermal dynamics of the APD-EGR between summer (June 15, 2020 to September 15, 2020) and winter (November 15, 2020 to February 15, 2021) in the Flint Hills Ecoregion. All temperature and soil moisture datasets were collected using Decagon/METER RT-1 and 5TM sensors to quantify the bulk heat flows through the APD-EGR system. The sensors were programmed to store in-situ temperature, moisture, and solar radiation measurements every 15 minutes.



**Figure 1.6.** APD-EGR substrate-plant interactions during the summer of 2020.  
(Images taken by M. M. Lekhon Alam in June 2020.)

## Chapter 2 - Literature Review

A green roof supports living vegetation on the roof of a building (Davis, 2015, Refahi and Talkhabi, 2015). Generally, there are two types of green roofs: extensive (with soil thickness less than 10–15 cm) and intensive (with soil thickness greater than 15–20 cm) (Fioretti et al., 2010, Feng et al., 2010, Spala et al., 2008, Jaffal et al., 2012).

There are many economic, ecological, and societal benefits associated with green roofing (Services, 2018). Green roofs improve stormwater management (Fioretti et al., 2010) and reduce air pollution (Yang et al., 2008, Li et al., 2010) and noise (Van Renterghem and Botteldooren, 2011). Green roofing reduces a city's carbon footprint by converting carbon dioxide to oxygen through photosynthesis (Li et al., 2010, Feng et al., 2010). Green roofs improve building energy efficiency by enhancing heat transfer through the roof (Fioretti et al., 2010, Sailor, 2008, Sailor et al., 2011, Jaffal et al., 2012). The reduced temperature near green roofing in the summer improves the efficiency of mechanical equipment in buildings (HVAC systems) (Services, 2018). Green roofs improve the longevity of roofing membranes by limiting the thermal stress to which they are subjected (Fioretti et al., 2010, Lin et al., 2013, Jaffal et al., 2012, Services, 2018). At the city level, green roofs provide a quasi-natural habitat for animals and birds (Schrader and Böning, 2006, Refahi and Talkhabi, 2015) and help mitigate the urban heat island effect (Alexandri and Jones, 2008, Wong et al., 2003, Takebayashi and Moriyama, 2007, Jaffal et al., 2012). Green roof characteristics (particularly plant health) are strongly associated with climate, microclimate, and substrate types and depth(s). For instance, green roof solutions and materials in Australia (design strategies, plants, substrates, etc.) may be different from those in a European climate (Williams et al., 2010). The substrates used on green roofs may also be very different, depending on materials or substrates readily available in a specific location.

Although green roofing is often used for energy savings and heat island mitigation, rarely has this technology been promoted for its ability to mitigate climate change. With reduced demand for heating and air conditioning, less carbon dioxide is released from power plants and furnaces. Sailor (2008) integrated green roof energy balance calculations into Energy Plus, a building energy simulation model supported by the U.S. Department of Energy (Getter et al., 2009b). Use of regionally adapted vegetation is critical to retain healthy plants on a green roof and help temper summer heat loads. Akther et al. (2018) statistically synthesized the effects of

influential factors, including design and hydrologic variables, on green roof performance and explored their impact in different climatic zones. These authors concluded that the differences in the influential variables and, thus, the performance of green roofs in different climatic zones (Akther et al., 2018; Getter et al., 2009a; Sailor et al., 2011). Figure 2-1 shows a typical cross-section of a green roof and its components (although many designed green roof profiles are unique).

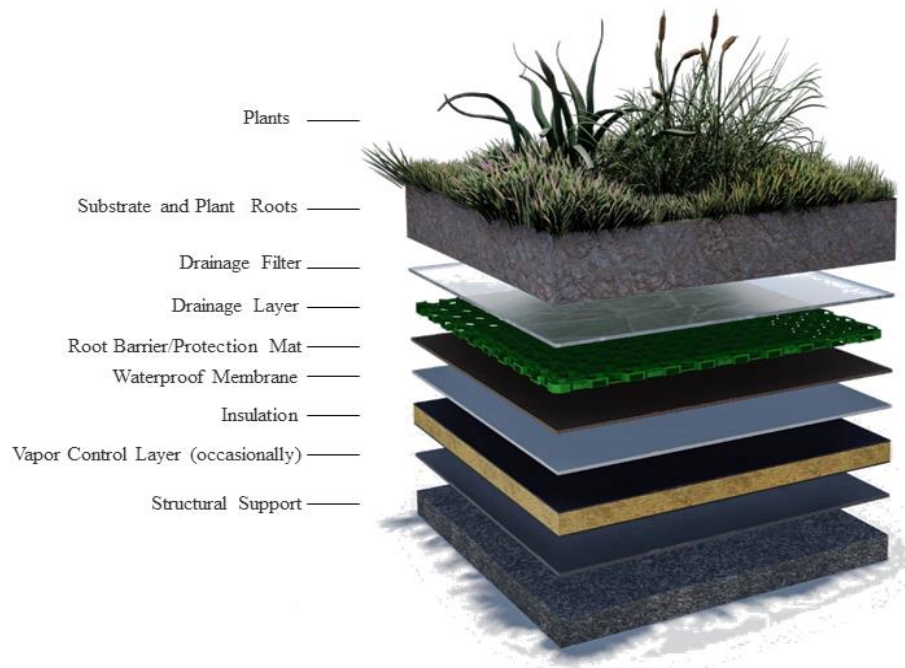


**Figure 2.1.** Basic components of green roof.

Alam, adapted from Shrestha (2019)

Significant research regarding the carbon (C) sequestration potential of green roofs was conducted by Dr. Kristin Getter and other researchers from Michigan State University between 2006 and 2009 (Getter et al., 2009b). Kristin Getter, one of the pioneers of green roof research told NBC that “the key to fighting global warming is capturing carbon from the atmosphere and storing it in new reservoirs that weren't storing carbon before, and in the whole scheme of things, green roofs are not the one answer to sequestering carbon, but they will certainly help” (Sohn, 2009). Getter et al. began by measuring the amount of carbon stored in aboveground vegetation on 12 typical green roofs in Michigan and Maryland. For two growing seasons, they also measured carbon above and belowground on an experimental roof at Michigan State University (Sohn, 2009, Getter et al., 2009a). After two years of study, it was concluded that although the

numbers varied from roof to roof and between different areas of the same roof, the entire green roof system sequestered  $375 \text{ g C}\cdot\text{m}^{-2}$  in aboveground and belowground biomass and substrate organic matter (Getter et al., 2009b).

Getter sought to establish her argument within a broader perspective and calculated that the metropolitan area of Detroit had approximately 65–85 million square meters of rooftop area. It was reported in *Environmental Science & Technology* that greening that entire area would be equivalent to removing 10,000 mid-sized SUVs or trucks from the roads for one year (Getter et al., 2009b, Sohn, 2009).

David Sailor, an engineer at Portland State University, believes that carbon sequestration in plant biomass is one of the most compelling co-benefits of green roofs (Sohn, 2009). Green roofs are considered effective in reducing atmospheric  $\text{CO}_2$  because they reduce the energy consumption of buildings and sequester carbon in plants and substrates (Kuronuma et al., 2018). Thus, they have the potential to help mitigate climate change (along with many other actions) (Project Drawdown, 2020).

This study has two essential parts (Fig. 2.2).

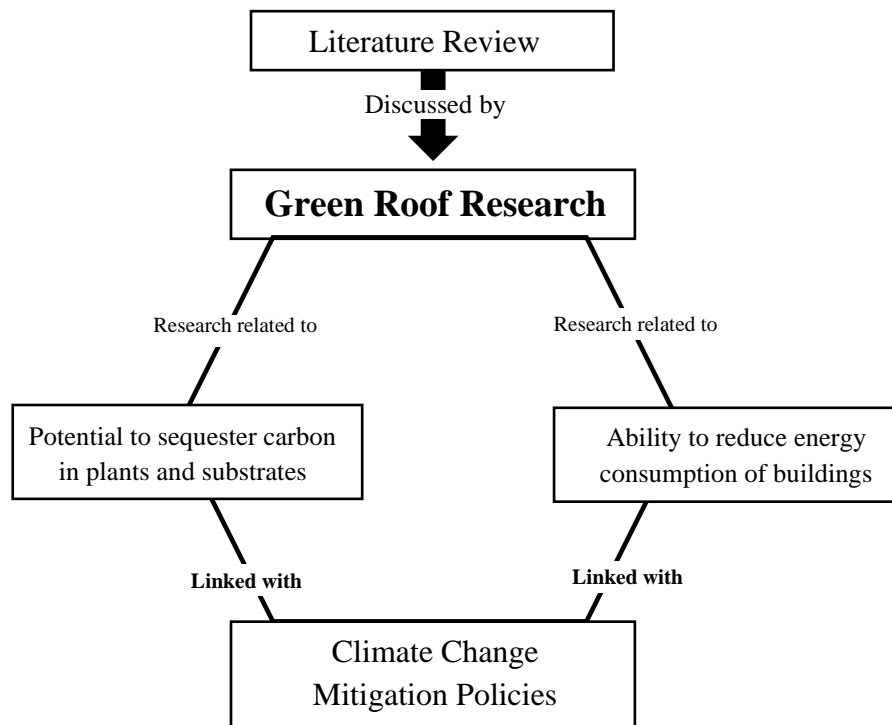


**Figure 2.2.** APD-EGR green roof literature review diagram.

### *Carbon sequestration by green roofs*

Green roofs are considered a practical means of reducing some types of pollution, reducing energy costs, retaining stormwater during rainfall events, and sequestering carbon in an age of climate change (Refahi and Talkhabi, 2015, Fioretti et al., 2010, Whittinghill et al., 2014). As with any forested or vegetation-covered area, a patch of green on top of a roof should theoretically reduce carbon dioxide levels in the air (Sohn, 2009). Plants breathe greenhouse gases as we breathe oxygen, storing carbon in their leaves and other tissues. However, until 2009, no one (according to one NBC news report) had measured how much carbon a green roof could sequester (Sohn, 2009). Significant research was conducted by Getter et al. in 2009b; they quantified the carbon sequestered in green roofs in Michigan and Maryland.

Although green roofs are often used for energy savings and heat island mitigation, rarely had this technology been promoted for its ability to mitigate climate change (Getter et al., 2009a). Getter and her colleagues cited research by Sailor (2008) regarding the ability of a green roof to reduce the energy consumption of a building by lowering the demand for heating and air conditioning, resulting in less carbon dioxide released from power plants, HVAC systems, and furnaces. In two years of extensive research, Getter et al. focused on establishing an argument regarding the carbon storage potential of extensive green roofs using two different methods.

Getter et al. reported that green roofs sequester carbon in plants and soils (Getter et al., 2009b). Photosynthesis removes carbon dioxide from the atmosphere and stores carbon in plant biomass, a process commonly referred to as terrestrial carbon sequestration (Getter et al., 2009b). Carbon is transferred to the substrate via plant litter and exudates. The length of time that carbon remains in the soil before decomposition has yet to be quantified for green roofs. Nonetheless, if net primary production exceeds decomposition, this manmade ecosystem will produce a net carbon sink, at least in the short term (Getter et al., 2009b).

To support these statements, Getter et al. conducted research using two different studies. The first study was performed on eight roofs in Michigan and four roofs in Maryland, ranging from one to six years in age. Twelve green roofs were composed primarily of the *Sedum* species, with substrate depths ranging from 2.5–12.7 cm. The aboveground plant material was harvested in the fall of 2006. The second study was conducted on a roof in East Lansing, Michigan (Getter et al., 2009b). Twenty plots were established on April 21, 2007, with a substrate depth of 6.0 cm.

In addition to a substrate-only control, the plots were sown with a single species of *Sedum* (*S. acre*, *S. album*, *S. kamtschaticum*, or *S. spurium*) (Getter et al., 2009b). These approaches to studying carbon sequestration for green roofs have been significant, guiding studies by other researchers.

In the first study, aboveground biomass was sampled in quadruplicate on eight extensive *Sedum*-based green roofs in Michigan and four green roofs in Maryland with a 13.0-cm ring during the fall of 2006, and dried in an oven at 70 °C for one week (Getter et al., 2009b). The samples were weighed, and ground using a Wiley mill to pass a 60-mesh stainless steel screen. To prevent moisture uptake, the samples were stored in glass vials in a desiccator prior to carbon analysis. Getter et al. used a Carlo Erba NA1500 Series 2 N/C/S analyzer (CE Instruments, Milan, Italy) to quantify total carbon concentration and accumulation by multiplying dry matter weight by total C concentration. They considered the location of each green roof (in either Maryland or Michigan) as a categorical independent variable, and substrate depth (cm) and age (in months) of the roof as independent variables in performing a regression analysis against grams of carbon per square meter of green roof as the dependent variable (using SAS version 9.1, PROC REG, NC, SAS Institute, Cary) (Getter et al., 2009b).

The second study was performed on the roof of the Plant and Soil Sciences Building on the campus of Michigan State University in East Lansing, Michigan. The study area was equipped with waterproofing systems and covered with a Xero Flor XF108 drainage layer (Xero Flor America LLC, Durham, NC) with a uniform depth of 6.0 cm. Each plot was covered with one of four species of *Sedum* typically used on U.S. green roofs: *Sedum acre* L. (biting stonecrop), *Sedum album* L. (white stonecrop), *Sedum kamtschaticum* var. *ellacombianum* Fisch. (stonecrop), and *Sedum spurium* Bieb. (Getter et al., 2009b). The plots were sown with 0.65 g of seeds of the treatment species from Germany resulting in a randomized complete block design with four replicates and five treatments. Getter and her colleagues shaded the entire study area and watered and weeded the roof to improve seed germination. Carbon analysis was performed after sampling aboveground biomass, belowground biomass (roots), and substrate carbon content over two growing seasons. They sampled every other month (June 30, 2007, August 23, 2007, October 17, 2007, April 15, 2008, June 12, 2008, August 15, 2008, October 13, 2008) to capture the full unpredictability of the green roof ecosystem, especially as different species exhibit different growth rates and peak biomass timing (Getter et al., 2009b).

Aboveground biomass was sampled and analyzed as in the previous study. Belowground samples were analyzed in two ways. Roots were removed from the retained sieved matter with forceps. The biomass was cleaned and dried for 2 d at 65 °C, ground, and analyzed for carbon (Getter et al., 2009b). The remaining sieved substrate (25 g) was oven-dried at 105 °C to remove moisture, ground with a roller mill, and analyzed for carbon (Getter et al., 2009b).

These methodologies are significant in terms of green roof carbon quantification as they were possibly the first to attempt this type of assessment (Sohn, 2009). They established that the studied green roofs sequester carbon from the atmosphere as follows: 375 g C·m<sup>-2</sup> in above- and below-ground biomass and substrate organic matter (Getter et al., 2009b).

Five years later, (Whittinghill et al., 2014) published research following the methods used by (Getter et al., 2009b). Whittinghill and her colleagues compared the carbon content of nine in-ground landscape systems and three green roof systems of varying complexities to determine their carbon sequestration potential. Soil and substrate samples were analyzed prior to planting in 2009; soil/substrate and aboveground and belowground biomass were analyzed at the end of the 2010 and 2011 growing seasons (Whittinghill et al., 2014). The study provided clear directions to measure aboveground biomass as a function of the crown volume index (CVI). Crown volume measures the mass of branches or foliage but does not include density measurements (Blozan, 2006). In the study, Whittinghill et al. estimated above-ground biomass for herbaceous perennials and grasses, deciduous, broadleaf evergreen, and narrow-leaf evergreen shrubs, and ornamental green roofs using plant dimensions based on allometric equations developed from destructive sub-sampling in a companion study (Whittinghill et al., 2014). They modeled allometric equations for shoot and foliar biomass as a function of crown volume index (CVI), calculated as:

$$\mathbf{CVI} = \mathbf{W1} \times \mathbf{W2} \times \mathbf{H} \text{ (Whittinghill et al., 2014)}$$

where CVI = crown volume index; W1 = crown width at widest point; W2 = crown width perpendicular to W1; H = plant height

Whittinghill et al. (2014) researched different landscape systems (including green roofs) and concluded that areas containing woody plants and shrubs (65.67 kg m<sup>-2</sup>, 78.75 kg m<sup>-2</sup>, and

62.91 kg m<sup>-2</sup>), and herbaceous perennials and grasses (68.75 kg m<sup>-2</sup> and 67.70 kg m<sup>-2</sup> for in-ground and green roofs, respectively) exhibited higher carbon content than other landscape systems. The native prairie mix (28.57 kg C m<sup>-2</sup>) had high carbon content due to the high volume of plant biomass. The vegetable and herb garden and vegetated green roof contained a moderate amount of carbon (54.18 kg C m<sup>-2</sup> and 11.03 kg C m<sup>-2</sup>, respectively). They reported that the three shrub landscape systems and herbaceous perennials and grasses were mulched, which may have contributed to soil carbon content over time (Whittinghill et al., 2014). More than 90% of the research methods were adapted from (Getter et al., 2009b). Mean percent carbon and grams of carbon per square meter were analyzed using an ANOVA model with the species as a fixed effect (Getter et al., 2009b, Whittinghill et al., 2014). Significant differences between treatments were determined (estimated) using multiple comparisons by LSD (least significant difference) (PROC MIXED, SAS version 9.1, SAS Institute, Cary, NC) (Whittinghill et al., 2014).

Li et al. (2010) attempted to determine the effect of a green roof on ambient CO<sub>2</sub> concentrations in Hong Kong. They quantitatively evaluated the impact of plants on CO<sub>2</sub> as an environmental pollutant. Their study had three parts: “(1) Field measurement of the difference in CO<sub>2</sub> concentrations in the middle of a small green roof and above pavers nearby; (2) Experiments to measure selected plant (vegetation) CO<sub>2</sub> absorption velocities and emission rates using a sealed glass chamber; (3) Computer simulation of CO<sub>2</sub> concentration distribution around a green roof using the measured CO<sub>2</sub> absorption velocity and emission rate to quantify the effects of the green roof on the ambient CO<sub>2</sub> concentration” (Li et al., 2010, p. 2644). Their methods and research location were significantly different from those in previous research (Getter et al., 2009a, Getter et al., 2009b).

Measurements were conducted on the rooftop of a six-story building in Hong Kong, which is a subtropical monsoon climate with a mean air temperature of 27.5 °C in summer. The roof area was 4 m x 4 m for growing selected vegetation. Li et al. ensured that other than the plants, there were no sinks or sources of CO<sub>2</sub> on or around the roof (Li et al., 2010). The CO<sub>2</sub> concentrations at locations P1 and P2 indicated in Fig. 2.3 were measured by an LI-7500 CO<sub>2</sub>/H<sub>2</sub>O analyzer in July and August 2009 (Yang et al., 2008, Li et al., 2010). Researchers used the LI-7500 to measure the concentration of vapor and CO<sub>2</sub>; a control box was connected to a computer for real-time measurement. P1 was located in the middle of plants in one of the green

roof plots; P2 was two meters from the plot (Li et al., 2010). The CO<sub>2</sub> concentration at P1 was measured for approximately 5 to 10 minutes, followed immediately by a measurement at P2. This measurement sequence was repeated throughout the day (Li et al., 2010).



**Figure 2.3.** Field measurement setup of Li et al. (2010).

Li and colleagues indicated that a green roof can function as a CO<sub>2</sub> sink, reducing the CO<sub>2</sub> concentration in the adjacent region. Sunshine irradiated directly on the green roof was simulated since plants take in CO<sub>2</sub> during daylight hours and to a higher degree in sunny conditions (Li et al., 2010). The research concluded that the effectiveness of a green roof is related to the condition of the vegetation, the position (relative to full sunshine) of the green roof, and the ambient airflow conditions at the sensor locations (Li et al., 2010). Li et al. discovered that the effect of a green roof on the ambient CO<sub>2</sub> concentration becomes more evident if the wind is light (speed of 0.5 m/s). They hope that other researchers will use their methods to investigate the effect of different plants (such as trees and shrubs) and their effect on pollutant concentrations (especially CO<sub>2</sub>) in urban areas. On a sunny day, a green roof may lower the CO<sub>2</sub> level nearby by as much as 2% (Li et al., 2010).

Another significant study was conducted by Yang et al. in Chicago, where it was concluded that the pollutants removed would increase to approximately 2047 metric tons if all rooftops in Chicago were covered with intensive green roofs (Yang et al., 2008). They argue that

the cost of installing green roofs is justified given the environmental benefits of having living vegetation on rooftops over the long run, and proposed green roofs to supplement the use of urban trees in air pollution control (Yang et al., 2008). Of course, green roof plants must be kept healthy to provide these benefits and little to no CO<sub>2</sub> will be taken in by plants during very cold winter months (when vegetation is dormant).

Klein et al. (2017) reported that during the dry season, common *Sedum* green roofs located in semi-arid regions emit a substantial amount of CO<sub>2</sub> during the day, increasing the high CO<sub>2</sub> concentration in the city (Klein et al., 2017). They discussed the limitations of green roofs and reported that nighttime CO<sub>2</sub> uptake by *Sedum* species does not fully compensate for the high daytime emissions. Both plot- and leaf-scale measurements indicated that CO<sub>2</sub> emissions were not fully compensated by nighttime uptake (Klein et al., 2017).

It is suggested that although carbon sequestration may only be a secondary benefit of green roofs, to improve the ecosystem, plant species other than *Sedum* species should be considered for use in green roofs, especially in the Mediterranean and other semi-arid climates (Klein et al., 2017). According to Getter et al., the carbon sequestered by growing biomass (375 g C·m<sup>-2</sup>) shortens the carbon payback period by two years, which may hamper the ability of a green roof to sequester carbon. The amount of carbon emitted by the decay of soil and plant material balances the carbon used in photosynthesis (Getter et al., 2009b). Nonetheless, the potential for offsetting the carbon debt of green roof materials is significant (Sailor, 2009, December 23) (Kuronuma et al., 2018, Getter et al., 2009a).

### ***Reduced energy consumption of buildings with green roofs:***

David Sailor is a leading researcher on the effects of green roofing, energy use in buildings, and the impact green infrastructure can have on cooling our cities (Sailor, 2009). He and his colleagues have developed tools to help quantify these impacts by integrating green roof energy balance into EnergyPlus, a building energy simulation model supported by the U.S. Department of Energy (Sailor, 2008, Getter et al., 2009b). Sailor's green roof model allows an energy modeler to explore green roof design options, including growing media thermal properties and depth and vegetation characteristics such as plant type, height, and leaf area index (Sailor, 2008). The model was tested in Chicago, Illinois, and Houston, Texas using observations

from a monitored green roof; a 2% reduction in electricity consumption and a 9 to 11% reduction in natural gas consumption were observed (Sailor, 2008, Getter et al., 2009a). Using a model of a generic building with a green roof area of 2000 m<sup>2</sup>, annual savings ranged from 27.2–30.7 GJ of electricity and 9.5–38.6 GJ of natural gas, depending on climate and green roof design (Getter et al., 2009b, Sailor, 2008). The green roof performance relies strongly on building location (climate), as Sailor has reported (2008).

Considering the national averages of CO<sub>2</sub> produced in generating electricity and burning natural gas (Hockstad and Hanel, 2018), these figures translate to 637–719 g C per m<sup>2</sup> of green roof for electricity and 65–266 g C per m<sup>2</sup> of green roof for natural gas each year (Getter et al., 2009b). An additional 25% reduction in electricity use may be possible due to indirect heat island reduction achieved from large-scale green roof use throughout an urban area (Akbari and Konopacki, 2005).

Sailor used an advanced building energy simulation platform (EnergyPlus) to implement the green roof model. EnergyPlus is a stand-alone building energy simulation model capable of modeling the hourly energy consumption of a building subject to user-specified construction, internal loads, schedules, and weather (Sailor, 2008). At its core, EnergyPlus relies on key elements of both the BLAST and DOE-2 programs (Sailor, 2008). The key features of EnergyPlus include “sub-hourly user-defined solution time steps, simultaneous solution of internal and external heat balance and loads, text-based weather-input files, advanced fenestration features (e.g., electrochromic glazings), transient heat conduction through building elements, daylighting controls, thermal comfort models, and atmospheric pollution calculations for on-site and remote energy conversion” (Sailor, 2008, p. 1468).

Sailor (2009) provided a green roof energy balance model for a traditional roof that was dominated by radiative forcing from the sun. Solar radiation is balanced by sensible (convection) and latent (evaporative) heat flux from soil and plant surfaces combined with the conduction of heat into the soil substrate and long-wave (thermal) radiation to and from the soil and leaf surfaces (Sailor, 2008). Ultimately, Sailor developed an important balance model for future reference, presented in Fig. 2.4.

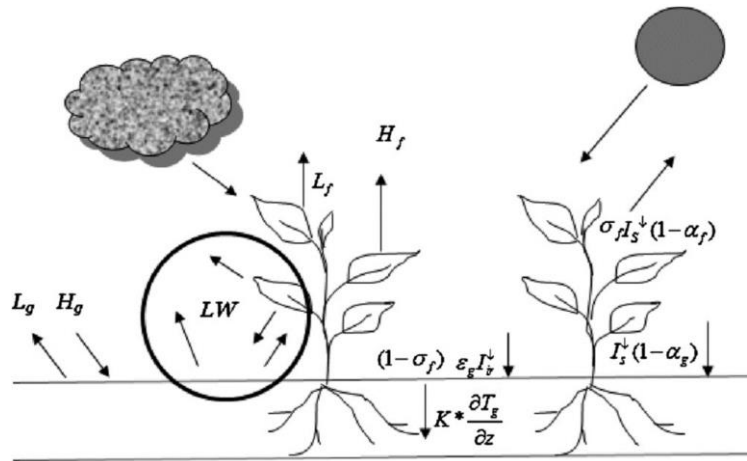


**Figure 2.4.** Energy balance for a green roof, including latent heat flux (L), sensible heat flux (H), shortwave radiation (Is), and incoming longwave radiation (Iir). Conduction into the soil and the complicated exchange of long-wave (LW) radiation within the canopy are also shown (Sailor, 2008). (diagram and text borrowed from Sailor)

The presented model divides the green roof heat balance into two parts: the balance at the foliage and at the soil surface (Jaffal et al., 2012). The heat balance equations are based on the models developed and validated by Sailor (2008) and Frankenstein and Koenig (2004). Sailor used many equations to generate the mathematical model (Jaffal et al., 2012) to determine the energy performance of buildings; the findings represent a significant advance in building design capabilities for the building energy modeling community (Sailor, 2008). Sailor indicated future research possibilities, including simulations, leading to quantitative estimates of potential energy savings with green roofs that can be integrated into life-cycle cost analyses (Sailor, 2008). He believes that exploring the building energy implications of green roof design options through computer simulation (EnergyPlus) can provide building designers with a method for evaluating their designs (Sailor, 2008).

Sailor et al. (2011) sought to integrate 2008 research findings and energy simulation programs in different locations. Their investigation included a total of eight buildings – new office and multi-family residential buildings in four cities representing diverse climatic conditions: Houston, Texas, New York City, Phoenix, Arizona, and Portland, Oregon (Sailor et al., 2011). Simulations were conducted for black and white membrane control roofs, with nine green roof variations, to analyze the effects of roof surface design on building energy consumption (Sailor et al., 2011).

This research (Sailor et al., 2011) provides fundamental knowledge regarding building energy performance with green roofs. They discovered that increases in soil depth and vegetative density improved building energy performance. Heating (natural gas) energy savings were greatest for residential buildings in colder climates (Sailor et al., 2011). Cooling energy (electricity) savings varied for different building types and cities (Sailor et al., 2011). They also analyzed the cost-effectiveness of different roof types (white, conventional black, and green roofs) and established several hypotheses. In all cases, a baseline green roof resulted in a heating energy cost savings compared to a conventional black membrane roof (Sailor et al., 2011). In six of the eight buildings, a white roof produced a lower annual energy cost than the baseline green roof (Sailor et al., 2011).

Further research was conducted at Lawrence Berkeley National Laboratory (also called the Berkeley Lab), strictly considering the economic costs and benefits of three roof types: black, white, and green (or vegetated). Berkeley Lab researchers found that white roofs were the most cost-effective over a 50-year time span (Chao, 2014). Although the high installation cost of green roofs sets them back in economic terms, their environmental and amenity benefits may at least partially mitigate their financial burden (Chao, 2014). According to Sailor et al., it mostly depends on the location (local climate) and building type (Sailor et al., 2011) and they researched these variables to justify their claims. Although the baseline green roof required more electricity consumption (cooling energy) and less gas consumption (heating energy) than the white roof, the net result was cost savings for the green roof over the white roof in New York and Portland residential buildings due to the colder climate (Sailor et al., 2011). Due to their different heating and cooling energy demands, the green roof performed better on residential buildings than on office buildings in Portland and New York (Sailor et al., 2011). Sailor and his colleagues also conducted research and concluded that a green roof with high vegetative cover outperformed a white roof in six of the eight buildings (Sailor et al., 2011).

Their research considers the relationship between two dependent variables (building energy performance depends on heating energy and cooling energy) and five main independent variables including soil depth, vegetative density, location (local climate), roof type (black, white, or green roof), and building type (office, residential, etc.).

A comprehensive study was performed by Jaffal et al. (2012); a schematic of the green roof model coupled with the building model is shown in Fig. 2.5 (Jaffal et al., 2012).

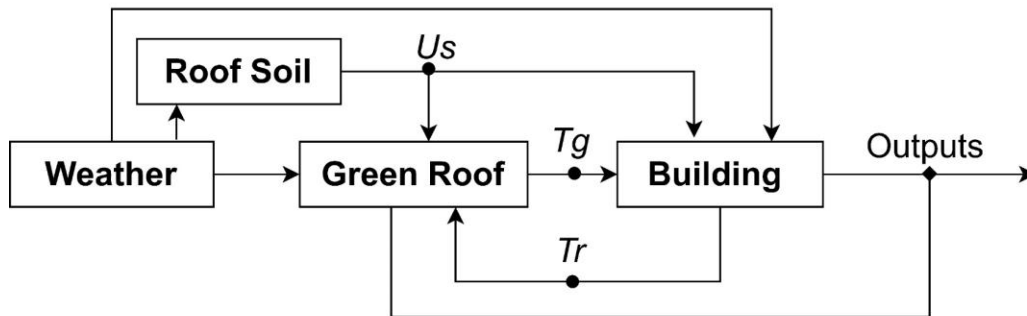


**Figure 2.5.** Coupling of green roof model with building thermal model (Jaffal et al., 2012) (diagram and text borrowed from Jaffal et al.).

This approach allows one to simplify the green roof system (substrate and canopy). A detailed calculation of the building thermal behavior is conducted in the building block (Fig. 2.5) using building simulation software such as TRNSYS or EnergyPlus. The detailed calculation includes the heat transfer through the roof slab  $U_s$  (considering its thermal mass), and the heat transfer between the inside surface of the roof  $T_g$  and the interior of the building  $T_r$ .

***Comprehensive approach reported by (Jaffal et al., 2012)***

Jaffal et al. (2012) discussed this approach by comparing the energy performances of a house with a conventional roof and an extensive irrigated green roof (Jaffal et al., 2012). They recommended a comprehensive approach for evaluating the impact of green roofs on building (single-family house) energy performance.

They suggested measuring the window-wall ratio and mean value of the internal heat gain. Researchers must consider the building location; thus, the local climate was evaluated to quantify building energy performance. Other independent variables in green roof research include plants, soil depth, and soil type (mixture) (Jaffal et al., 2012). After fixing all variables, dynamic simulations such as TRNSYS and EnergyPlus were performed for at least one year using the standard TM2 meteorological file for the specific location (Jaffal et al., 2012). They

recommended selecting set-point temperatures for winter and summer periods. For the summer period, there are two cases: cooling demand (for a set-point temperature) and indoor air temperature (free-floating, without cooling) (Jaffal et al., 2012).

For a green roof, the soil and foliage temperature values ( $T_g$  and  $T_f$ , respectively) should be assessed based on the soil and foliage heat balance model/methods of (Sailor, 2008), enabling comparison of the following parameters (Jaffal et al., 2012) for conventional and green roofs (Fig. 2.6).

- The temperature of the exterior surface of the roof slab ( $T_r$ )
- The heat flux through the roof to the inside of the building ( $q''_{ri}$ )
- The indoor air temperature ( $T_i$ )
- The heating and cooling demand ( $Q_h$  and  $Q_c$ , respectively)

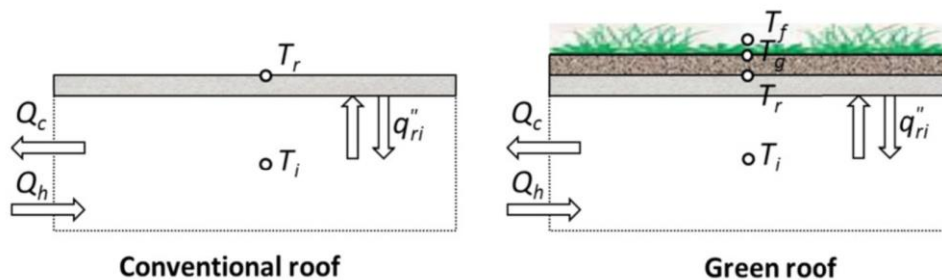


**Figure 2.6.** Studied parameters for conventional and green roofs (Jaffal et al., 2012).

According to Jaffal et al., the temperature evolution and the flux through the roof should be presented using climatic data for three typical days at the location. They suggested using the day with the minimum yearly temperature, the day with the maximum solar radiation for the winter season, and the day with the annual maximum temperature for the summer season as typical days for evolution. This approach could help provide a detailed parametric study of the effects of different green roof system configurations. The model quantifies the variation in the summer indoor air temperature and the cooling and heating demand, first as a function of two of the most influential parameters: the leaf area index (Del Barrio, 1998, Takakura et al., 2000, Kumar and Kaushik, 2005, Wong et al., 2003, Jaffal et al., 2012) and the level of roof insulation (Santamouris et al., 2007, Niachou et al., 2001, Castleton et al., 2010, Jaffal et al., 2012) and then for different climate zones.

Another study was conducted in a Mediterranean climate by (Moghbel and Erfanian Salim, 2017); their main objective was to evaluate the effect of green roofs on Tehran's microclimatic conditions and air quality parameters. They installed air temperature, relative humidity, and carbon dioxide concentration data loggers on two buildings with different roof covers (green and bitumen roofs). These two researchers used two HD37AB1347 measuring probes from Delta OHM Company (Italy) to measure CO<sub>2</sub> concentration, air temperature, and humidity in both positions over a 15-minute period. They used two Opus 10 temperature data loggers from Lufft Company (Germany), installed directly below the roof to assess the effect of roof materials on indoor thermal conditions and the heat exchange and energy consumption of each building (Moghbel and Erfanian Salim, 2017). A Flir Extech IRC30 thermal camera (USA) was positioned to capture thermographic images of the external roof surface temperature. Moghbel and Erfanian focused on studying the impact of green roofs on urban microclimate, especially in summer (Moghbel and Erfanian Salim, 2017). They used statistical analyses such as Kolmogorov–Smirnov and Shapiro-Wilk tests using SPSS to determine the normality of the collected data (Moghbel and Erfanian Salim, 2017).

Their results demonstrated that a green roof reduced CO<sub>2</sub> concentration (by 27.98 ppm and 20.71 ppm compared with the reference roof), and that interior spaces of buildings with a green roof exhibited a lower measured air temperature than buildings with a bitumen roof.

### ***The Importance of Green-Roof Substrates and Living Vegetation***

In combination, green-roof substrates and living vegetation have the potential to sequester C from the environment (Getter et al., 2009a, Whittinghill et al., 2014), thus helping reduce global warming impacts (Jaffal et al., 2012). The substrate's water-holding capability (Best et al., 2015), which helps support living vegetation, is dependent on the substrate type and depth. In combination with living vegetation (well-adapted to the regional climate and local microclimate), a green roof's substrate depth and composition can be designed to optimize potential benefits and reduce problems related to climate change (Ismail and Abdullah, 2016). In addition to the selection of substrates and plant species, the actual as-built conditions will also dramatically impact the survival and health of vegetation, although the effects of subsurface variability (especially where water pools above the filter fabric or within and beneath the

drainage layer) may not fully be seen until after irrigation is eliminated or is significantly reduced.

***Green roofs and climate change mitigation and adaptation programs, policies, and practices:***

The following tagline from the website Climate Action highlights the potential for green roofs to play an important role in climate change programs, policies, and practices: “Green roofs, a concept often associated with the fantasy hobbit land of the shires, have had a surge in popularity in recent years, being introduced to major cities to help reduce the impacts of climate change” (Knight, 2011).

Green roofs are a climate change mitigation strategy in two ways. They reduce CO<sub>2</sub> from the atmosphere (Getter et al., 2009b, Whittinghill et al., 2014) and reduce energy consumption (Sailor, 2008). Green roofs help maintain building temperature by regulating temperature variability, insulating from cold weather in the winter, and absorbing heat in summer (Sailor et al., 2011). Additionally, green roofs can free up funds for other initiatives by reducing central heating and air-conditioning costs (Sailor et al., 2011, Knight, 2011).

In this section, concepts related to climate change mitigation and adaptation programs, policies and practices, as well as a discussion of the importance of these actions, are introduced.

Adaptation to climate change requires an appraisal of future climate change scenarios and the development of mitigation and adaptation strategies to modify current practices to enable future human existence in changed environmental conditions (Cooper and Lemckert, 2012).

***Programs, Policies and Practices for Climate Change Adaptation and Mitigation***

Although many program and policy responses are developing at local and regional levels, Hamlin and Gurrán believe that only a few attempts have been made to develop strategies to adapt to the inevitable impacts of enhanced climate change. However, we should remember that ‘adaptation’ is a supporting feature of many ongoing programs and policies intended to mitigate local contributions to climate change, such as advocacy and efforts by planners to increase urban densities to reduce car dependency (Hamlin and Gurrán, 2009). In some cases, mitigation and adaptation are complementary; in other cases, these program or policy goals may conflict

(Hamin and Gurran, 2009; Laukkonen et al., 2009). However, it is argued that the ultimate goal of both is to minimize the undesirable consequences of climate change (Sharifi, 2020). To this end, mitigation mainly focuses on the long-run reduction of risks. At the same time, adaptation is aimed at reducing the current risks that exist due to historical emissions and/or because of failure to achieve mitigation targets (Sharifi, 2020).

The issue of adaptation alongside mitigation has emerged as one of the most pressing issues faced by nations and cities (Hamin and Gurran, 2009). It is not enough to concentrate on one or the other; a combination produces the most sustainable results. Sometimes adaptation and mitigation do not complement each other, which can be counterproductive (Laukkonen et al., 2009). Elisabeth M. Hamin and Nicole Gurran argue the following:

“While mitigation planning works to reduce current and future greenhouse gas emissions, including emissions that are generated through the built environment and transportation sectors, adaptation seeks to adjust the built and social environment to minimize the negative outcomes of now-unavoidable climate change. Thus, mitigation and adaptation must be treated as twin issues.” (Hamin and Gurran, 2009, p. 238)

The Intergovernmental Panel on Climate Change (IPCC) Third Assessment report provides the definition of “adaptation” (McCarthy et al., 2001); in their Fourth Assessment report (IPCC Climate, 2007), the IPCC argues that neither adaptation nor mitigation alone can prevent all climate change impacts. The panel states:

“Adaptation is necessary both in the short term and longer-term to address impacts resulting from the warming that would occur even for the lowest stabilization scenarios assessed. [However] unmitigated climate change would, in the long term, be likely to exceed the capacity of natural, managed, and human systems to adapt.” (Hamin and Gurran, 2009, p. 238; IPCC Climate, 2007)

Mitigation is widely discussed and successfully applied in different contexts at international, national, regional, local, and even individual levels. It includes technical and infrastructure investments, renewable energy implementation (to reduce climate change and improve energy security), and improving energy efficiency (Laukkonen et al., 2009). Mitigation and adaptation programs, policies, and practices are important at global and regional levels to address global warming and rising sea levels. (Laukkonen et al., 2009). Climate change is happening (with increasing temperatures, drought, and flooding), and there is a need to act now

(Laukkonen et al., 2009; UNDP, 2008). Strategies such as implementing green roofs are already being used worldwide to mitigate climate change (Knight, 2011). Future research questions include: How to adapt regional architecture/planning (including green roofs) to ensure future human survival with climate change? What techniques to improve the effectiveness of green roof systems are currently being used in various parts of the world to help mitigate climate change?

The effects of climate change have been well-documented by NASA, including some serious issues. According to (Potter and Cabbage, 2017) global average temperatures have increased steadily in the last 150 years; at the time, the year 2020 tied with 2016 for the hottest year since recordkeeping began in 1880 (Libonati et al., 2022). The average temperature was 0.99 °C above the mid-twentieth century mean (Potter and Cabbage, 2017). The world's nine warmest years since recording began have all occurred since 2005, with the five warmest occurring since 2010 (Potter and Cabbage, 2017). Since the beginning of the 21<sup>st</sup> Century, it has been acknowledged that observed and anticipated climate warming and associated future mean sea-level rise are likely to have far-reaching impacts on coastal zones (Nicholls and Cazenave, 2010a), and that delta regions are exposed to the most potent threat of mean sea-level rise (Vörösmarty et al., 2009).

Significant research studies have drawn our attention to some of the critical actions communities undertake to mitigate climate change. One is changing building codes to reflect the need for more natural cooling (using green roofs and other cool roof strategies) and thus lessen the contribution of buildings to the heat island effect (Hamin and Gurrán, 2009). (Hamin and Gurrán, 2009) Jaffal et al. (2012) reported that the impact of green roofs on the environmental performance of buildings and cities (water management, energy, acoustic, biodiversity, etc.) remains an intriguing subject for research. Evaluating and understanding the effect of green roofs on building energy performance (especially for specific regions, cities, and locations) requires further research in these areas (Jaffal et al., 2012). Because green roofs rely on living plants to take in CO<sub>2</sub> at different times of the day, it is important to understand and appropriately respond to the ecoregional and site-specific contexts (Dvorak & Skabelund, 2021) and to monitor inputs and outputs (Skabelund, et al., 2015). Addressing these needs, my research sought to evaluate the climate change potential of green roofs by quantifying their urban heat island indicators and capacity to sequester carbon.

## **Understanding Total Organic Carbon (TOC) and Total Nitrogen (TN) in Soil**

Soil and sediment organic carbon and soil organic nitrogen (SOC and SON) are mainly derived from the decomposition of plants and animals, or come from anthropogenic sources, such as chemical contaminants, fertilizers, and organic-rich waste (Avramidis et al., 2015). Globally, the amount of SOC is more than twice that in the atmosphere or in living vegetation (Rice et al., 2021). SOC is an extremely important soil-health indicator because it influences almost all soil biological, chemical, and physical properties and processes and is typically related to the amount of organic matter in a soil. Loss of SOC accelerates soil-health problems, such as soil erosion, and decreases soil aggregation (Rice et al., 2021).

The amount of organic matter (OM) and SOC in the soil is essentially regulated by net primary production, the distribution of photosynthates into roots and shoots, and the rate at which these various organic compounds decompose (Batjes, 1996). Plant residues (litter) that fall on the soil are gradually altered through physical fragmentation, faunal and microfloral interactions, mineralization, and humus formation (Batjes, 1996). Soils contain several important C pools and play an essential role in the global C cycle. Total soil C consists of organic C and inorganic C, with organic C being part of the SOM. The estimated amounts of organic C stored in world soils range from 1100 to 1600 Pg—more than twice that in living vegetation (560 Pg) or the atmosphere (750 Pg) (Rice et al., 2021).

### ***Origin and factors affecting SOC***

Plant residues are decomposed by soil microorganisms, with most of the plant C being released to the atmosphere as CO<sub>2</sub>. Approximately 10 to 20% of the C in plant residues becomes SOM, often referred to as “humus” (Rice et al., 2021). The theoretical potential for soil C storage is a function of climate and basic soil characteristics, while the amount of C residing in the soil is a function of plant and soil management (Rice et al., 2021). Tillage and organic residue input are two primary drivers influencing organic C levels in soils (Rice et al., 2021). Soil disturbance (i.e., tillage) disrupts soil aggregates and decreases physical protection by exposing C in soil aggregates to microbial decomposition, which results in a conversion of organic C to CO<sub>2</sub> (Rice et al., 2021). Likewise, the presence of plant/crop roots can release exudates into the soil, contributing to greater macroaggregate formation by increasing the microbial biomass and fungal

networks (Rice et al., 2021), which can potentially increase or sustain soil C. In grassland systems, perennial crops also tend to increase the SOC because there is no tillage (i.e., no disturbance), and organic C is added through root turnover (Rice et al., 2021).

### ***Biological effects***

The biological benefits of SOC primarily relate to nutrient cycling by soil microorganisms for C and energy (Rice et al., 2021). Soil microorganisms convert complex plant and animal materials into simpler compounds (Rice et al., 2021). The primary SOM decomposers (i.e., consumers) include bacteria, fungi, earthworms, insects, protozoa, insects, and nematodes (Rice et al., 2021).

### ***Physical effects***

The physical benefits of SOC relate to the formation and stabilization of soil aggregates. Several studies have reported a high correlation between soil aggregation and SOC (McVay et al., 2006; Wilson et al., 2009). The decomposition of protected SOC can become slow due to the clay barrier, thus promoting soil C sequestration. The soil health benefits of greater soil aggregation include reduced crusting, compaction, and bulk density (Diaz-Zorita and Grosso, 2000), enhanced soil structure (adding compost to a sandy or clay soil) for greater water infiltration and water holding capacity (Rice et al., 2021), and improved aeration for root growth and microbial activity. As tillage intensity increases, soil microbial activity increases right after the tillage, and microaggregates are dispersed, releasing SOM from protection (Puget et al., 2000).

### ***Functions of SOC***

Soil OM imparts many beneficial biological, chemical, and physical properties to the soil, specifically improving its structure (Dexter et al., 2008), supporting water infiltration and retention (Boyle et al., 1989), reducing erosion through increased infiltration, decreased runoff, and more large aggregates (King et al., 2019), and storing C for climate-change mitigation (Lal and Follett, 2009; Paustian et al., 2016, Rice et al., 2021).

## **SOM stores C for climate change mitigation**

Recent concerns about increasing atmospheric CO<sub>2</sub> levels and global warming have resulted in increased interest in the sequestration of plant C by SOM. Long-term crop rotations

and optimum N fertilizer practices can result in higher equilibrium SOM contents due to greater residue additions and/or lower decomposition (Sikora and Stott, 1997). Organic C makes up approximately 58% of SOM by weight. This constant allows for the determination of SOM by direct measurement of organic C (Sikora and Stott, 1997).

Although soils contribute a major share (37%, mainly as nitrous oxide [N<sub>2</sub>O] and methane [CH<sub>4</sub>]) to agricultural emissions (Tubiello et al., 2015), improved soil management (or new strategies, such as implementing green roofs) can substantially reduce these emissions and sequester some of the CO<sub>2</sub> removed from the atmosphere by plants as C in SOM (from this perspective, this discussion of soil C refers solely to organic C) (Paustian et al., 2016). So, we can decrease GHG emissions and sequester C through wise soil management practices in green roof systems that increases OM and tightens the soil N cycle (Paustian et al., 2016).

Interest in developing aggressive soil C sequestration strategies has been heightened by recent assessments, which project that substantial terrestrial C sinks will be needed to supplement large cuts in GHG emissions to achieve GHG stabilization levels of 450 ppm CO<sub>2</sub> equivalent or below, consistent with the goal of a mean global temperature increase of less than 2°C (Ciais et al., 2014). Soil C sequestration is one of only a few strategies that could be applied at large enough scales (Ciais et al., 2014) and potentially at low cost. For example, the French government has proposed (Paustian et al., 2016) increasing soil C concentrations in a large portion of agricultural soils across the globe by 0.4% per year, in conjunction with the Conference of the Parties to the UN Framework Convention on Climate Change (UNFCCC) negotiations held in December 2015 (Paustian et al., 2016). This would produce a C sink increase of 1.2 Pg C per year (Paustian et al., 2016).

So, it being understood that soil C sequestration could be a vital component in future climate-change mitigation, investigating green roof systems (substrate + plant mix type + depth) in the Flint Hills Ecoregion, that could sequester large amounts of C in the soil/substrate, makes sense. Soil C sequestration is related to climate, soil/substrate type and depth, and types and sizes of vegetation (Lal and Follett, 2009; Paustian et al., 2016; Rice et al., 2021). Over long periods of time, C storage in the soil varies, mainly as a result of climatic, geological, and soil-forming factors (Batjes, 1996), while over shorter periods of time, it is mainly vegetation disturbances or succession and changes in land-use patterns that affect storage (Batjes, 1996).

## **Relationship between Soil Heat Storage and Building Energy Performance**

To understand the relationship between the rate of change in soil heat storage (*Q-value*), and a green roof's role in improving a building's energy performance, the definitions of some thermal transport properties are required, such as thermal conductivity, thermal diffusivity, specific heat capacity, volumetric heat capacity, thermal energy storage, and thermal resistance. The thermal energy storage capacity of a substance improves the overall energy performance of a building within particular climates.

### ***Heat Transfer***

Heat is energy that transfers between two materials due to temperature differences. Heat flows from the object of higher temperature to the object of lower temperature until thermal equilibrium is achieved. Methods of heat transfer include thermal conduction, convection, and radiation (Towell, 2020).

Conduction is the transfer of energy from one molecule to another through direct contact. Convection is the transfer of thermal energy through the movement of a liquid or gas. Radiation is the transfer of heat through electromagnetic waves. (See Figure 2.7.)

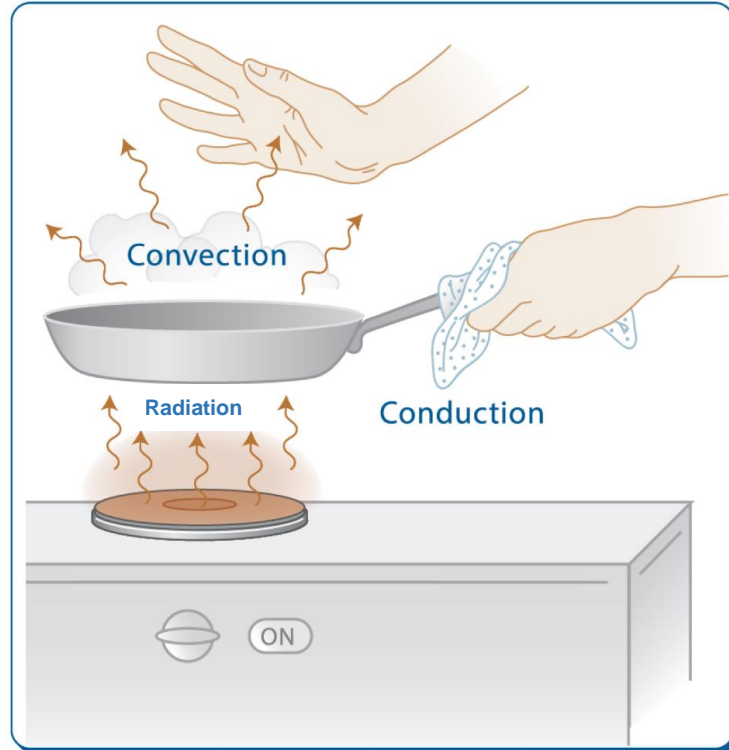


**Figure 2.7.** Cooking stove illustration demonstrating heat transfer through radiation, convection, and conduction (Selker and Or, 2021).

### ***Thermal Conductivity ( $\lambda$ )***

Thermal conductivity is a measure of how easily heat energy moves through a material or how well that material can transfer heat. How well heat conduction occurs depends on the thermal properties of the material (Towell, 2020). It is denoted in this study by the Greek letter  $\lambda$  (Lambda). The SI unit of conductivity is watts/meter  $\times$  Kelvin (W/mK).

Thermal conductivity is the rate of steady-state heat flow through a unit area of a homogeneous material induced by a unit temperature gradient in a direction perpendicular to that unit area.

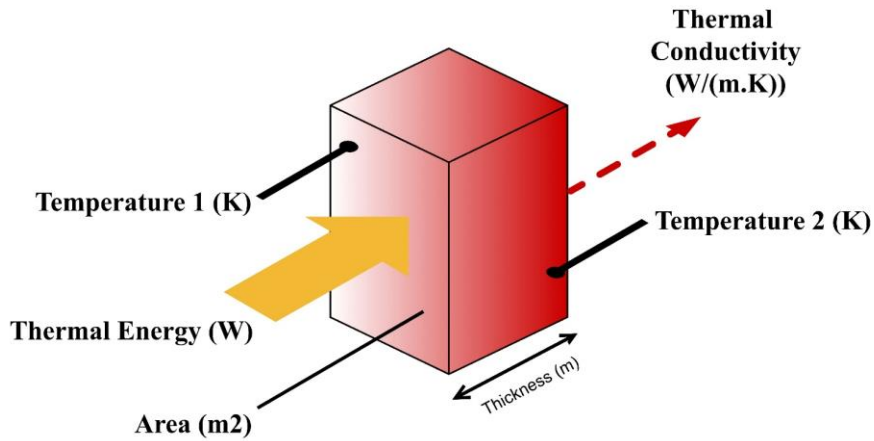


**Figure 2.8.** Thermal conductivity of a specimen.

Where  $L$  is the thickness of the specimen in meters (m);  $T$  is the temperature in Kelvin (K);  $q$  is the heat flow rate ( $W/m^2$ ), the thermal conductivity formula is:

$$\lambda = q \frac{L}{\Delta T} \dots\dots\dots (a)$$

***Thermal Resistance (R-Value)***

How well heat can move through an object depends not only on that object's conductivity, but on the size and shape of the object as well. Thermal resistance is the temperature difference, at a steady state, between two defined surfaces of a material that induces a unit heat flow rate through a unit area (measured in  $K \cdot m^2/W$ ). According to this definition, Figure 2.8, and Equation (a), Equation (b), therefore, can be used to determine the thermal resistance (*R-Value*).

$$R = \frac{\Delta T}{q} = \frac{L}{\lambda} \dots\dots\dots (b)$$

As indicated in Equation (b), the value of the thermal resistance can be determined by dividing the thickness of the specimen by its thermal conductivity.

### ***Specific Heat Capacity***

Heat capacity is the heat required to raise the temperature of a body by one degree. The specific heat capacity is defined as the quantity of heat (in joules ( $J$ )) absorbed per unit mass (kg) of the substance when its temperature increases by 1 K (or 1 °C). The formulas used to describe these relationships are  $J/(kg\ K)$  or  $J/(kg\ ^\circ C)$ .

### ***Volumetric Heat Capacity***

The volumetric heat capacity of a material is the heat capacity of a sample of the substance divided by the volume of the sample. It is the amount of energy that must be added, in the form of heat, to one unit of volume of the material in order to cause an increase of one unit in its temperature. The SI unit of volumetric heat capacity is joule per kelvin per cubic meter, ( $J \cdot K^{-1} \cdot m^{-3}$ ).

### ***Volumetric Water Content, $\theta_v$***

The volumetric water content is the ratio of the volume of water to the unit volume of soil. The volumetric soil water content ( $\theta_v$ ) is expressed in  $cm^3$  water per  $cm^3$  of soil. Volumetric water content is a numerical measure of soil moisture. It is simply the ratio of water volume to soil volume.

### ***U-value***

Thermal transmittance, also known as U-value, is a measure of the heat transmission through a building part (such as a wall or window) or a given thickness of a material (such as insulation) with lower numbers indicating better insulating properties.

### ***Thermal Energy Storage***

Thermal energy storage (TES) allows the storage of heat and cold to be used later. High-temperature thermal storage (HTTS) in soils is a promising energy-saving technology for space heating of buildings.

### ***Thermal Energy Storage and its Effect on Building Energy Performance***

Energy systems worldwide are experiencing a transformation spurred by the need to reduce carbon dioxide emissions to prevent climate change impacts (Mughees, 2022). Boosting the proportion of renewable energies that allow the power sector (which is responsible for two-thirds of global emissions) to decarbonize is critical to meeting international energy commitments (Mughees, 2022). In the United States, buildings account for 40% of total energy consumption. Of that, almost half is consumed in heating and cooling, which includes space heating and cooling as well as water heating and refrigeration. One-fifth of all energy produced goes towards thermal loads in buildings (BerkeleyLab, 2021).

On the road to low-carbon, environmentally friendly, and energy-efficient buildings, thermal energy storage provides a wide variety of options and advantages for lowering energy consumption and greenhouse gas emissions (Mughees, 2022). Thermal energy storage solutions might operate on principles of thermochemical, latent, or sensible energy storage and can be used in both active and passive applications in buildings (Mughees, 2022).

Active applications allow a reduction in peak load demand by virtue of the stream of stored energy and lowering the power requirements of cooling or heating equipment. It furthermore increases system efficiency by changing the operating range, to avoid partial load operations and reducing sporadic input through repeated starting and stopping (Mughees, 2022). Sensible heat storage is extensively used for building applications. In essence, it entails storing and releasing heat by raising or reducing the temperature of a large thermal capacity, storage medium. Most storage materials have a thermal energy storage capacity of around  $100 \text{ MJ/m}^3$ , of which water is the most feasible accessible medium. At a temperature gradient of  $60^\circ \text{ C}$ , water has a storage capacity of  $250 \text{ MJ/m}^3$  (Mughees, 2022).

## *Application of Thermal Energy Storage Solutions in APD-EGR Research Settings*

Quoted from the Lawrence Berkeley National Laboratory (Berkeley Lab):

**“Could a tank of ice or hot water be a battery?”** Yes! If a battery is a device for storing energy, then storing hot or cold water to power a building’s heating or air-conditioning system is a different type of energy storage” (BerkeleyLab, 2021).

To overcome some of the limitations of traditional water-based thermal energy storage, Berkeley Lab scientists are developing next-generation materials and systems to be used as heating or cooling mediums (BerkeleyLab, 2021).

Rooftop gardening has the potential to work as a water-based thermal energy storage medium, and it is exactly the case happening in the research setting at APD-EGR. The thermal energy storage of a green roof system is soil that can absorb heat throughout the day and prevent the interior of the building from heating up. As a result, green roof soil functions as an individual cooling system by lowering temperature spikes during the day. At night, a green roof can also work like a Trombe wall or thermal storage roof. After the direct and indirect solar gains are made during the day, the roof can radiate heat when the environmental temperature drops at night. As per the definition made by Berkeley Lab, a green roof substrate can potentially work like a battery since it has the potential to store thermal energy.

It may seem peculiar to consider soil (green roof substrate) as a thermal storage material for a building’s roof system, but when one factors in the moisture in the soil, the potential heat capacity of the soil increases. Soil thermal storage capacity is influenced by a wide range of soil characteristics, including (Ochsner, 2019):

- Air-filled porosity
- Water content
- Bulk density
- Texture
- Mineralogy
- Organic matter content
- Soil structure
- Soil temperature

Generally, since the thermal conductivity of air is so low, air-filled porosity exerts a dominant influence on soil thermal conductivity. The higher the air-filled porosity is, the lower the thermal conductivity is (Ochsner, 2019). Soil thermal conductivity increases as water content increases, but not in a purely linear fashion (Ochsner, 2019). For dry soil, relatively small increases in the water content can substantially increase thermal contact between mineral particles because the water adheres to the particles, resulting in a relatively large increase in the thermal conductivity (Ochsner, 2019).

An increase in thermal conductivity means a decrease in thermal resistance. The thermal resistance of a material is the inverse of thermal conductivity. i.e., thermal conductivity has units of  $W\ m^{-1}\ K^{-1}$ , and thermal resistivity has units of  $K\ m\ W^{-1}$ . Thermal conductivity is the ability of a material to conduct heat, so thermal resistance is how much a material resists heat flow. All these factors (like the porosity of the soil, thermal conductivity, and thermal resistance) regulate soil thermal storage capacity in a green roof system.

One can appreciate that fluctuating moisture content of soil will impact soil thermal storage. Phase-change materials have a number of potential applications, including thermal management of batteries (to prevent them from getting too hot or too cold), thus achieving thermal comfort while reducing building energy consumption (BerkeleyLab, 2021). In buildings, phase-change materials could be added to walls, acting like a thermal battery for the building. When the ambient temperature rises above the material's melting point, the material changes phase and absorbs heat, thus cooling the building (BerkeleyLab, 2021).

Conversely, when the temperature drops below the melting point, the material changes phase and releases heat (BerkeleyLab, 2021). The most common example of a phase change material is water; and thus, green roof substrates can also work as thermal mass for buildings, particularly in the context of the Flint Hills Ecoregion at Manhattan, Kansas. This study explored the potential of green roof substrate as a thermal battery from in-situ measurement.

Soil moisture dynamics and their influence on the rate of change in soil heat storage was analyzed using data collected in the summertime and wintertime in Manhattan, Kansas. Since the substrate properties of Kansas BuildEx® (K) and rooflite® (R) are different (see Table 3.4) and the substrate depths are different (4-inch vs. 8-inch), it was hypothesized that their interaction

would be significantly different. After data and graphical analyses, the research explains which soil scenarios (depth + substrate) at APD-EGR are better for the energy performance of a building.

Typically soil heat research will find multiple factors responsible for the thermal outcomes. In the building (at APD-EGR), there are two boundaries: (Figure 2.9 (b)) soil surface and the building interior (Figure 2.9 (c)). It is easy to misunderstand the building's interior boundary as passive; however, the HVAC systems of Seaton-Regnier buildings maintain a steady interior temperature. Thus, there is always heat flowing to or from the building interior, and this flow of heat also changes with exterior conditions. All the test locations at APD-EGR (Figure 2.9 (b)) have similar assemblies and interior conditions underneath the green roofs. Therefore, the experiment controlled this variability and assumed the change in heat in the engineered soil was due to the APD-EGR substrate properties and the interaction of each substrate type with the environment (including vegetation, weather conditions, shading, precipitation, irrigation, etc.).

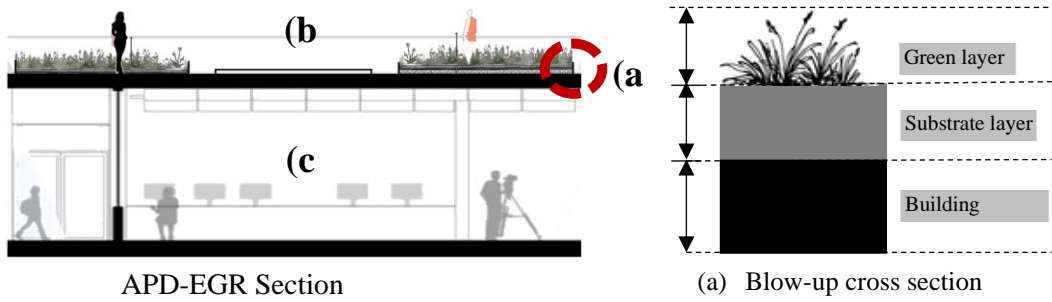


**Figure 2.9.** Thermal test sites assemblies (simplified) at APD-EGR.  
(Photographs by M. M. Lekhon Alam taken in 2021, at the APD-EGR)

## Chapter 3 - Research Context and Methods

### Research Setting

Between July 2017 and June 2018, KSU's APD-EGR was constructed above the Seaton–Regnier Hall studios in the Flint Hills Ecoregion in Manhattan, Kansas (39.1897°N, 96.5831°W). The depths of the beds in the construction were approximately 4 in/10 cm, 6 in/15 cm, and 8 in/20 cm (Figure 3.1). This study focused on only the 48 shallowest and deepest plots. Actual depths following implementation within each of the three beds (depths) ranged from 2.4–5.2 inches (6.1–13.2 cm) for the 4-inch bed, 4.5–7.5 inches (11.4–19.1 cm) for the 6-inch bed, and 6.5–10.1 inches (16.5–25.7 cm) for the 8-inch bed (per eight measurements in each plot taken June 22, 2018, by Lee Skabelund and averaged for each of the 72 plots by Priyasha Shrestha).

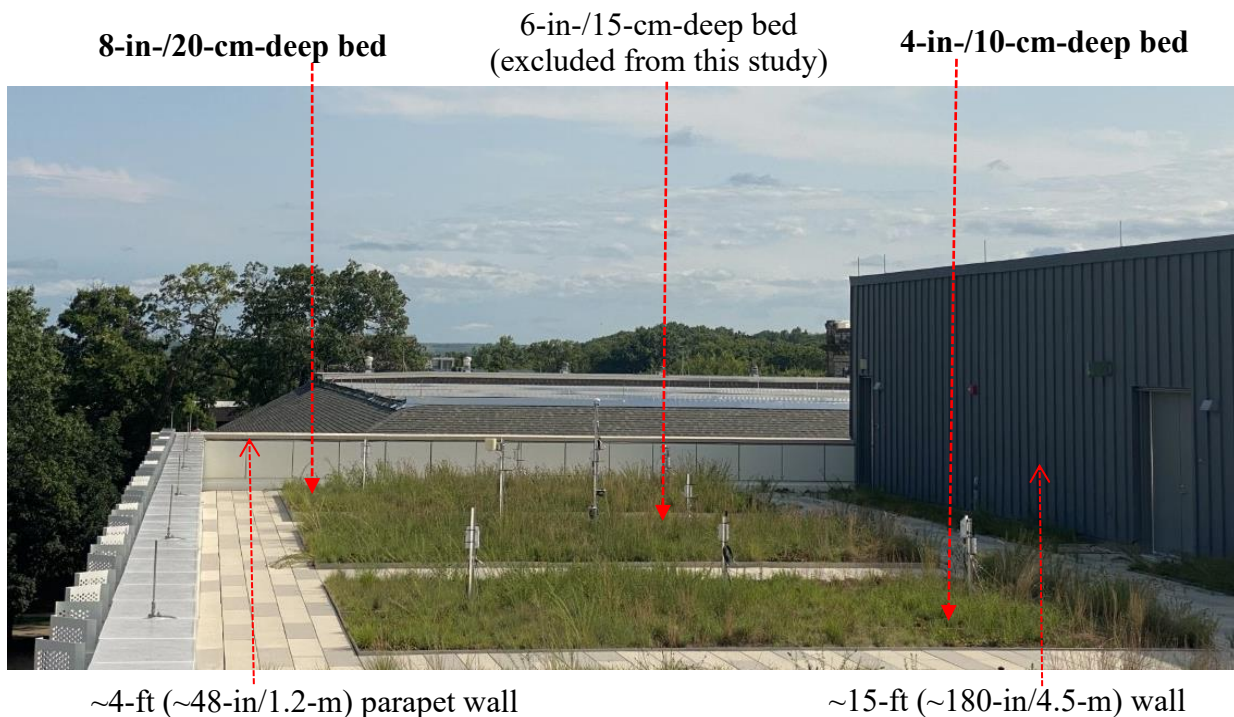


**Figure 3.1.** Illustration of the APD-EGR site at KSU showing the positions of the three beds, with the 4-in bed situated closest to the camera (i.e., on the north side).

(Image taken by M. M. Lekhon Alam on July 15, 2021.)

The cross-section of the APD-EGR appearing in Figure 3.3 illustrates the components of the green roof system. A total of 48 roughly 4 x 4-ft (1.2 x 1.2-m) APD-EGR plots were

established for the two examined substrate depths (4 and 8 in/10 and 20 cm), with 24 plots in each bed (Figure 3.2).

Manhattan, Kansas has a continental climate, as per the Koppen–Geiger climate classification, with an average annual precipitation of 35.62 in (904.75 mm), based on 30-year averages (Knapp, 2017). Based on 20-year weather data from the National Oceanic and Atmospheric Administration (NOAA, 2000–2019), the highest monthly mean maximum temperature for 2000–2019 was 92.1°F or 33.4°C (in July), while the lowest monthly mean minimum temperature was 18.6°F or -7.5°C (in January) (NOAA, 2019; refer to Appendix A). Air, surface, and subsurface temperatures on the APD-EGR frequently exceed 90°F (32.2°C) from June to August.



**Figure 3.2.** A roughly 4 x 4-ft/1.2 x 1.2-m plot on the APD-EGR, with a surface temperature sensor cover visible. (Image taken by M. M. Lekhon Alam on July 10, 2020.)

Figure 3.3 shows a section of the APD-EGR and the components of the green roof system. Vegetation has been planted atop a substrate layer, supported by a filter fabric, a gravel leveling layer, a drainage panel, a root barrier, a water-proofing membrane, and insulation, all laid atop the roof structure.

Seventeen plant species (eight *Sedum*, seven graminoids, and two forbs) were planted as live plugs in the roof plots on the APD-EGR in October 2017. Due to less-than-ideal plant stock (especially the use of root-bound plant stock for many warm-season grass plugs) and poor overwintering performance, 116 plants in the 4-in bed (including 72 graminoids) had to be replanted in May and June of 2018 (Shrestha, 2019).

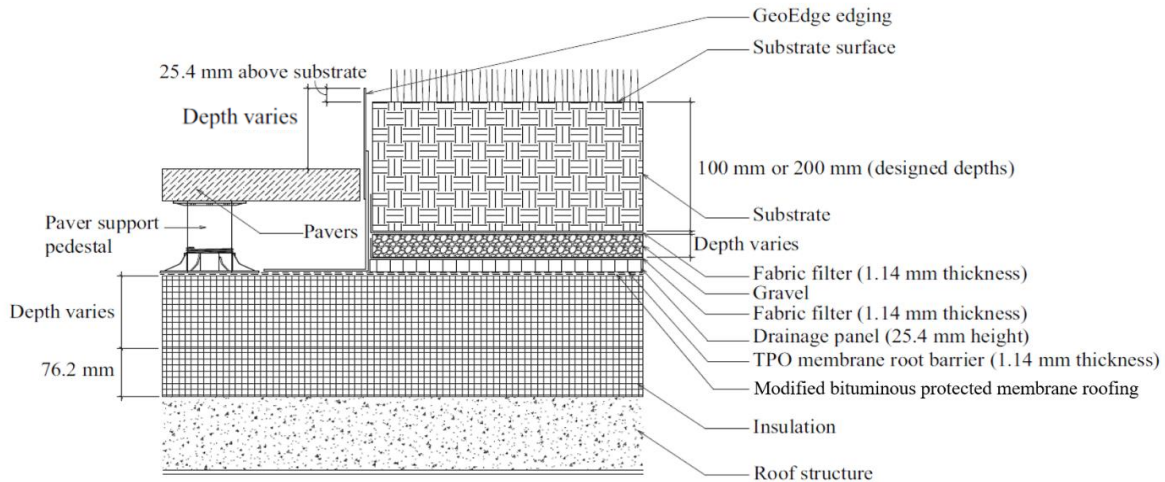


**Figure 3.3.** Section of the APD-EGR showing the green roof components.  
(Adapted by M. M. Lekhon Alam from the APD-EGR construction drawings.)

The plots had one of two types of substrates—the sandy, dense K type (Kansas BuildEx®) or a more-porous R type (rooflite® extensive mc). Vegetation was planted on the APD-EGR in three mixes of 18 plants (three plants of each species for each mix type) — six *Sedum* (type A), two *Sedum* + four native grasses (type B), and four native grass-like plants + two native forbs (type C). Each species was planted in repeat order (1–6) three times designated plots (see Table 3.1). The grasses and forbs are native to, or currently commonly found in, the Flint Hills Ecoregion. The species assigned to each mix are also reported in Table 3.1.

**Table 3.1.** Plant mixes planted on the ARD–EGR.

<b>All <i>Sedum</i> species (Mix type A)</b>	<b><i>Sedum</i> + grass species (Mix type B)</b>	<b>Native grasses + forbs (Mix type C)</b>
<i>Sedum album</i> f. <i>murale</i> (1)	<i>Bouteloua curtipendula</i> (1)	<i>Carex brevoir</i> (1)
<i>Sedum ellacombeanum</i> (2)	<i>Bouteloua dactyloides</i> (2)	<i>Dalea purpurea</i> (2)
<i>Sedum hybridum</i> ‘Immergrüchen’ (3)	<i>Bouteloua gracilis</i> (3)	<i>Koeleria pyrammidata</i> (3)
<i>Sedum kamschaticum</i> var. <i>floriformum</i> ‘Weihenstephaner Gold’ (4)	<i>Schizachyrium scoparium</i> (4)	<i>Packera obovata</i> (4)
<i>Sedum sexangulare</i> (5)	<i>Sedum reflexum</i> (5)	<i>Schizachyrium scoparium</i> (5)
<i>Sedum spurium</i> (6)	<i>Sedum rupestre</i> (6)	<i>Sporobolus heterolepis</i> (6)

This study focused on the 4-in-/10-cm- and 8-in-/20-cm-deep substrate plots (four plots for each unique substrate type and vegetative mix), considering: 1) the ease of making

comparisons between two distinct depths, one depth being the shallowest and the other the deepest of the three established APD-EGR beds or plot depths; and 2) the bulk heat flow through the roof, and the soil biological properties, total microbial biomass, and C-storage performance of the two substrate types were expected to show the most significant differences for the two substrate depths. The statistical comparison of datasets, evaluation of recorded evidence, and their explanations were expected to demonstrate how one condition (either the shallowest or deepest depth) performed better as a climate mitigation strategy than the other by considering the two substrate types and the documented climatic conditions influencing the APD-EGR.

**Table 3.2.** Research settings for the APD-EGR considering two substrate types, three vegetative plant mixes, two bed depths, and four plots sampled for each plot type (a combination of depth, substrate type, and plant mix)

<b>Initial APD-EGR carbon sequestration study in Manhattan, Kansas, USA</b>													
<b>Composites*</b>	<b>4-in-/10-cm-deep bed</b>						<b>8-in-/20-cm-deep bed</b>						<b>Total replicates</b>
	24 Plots												
	A		B		C		A		B		C		
	<i>Sedum</i> only		<i>Sedum</i> + native grass		native grasses + forbs		<i>Sedum</i> only		<i>Sedum</i> + native grass		native grasses + forbs		
<b>KA</b>	4						4					<b>8 KA</b>	
<b>KB</b>			4						4			<b>8 KB</b>	
<b>KC</b>					4						4	<b>8 KC</b>	
<b>RA</b>		4						4				<b>8 RA</b>	
<b>RB</b>				4						4		<b>8 RB</b>	
<b>RC</b>						4					4	<b>8 RC</b>	

\*The first letter represents the substrate type, the second letter the plant mix type.

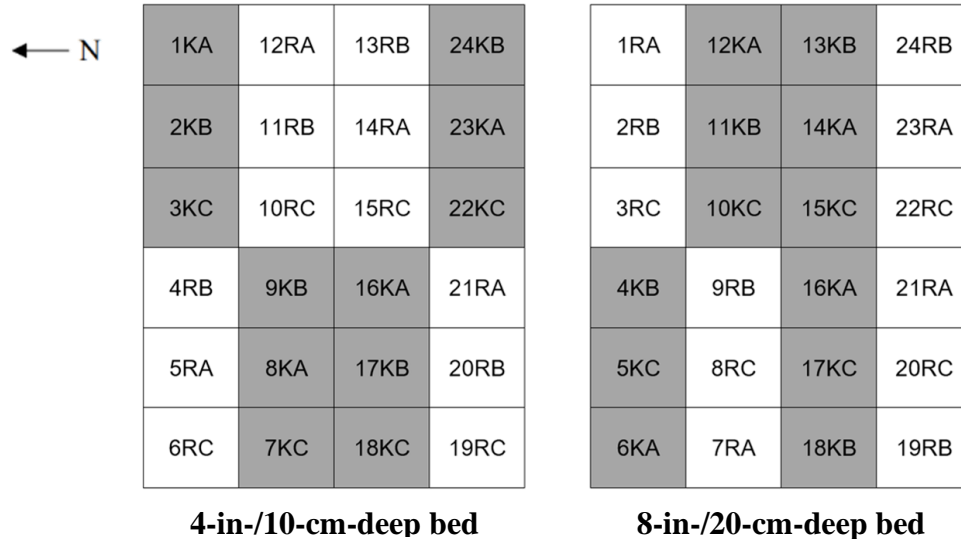


**Figure 3.4.** Layouts of the beds containing plant mix types A, B, and C in the K (gray boxes) and R substrates in the 4- and 8-in-deep beds, with the plots in each bed numbered from 1 to 24.

The two substrates (or grow media), K and R, had both previously been specified and used on other KSU green roofs (East Memorial Stadium for K and Regnier Hall for R), and both were deemed promising for growing *Sedum* and prairie plants on campus (Shrestha, 2019). Professor Skabelund of KSU selected the plant species in collaboration with Richard Sutton and Robert Grese, based on past precedents of plants that had done well on green roofs in Lincoln, Nebraska and Ann Arbor, Michigan (Shrestha, 2019). The grasses and forbs selected were native to, or found growing in, the Flint Hills Ecoregion. The designer adopted a systematic numbering system to lay out each plot plant species. Initially, randomizing the plant mixes was attempted. However, according to Skabelund (Shrestha, 2019), to avoid an undesired clustering of the same species in one location, the plants were numbered in increasing numeric order, as shown in Table 3.1 and Figure 3.5.



**Figure 3.5** Plant layouts for plant mix types A, B, and C (after Shrestha, 2019).

## Substrate constituents and characteristics

According to Tim Sharp from Blueville Nursery (JL, pers. comm. October 1, 2018), substrate K (called Kansas Build-Ex by the APD-EGR research team) is made with mason sand, fine-grade peat moss, and cattle-manure compost mixed in equal proportions with Buildex lightweight aggregate (expanded shale) (Shrestha, 2019). The type R substrate is a proprietary mix manufactured by Skyland LLC and is a blend of lightweight mineral aggregates and organic components, such as compost approved by USCC STA (rooflite® extensive 800 specifications). Figure 3.6 shows the ~8-inch plots with the two substrate types and mix type C plants.



**Figure 3.6.** Substrate types K (left) and R (right) planted with native grass + forbs (mix type C) on the APD-EGR. (Images taken by Allyssa Decker during the first growing season in 2018.)

## Substrate chemical characteristics

In March 2018, substrate samples were collected consistently from the centers of each of the green-roof plots. Samples from the same depth and substrate type were combined and sent to the KSU Soil Testing Laboratory (Manhattan, Kansas) for analysis (Shrestha, 2019). Testing was performed for nutrients, OM, electrical conductivity (EC), cation exchange capacity (CEC), pH, and percentage of sand, silt, and clay in both substrates. Table 3.3 shows the results of these soil analyses for the 4-in-deep bed. The N, phosphorus (P) and potassium (K) values were slightly higher for the K than the R substrate, but both were found to be alkaline, albeit with type R having a slightly higher pH value than type K. The protocols used by the KSU Soil Testing Laboratory for conducting the tests are reported in Appendix B.

**Table 3.3.** Soil test results for substrate types K and R from the 4-in-deep APD-EGR bed (the tests were conducted by the KSU Soil Testing Lab in April 2018).

<b>Chemical property</b>	<b>Substrate K</b>	<b>Substrate R</b>
Calcium (Ca) ppm	1257	1503
Copper (Cu) ppm	0.3	0.6
EC dS/m	0.7	0.85
Magnesium (Mg) ppm	117	110
Manganese (Mn) ppm	2.0	3.2
Sodium (Na) ppm	17.8	29.3
pH	7.9	8.4
Nitrate N (NO <sub>3</sub> -N) ppm	4.7	2.1
Potassium (K) ppm	116	89.7
Phosphorus (P)-M ppm	85.0	59.9
Zinc (Zn) ppm	1.2	3.1
Iron (Fe) ppm	15.8	19.2
CEC meq/100 g	7.63	8.79

***APD-EGR substrates, K and R, affect soil moisture***

The laboratory analyses reported and discussed by Decker (2021) established that, for two APD-EGR depths (4 and 8 inch), substrate type K held more water (by volume) in the substrate profile than type R. The physical properties per the 2018 laboratory analysis of the APD-EGR substrate samples for the two substrate types, K and R, are presented in Table 3.4.

**Table 3.4.** Type K and R substrate properties as tested at and reported by the Turf and Soil Diagnostics Laboratory in Linwood, Kansas in 2018.

<b>Property</b>	<b>Substrate K</b>	<b>Substrate R</b>
Clay (<0.002 mm)	2.9%	1.3%
Silt (0.002–0.063 mm)	4.5%	5.8%
Sand (0.063–2.0 mm)	67.6%	52.4%
Larger particles (>2 mm)	25%	40.5%
Dry bulk density (g/cm <sup>3</sup> )	1.47	0.98
Saturated density (g/cm <sup>3</sup> )	1.77	1.33
Maximum water retention	29.5	35.0
Total pore space (%)	42.5%	58.0%

One year later, K and R substrate samples were obtained from Blueville Nursery Inc. (Manhattan, Kansas) and sent again to the Turf and Soil Diagnostics Laboratory in March 2019. The test results for the physical characteristics of the two substrates are given in Table 3.5. Average water holding capacity or “roof capacity” (Decker, 2021) for K and R for two depths are provided in Table 3.5. (a).

**Table 3.5.** Green-roof porosity, pH, EC, and OM test results for substrate types K and R (substrate tests conducted by Turf and Soil Diagnostics in Linwood, Kansas in March 2019).

<b>Characteristic</b>	<b>Unit</b>	<b>Substrate K</b>	<b>Substrate R</b>
Initial sample wt.	kg	3.128	2.151
Sample volume	m <sup>3</sup>	0.0019	0.0020
Initial sample height	cm	10.4	10.8
Final sample height	cm	10.4	10.7
Sample wt. after draining	kg	3.3	2.6
Air-filled porosity	%	13	23
pH		7.0	7.6
OM	%	1.9	2.2

**Table 3.5(a).** Average water holding capacity for K and R for 4-inch and 8-inch beds (Decker, 2021).

<b>Depth</b>	<b>R</b>	<b>K</b>
<b>4-inch</b>	0.26%	0.41%
<b>8-inch</b>	0.21%	0.34%

The percentages are essentially the volume of water held in a substrate/soil profile after drainage ceases divided by total volume of the soil profile (Decker, 2021).

## The Flint Hills Ecoregion and Regional-Scale Green Roof Studies

Globally increasing vulnerabilities to natural and human-made disasters are a consequence of climate change (Laukkonen et al., 2009). According to the United Nations Development Program (United Nations Development, 2007), it is necessary to ensure future human well-being and perhaps survival by inventing and implementing place-appropriate mitigation and adaptation strategies worldwide and doing so in ways that align with regional architecture, planning/design, and development (Langemeyer, J., et al., 2020). It is argued that implementing green roofs in substantial numbers worldwide (Knight, 2011) can help reduce global-warming impacts at regional and global scales (Laukkonen et al., 2009).

The use of regionally adapted vegetation is critical. Akther et al. (2018) synthesized the effects of the influential factors statistically, including the design and hydrological variables on green-roof performance, exploring their impact in different climatic zones. These authors concluded that the performance of green roofs in different climatic zones is meaningfully different (Akther et al., 2018). Therefore, we need more ecoregion-focused green roof research.

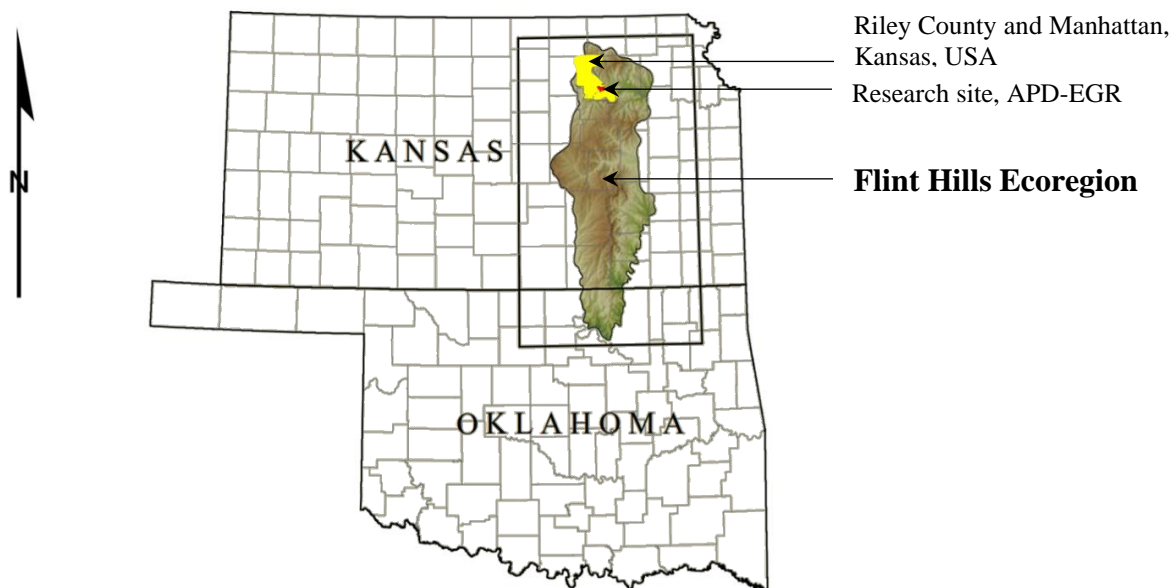


**Figure 3.7.** Flint Hills Ecoregion in Kansas.

(Adapted by M. M. Lekhon Alam from Chapman et al., 2001.)

The Flint Hills Ecoregion (Figure 3.7) is defined by gently sloping, prairie-dominated hills of limestone and shale (Anderson and Fly, 1955). Hot continental summer temperatures and cool winters (accentuated by cold Arctic blasts) are prevalent in this region. Tallgrass prairie is the dominant vegetation (Anderson and Fly, 1955). Soils along ridgelines are typically thin, and may be comparable to green-roof substrates, especially in terms of the harsh growing conditions they induce on vegetation.

The US Environmental Protection Agency has designated the Flint Hills as an ecoregion, distinct from other grasslands of the Great Plains (Chaplin et al., 2007). The research site in Manhattan, Kansas has a continental climate, characterized by warm, wet summers and dry, cold winters (KSU, 2012). The continental climate accounts for substantial daily and seasonal temperature fluctuations, with the ecoregion typically receiving 30–38 in (760–965 mm) of annual precipitation, most of it falling during the growing season, especially in April to September (Tollerud et al., 2018). Nevertheless, very dry periods can occur throughout the year, including during the growing season. The climate of this region is one of the most critical variables in this study.

Figure 3.8 shows the concept map for this study. Important notes about variables and temperature and soil moisture sensors are provided below the concept map.

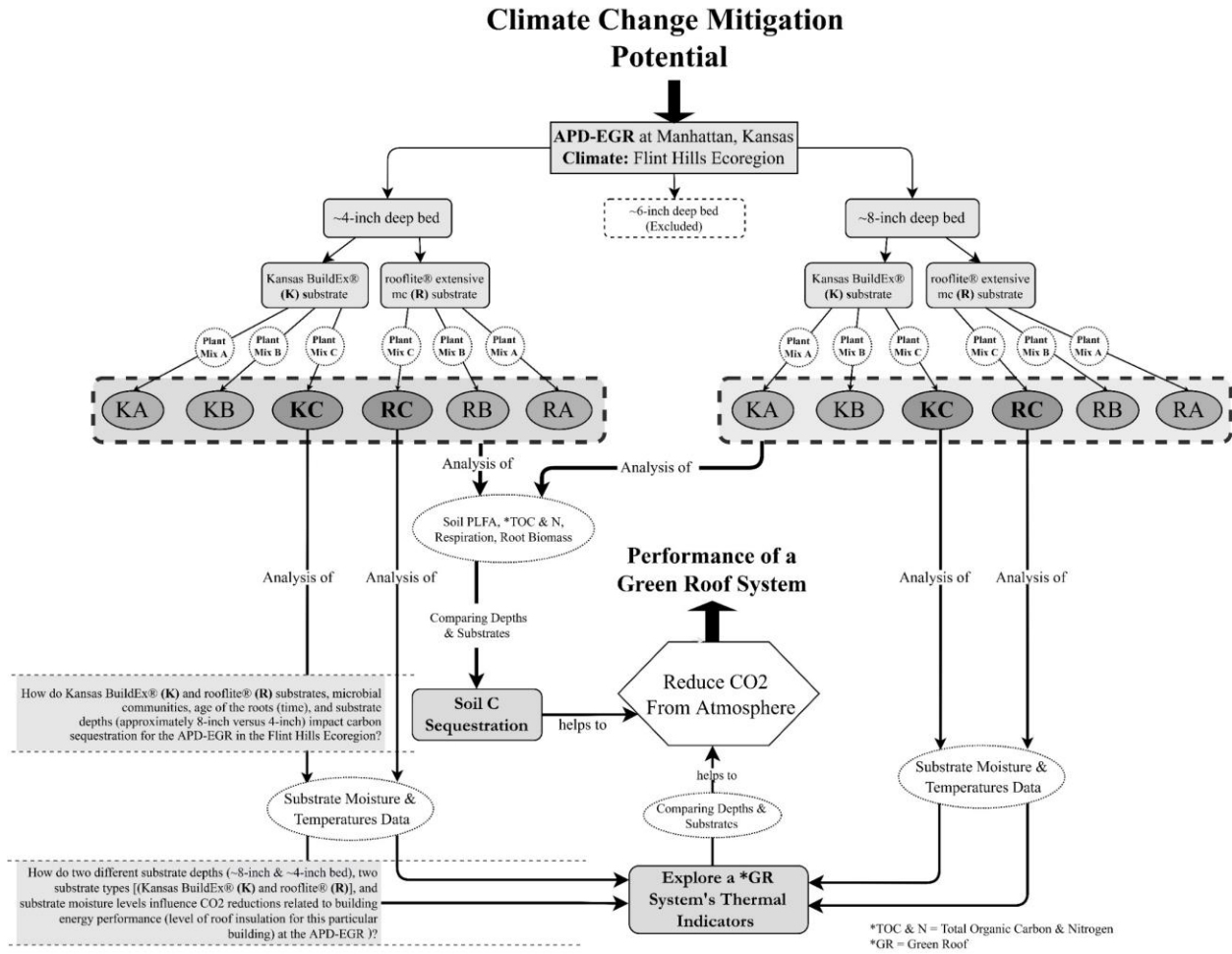


**Figure 3.8.** Concept map for the research project.  
(Diagram by author.)

- The two primary variables employed in this study were: 1) the two different substrates (K and R) with three different belowground biomass samples (KA, KB, KC and RA, RB, RC); and 2) the two bed depths, ~4 in/10 cm and ~8 in/20 cm.
- The aboveground biomass (different plant types) was excluded from the variables.
- All temperature and soil moisture sensors referenced were placed in plant mix type C by other APD-EGR researchers in mid-March 2018.

## **Research approach**

This study aimed to examine the impact of the selected APD-EGR beds and plots in terms of C sequestration and to evaluate the climate change mitigation potential of the APD-EGR for two different substrate depths and types of engineered growing media. The study was focused on the 4-inch (10.16 cm) and 8-inch (20.32 cm) substrate depths.

The necessity for the study was to provide evidence to understand the APD-EGR's contribution to C sequestration, focusing on the two substrates at two depths (shallowest and deepest). A quantitative approach was used to assess data collected, which is very common in scientific research in this type of life and physical science research.

### ***Variables related to the research hypotheses:***

Plant (vegetation) mix type, soil (substrate) type, substrate depth, and time (age of the green roof) were the independent variables used in this study. Conversely, the primary dependable variables were building energy performance (heating and cooling), environmental CO<sub>2</sub> sequestration, substrate/soil moisture, microbial biomass, root biomass, and so on.

### ***Hypotheses:***

- Green roofs remove CO<sub>2</sub> directly from the atmosphere to a greater degree when there is: 1) greater substrate depth (as in the 8-inch APD-EGR bed); 2) a substrate with a relatively high water-holding capacity (as should be the case for substrate type K, given that this substrate was less porous); 3) a greater abundance of soil (substrate) microbes; and 4) a higher content of OM and more root biomass (which should change with the age of the green roof, but which may be higher at the outset for substrate type R, given its physical, material composition).
- As an intervention with significant climate change mitigation potential for the Flint Hills Ecoregion, improved building energy performance can help remove CO<sub>2</sub> from the environment more effectively with a greater soil depth and moisture content, and higher R-values.

Multiple null hypotheses were generated from these hypotheses, and a crucial step in null hypothesis testing was to find the likelihood of the sample result if the null hypothesis was correct. This probability is called the *p*-value (Leavy, 2017). Statistical equations, procedures, and rules were followed in this study to find the *p*-value and support or reject any null hypothesis.

## **Methodology and methods**

For this study, a combined quantitative and observational research methodology was employed. The classic form of data collection in naturalistic or field research is observation of research variables in the context of a natural scene or system (Hoepfl, 1997). Observational data are used for the purpose of description—of settings, activities, and the meanings of what is observed from the perspective of the researchers (Hoepfl, 1997). Here, the independent variables were established at the outset by varying the green-roof substrate types, depths, and vegetative mixes in order to observe the effects on different dependent variables.

- 1) Researchers observed changes on the two green roof beds and collected data from the plots, which were later quantitatively and qualitatively analyzed following experimental methods.
- 2) Like experimental methods, dependent variables are measured by the researcher (Thomas et al., 2015).
- 3) A quantitative observation is an objective method of data analysis that measures research variables using numerical and statistical parameters (Thomas et al., 2015). The study did not use a perfect formal experimental method for this research. It was observational research with systematic data collection and analysis.

This quantitative observation is also directed to standardized observation because it measures research variables using definite parameters as discussed in further detail below (Hoepfl, 1997). Therefore, the different methods and research settings needed to be fixed to allow an exploration of building energy performance and soil C sequestration in the APD-EGR.

## a) Methods For Estimating Soil C Sequestration

In this study, the soil (substrate) C sequestration potential of the APD-EGR was estimated by measuring the microbial biomass (PLFA analysis), TOC and N, biological activity and decomposition (soil respiration), and root biomass of the two different substrates (K and R) from two growing seasons (2019 for PLFA, TOC, and N, and 2020 for root biomass, PLFA, soil respiration, TOC, and N) in order to compare these variables across two depths (approximately 4 inches and approximately 8 inches) for 24 green-roof plots at each depth.

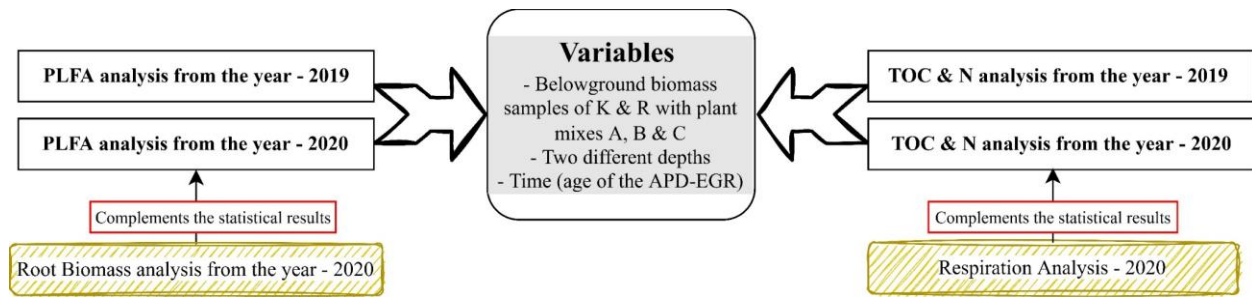


**Figure 3.9.** Research design for estimating soil C sequestration.

The PLFA, root biomass, and soil respiration analyses (indoor portion) of the two substrate types and substrate depths were conducted in the KSU Department of Agronomy Soil Microbial Agroecology Laboratory (SMAL). The procedures adopted for the PLFA laboratory analyses are documented in Appendix C, the TOC, and N procedures in Appendix D, and the soil respiration procedures in Appendix E.

Additionally, root biomass analyses were performed for the volume of the core in order to complement the PLFA analyses, thereby helping the research team to understand better the C dynamics in the two substrate types and depths. These observational approaches and studies were undertaken to gather further data related to C sequestration on the APD-EGR. It is important to note that the aboveground plant biomass was collected at the end of each growing season in 2018, 2019, and 2020, but these data were not required for this study because the aboveground biomass was excluded from the research variables.



**Figure 3.10.** Collecting soil samples for the soil PLFA, TOC and N analyses from the APD-EGR in 2019.  
(Image taken by Allyssa Decker on October 3, 2019.)

- In the second growing season, 48 substrate samples were collected from the 4-inch-deep and 8-inch-deep beds of the APD-EGR to use in the PLFA, TOC, and N analyses. The samples were collected on October 3, 2019 (7:30–11:30 am) and stored in a refrigerator until they were analyzed.
- In the third growing season, 48 samples were collected from the 4-inch and 8-inch beds of the APD-EGR for PLFA, TOC, and N analysis on July 30, 2020 (7:15–11:30 am). More samples from the same 48 plots were collected for soil respiration analysis on August 6, 2020, and root biomass analysis at the end of the third growing season, on November 6, 2020 (8:30 am–2:30 pm). The samples were stored in a refrigerator until they were analyzed.

### **PLFA analysis**

The study of PLFA (Phospholipid fatty acid) was focused on estimating the microbial biomass, with the understanding that microbes are an early indicator of changes in total soil SOC. In 2019 and 2020, PLFA analyses were conducted to determine the microbial biomass and the proportions of microbial communities, including the arbuscular mycorrhizal fungi (AMF),

gram-positive bacteria, gram-negative bacteria, actinomycetes, and saprophytic fungi as dependent variables (Quideau et al., 2016). Time (age of the APD-EGR), soil (substrate) type, plant (vegetation) mix type, and substrate depth were the independent variables in these experiments. The total lipids were extracted from freeze-dried soil using a modification of the Bligh and Dyer lipid-extraction method (Bligh and Dyer, 1959; White and Rice, 2009). Substrate sampling protocols and the laboratory procedures used to conduct the PLFA analyses at the SMAL are described in more detail below.

The PLFA analysis involved two primary protocols: 1) an outdoor portion, involving protocols for collecting soil samples from the APD-EGR; and 2) an indoor portion, involving protocols for analyzing soil samples in the laboratory. The protocol is described in Appendix C.

### **Soil sampling protocols (outdoor portion)**

The protocols for collecting soil samples from the APD-EGR are given below.

#### ***Soil sampling protocols for PLFA analysis (Protocol 1)***

Note that substrate samples were taken from the 4-inch/10-cm and 8-inch/20-cm beds in 2019 and 2020.

- **Step 1:** Label all plastic bags before collecting samples from each APD-EGR bed.
- **Step 2:** Identify uniform areas near plants in the plots to be tested. Avoid sampling areas that might give misleading results, such as barren areas in a plot.
- **Step 3:** From each area, take enough samples from the two beds (4-inch and 8-inch) to properly represent the area, referring to Figure 3.5 for each plot location and sample number. Make sure that the probe reaches the bottom of the plot (which is the upper surface of the filter fabric at the base of the substrate in each plot). Keep the samples for each plot separate in bags to organize each sample. Clean the probe with acetone after use in each plot.
- **Step 4:** Repeat this substrate sampling procedure for each bed and plot. The PLFA samples were stored at -4°C prior to analysis.



**Figure 3.11.** Lekhon and Tonima collecting soil samples for PLFA, TOC, and N analyses from the APD-EGR in 2020 (outdoor portion).

(Image taken by Lee Skabelund on July 30, 2020.)



**Figure 3.12.** Collecting soil samples for respiration analysis from the APD-EGR's 4- and 8-in-deep beds in 2020 (outdoor portion).

(Image taken by Lee Skabelund on August 6, 2020.)

## **Root biomass**

Plant roots play a crucial role in C and nutrient cycling, promoting soil formation and structural stability, and shaping soil microbial communities. Roots are therefore key players in many ecosystem processes (Philippot et al., 2013; Bardgett et al., 2014). At the same time, roots are highly responsive to their environment, unfolding their physical and functional characteristics with respect to plant growth conditions (Gregory, 2006; Hodge et al., 2009). The most commonly investigated root parameter in studies of plant responses to environmental change is root biomass because it is closely linked to the energy investment of plants in their root systems or, in other words, the amount of C that is allocated below ground (Fageria, 2012). This makes it one of the most relevant root parameters for soil C modeling and for identifying efficient climate change mitigation options (Bolinder et al., 2007; Hirte et al., 2017).

### ***Procedure for root biomass analysis***

Substrate samples were taken from the 4-inch- and 8-inch-deep beds on November 6, 2020. The root biomass was estimated by extracting the roots from soil cores (Wilsey and Polley, 2006). Note that root biomass is typically carried over from year 1 to year 2, so it is appropriate to refer to root biomass as “peak biomass” rather than “productivity” (Wilsey and Polley, 2006). For the APD-EGR, soil samples were collected from each of the 4-inch and 8-inch plots (with 48 samples in total).

- Volumetric cores were taken from the 4-inch- and 8-inch-deep beds, thus producing four replications (reps) for each unique plot type (plant mix and soil type). The samples were collected at a consistent distance (~3–6 cm) from a plant selected near the southeastern corner of each plot. A 2-inch- (5.08-cm-) diameter corer was used to collect one core per plot (employing a hand trowel, as needed). Although the APD-EGR plots had four replicates (or reps), these reps were not combined, so that statistical analyses could be used to compare and contrast the findings among all 48 plots in the 4-inch- and 8-inch-deep beds.

- Some substrate cores did not come out as complete and consistent core lengths given the sandy and gravelly nature of the substrate. Because the volume of a cylinder is  $V = \pi r^2 h$ , we needed to keep track of each core depth and height (h). The most effective approach was to measure the core depths (h) manually during the sampling process, allowing the collection of “substrates with roots” from the 2-inch-diameter (5.08-cm-diameter) volumetric core using a soil probe, and then using a trowel, as needed.
- In the laboratory, each core required visual observation in order to first remove the coarse material (Wilsey and Polley, 2006). Large roots were hand-picked from the soil samples, and then the substrate samples were passed through 4-, 2-, and 1-mm sieves, respectively, with the roots being collected with tweezers from each sieve. All the roots were gathered in metal tins and washed over a 0.25-mm screen/sieve. The metal tins were labeled with plot numbers and weighed before the roots were placed in them. . Because only the K-type substrate had ~2% of clay a root washer was not needed to separate the clay from the roots. Note that the samples were refrigerated until the roots were washed.
- After washing, the root samples in the metal tins were oven-dried at 55–60°C for 48 hours (Frasier et al., 2016), then weighed (metal tin + dry roots) using a precision scale. The final step was to calculate the root biomass density ( $p = m/V$ ) for the volume of the core, using the formula  $V = \pi r^2 h$ .

Since 2020 was the third growing season, the APD-EGR was expected to have developed relatively stable root systems and root biomass in the two substrate types. This was not verified in any scientific way but was our research team’s working assumption.

To explore the extent of the soil microbes and their effects on the C sequestration potential, data regarding the root biomass, microbial biomass, and total C in the soil was necessary. The aboveground biomass assesses productivity (Lauenroth et al., 1986; Barrachina et al., 2015), which co-relates or translates to how much C is occurring belowground. Thus, it was possible to explain the main points of this study (and complement the PLFA results) by directly measuring or determining the relative density of the root biomass.



**Figure 3.13.** Collecting and analyzing root biomass samples from the 4-inch-/10-cm- and 8-inch-/20-cm-deep beds. (Images taken by M. M. Lekhon Alam on November 6, 2020.)

### Soil respiration analysis

Soil respiration reflects the capacity of soil to sustain plant growth, the soil fauna, and microorganisms. It can be used to estimate nutrient cycling in the soil and the soil's ability to sustain plant growth (US Department of Agriculture [USDA], n.d.). Soil respiration is a measure of the CO<sub>2</sub> released from the soil from the decomposition of soil organic matter (SOM) by soil microbes and respiration from plant roots and the soil fauna (USDA, n.d.). It is an important indicator of soil health because it measures the level of microbial activity, SOM content, and its decomposition. In the short-term, high soil respiration rates are not always better, however—this may indicate an unstable system and the loss of SOM because of excessive tillage, or other factors that degrade soil health (USDA, n.d.). This was measured using the laboratory protocols documented in Appendix E.

As with the PLFA analysis, the soil respiration analysis has two primary protocols: 1) an outdoor portion, involving protocols for collecting soil samples from the APD-EGR; and 2) an indoor portion, involving protocols for analyzing soil samples in the laboratory, as reported in Appendix E.

***Soil sampling protocols for soil respiration analysis (outdoor portion)***

Substrate samples were taken from the 4-inch/10-cm- and 8-inch/20-cm-deep beds in 2020. The protocols for collecting soil samples for the soil respiration analysis from the APD-EGR followed *Protocol 1*. The soil respiration samples were stored at  $-4^{\circ}\text{C}$  prior to analysis. The soil respiration test is a way to measure how much biological activity is occurring in the soil. The independent variables for these experiments were the two depths (4 inch vs. 8 inch) with the three different belowground biomass samples (A, B, and C), and the two substrates, K and R. The findings were expected to complement TOC and N analysis results from 2019 and 2020.



**Figure 3.14.** Soil laboratory activities (indoor portion)—preparing soil samples for PLFA analysis. (Images taken by M. M. Lekhon Alam and James Lin on October 10, 2019, at the Department of Agronomy, KSU.)



**Figure 3.15.** Soil laboratory activities (indoor portion)—preparing soil samples for respiration analysis. (Images taken by M. M. Lekhon Alam on September 11, 2020, at the Department of Agronomy, KSU.)

## TOC and N analyses

Important parameters for estimating the environmental status of terrestrial and aquatic ecosystems are the TOC and TN contents in soils and sediments. Soil TOC and N analysis were performed for this study in 2019 and 2020. The substrate sampling protocols, and laboratory procedures used to conduct the TOC and N analyses performed at the KSU Soil Testing Laboratory are described in more detail below.

The TOC and TN analyses had two primary protocols: 1) an outdoor portion, involving protocols for collecting soil samples from the APD-EGR; and 2) an indoor portion, involving protocols for analyzing soil samples in the laboratory, as reported in Appendix D.

### *Soil sampling protocols for TOC and N analysis*

Substrate samples were taken from the 4-inch/10-cm and 8-inch/20-cm beds in 2019 and 2020. The protocols for collecting the soil samples for TOC and N analysis from the APD-EGR followed Protocol 1. The soil TOC and N samples were stored at -4°C prior to analysis. The independent variables for these experiments were time (age of APD-EGR), the two depths (4-inch/10-cm and 8-inch/20-cm), the three different belowground biomass samples, A, B, and C, and the two substrates, K and R. The findings were expected to complement the soil PLFA analysis from 2019 and 2020.

### **Statistical data analysis**

Three-way analysis of variance (ANOVA), repeated-measure ANOVA, and Tukey's honestly significant difference (HSD) post-hoc analysis were conducted using SAS Proc Mixed and SPSS Statistics 29 software in order to identify a treatment (substrate + plant mix type + depth) that would potentially sequester the largest amount of C from green roofs in the Flint Hills Ecoregion (see the research design in Figure 3.9). Two three-way ANOVAs were used to evaluate the effect of three belowground biomass samples of plant mixes (types A, B, and C), two substrates (K and R) and two soil depths (4inch and 8 inch) on root density and soil respiration, and their interactions.

For the soil PLFA, TOC, and N analyses from 2019 and 2020, SAS Proc Mixed software (SAS Institute Inc., Cary, NC, USA) was used for the normally distributed data. Each bed of the experimental site incorporated a strip-plot or strip-block design, with four blocks per bed. The strip-plot design was incorporated so that any confounding variables occurring due to spatial variability (for example, the direction of drainage), which might affect responses in the strip factors (substrate and mix), would be distributed uniformly among blocks. All error bars were reported as standard errors. Differences were determined at the  $p < 0.05$  significance level using the least squares means separation (LSMEANS) and Tukey's HSD adjustment for multiple comparisons. Post hoc analyses of the treatment means were conducted using paired t-tests ( $p \leq 0.05$ ).

***Soil-sampling timeline***

On the prairie, the maximum aboveground biomass generally occurs in early August (Jarchow and Liebman, 2011), which prompted the collection of all the soil samples (excluding the root biomass) in the last week of July 2020. Table 3.6 provides the soil sampling dates, times, and procedures for 2019 and 2020.

**Table 3.6.** Soil sampling details for the APD-EGR for 2019 and 2020

<b>Soil sampling at APD-EGR in 2019 and 2020 (protocols and timelines)</b>					
<b>Date</b>	<b>Analysis</b>	<b>Collected from</b>	<b>Total samples</b>	<b>Collection time</b>	<b>Experiment location and lab protocols</b>
10/3/2019	Soil PLFA	Each plot of 4- and 8-in-deep beds	48	7:30–1:30 am	SMAL Indoor lab protocols reported in Appendix C
10/3/2019	TOC and N	Each plot of 4- and 8-in-deep beds	48	7:30–11:30 am	KSU soil-testing lab Indoor lab protocols reported in Appendix D
7/30/2020	Soil PLFA	Each plot of 4- and 8-in-deep beds	48	~7:15–11:30 am.	SMAL Indoor lab protocols reported in Appendix C
7/30/2020	TOC and N	Each plot of 4- and 8-in-deep beds	48	~7:15–11:30 am	KSU soil-testing lab Indoor lab protocols reported in Appendix D
8/6/2020	Soil respiration	Each plot of 4- and 8-in-deep beds	48	~8:45 am–12:45 pm	SMAL Indoor lab protocols reported in Appendix E
11/6/2020	Root biomass	Each plot of 4- and 8-in-deep beds	48	~8:45 am–12:45 pm	SMAL Complete protocols included

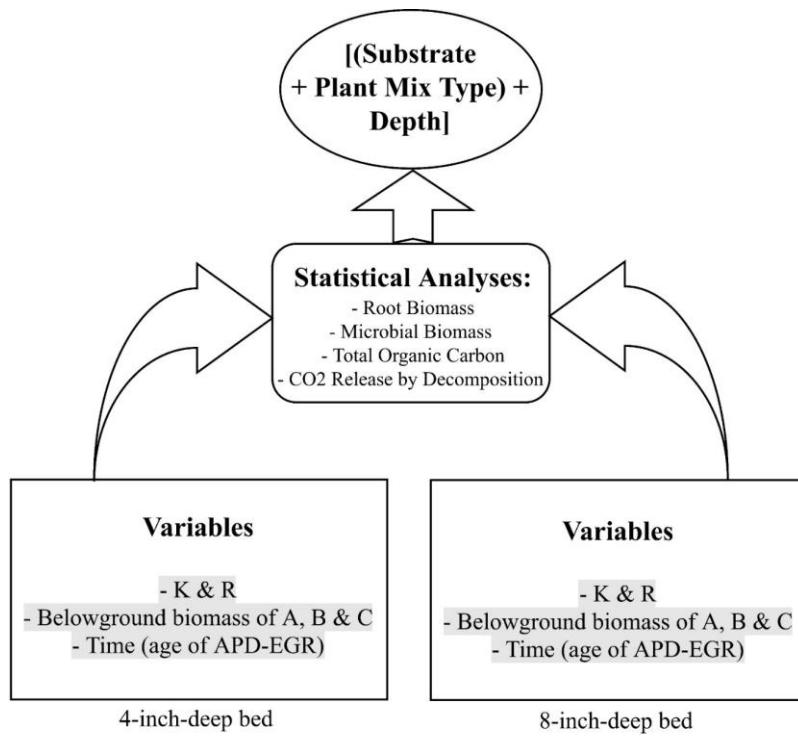


**Figure 3.16.** Experimental design and data analysis procedures for comparing the soil C sequestration potential of different APD-EGR beds. (Diagram by author.)

## (b) Methods for Investigating the Role of Green Roof Systems in Improved Building Energy Performance

According to Sailor, building energy performance related to green roofs relies significantly on the climatic location (Sailor, 2008). Most green roof energy performance research concerns the relationship between two dependent variables (namely, building energy performance and the energy expended in heating and cooling the building) and five primary independent variables including soil depth, vegetative density, climatic location, roof type (black, white, or green), and building types (office, lodging, or residential).

Within this study, all necessary sensors were installed at the APDesign Experimental Green Roof (APD-EGR), and the sensors were programmed to record and store temperature, soil moisture, and solar radiation readings every fifteen minutes.



**Figure 3.17.** Installing temperature sensors, checking sensor readings, and an assortment of temperature and soil moisture sensors at APD-EGR

(Photographs by M. M. Lekhon Alam & Lee R. Skabelund, taken in 2020, at the APD-EGR.)

### *Sensor Map of the APD-EGR and Installation Timeline*

For this research, it was essential to acquire surface and sub-surface temperature data from two beds, the shallowest (4-inch/10-cm deep) and deepest (8-inch/20-cm deep) among the three green roof depths. Decagon/METER data-loggers and soil moisture and temperature sensors (5TM sensors), along with a weather station (including precipitation, air temperature and relative humidity, wind speed and direction, and solar radiation), were originally installed in mid-March 2018. Surface temperature sensors (RT-1 sensors) were installed in mid-March and mid-June of 2020. Data examined for this study included the following time periods:

On March 17, 2020, Professor Lee Skabelund installed six RT-1 soil temperature sensors on the 8-inch deep APD-EGR bed (see Figure 3.19). Additional RT-1 sensors (METER Group, Inc. USA) along with METER data-loggers were installed on the 4-inch bed June 11, 2020. These RT-1 surface temperature sensors were placed on plots with plant mix type C.

The Kansas State University Green Roof Research Team used the ZENTRA Cloud to visualize the measurements of all sensors in the three beds of different substrate depths. ZENTRA Utility enables one to interact with the METER data logger over a Bluetooth low-energy wireless connection. Using a computer, smartphone or tablet, one can view information about each data-logger and attached sensors remotely, configure the logger, and test long-range telemetry communications (METERGROUP, 2020).

In Figure 3.18, the diamonds show each data logger location. P1, P2, P3, and P4 indicate plots with a 5TM sensor located sub-surface in the middle of each monitored plot. The number following each "P" show the port that each 5TM sensor was plugged into between July 12, 2018 and July 22, 2019, when sub-surface data was collected and analyzed for this research.

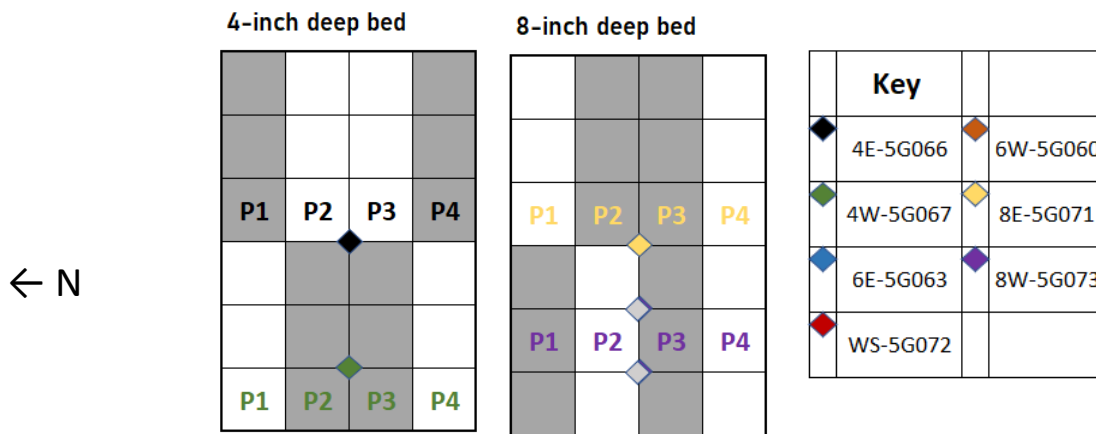


**Figure 3.18.** Sensor map of the APD-EGR, Kansas State University. Sub-surface sensors were placed in the eight C plots in mid-March 2018.

(Figure created by Allyssa Decker and Lee Skabelund.)

Plots are marked with a yellow color where the twelve RT-1 sensors were placed (six sensors on 4-inch-deep beds and six sensors on 8-inch-deep beds).

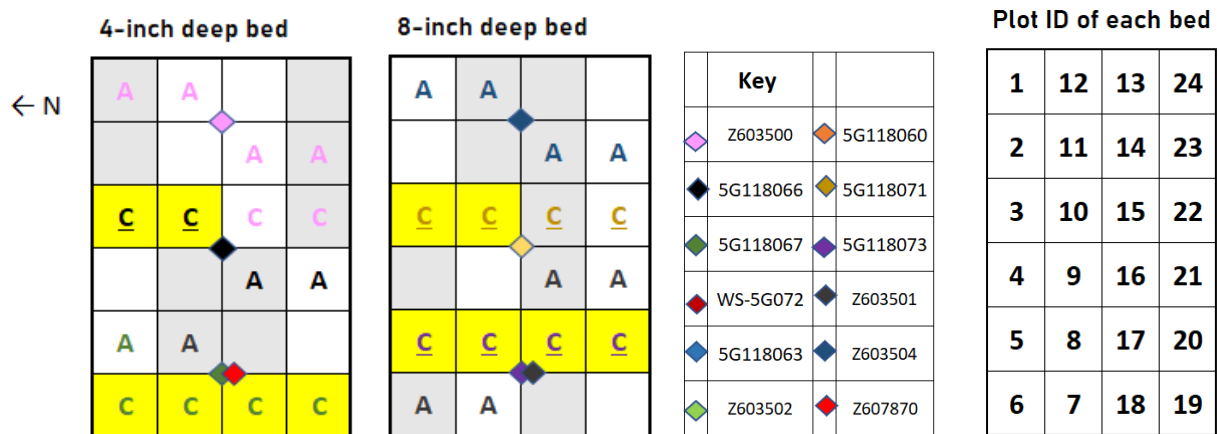


**Figure 3.19.** The latest sensor map of the APD-EGR, marking surface temperature RT-1 sensors in 4-inch & 8-inch-deep beds, lasting until June 11, 2020.

(Figure created by Allyssa Decker and Lee Skabelund.)

Figure 3.19 includes the key showing the identification numbers (**ID**) of the data loggers deployed on the APD-EGR. One can download any necessary sensor data from the ZENTRA Cloud by clicking the Key ID on the computer or in the Zentra app using a smartphone. The

temperature measurements were assumed to be accurate surface temperature readings for the APD-EGR. The METER 5TM (sub-surface readings) and METER RT-1 (surface) sensor information is shown in Table 3.7.

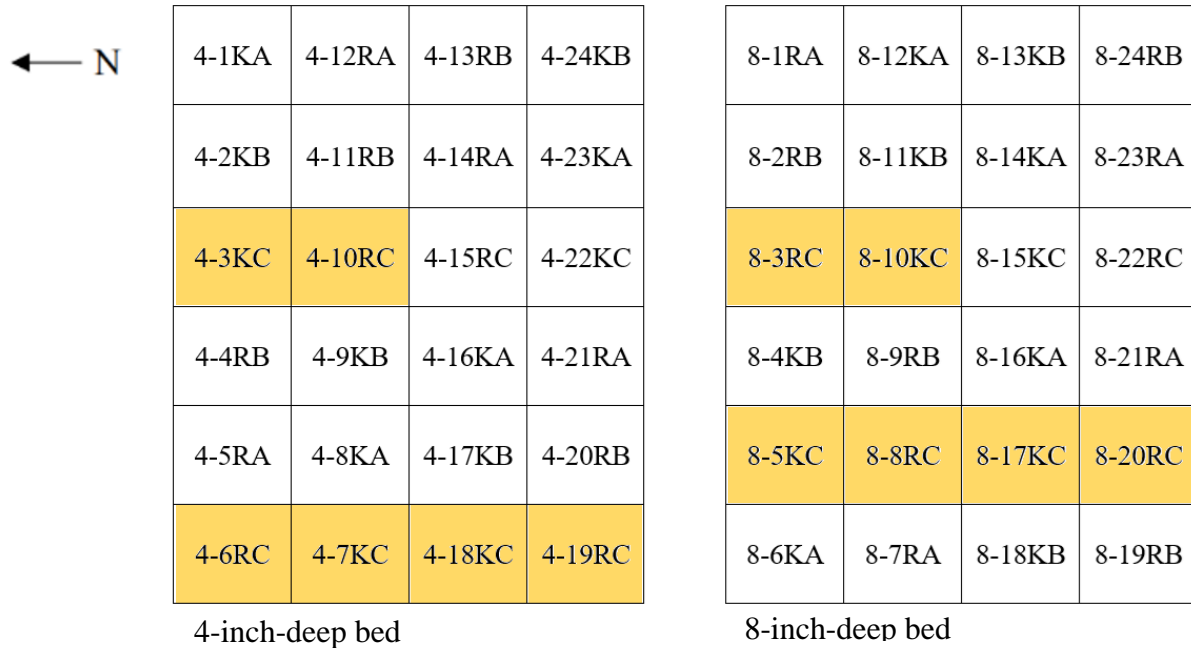
**Table 3.7** KSU APD-EGR data logger information.

Sensors Provide Soil Moisture & Temperature Data			Research Plots for Energy Performance		Sensors Provide Surface Temperature Data		
Sensor Type	Port	Datalogger (Group 1)	Depth	GR Cell	Datalogger (Group 2)	Port	Sensor Type
5TM	1	5G118066	4-inch bed	3KC	Z607870	6	RT1
5TM	1	5G118067	4-inch bed	6RC	Z607870	4	RT1
5TM	2	5G118067	4-inch bed	7KC	Z607870	3	RT1
5TM	2	5G118066	4-inch bed	10RC	Z607870	5	RT1
5TM	3	5G118067	4-inch bed	18KC	Z607870	2	RT1
5TM	4	5G118067	4-inch bed	19RC	Z607870	1	RT1
5TM	1	5G118071	8-inch bed	3RC	Z603504	6	RT1
5TM	1	5G118073	8-inch bed	5KC	Z603501	6	RT1
5TM	2	5G118073	8-inch bed	8RC	5G118071	5	RT1
5TM	2	5G118071	8-inch bed	10KC	Z603504	5	RT1
5TM	3	5G118073	8-inch bed	17KC	Z603501	5	RT1
5TM	4	5G118073	8-inch bed	20RC	5G118073	5	RT1

Data-logger WS-5G072 (labeled EGRw072 in Zentra Cloud), was placed in the middle of the 6-inch-deep bed along with solar radiation and air temperature sensors. The quantification of urban heat island indicators and their potential to reduce CO<sub>2</sub> were conducted using data collected on the 4-inch/10-cm and 8-inch/20-cm APD-EGR beds with the data sets noted in Table 3.7.

***Instrumentation at the APD-EGR for the Research***

After installing the RT-1 sensors and checking on the previously installed 5TM sensors, temperature data, soil moisture data, and solar radiation values were available for examination and analysis. The following three sets of data were analyzed to understand better the surface and sub-surface temperature dynamics of an experimental green roof in the Flint Hills Ecoregion. The units for these data sets are noted: 1. sub-surface (soil) temperatures (°C), 2. surface temperatures (°C), 3. soil moisture content (m<sup>3</sup> water/m<sup>3</sup> soil), and 5. solar radiation (W/m<sup>2</sup>).



KA,’ ‘KB,’ and ‘KC’ indicate a Kansas BuildEX® (**K**) substrate plot—planted with *Sedum* only (**A**), *Sedum* and native grass mix (**B**), and native grasses and forbs (**C**). ‘RA,’ ‘RB,’ and ‘RC’ indicate a rooflite® extensive mix (**R**) substrate plot—planted with *Sedum* only (**A**), *Sedum* and native grass mix (**B**), and native grasses and forbs (**C**). The study related to thermal analysis chose to be conducted only in C plots, and the rationale for using C plots is given below.

**Figure 3.20.** Sensor map of the in 4-inch & 8-inch-deep beds, including the plot IDs, with RT-1 & 5TM surface temperature sensors marked in yellow. (Diagram by author.)

Twelve METER RT-1 soil temperature sensors were positioned at the substrate surface. Furthermore, Decagon/METER 5TM soil moisture and temperature sensors (METER Group, Inc. USA), had been placed in the center of the Plant Mix C plots in June 2018, with one sensor placed in the middle of the green roof profile (2 inches from the surface for the 4-inch plots and 4 inches from the surface in the 8-inch plots). The 4-inch and 8-inch APD-EGR beds with these sensor data sets were able to meet the needs of quantifying both soil moisture and temperature fluctuations and trends and thus to assess urban heat island indicators and their potential to reduce CO<sub>2</sub>. The three K plots (4-3KC, 4-7KC, and 4-18KC), and the three R plots (4-6RC, 4-10RC, and 4-19RC) were 4-inch/10-cm deep beds, whereas the three K plots (8-5KC, 8-10KC, and 8-17KC) and the three R plots (8-3RC, 8-8RC, and 8-20RC) were 8-inch/20-cm deep beds (refer to Fig. 3.20).

#### ***Rationale for the Use of Only Plant Mix C Type (Native Grasses and Forbs) Plots***

As a part of this study, root biomass from the 4-inch/10-cm and 8-inch/20-cm beds were examined. Native short grass roots had significantly more subterranean biomass than *Sedum* spp., findings that are supported by Sutton (2013). Using the three-way ANOVA, the subterranean biomass samples containing grasses (B and C) appeared overall to have significantly higher root density than *Sedum* plots in both 4-inch and 8-inch beds (these findings will be explained further in subsequent chapters). I hypothesized that the C-type plots would potentially have the most thermal conductivity and the most interactions with soil moisture. Therefore, instrumentation was performed in C-type plots to conduct thermal analyses of APD-EGR (excluding comparisons of APD-EGR plant types and plant mixes A, B and C).

### Proposed Methods for Thermal Analysis

The study did not follow the most common methodology to estimate thermal resistance (the *R-value*) by dividing the thickness by the known thermal conductivity of the specimen. This study explains why it is sometimes impractical to determine soil R-values from known values of conductivity. The proposed methodology had several limitations and challenges because the thermal resistance of the material was unknown (Yüksel, 2016), and the thermal conductivity of substrates (K and R) fluctuated rapidly at the APD-EGR site. Therefore, in situ measurements of soil moisture and surface temperature were used as inputs to determine whether the substrate *R-value* or the rate of change in heat storage (*Q-value*) should be further explored in this research.

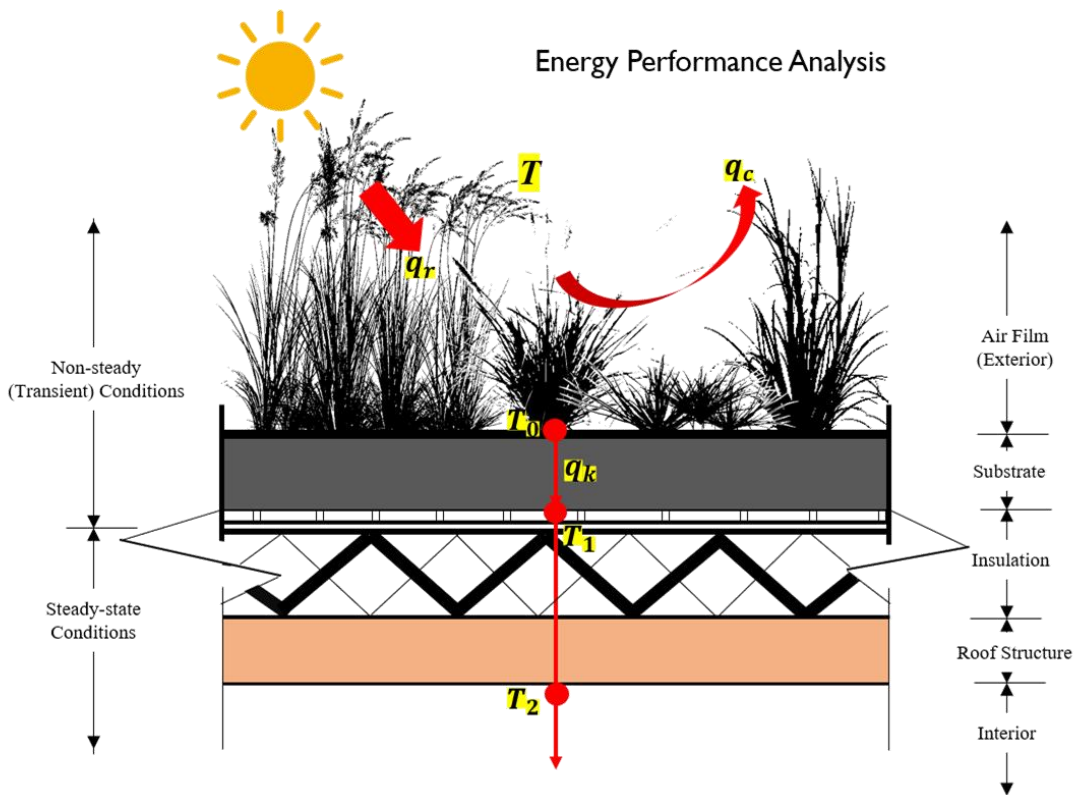


**Figure 3.21.** APD-EGR heat transfer model.

$T$ = Adjacent air temperatures;  $q_r$  = direct radiation from the sun;  $q_c$  = heat loss/gain by convection;  $q_k$  – soil moisture data;  $T_0$  = soil surface temperatures and,  $T_1$  = Sub-surface temperatures and,  $T_2$  = Building interior temperatures

### **In situ observations**

- Initially, the study explored the possibility of determining the thermal resistance *R-value* from the in-situ measurement of soil surface temperatures and soil moisture from the APD-EGR system. The resultant thermal resistance (R-value) represented the inside and outside of the soil surface and did not include air films. This means that the temperature of concern was the soil surface and subterranean temperatures, as opposed to the recorded air temperature.
- Secondly, the study explored the possibility of explaining the effect of green roof soil moisture on building energy performance by estimating the rate of change in heat storage within the soil layer (*Q-value*). An approximation of this *Q-value* was achieved using the sub-surface temperature of the two substrate types and soil moisture data from the APD-EGR sensors.

This research was inspired by the summation technique provided in ASTM C1155 (Materials, 2013), but adapts this technique by introducing a new way of determining the R-value of the building envelope component. This calculation procedure uses aggregated data on soil moisture content and differences in surface temperatures over time at APD-EGR. The study compares the relative thermal dynamics of the APD–EGR between summer (June 15, 2020 to September 15, 2020) and winter (November 15, 2020 to February 15, 2021) in the Flint Hills Ecoregion.

### ***The Summation Technique of in-situ Measurements***

For each time interval, starting from the time of the first measurement, the estimate of thermal resistance for each plot was calculated (specified from two beds of APD-EGR (Materials, 2013)):

$$R_e = \frac{\sum_{k=1}^M \Delta T_{sk}}{\sum_{k=1}^M q_k} \dots\dots\dots (1)$$

Where:

- $R$  = thermal resistance, in  $m^2 \cdot K/W$
- $q$  = heat flux, in  $W/m^2$
- $\Delta T$  = the temperature difference across the object
- $e$  = estimate
- $M$  = the number of values of  $\Delta T$  and  $q$  in the source data
- $s$  = surface,  $I$  = indoor,  $o$  = outdoor
- $k$  = the step counter for the summation of time-series data

### ***Perpendicular Heat Flow***

This study assumed that heat flow was perpendicular (and one dimensional) to the surface of the building and the two green roof beds. The temperature difference ( $\Delta T_s$ ) for each surface was obtained by subtracting the outside soil-surface temperature from the inside sub-surface temperature for each time interval (Materials, 2013). The data collected by the APD-EGR 5TM and RT1 sensors were used (5TM sensors for temperatures inside the substrate profile and RT1 sensors for outside or surface temperatures).

$$\Delta T_s = T_1 (sub-subface) - T_0 (surface) \dots\dots\dots (2)$$

### ***Necessary Equations to Determine Heat Flux ( $q$ ) from In-Situ Measurement***

The most critical part of this thermal study is determining the heat flux value ( $q$ , measured in  $W/m^2$ ) for two different substrates (**K**= Kansas BuildEx® and **R**= the rooflite® extensive mc). Heat transport in soils results from energy transfer mechanisms, primarily near the soil surface, and the result of dynamic thermal properties of the soil (Selker and Or, 2021). Heat may be transported in soils by conduction, radiation, and by convection with air or water flow (Selker and Or, 2021). While conduction is generally considered the dominant mechanism for heat transport, convection and radiation are also worthy of careful consideration in the soil section (Alam et al., 2015).

## *Conduction of Heat in Soil*

The value of soil temperature at any given moment is an important factor for many physical, biological, and chemical soil processes. Temperature governs (Hillel, 2003):

1. evaporation and aeration,
2. the types and rates of chemical reactions that take place in the soil, and
3. influences biological processes, such as seed germination, seedling emergence and growth, root development, and microbial activity.

Soil temperature varies in response to changes in radiant, thermal, and latent energy exchange processes that take place primarily through the soil surface (Hillel, 2003, p. 215). The effects of these phenomena are propagated into the soil profile by a complex series of transport processes, the rates of which are affected by time-variable and space-variable soil properties (Hillel, 2003, p. 215). Writer and soil scientist Dr. Daniel Hillel has produced explanations and simplifications of these processes in a series of formulas. This study also uses an equation to estimate soil specific heat capacity developed by environmental engineer Dr. Wilfred Brutsaert (1982).

**Step 1:** The first law of heat conduction, known as *Fourier's law*, states that the flux of heat,  $q$ , in a homogeneous body is in the direction of, and proportional to, the temperature gradient (Hillel, 2003, p. 216):

$$q = - \lambda \nabla T \dots\dots\dots (3),$$

Where,  $\lambda$  = Soil thermal conductivity, ( $\text{J m}^{-1} \text{s}^{-1}\text{C}^{-1}$ )

**Step 2:** In vertical one-dimensional form, this law is written,

$$q = - \lambda \frac{dT}{dz} \dots\dots\dots (4)$$

In this equation  $z$  represents soil depth ( $z = 0$  being the soil surface) and  $dT/dz$  is the temperature gradient in any direction (Hillel, 2003, p. 216). The negative sign in these equations conveys that heat flows (or transfers) from areas of higher to lower temperature (i.e., in the direction of, and in proportion to, a *negative* temperature gradient).

**Step 3:** While thermal conductivity in soils is in principle independent of water vapor movement, the  $\lambda$  in Eq. 4 should be considered as the *apparent* soil thermal conductivity (Selker and Or, 2021, Hillel, 2003). This is because latent heat transfer in the form of water vapor (energy liberated or consumed due to water changing between liquid and vapor states) cannot be separated from conduction in moist soils. That is,  $\lambda = \lambda^* + D_{\text{vapor}} \times L$ , where  $\lambda^*$  represents the instantaneous thermal conductivity,  $D_{\text{vapor}}$  is thermal vapor diffusivity, and  $L$  (2.449 MJ/kg or 585 cal/g) is latent heat of vaporization (Hiraiwa and Kasubuchi, 2000).

In Figure 3.22, a key observation is that  $\lambda$  depends on the minerals which make up the soil, the porosity of the soil, and the water content of the soil or sample being analyzed (Selker and Or, 2021, p. 248). The thermal conductivity of the constituent parts of soil can vary 400-fold, with quartz having fifteen times the conductivity of water, which in turn is about twenty times as conductive as air (Selker and Or, 2021, p. 248).

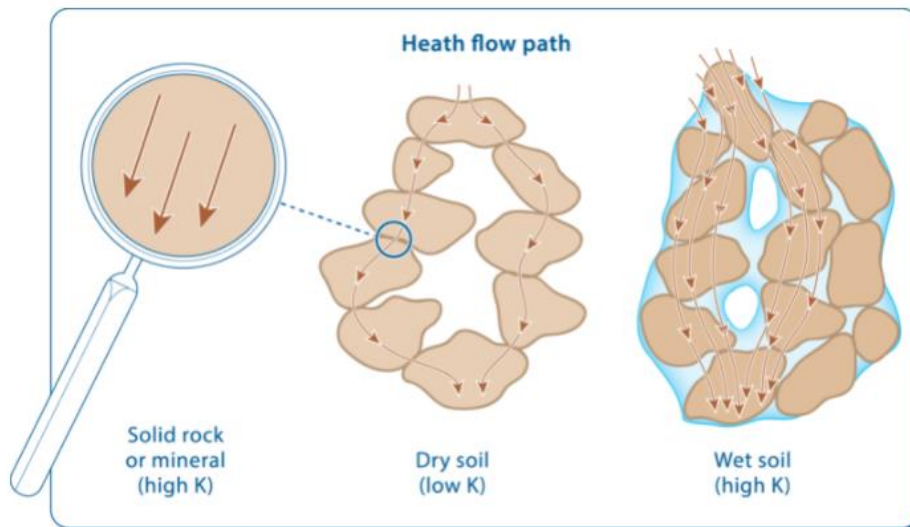


**Figure 3.22.** Illustration of heat flow in soils, emphasizing the role of mineral composition, porosity, and water content (Stephens et al., 2018; Selker and Or, 2021)

**Step 4:** Equation (3) is sufficient to describe heat conduction under steady-state conditions, where the temperature at each point in the conducting medium is invariant, and the flux is constant in time and space (Hillel, 2003, p. 219). To account for non-steady (transient) conditions, a second law analogous to Fick’s second law of diffusion as embodied in Eq. (11) is necessary (Hillel, 2003, p. 219). Hillel states: “To obtain the second law of heat conduction, we invoke the principle of energy conservation in the form of the continuity equation, stating that, in the absence of internal sources or sinks of heat, the time rate of change in heat content of a volume element must equal the change of flux with distance” (Hillel, 2003, 219). Selker and Or (2021) provide detailed explanations (adopted from Hillel’s statements) and a series of equations in their book *Soil Hydrology and Biophysics* (2021), to determine the conservation of energy equation for a soil/substrate type:

$$\rho_s c_s \frac{\partial T}{\partial t} = - \nabla \cdot q \dots\dots\dots (5)$$

Where Equation (5) is the three-dimensional form of the equation,  $\rho_s$  is soil bulk density,  $c_s$  is the specific heat capacity of soil (the amount of heat required to raise the temperature of a unit mass of moist soil by 1°C), and  $\partial T/\partial t$  is the rate of temperature change. The symbol  $\nabla$  (del) is the shorthand representation of the three-dimensional gradient (Hillel, 2003, 219). Equations (5), (3), and Fourier’s law, when combined, result in a general three-dimensional form (Selker and Or, 2021, p. 253):

$$\rho_s c_s \frac{\partial T}{\partial t} = - \nabla \cdot (\lambda \nabla T) \dots\dots\dots (6)$$

**Step 5:** For the APD-EGR energy model (Figure 3.21), with gradients in the perpendicular z-direction (which is not unusual in soils, which tend to be at the same temperature at any depth), the equation is (Selker and Or, 2021, p. 253):

$$\rho_s c_s \frac{\partial T}{\partial t} = - \frac{\partial}{\partial z} \left( \lambda \frac{\partial T}{\partial z} \right) \dots\dots\dots (7)$$

**Step 6:** Three parameters describe the essential physical properties of the thermal dynamics of the soil. If the properties of the soil are uniform in space and time, they can be aggregated into a single value. For these calculations, this study adopts the methodology commonly found in the literature. The expression is simplified using the soil's volumetric heat capacity:

$$(C_v = \rho_s c_s) \dots\dots\dots (9)$$

$C_v$  may be approximated as (Brutsaert, 1982; Selker and Or, 2021, p. 253):

$$C_v \cong 1.94 \cdot (1 - sp - \varphi) + 4.189 \cdot \theta_v + 2.50 \cdot \varphi \quad [MJ\ m^{-3}\ C^{-1}] \dots(10)$$

where  $sp$  is the soil porosity (*porosity is a measure of the total pore space in the soil*),  $\theta_v$  is the volumetric water content, and  $\varphi$  is the fractional volume of soil organic matter. The terms on the right-hand side of Eq.10 account for the contributions of soil solids, water, and organic matter respectively to volumetric heat capacity (Selker and Or, 2021). The ratio of the thermal conductivity ( $\lambda$ ) to the volumetric heat capacity of a homogenous soil ( $C_v$ ) is referred to as the *thermal diffusivity* ( $D_H$ ). Thus,

$$D_H = \lambda/C_v \dots\dots\dots (11)$$

The variable  $D_H$  is a useful measure of the rate of change in the soil layer temperature. The rate at which the heat content of a layer of soil changes depends on the volumetric heat capacity ( $C_v$ ) and the rate of temperature change of the soil volume per unit time (Snyder and Paw, 2001). For a unit surface area, the rate of change in heat storage within the soil layer is expressed as  $-C_v \frac{\partial T_{soil}}{\partial t} \Delta Z$  (Snyder and Paw-U; 2001, Philip, 1961).

Thus, one can calculate the rate of change in heat storage within the soil layer:

$$Q = -C_v \frac{\partial T_{soil}}{\partial t} \Delta Z \dots\dots\dots (12)$$

where,  $\partial T_{soil}$  is soil subsurface temperature difference and  $\partial t$  is the time interval.

Solving the aforementioned equations allows one to obtain a description of how temperature varies in space and time in the soil or substrate, and thus the values of three parameters, 1) the volumetric soil heat capacity ( $C_v$ ), 2) thermal conductivity ( $\lambda$ ), and 3) thermal diffusivity ( $D_H$ ), are required through measurement or calculation. Together, they ( $C_v$ ,  $\lambda$  and  $D_H$ ) are called the thermal properties of soils (Hillel, 2003, p. 220).

**Step 7:** Volumetric heat capacity ( $C_v$ ) for each time interval was calculated using Equation (10). These heat capacity values were then input into Equation (12) to output heat flux ( $q$ ) for each of the 12 C plots (six plots in each of the APD-EGR 4-inch/10-cm and 8-inch/20-cm beds). Finally,  $q$  values can be used in equation (1) to obtain  $R_e$  values—suggested for future research.

### Other Constant Values Required for Calculating $C_v$

Table 3.8 Dry bulk density and porosity of the two APD-EGR substrates, K and R per (Decker, 2021).

Soil Types	K	R
*Bulk density ( $\text{g}/\text{cm}^3$ )	1.47	0.98
Total pore space (%), $n$	42.50	58.00
<b>Soil Porosity, <math>sp</math></b>	0.425	0.58

\*Bulk density is usually expressed in megagrams per cubic meter ( $\text{Mg}/\text{m}^3$ ) but the numerically equivalent units of  $\text{g}/\text{cm}^3$  and  $\text{t}/\text{m}^3$  are also used ( $1 \text{ Mg}/\text{m}^3 = 1 \text{ g}/\text{cm}^3 = 1 \text{ t}/\text{m}^3$ ) (Cresswell and Hamilton, 2002).

### ***Estimating $\phi$ , the Fractional Volume of Substrate Organic Matter***

Table 3.9 provides substrate Organic Matter (OM) percentages estimated by the Kansas State Soil Testing Lab on August 24, 2021. A modified version of the loss on ignition method (Combs and Nathan, 1998) was performed at the lab. Table 3.9 below reports OM on a mass basis (as opposed to a volumetric basis). The testing protocols used by the KSU Soil Testing Lab are described in Appendix D.

**Table 3.9** Mass percentage of substrate Organic Matter (OM) for the selected twelve plots.

<b>Plot ID</b>	<b>Organic Matter %</b>
4-19RC	4.0
4-18KC	1.7
4-10RC	3.8
4-7KC	2.4
4-6RC	3.6
4-3KC	2.0
8-20RC	1.4
8-17KC	1.4
8-10KC	2.1
8-8RC	2.7
8-5KC	1.6
8-3RC	2.7

### ***Converting Mass Percentage of Soil OM to Fractional Volumes of soil OM***

A table from the book, *Evaporation into the Atmosphere* (Brutsaert, 1982), was consulted for the density of soil organic matter:

**Table 3.10** Properties of soil components at 293 K per (Brutsaert, 1982).

Soil Components	Density $\rho$ ( $kg\ m^{-3}$ )
Soil minerals	2650
<b>Soil Organic Matter (OM)</b>	<b>1300</b>
Water	1000
Air	1.20

Fractional volumes of soil OM are converted in Table 3.11 using soil bulk density (from Table 3.8), soil OM density (from Table 3.10), and organic mass percentage (%) from Table 3.9:

**Table 3.11** Fractional volume of soil Organic Matter (OM) for the selected twelve plots. (Table by author.)

Plot ID	Volume fraction of soil OM $\phi$
4-19RC	0.045231
4-18KC	0.019223
4-10RC	0.042969
4-7KC	0.027138
4-6RC	0.040708
4-3KC	0.022615
8-20RC	0.015831
8-17KC	0.015831
8-10KC	0.023746
8-8RC	0.030531
8-5KC	0.018092
8-3RC	0.030531

***Determining  $C_v$  with the Volumetric Water Content (primary variable  $\theta_v$ )***

$C_v$  was calculated for each 15-minute time interval using in-situ soil moisture content measurements for the twelve selected plots. The  $C_v$  value is used to determine  $R_e$  and to indicate the relationship between soil moisture contents and heat resistance of K and R soil types.

***Possibility of Determining  $R_e$  in the Context of the APD-EGR***

The length of time and number of in-situ values providing acceptable  $R_e$  values were very important for the accuracy of the study. Initially, this study set out to estimate  $C_v$  (from Eq 10) and report  $R_e$  (using Eq 12 and then Eq 1) for selected data recorded at each sensor location. Furthermore, the study initially aimed to determine  $R_e$  values from each selected plot at the APD-EGR every 15 minutes. However, obstacles to approximating the thermal resistance value were encountered.

In soil–plant–atmosphere systems, the energy balance equation is given by three soil heat flux researchers (Roxy et al., 2014):

$$R = G^* + L + H \dots\dots\dots (13),$$

where  $G^*$  is the soil heat flux at the surface,  $R$  is the net radiation,  $L$  is the latent heat flux, and  $H$  is the sensible heat flux. The ground heat flux is of comparable magnitude to the latent heat flux and thus constitutes an important term in the surface energy balance (Langer et al., 2011; Roxy et al., 2014, p. 742). Generally, the soil heat flux term in the energy balance equation is neglected, but this is not agronomically justified considering the associated sub-soil migration of moisture. Soil heat flux is difficult to measure because it includes conduction and convection heat transfer processes (Heitman et al., 2010; Roxy et al., 2014, p. 742). In various studies, it has been found that soil heat flux is estimated from soil temperature profile measurements; by using the temperature gradient method, soil heat flux  $G$  is calculated with the following Equation (14) (Oncley et al., 2007):

$$G = \lambda \frac{\Delta T_s}{\Delta z} \dots\dots\dots (14),$$

where  $\lambda$  is the thermal conductivity of the soil,  $\Delta T_s$  temperature difference of two soil surfaces (Equation 2), and  $\Delta z$  is the width of the layer. The most common method of measuring soil heat flux  $G$  in the field is to place an SHF sensor at a depth below the surface (Gao et al., 2017). The thermal conductivity can also be calculated from the thermal diffusivity ( $k$ ) using the following equation (Roxy et al., 2014).

$$\lambda = D_H C_v \dots\dots\dots (15)$$

To estimate soil heat flux  $G$ , one must know or input the thermal conductivity ( $\lambda$ ) or the thermal diffusivity ( $D_H$ ) in Equation (12).

The soil surface heat flux ( $G^*$ ) can be written as (Roxy et al., 2014):

$$G^* = G + Q \dots\dots\dots (16),$$

where  $Q$  is the rate of change in soil heat storage (Philip, 1961).

The above equation is strongly related to thermal conduction and convection and therefore, in moist, warm soils, a third term that accounts for the thermal convection should be included so that the ground heat flux becomes (Roxy et al., 2014):

$$G^* = G + Q + C_w \Delta T_s \dots\dots\dots (17),$$

where  $C_w$  is the water volumetric heat capacity and its value can be chosen from (Garratt, 1994).

From all of the above equations, one can see that it is difficult to determine soil heat flux ( $G$ ) without at least inputting the thermal conductivity ( $\lambda$ ) or the thermal diffusivity ( $D_H$ ). The thermal conductivity of soils is numerically relative, which frequently changes due to variant soil moisture, organic materials, and other soil properties. The primary aim of this study is to assess the effect of moisture content in the green roof system, to improve building energy performance. Determining soil heat flux ( $G$ ) from the literature would exclude moisture content from this in-situ research scenario and focus instead on the primary independent variable.

If future research is primarily focused on determining heat flux of different soil types at APD-EGR, the above equations can be used to determine the approximate  $G$  and  $G^*$  for the APD-EGR system at Manhattan, Kansas.

### ***Possible Solutions for this Research Setting***

From the above discussion, it is clear that determining the thermal resistance (R-value) of soil is a lengthy process and requires incremental development in research. For this study,  $Q$  was estimated as the rate of change in heat storage of a layer of soil between the surface  $z_1 = 0$  and some depth  $z_2 = 0.1$  (for the 4 – inch – deep bed) and  $z_2 = 0.2$  (for the 8-inch-deep bed).  $C_v$  was estimated (using Eq 10) and then  $Q$  was determined using equation 12:

$$Q = -C_v \frac{\partial T_{soil}}{\partial t} \Delta z$$

This value was used to determine soil heat flux at the surface following the methods shown by Philip (1961). For in-situ measurement, the research setting should use heat flux sensors ideally on two surfaces  $z_1$  and  $z_2$  in the APD-EGR research settings.

The sensible and latent heat fluxes can be calculated using the equation series provided by Oncley et al., (2007), and other values for the input in equation (13) can be approximated from Roxy et al. (2014). Soil heat flux sensors were not placed at the research site at APD-EGR due to the lack of time and resources, and the study did not use an approximate value for  $\lambda$  and  $D_H$  to try to understand the thermal dynamics related to the soil moisture content in the Flint Hills Ecoregion. If the study used known values of  $\lambda$  and/or  $D_H$  —it might not give the exact interpretations of soil moisture with its thermal conductivity (Selker and Or, 2021) because thermal conductivity ( $\lambda$ ) and diffusivity ( $D_H$ ) of soils are affected by moisture (Selker and Or, 2021). Therefore, the study could not determine the R-value from the collected 5TM and RT-1 data sets.

Since the primary purpose of this study was to understand the dynamics between soil moisture and thermal storage in the soil, this can be explained (explanations are in Chapter 4) and explored using the changes in  $Q$  values in different substrates and depths at APD-EGR.

Finally, the study determined the rate of change in heat storage within the soil and observed its interactions with the soil moisture content. Therefore, the moisture content was determined to be the primary independent variable with two depths (4-inch vs. 8-inch) and substrates (K and R), and the focus dependent variable was the rate of heat storage within the substrate layers.

### ***Duration of Test***

According to ASTM C1155 (Materials, 2013), and other journal articles (Roxy et al., 2014), (Oncley et al., 2007), (Gao et al., 2017), the test should last one or more multiples of 24 hours, because this length of time is a dominant weather station temperature cycle (Materials, 2013). If one obtains temperature and heat flux data for an insufficient duration, the calculation in Equation (1) may be significantly biased by not obtaining the temperature history prior to the onset of heat transfer measurement or the post-measurement heat flux that resulted from the temperature history prior to the cessation of measurement. Since our test lasted for roughly 90 multiples of 24 hours it was unnecessary to perform sufficient data criteria or the convergence factors. Values were retrieved every 15 minutes so the variance ( $V$ ) of  $Q$  value  $V(Q)$  was also optional.

Flanders (1992) explains the requisite choice of  $n = 12$  h for the time lapse in their summation technique. Per ASTM guidance, a researcher can choose other values of  $n$ , between 6 and 48 hours, for the time-lapse time intervals (Materials, 2013).

### ***Calculation of Mean Soil Heat Storage and Mean Temperature***

The final  $Re$  obtained at any one sensor location did not adequately represent the building envelope component chosen, even where thermal anomalies were absent. The rate of change in heat storage within the soil layer was calculated from the area-weighted averages of the final values of  $Q$ , using appropriate groupings of two (plots with K substrate and plots with R substrates, Table 3.12) at each bed (4-inch/10-cm and 8-inch/20-cm) of sensors in representative subsections. The APD-EGR sensor site covers equal areas of the building component (roughly 1.2 x 1.2 meters).

### ***Sensors Associated with Equal Areas of the Plots at APD-EGR***

The mean numeric value of the rate of soil heat storage change was calculated after every 6 hours ( $n = 6$ ) ( $Q_6$ ) for each building green roof component subsection (the APD-EGR plots). This was done using six 5TM sensors and six RT-1 sensors in six plots for each depth (4-inch and 8-inch). It was calculated using values of  $Q$  from Equation 12 for each sensor site ( $j$ ) (Materials, 2013) as follows:

$$Q_6 = \frac{[\sum_{j=1}^N Q_{ej}]}{N} \dots\dots\dots (18)$$

$N$  = number of values of  $Q$  every 6 hours ( $N \geq 3$ )

$e$  = estimate

$j$  = counter for summation of sensor sites; the research settings at APD-EGR had six sensor sites per bed (each depth of 4 inch and 8 inch).

Similarly, the estimated mean moisture ( $Moi$ ) content was calculated every 6 hours ( $n=6$ ), using the values of moisture content data from the dataloggers for each sensor site ( $j$ ) (Materials, 2013):

$$Moi_6 = \frac{[\sum_{j=1}^N Moi_{ej}]}{N} \dots\dots\dots (19)$$

where  $N$  = number of values of  $Moi$  every 6 hours ( $N \geq 3$ )

The study determined the mean soil moisture ( $Moi_6$ ) and the mean of  $Q_6$  (the rate of change in heat storage within the soil) after every 6 hours ( $n=6$ ) to determine the interaction of soil moisture content and the Q-value of different substrates (Kansas BuildEx® (K) and rooflite® extensive mc (R) substrates) at different depths (approximately 4-inch/10-cm and 8-inch/20-cm deep). Graphical analyses were performed using the overall mean of  $Q_6 - value$  from three sensor sites in each bed (3-KC plots and 3-RC plots) every 6 hours, and the overall mean of  $Moi_6 - value$  from three sensor sites in each bed (3-KC plots and 3-RC plots) every 6 hours. The overall mean  $m(Q)_{(Plot Type)-(bed depth)}$  was calculated according to the following Equation:

$$m(Q)_{(Same\ Plot\ Type)-(bed\ depth)} = \frac{[\sum Q_6 - values\ of\ three\ same\ type\ plots\ from\ each\ bed^{**}]}{N_{Q_6}}$$

$N_{Q_6} = 3$ ; three  $Q_6$  – value of three similar plots from each bed ( $N_6 \geq 3$ ).

\*\* The plot groupings for determining overall mean of  $Q_6$  – values are reported in the Table 3.13

$$mMoi_{(Same\ Plot\ Type)-(bed\ depth)} = \frac{[\sum Moi_6 - values\ of\ three\ same\ type\ plots\ from\ each\ bed^{**}]}{N_{Moi_6}}$$

$N_{Moi_6} = 3$ ; three  $R_6$  – value of three same type plots from each bed ( $N_6 \geq 3$ ).

\*\* The plot groupings for determining overall mean of  $Moi_6$  – values are reported in the Table 3.13

**Table 3.12** Sensor site groupings for the overall mean of  $m(Q)$  and  $m(Moi)$  calculations. (Table by author.)

<b>Sensor Site Groupings</b>	
4-inch (10 cm) deep sensor sites ( <i>j</i> )	8-inch (20 cm) deep sensor sites ( <i>j</i> )
<b>KCs-4</b>	<b>KCs-8</b>
4-3KC	8-5KC
4-7KC	8-10KC
4-18KC	8-17KC
<b>RCs-4</b>	<b>RCs-8</b>
4-6RC	8-3RC
4-10RC	8-8RC
4-19RC	8-20RC

In Table 3.12 there are four groups of soil type substrates shown [(Kansas BuildEx® (**K**) and rooflite® (**R**)], including two distinct soil types in each bed. Table 3.13 shows the symbols used in this thermal analysis study and for statistical analyses.

**Table 3.13** Selected symbols used in the thermal analyses. (Table by author.)

Symbol	Reports	From (Plots   Bed Depth)
$mQ_{KCS-4}$	Overall mean of $Q_6$	4-3KC, 4-7KC, 4-18KC   4-inch
$mQ_{RCS-4}$	Overall mean of $Q_6$	4-6RC, 4-10RC, 4-19RC   4-inch
$mQ_{KCS-8}$	Overall mean of $Q_6$	8-5KC, 8-10KC, 8-17KC   8-inch
$mQ_{RCS-8}$	Overall mean of $Q_6$	8-3RC, 8-8RC, 8-20RC   8-inch
$mMoi_{KCS-4}$	Overall mean of $Moi_6$	4-3KC, 4-7KC, 4-18KC   4-inch
$mMoi_{RCS-4}$	Overall mean of $Moi_6$	4-6RC, 4-10RC, 4-19RC   4-inch
$mMoi_{KCS-8}$	Overall mean of $Moi_6$	8-5KC, 8-10KC, 8-17KC   8-inch
$mMoi_{RCS-8}$	Overall mean of $Moi_6$	8-3RC, 8-8RC, 8-20RC   8-inch

The performance of green roof system depends significantly on local climate and weather. Our thermal analysis compares the thermal dynamics of our APD-EGR between summertime (**June 15, 2020- September 15, 2020**), and wintertime (**November 15, 2020- February 15, 2021**) in the Flint Hills Ecoregion. All data sets were collected using RT-1 and 5TM sensors at APD-EGR.

- The overall mean of  $Q_6$  approximated from the data collected from the APD-EGR in the summertime (June 15, 2020 to September 15, 2020) is expressed as  $SmQ_{KCS-4}$ ,  $SmQ_{RCS-4}$ ,  $SmQ_{KCS-8}$ , and  $SmQ_{RCS-8}$ .
- The overall mean of  $Q_6$  approximated from the data collected from APD-EGR in the wintertime (November 15, 2020 to February 15, 2021) was expressed as  $WmQ_{KCS-4}$ ,  $WmQ_{RCS-4}$ ,  $WmQ_{KCS-8}$ , and  $WmQ_{RCS-8}$ .

- The overall mean of  $\mathbf{Moi}_6$  approximated from the data collected from the APD-EGR in the summertime (June 15, 2020 to September 15, 2020) was expressed as  $\mathbf{SmMoi}_{KCS-4}$ ,  $\mathbf{SmMoi}_{RCS-4}$ ,  $\mathbf{SmMoi}_{KCS-8}$ , and  $\mathbf{SmMoi}_{RCS-8}$ .
- The overall mean of  $\mathbf{Moi}_6$  approximated from the data collected from the APD-EGR in the wintertime (November 15, 2020 to February 15, 2021) was expressed as  $\mathbf{WmMoi}_{KCS-4}$ ,  $\mathbf{WmMoi}_{RCS-4}$ ,  $\mathbf{WmMoi}_{KCS-8}$ , and  $\mathbf{WmMoi}_{RCS-8}$ .

### *Special Considerations in Determining Net Heat Change (Q)*

The minus sign indicates that spontaneous processes always tend to eliminate gradients (i.e., slopes). If a field (e.g., a temperature field) increases in one direction, then the associated flow (e.g., conductive heat transfer) will be in the opposite direction. This scenario arises throughout physics. We know that Fourier's Law is:

$q = -\lambda \frac{dT}{dz}$ , the negative sign in Fourier's equation indicates that the heat flow is in the direction of negative gradient temperature and that serves to make heat flow positive.

From Equation (12), the rate of change in heat storage within the soil, we arrive at the following expression.

$$Q = -C_v \frac{\partial T_{soil}}{\partial t} \Delta Z = -C_v \frac{(T_{Soil_0} - T_{Soil_1})}{\partial t} \Delta Z$$

- $\frac{\partial T_{soil}}{\partial t}$  is the time rate of temperature change within the soil layer
- $T_{Soil_0}$  is the temperature of the soil 15 minutes prior
- $T_{Soil_1}$  is the present temperature
- $C_v$  is the volumetric heat capacity of the soil
- The negative sign describes the direction of heat transfer

The rate of change in heat storage within the soil is *net change, Q*, which means that it is the result of the building and soil surface heat flows interacting together.

Generally, the rate of change in heat storage within the soil is net change, Q, which is positive downwards (Snyder and Paw-U, 2001). Therefore, there are two cases of one-dimensional heat transfer problems, considering equation (12):

### Case 1

**Q is positive (+ve), or  $\frac{\partial T_{soil}}{\partial t}$  is negative (-ve).** [Here, the temperature of the soil 15 minutes before,  $T_{Soil_0} < \text{Present Temperature, } T_{Soil_1}$ .]: If  $T_{Soil_1}$  is greater than  $T_{Soil_0}$  this means  $\partial T_{soil} = T_{Soil_0} - T_{Soil_1} = -ve$  (negative), which means the soil is warming. *If this happens in the heating season (wintertime), that means that the soil is buffering heat loss from the building.* This condition of the substrate during the wintertime in a green roof system will reduce the heating load of a building. But if  $T_{Soil_1} < T_{Soil_0}$ , this means  $\frac{\partial T_{soil}}{\partial t}$  is positive (+ve), which means that the roof *is wicking heat away from the building in the wintertime* of the year.

Heating season is a period in the year (determined by mean climatic indicators of many years) when it is necessary to provide heat to buildings and premises to ensure comfortable living and working thermal conditions for occupants. The cooling load is the amount of heat energy that would need to be removed from a space to maintain the temperature in an acceptable range.

### Case 2

**Q is negative (-ve) or,  $\frac{\partial T_{soil}}{\partial t}$  is positive (+ve)** [Here, the temperature of the soil 15 minutes before,  $T_{Soil_0} > \text{Present Temperature, } T_{Soil_1}$ .]: If  $T_{Soil_0}$  is greater than  $T_{Soil_1}$ , this means  $\partial T_{soil} = T_{Soil_0} - T_{Soil_1} = +ve$  (positive). This, in turn, means that the soil is cooling, and *if this happens in the cooling season (summertime), the soil is buffering heat gain entering the building.* This condition of the substrate during the summertime in a green system will reduce the cooling load of a building. But if  $T_{Soil_0} < T_{Soil_1}$ , this means the condition *is increasing the heat gain of*

the building in the summertime of the year. This thermal state is not energy efficient in the summertime.

**Case 3, particular to the conditions at APD-EGR:**

$Q$  is zero (0) or,  $\frac{\partial T_{soil}}{\partial t}$  is zero (0) [The temperature of the soil 15 minutes before,  $T_{Soil_0}$  = present Temperature,  $T_{Soil_1}$ ]: This is a rare and complicated scenario in terms of soil physics and building science. An observation like this indicates different thermal dynamics if it occurs in the building’s envelope (the separator between interior and exterior spaces) or on the ground/earth.

If there is not a net change in ground heat storage, the soil is in equilibrium, and the heat is neither flowing in nor out. However, at the APD-EGR this can occur during either the heating season or the cooling season.

At the APD-EGR this condition indicates steady state heat flow: heat is flowing to or from the building at a steady rate while not changing heat stored in the soil.

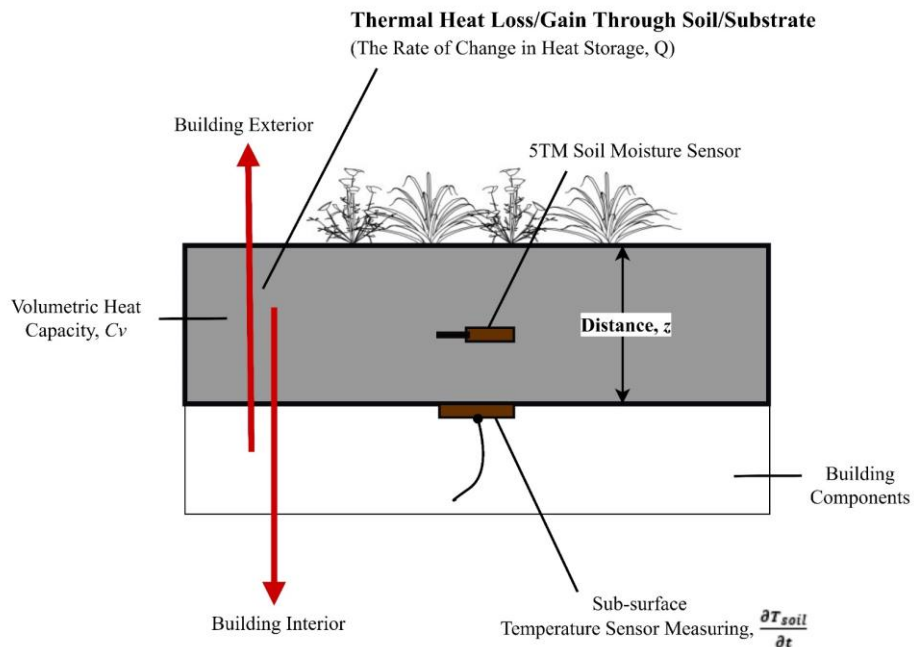


**Figure 3.23.** Diagram depicting thermal energy loss and gain through the soil layer at the APD-EGR with volumetric heat capacity,  $C_v$ . (Diagram by author.)

Soil heat flow direction is critical for this research. The primary purpose of this study is to explore the soil moisture content in two different substrates [(Kansas BuildEx® (**K**) and rooflite® (**R**)] from two different depths (4 inch/10-cm and 8 inch/20-cm) and to explain how the soil moisture/volumetric water content affects the rate of change in heat storage (*Q-value= net change*) at APD-EGR.

For homogeneous soils  $C_v$  may be considered as independent of  $z$  (constant with depth) (Selker and Or, 2021). However, the study is designed in such a way that soil porosity (*sp*), and the fractional volume of soil organic matter ( $\phi$ ) are assumed to remain constant because: i) the sensor plots sizes are very small (~roughly 1.2m x 1.2m); ii) only mix C plots (native grasses and forbs) were chosen (because the root biomass analysis confirms the highest concentration of organic material in C plots); iii) soil porosities of two different substrates were determined through lab analysis and should remain the same for at least one year. The soil moisture content (recorded as volumetric water content ( $\theta_v$ ) by the dataloggers connected to the 5TM sensors) is dependent on weather conditions at the APD-EGR.

The study considered  $C_v$  to be dependent on the volumetric water ( $\theta_v$ ) of the twelve selected plots (4-3KC, 4-7KC, 4-18KC, 4-6RC, 4-10RC, 4-19RC, 8-5KC, 8-10KC, 8-17KC, 8-3RC, 8-8RC, and 8-20RC). Thus, the rate of change in heat storage within the soil layer of each homogeneous soil/substrate plot (Kansas BuildEx® (**K**) or rooflite® (**R**) substrates) depended on volumetric water content ( $\theta_v$ ), and the depth ( $\Delta z$ ) of plots. Another critical independent variable of this study was local climate and weather.

Therefore, substrate types, substrate depths, and volumetric water content of each plot were determined to be the independent variables. The primary dependent variable of this study was the rate of change in heat storage (approximated *Q-value= net change*) of each plot in two different depths. Most of the water holding capacity of a green roof system is dependent on the substrate type and depth (Best et al., 2015). The study discusses critical factors such as directions, thermal buffers related to soil moisture content and their effect on net change.

### ***Research Time Period / In-situ Data Collection Duration***

In Manhattan, Kansas, the summers are hot, humid, wet, and mostly clear. The winters are very cold, snowy, windy, and partly cloudy. Over the course of the year, the temperature typically varies from 20°F to 92°F and is rarely below 3°F or above 101°F (Weatherspark, 2020-2021).

### ***Average Temperature in Manhattan, Kansas, United States***

Based on 1972-2021 weather data k (Weatherspark, 2020-2021), the hot season lasts for 3.5 months, from June 1 to September 16, with an average daily high temperature above 81°F. The hottest month of the year in Manhattan is July, with an average high of 91°F and low of 69°F. The cold season lasts for 3.0 months, from November 26 to February 26, with an average daily high temperature below 50°F. The coldest month of the year in Manhattan is January, with an average low of 20°F and high of 41°F (Weatherspark, 2020-2021).

The wetter season lasts 5.8 months, from April 6 to September 29, with a greater than 25% chance of a given day being a wet day. The month with the most wet days in Manhattan is June, with an average of 12.3 days with at least 0.04 inches (1.02 mm) of precipitation. The drier season lasts 6.2 months, from September 29 to April 6. The month with the fewest wet days in Manhattan is January, with an average of 2.7 days with at least 0.04 (1.02 mm) inches of precipitation (Weatherspark, 2020-2021).

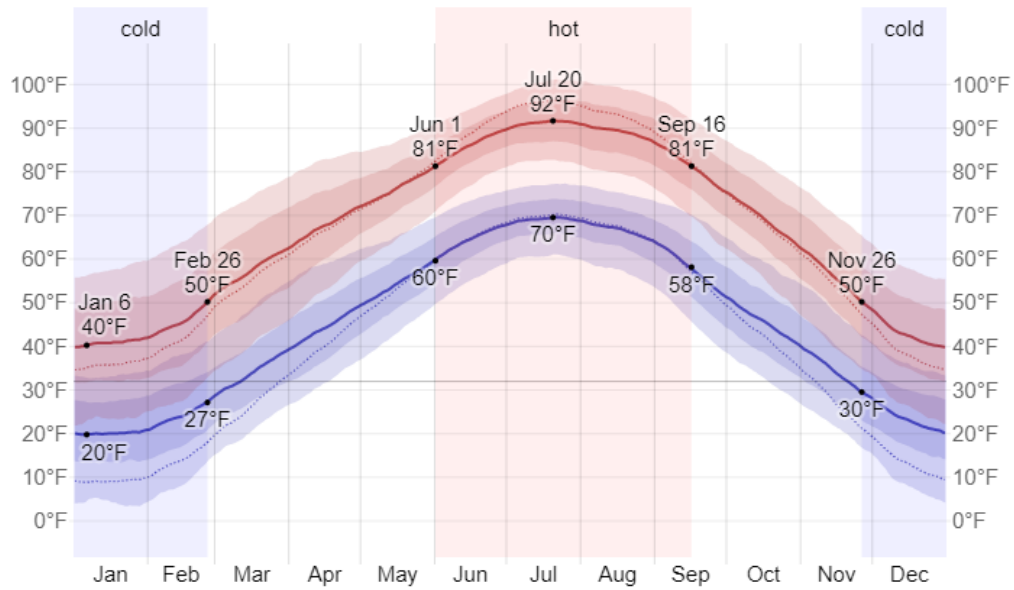


**Figure 3.24.** Average (1972 - 2021) high and low temperatures in Manhattan, Kansas, USA (Weatherspark, 2020-2021).

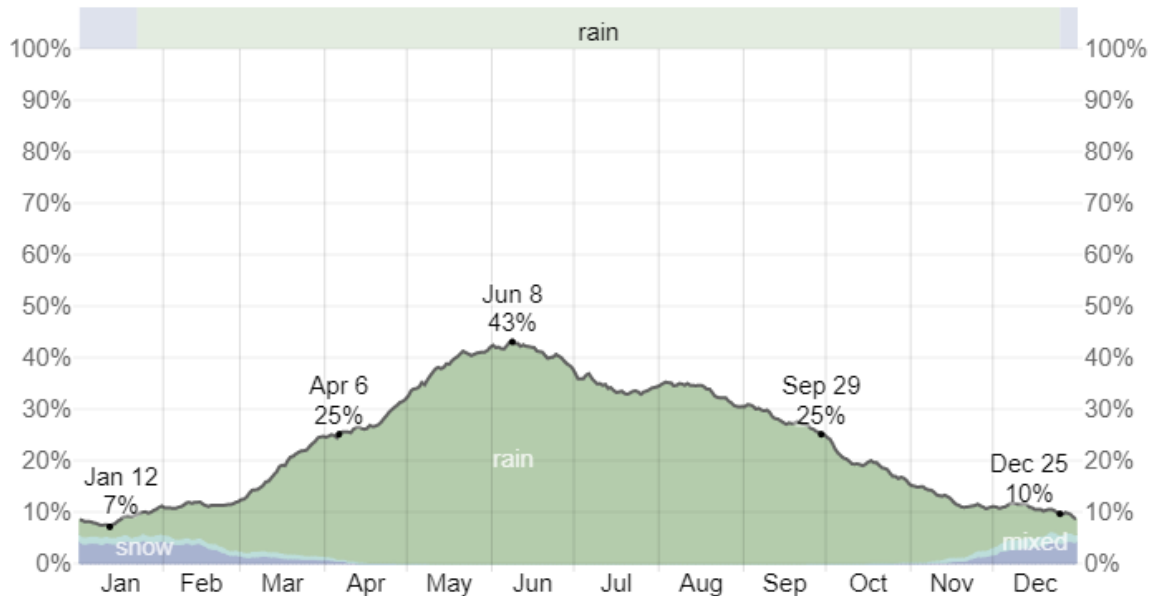


**Figure 3.25.** Average (1972 - 2021) daily chance of precipitation in Manhattan, Kansas, USA (Weatherspark, 2020-2021).

The percentage of days in which various types of precipitation are observed, excluding trace quantities: rain alone, snow alone, and mixed (both rain and snow fell in the same day).

Using the above graph (Figure 3.24), it was decided that a comparison of the thermodynamics of the APD-EGR would be made between summer (June 15, 2020 to September 15, 2020) and winter (November 15, 2020 to February 15, 2021). The in-situ data collection timeline and total continuous duration of data collection are given below in Table 3.15.

**Table 3.14** Total Data Collection Points and Duration.

<b>Time</b>	<b>Date</b>	<b>Total Days</b>	<b>Total Continuous Hours</b>	<b>Total Intervals for data collection (Data Points)</b>
<b>Summer</b>	Jun 15, 2020 - Sep 15, 2020	93	2232	8928
<b>Winter</b>	Nov 15, 2020 - Feb 15, 2021	93	2232	8928

Therefore, substrate types, depths, and time (summer vs. winter) were determined to be the independent variables for this study. The aim of this study was to explore how the heat storage rate changes within the soil or substrate layer at different moisture content (volumetric water content) in two extreme weather conditions (during average high and low temperatures in the Flint Hills Ecoregion at Manhattan, Kansas USA). All the findings related to the results are discussed in Chapter 4 (b), and the detailed discussions are in Chapter 5 (b).

## Chapter 4 - Results

### (a) Soil C Sequestration

In this chapter, all statistical outcomes and significant values have been discussed with necessary graphs and charts. Statistical analysis procedures have also been discussed in this section. Results from these chapters have been explained broadly with the required literature in chapter 5. Eight thermal graphs from in-situ measurements from summertime and wintertime have also been included here for the discussion. All tables and figures of each major section (a and b) in Chapter 4 were prepared by the author.

#### **Factors studied for the APD-EGR at KSU**

The factors involved in the statistical analyses are given below:

- **Two bed depths:** one bed approximately 4 inches deep (~10 cm) and one bed approximately 8 inches deep (~20 cm), each with 24 plots per depth.
- **Two substrates (soil types):** Kansas BuildEx® (K), with relatively high bulk density, low pore space, and higher water-holding capacity, and rooflite® (R), with relatively low bulk density, high pore space, and lower water-holding capacity:
  - 12 plots with K substrate in each bed.
  - 12 plots with R substrate in each bed.
- **Three plant mixes:** vegetation planted in three mixes of 18 plants (refer to Figure 3.1), with six species in each plot:
  - To ease the statistical analysis, in some cases, we used 0, 1, and 2 where, 0 = *Sedum* only, plant mix type A; 1 = *Sedum* + native grass, plant mix type B; 2 = native grasses + forbs, plant mix type C).

#### **Statistical analysis procedures for separate bed analysis**

Total organic C, N, and microbial biomass (MB) (from the soil PLFA analysis) were collected one time each for 2019 and 2020 and statistically analyzed using SAS Proc Mixed software (SAS Institute Inc., Cary, NC, USA), using the following steps:

- 1) First, the data were sorted by different bed depth (4-inch/10 cm vs. 8-inch/20 cm) and analyzed for each separately.
- 2) The substrate type and plant mix were analyzed as a strip-plot with four replications in each bed (strip-plot or strip-block were random effects), with year as a repeated measure.
- 3) The data presentation was informed by the mixed model analysis. If interactions were found to be nonsignificant, the main-effect means were presented. If the year interactions were significant, then it was presented as means by year.

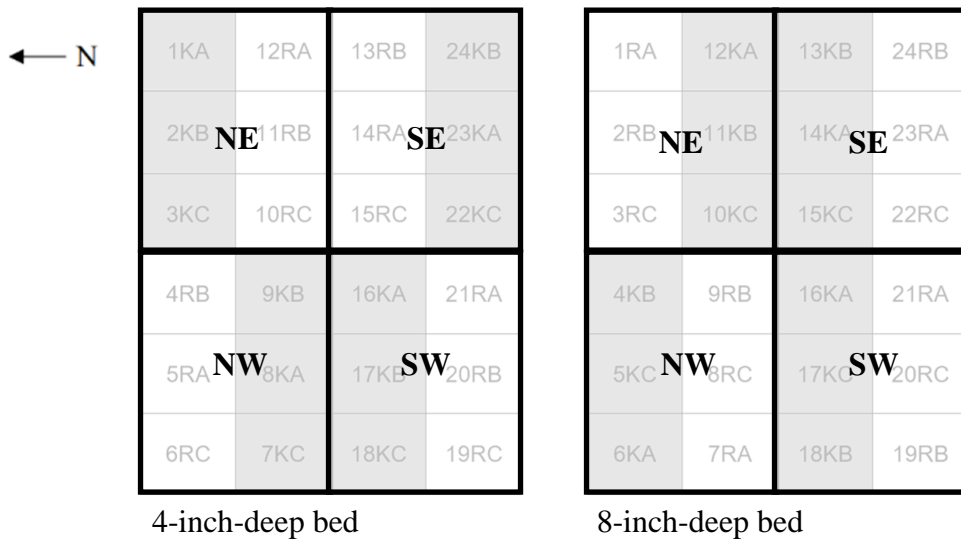


**Figure 4.1.** Four blocks (NE, NW, SE, SW) in the 4-inch- and 8-inch-deep beds, as allocated by the strip-plot design. (Diagram by author.)

Each bed in the experimental (APD-EGR) site incorporated a strip-plot or strip-block design, with four blocks per bed. The strip-plot design was used so that any confounding variables occurring due to spatial variability (for example, the direction of drainage), which may influence responses in the strip factors (substrate and mix), would be distributed uniformly among the blocks. Figure 4.1 shows the four blocks in the 4-inch and 8-inch-deep beds.

Mixed models are used when there is a mixture of fixed treatment effects and random effects (SAS Institute, n.d.). Mixed models recognize that observed data consists of two parts (Abdulnabi, 2004): 1) fixed effects; and 2) random effects. In this way, the fixed effects define

the expected values of the observations, whereas the random effects define the variance and covariances of the observations (Abdulnabi, 2004).

### ***Repeated-measures analysis***

Repeated measures are response outcomes that are measured on the same subject. Commonly, these measurements are made over a specified period of time (Abdulnabi, 2004). However, repeated measures can also refer to multiple measurements on an experimental unit under different conditions or in different places (Abdulnabi, 2004). Time is called a “within-subject” effect because there are different measurements at different times on the same subject (Abdulnabi, 2004). Explanatory variables, such as depth or soil type are called “between-subject” effects because their values change only from subject to subject; there is no different value for them at different times for the same subject (Abdulnabi, 2004). The effects of interest in the repeated-measures analysis used in this study are the interactions between the two types of effects, TREATMENT\*TIME.

### ***Repeated-measures ANOVA***

Repeated-measures ANOVA is the equivalent of the one-way ANOVA, but for related, not independent, groups and is the extension of the dependent t-test (Statistics, n.d.). The dependent t-test (also called the paired t-test or paired-samples t-test) is used to compare the means of two related groups to determine whether there is a statistically significant difference between those means (Statistics, n.d.). A repeated-measures ANOVA is also referred to as a within-subjects ANOVA or an ANOVA for correlated samples. All these names imply the nature of the repeated-measures ANOVA—a test to detect any overall differences between related means (Statistics, n.d.).

An F-statistic is a value obtained when running an ANOVA or a regression analysis to find out if the means between two populations are significantly different. It is like a t-statistic from a t-test. A t-test indicates if a single variable is statistically significant and an F test indicates if a group of variables is jointly significant (Statistics, n.d.).

**Total Organic Carbon (TOC) (derived from soil samples collected in 2019 and 2020)**

The TOC data collected in 2019 and 2020 were statistically analyzed for each separate bed, ~4-inch (~10-cm) and ~8-inch (~20-cm), to identify any significant interactions. The results of those statistical analyses are discussed below.

**Table 4.1.** Test of fixed effects on TOC of the 4-inch-deep bed (SAS output).

Effect	Num DF	Den DF	F value	Pr > F
Substrate	1	3	25.04	<b>0.0154**</b>
(Plant)Mix	2	6	1.12	0.3861
Substrate*(Plant)Mix	2	6	2.28	0.1833
Year	1	18	2.37	0.1408
Substrate*Year	1	18	2.43	0.1365
(Plant)Mix*Year	2	18	0.67	0.5248
Substrate*(Plant)Mix*Year	2	18	1.51	0.2474

\*\*Significant at the 5% level

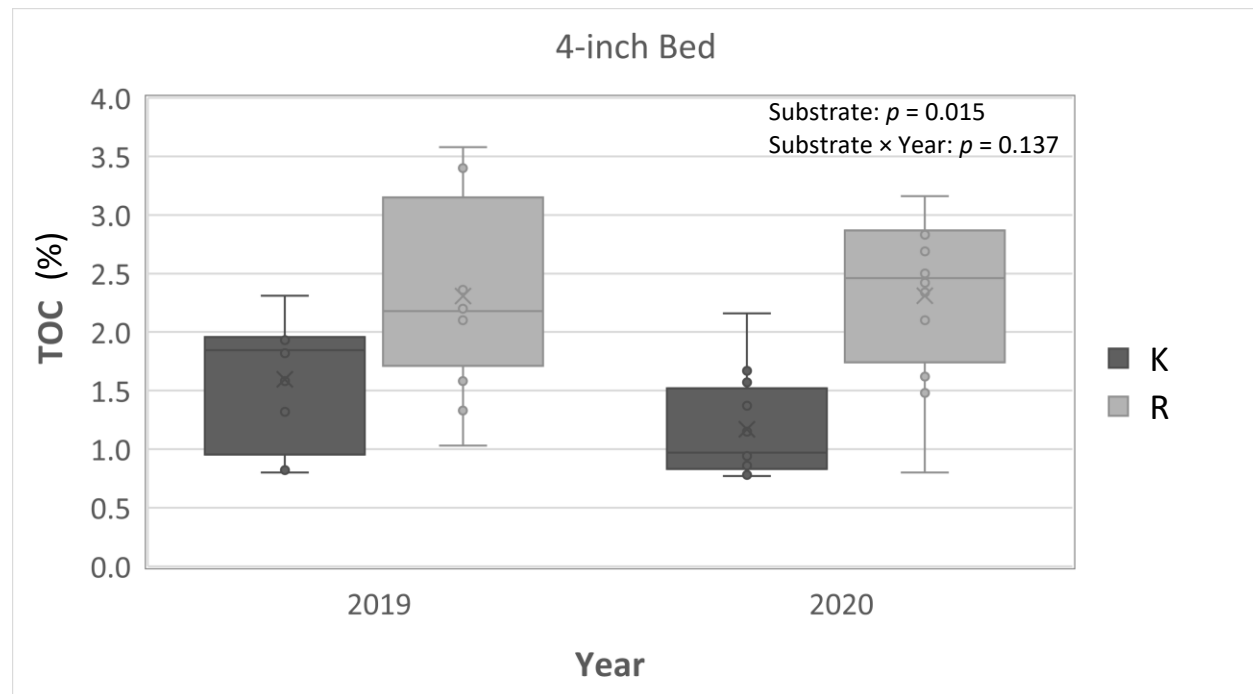


**Figure 4.2** Descriptive statistics, with box-and-whisker plots showing the data distribution for TOC from the two substrates (K and R) of the 4-inch-deep bed (comparing TOC with year).

From the ANOVA test of the 4-in-deep bed, TOC differed significantly between the two substrates, being higher for R than K (Figure 4.2, Table 4.1) ( $F[1, 3] = 25.04, p = 0.0154$ ).

**Table 4.2.** Test of fixed effects on TOC of the 8-inch-deep bed (SAS output).

Effect	Num DF	Den DF	F Value	Pr > F
Substrate	1	3	4.82	0.1157
(Plant)Mix	2	6	0.31	0.7458
Substrate*(Plant)Mix	2	6	0.36	0.7142
Year	1	18	7.60	<b>0.013**</b>
Substrate*Year	1	18	34.37	<b>&lt;.0001***</b>
(Plant)Mix*Year	2	18	0.75	0.4858
Substrate*(Plant)Mix*Year	2	18	0.13	0.8759

\*\*\*Significant at the 1% level, \*\*significant at the 5% level,

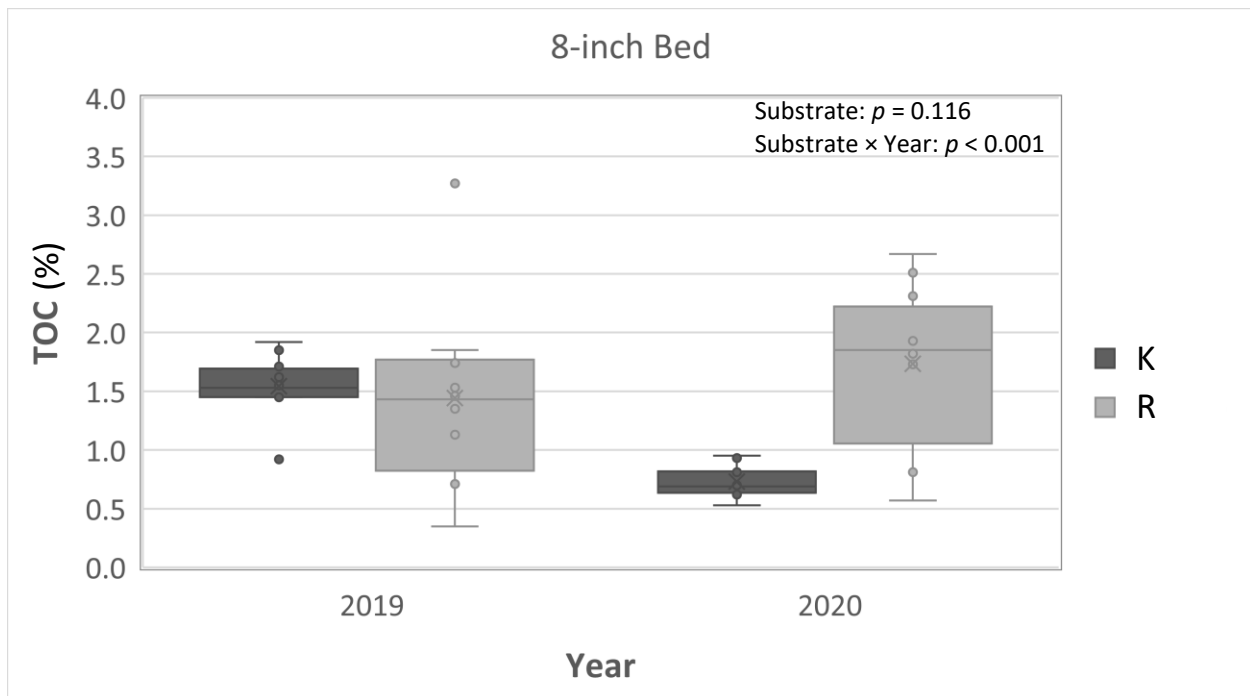


**Figure 4.3** Descriptive statistics, with box-and-whisker plots showing the data distribution for TOC from the two substrates (K and R) of the 8-inch-deep bed (comparing TOC with year).

From the ANOVA of the 8-inch-deep bed, the TOC was significantly different between the two years (2019 and 2020) and higher for substrate R in 2020 compared to 2019 (Figure 4.3, Table 4.2) ( $F[1, 18] = 7.60, p = 0.013$ ). There was a significant two-way interaction between the two years (Figure 4.4) and the two substrates (K and R) ( $F[1, 18] = 34.37, p < .0001$ ), as shown in Table 4.2.

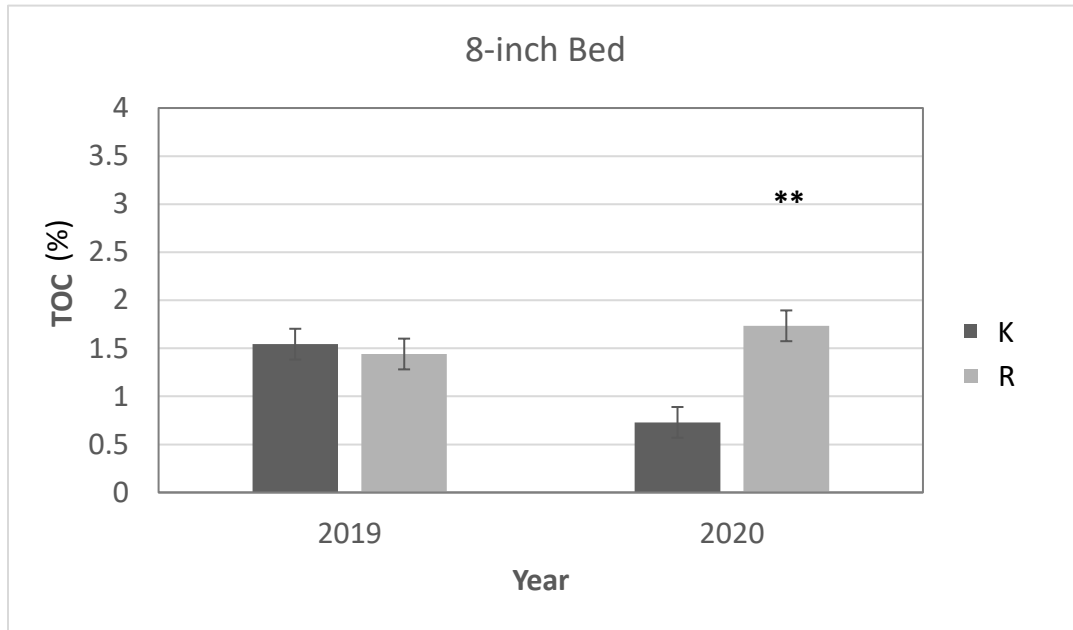


**Figure 4.4.** TOC means and standard errors from the 8-in-deep bed (comparing means of TOC from the two substrates (K and R) with year). \*\*Significant effect of TOC in two years ( $\alpha = 0.05$ ). Vertical bars denote upper and lower standard errors.

From Figure 4.4, it can be seen that the two-way substrate-by-year interaction is significantly different for TOC in the 8-inch bed due to a decrease in TOC in the K plots (Figure 4.4) in 2020 compared to 2019.

The SAS output for the statistical analyses by different bed (4-inch and 8-inch) and year (with year as the repeated measure) of TOC variations are reported in Appendix F.

### Total Nitrogen (TN) (derived from soil samples collected in 2019 and 2020)

The TN data collected in 2019 and 2020 were statistically analyzed by separate bed (4-inch and 8-inch), considering year as the repeated measure, to reveal significant interactions. The results of those statistical analyses are discussed below. Table 4.3 presents the F-test results with significant interactions for the 4-inch-deep bed.

**Table 4.3.** Test of fixed effects on TN of the 4-inch-deep bed (SAS output).

Effect	Num DF	Den DF	F Value	Pr > F
Substrate	1	3	21.19	<b>0.0193**</b>
(Plant)Mix	2	6	1.07	0.4008
Substrate*(Plant)Mix	2	6	1.33	0.3323
Year	1	18	1.58	0.2252
Substrate*Year	1	18	2.46	0.1339
(Plant)Mix*Year	2	18	0.15	0.8623
Substrate*(Plant)Mix*Year	2	18	1.58	0.2329

\*\*Significant at the 5% level.

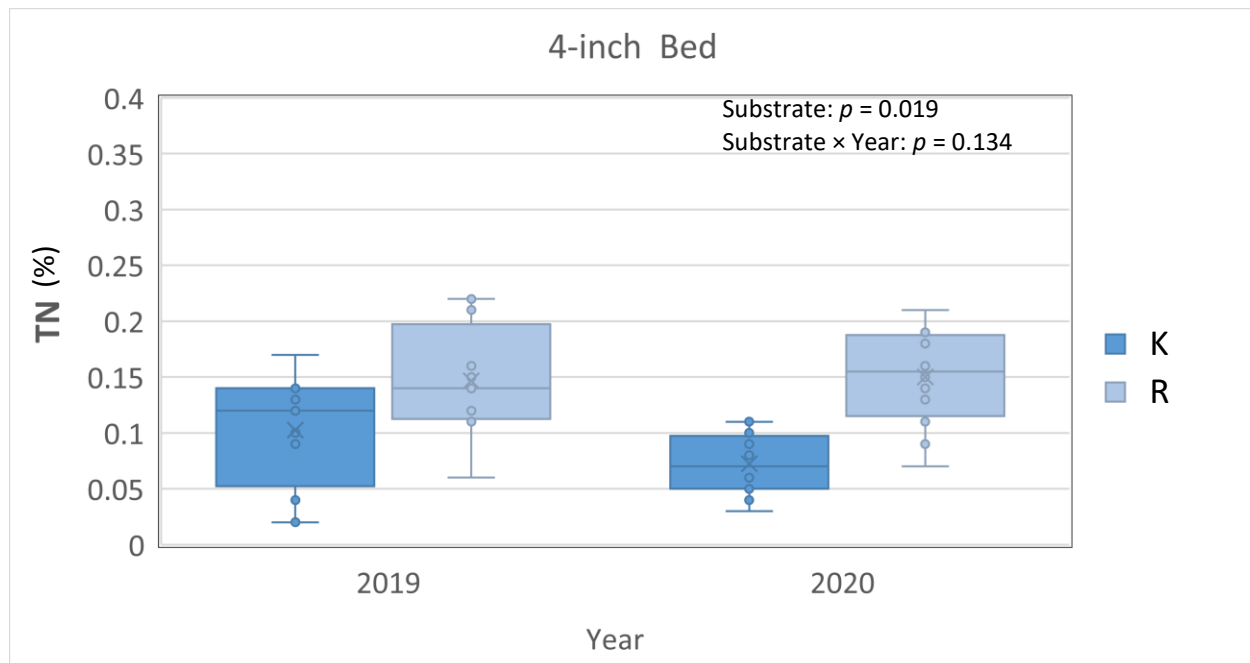


**Figure 4.5.** Descriptive statistics, with box-and-whisker plots showing the data distribution for TN from the two substrates (K and R) of the 4-inch-deep bed (comparing TN with year).

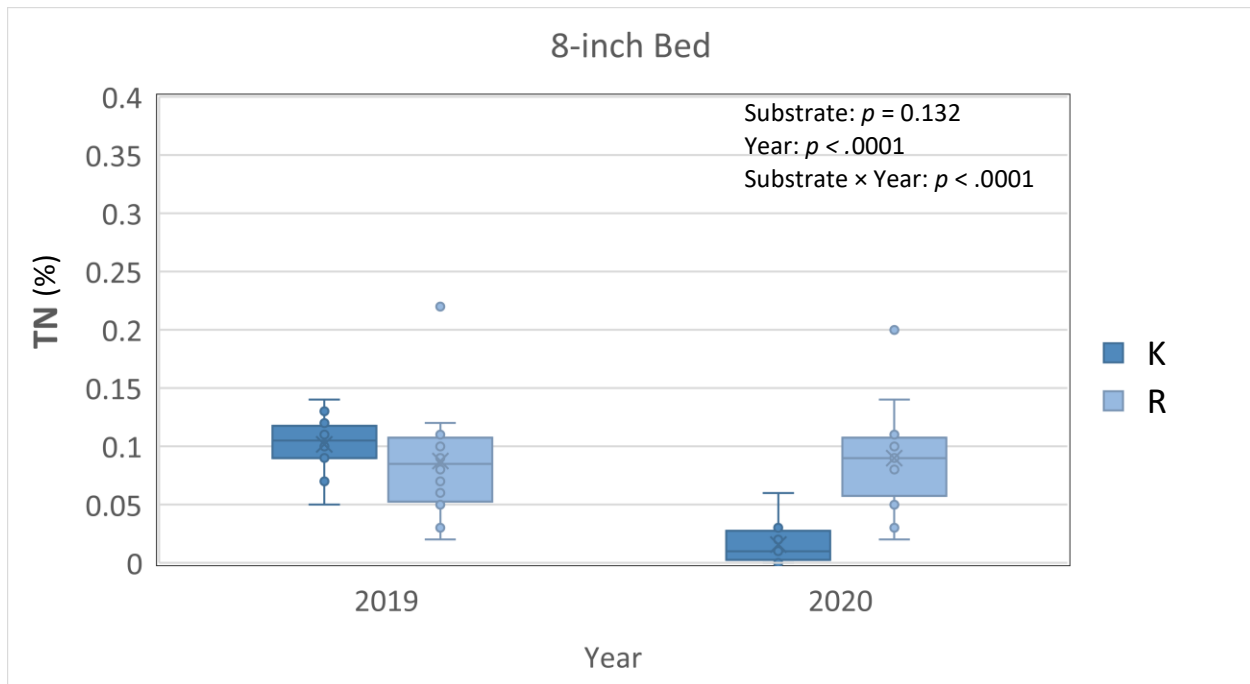
The TN was found to differ significantly different between the two substrates (K and R) in the 4-inch-deep bed ( $F[1, 3] = 21.19, p = 0.019$ ) (Table 4.3). Also, the TN in substrate R was higher than in K in the 4-inch-deep bed (Figure 4.5).

Table 4.4 presents the F-test results with significant interactions for the 8-inch-deep bed.

**Table 4.4.** Test of fixed effects on TN of the 8-in-deep bed (SAS output).

Effect	Num DF	Den DF	F Value	Pr > F
Substrate	1	3	4.23	0.1321
(Plant)Mix	2	6	0.09	0.9147
Substrate*(Plant)Mix	2	6	0.46	0.6506
Year	1	18	33.78	<.0001***
Substrate*Year	1	18	37.96	<.0001***
(Plant)Mix*Year	2	18	1.16	0.3362
Substrate*(Plant)Mix*Year	2	18	0.35	0.7108

\*\*\*Significant at the 1% level.



**Figure 4.6.** Descriptive statistics, with box-and-whisker plots showing the data distribution for TN from the two substrates (K and R) of the 8-inch-deep bed (comparing TN with year).

From the ANOVA (F-test) of the 8-inch-deep bed, TN appeared to be significantly different between the two years (2019 and 2020), and higher for substrate R in 2020 than in 2019 (Figure 4.6, Table 4.4), ( $F[1, 18] = 33.78, p < 0.0001$ ). There was significant two-way interaction between the years (Figure 4.7) and substrates (K and R) ( $F[1, 18] = 37.96, p < .0001$ ), as shown in Table 4.4.

From Figure 4.7, it can be seen that the two-way substrate-by-year interaction is significantly different for TN in the 8-inch-deep bed due to a decrease in TN in substrate K (Figure 4.7) in 2020 compared to 2019.

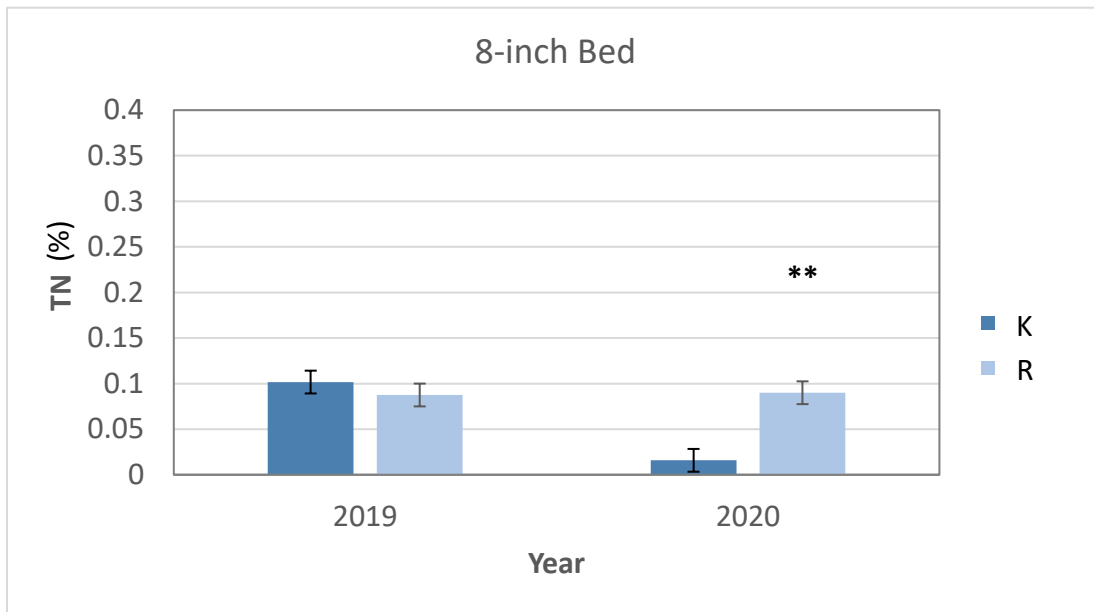


**Figure 4.7.** TN means and standard errors from the 8-inch-deep bed (comparing the means of TN from the two substrates (K and R) with year). **\*Significant effect of TN in two years ( $\alpha = 0.05$ ).** Vertical bars denote upper and lower standard errors.

The SAS output for the statistical analyses by the different bed (4 inch and 8 inch) and year (year as the repeated measure) of the TN variables are reported in Appendix G.

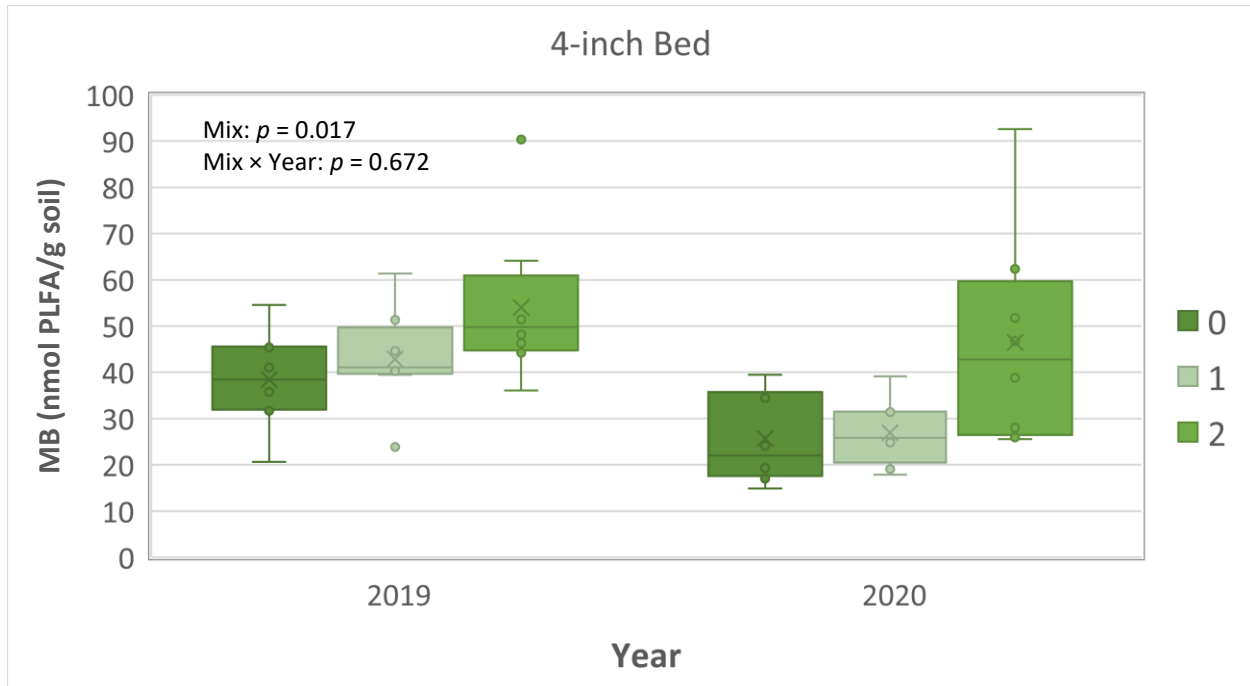
### Microbial Biomass (MB) (derived from soil samples collected in 2019 and 2020)

The MB data collected from the PLFA analyses in 2019 and 2020 were statistically analyzed by bed (4-inch and 8-inch), considering year as the repeated measure to reveal significant interactions. The results of those statistical analyses are discussed below. Table 4.5 provides the F-test results with significant interactions from the 4-inch-deep bed.

**Table 4.5.** Test of fixed effects on MB of the 4-inch-deep bed (SAS output).

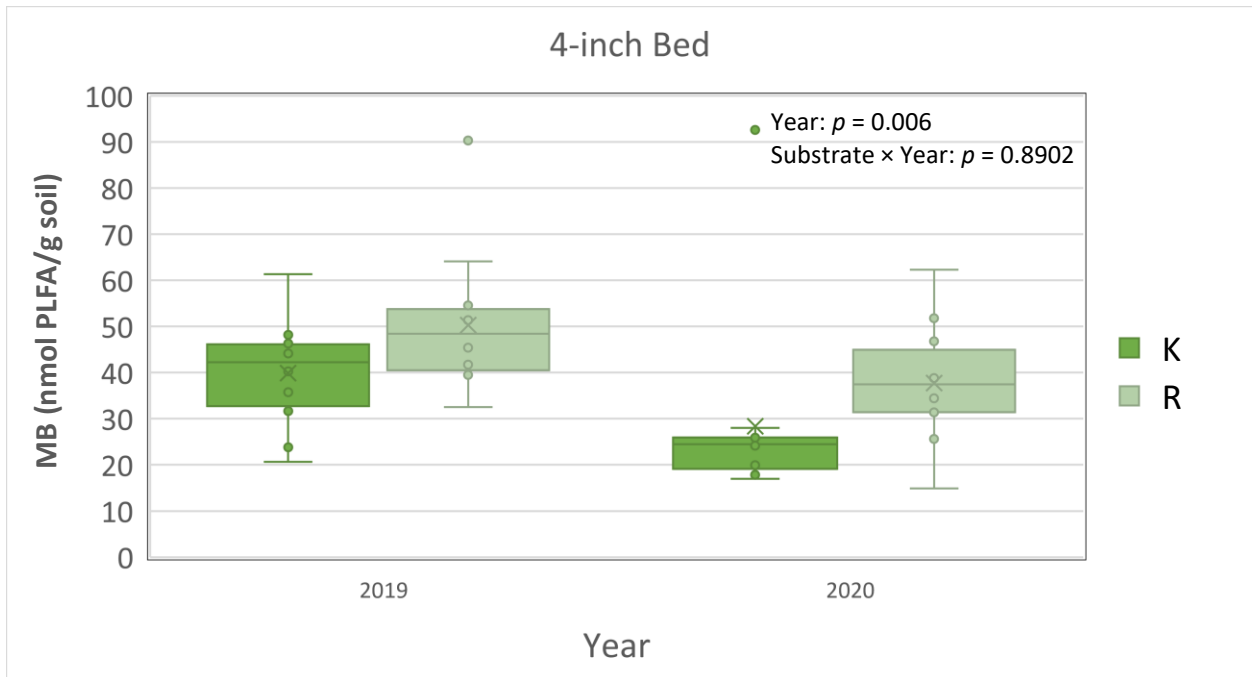
Effect	Num DF	Den DF	F Value	Pr > F
Substrate	1	3	5.6	0.0988
(Plant)Mix	2	6	8.64	<b>0.0171**</b>
Substrate*(Plant)Mix	2	6	0.41	0.6837
Year	1	18	9.88	<b>0.0056**</b>
Substrate*Year	1	18	0.02	0.8902
(Plant)Mix*Year	2	18	0.41	0.672
Substrate*(Plant)Mix*Year	2	18	0.77	0.4773

\*\*Significant at the 5% level.



**Figure 4.8.** Descriptive statistics, with box-and-whisker plots showing the data distribution for MB from the three plant mixes (A, B, and C) of the 4-inch-deep bed (comparing MB with year). (0—*Sedum* only, plant mix type A; 1—*Sedum* + native grass mix, plant mix type B; 2—native grasses + forbs, plant mix type C).

The MB was found to be significantly different in the 4-inch-deep bed among the belowground biomass samples of plant mix types A, B, and C ( $F[2, 6] = 8.64, p = 0.0171$ ) (Table 4.5). Figure 4.8 indicates that the below-ground MB in plant mix type C was higher than in plant mix types B or A in the 4-inch-deep bed ( $p = 0.0171$ ). The statistical analyses from the 4-inch-deep bed also showed that year (MB data from 2019 and 2020) had a significant effect ( $F[1, 18] = 9.88, p = 0.0056$ ) (Table 4.5, Figure 4.8), with an overall higher microbial concentration in substrate R compared with K (Figure 4.9).



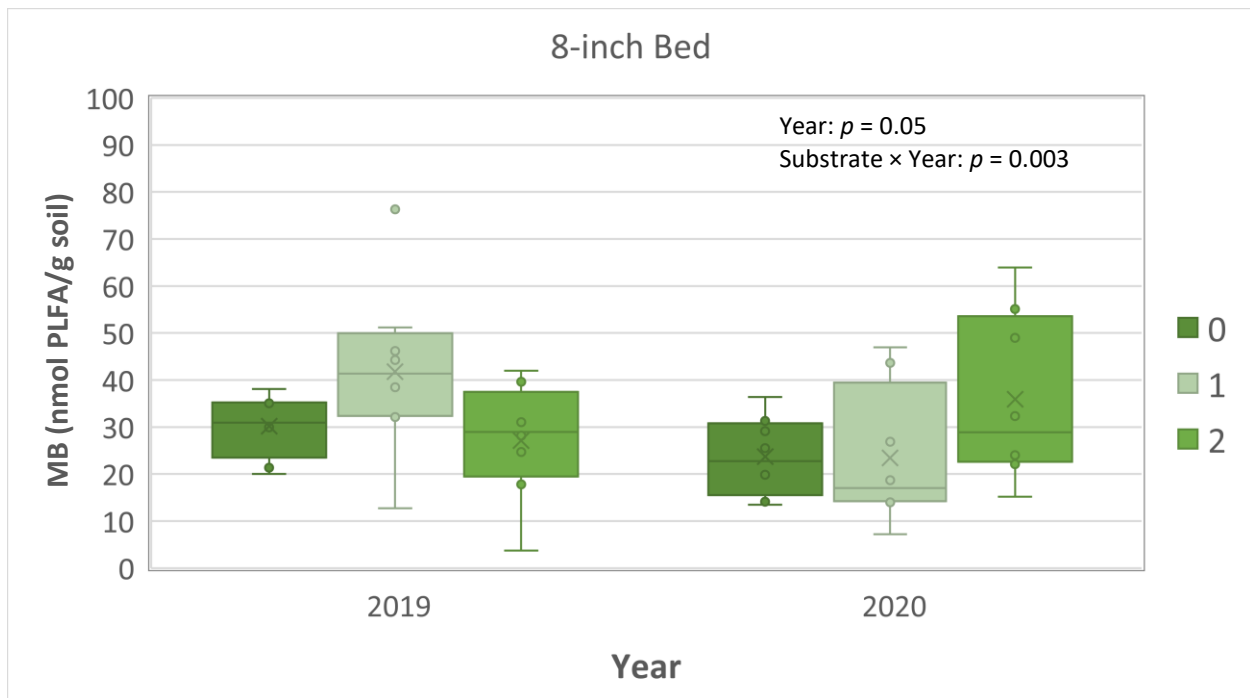
**Figure 4.9.** Descriptive statistics, with box-and-whisker plots showing the data distribution for MB from the two substrates (K and R) of the 4-inch-deep bed (comparing MB with year).

Table 4.6 provides the F-test results with significant interactions from the 8-inch-deep bed.

**Table 4.6.** Test of fixed effects on MB of the 8-in-deep bed (SAS output).

Effect	Num DF	Den DF	F Value	Pr > F
Substrate	1	3	2.96	0.1837
(Plant)Mix	2	6	0.62	0.5668
Substrate*(Plant)Mix	2	6	0.85	0.4728
Year	1	18	4.35	<b>0.0516**</b>
Substrate*Year	1	18	11.73	<b>0.003***</b>
(Plant)Mix*Year	2	18	9.37	<b>0.0016***</b>
Substrate*(Plant)Mix*Year	2	18	1.69	0.2129

\*\*\*Significant at the 1% level, \*\*significant at the 5% level.



**Figure 4.10.** Descriptive statistics, with box-and-whisker plots showing the data distribution for MB from the three plant mix types (A, B, and C) of the 8-in-deep bed (comparing MB with year). (0—*Sedum* only, plant mix type A; 1—*Sedum* + native grass mix, plant mix type B; 2—native grasses + forbs, plant mix type C).

From the ANOVA (F-test) of the 8-inch-deep bed, MB was significantly different between the two years (2019 and 2020) ( $F[1, 18] = 4.35, p = 0.0516$ ) (Table 4.6, Figure 4.10). Figure 4.11 and Table 4.6 indicate that the two-way substrate-by-year interaction was significantly different for MB in the 8-inch-deep bed due to a decrease in MB in the K substrate plots in 2020 compared with 2019 ( $F[1, 18] = 11.73, p = 0.003$ ).

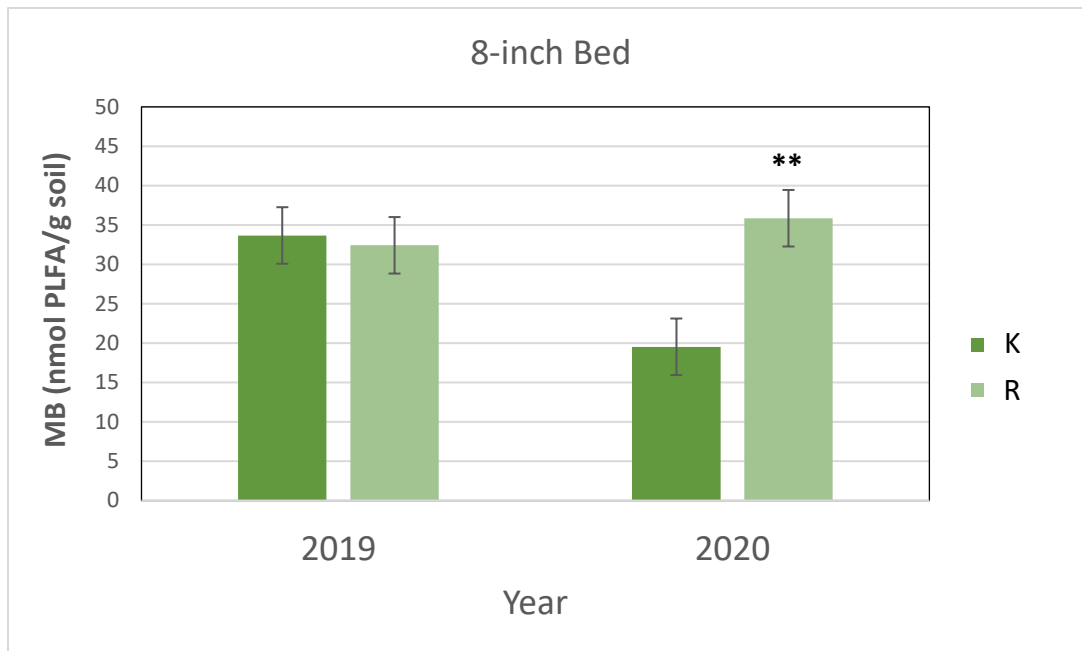


**Figure 4.11.** MB means and standard errors from the 8-inch-deep bed, comparing the means of MB from the two substrates (K and R) with year. **\*\*Significant effect of MB in two years ( $\alpha = 0.05$ ).** Vertical bars denote upper and lower standard errors.

The two-way plant-mix-type-by-year interaction was significantly different for MB in the 8-inch bed due to a decrease in MB in the plant mix type B plots in 2020 compared to 2019 ( $F[2, 18] = 9.37, p = 0.0016$ ), as shown in Figure 4.12 and Table 4.6.

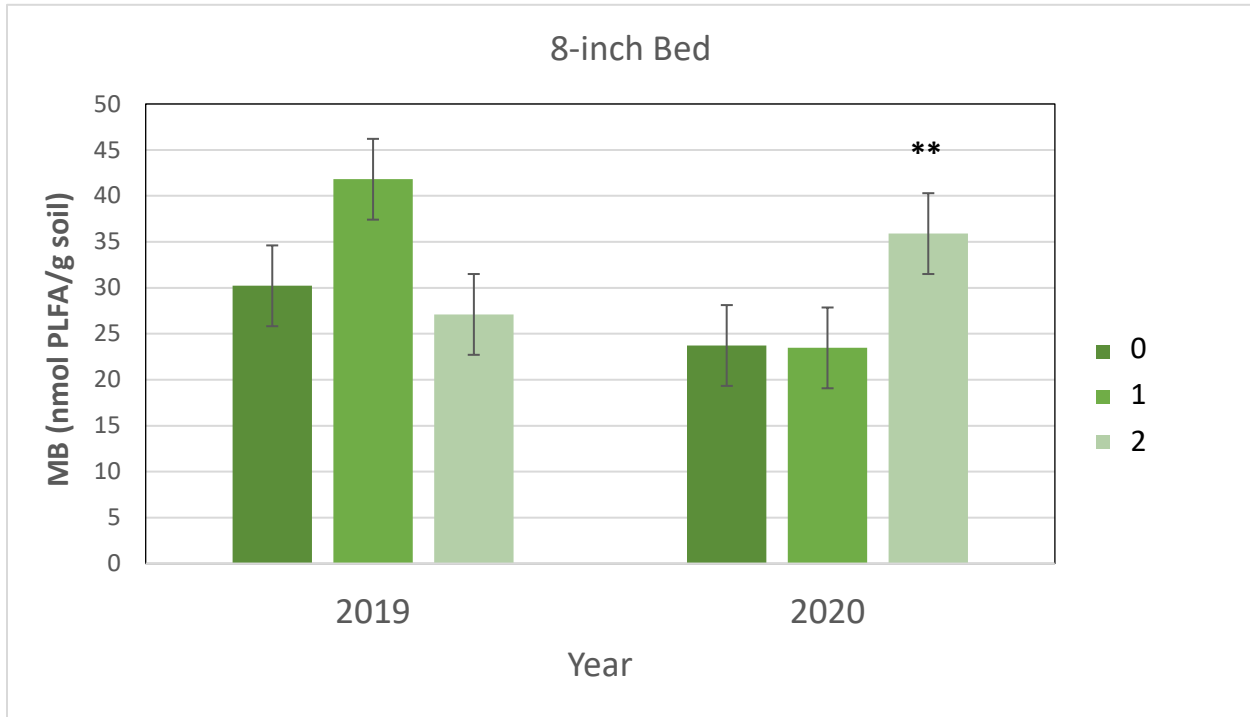


**Figure 4.12.** MB means and standard errors from the 8-inch-deep bed, comparing means of MB from the three plant mixes (A, B, and C) within the year. **\*\*Significant effect of MB in the two years ( $\alpha = 0.05$ ).** Vertical bars denote upper and lower standard errors. (0—*Sedum* only, plant mix type A; 1—*Sedum* + native grass mix, plant mix type B; 2—native grasses + forbs, plant mix type C).

The SAS output for the statistical analyses of MB for the 4-inch and 8-inch beds and year (with the year as the repeated measure) is reported in Appendix H.

Considering the statistical analyses presented above, the following section summarizes the results and discusses known, likely, and potential influences and interrelationships.

### *Summary of the statistical results from the repeated-measures ANOVA*

- 1) In the 4-inch-deep bed, the TOC and TN were higher for substrate R than K, and the MB was higher in the below-ground biomass of plant mix type C (native grasses + forbs) compared to the biomass of plant mix type A (*Sedum* only) and B (*Sedum* + native grasses).
- 2) The two-way substrate-by-year interactions for TOC, TN, and MB in the 8-inch-deep bed were due to decreases in the K substrate plots in 2020 compared to 2019.
- 3) Similarly, the two-way plant-mix-type-by-year interaction for MB in the 8-inch-deep bed was due to a decrease in MB in the plant mix type B (*Sedum* + native grasses) plots in 2020 compared to 2019.

To obtain more in-depth interpretations, statistical analyses of the root biomass and soil respiration data from 2020 were performed. The root biomass and respiration data complemented the repeated-measures ANOVA results and helped to the research team understand better the green roof's role in mitigating climate change in the Flint Hills Ecoregion. For root biomass and soil respiration, statistical data were evaluated using IBM SPSS Statistics 29 software. Significant differences were tested between the different dependent and independent variables using three-way ANOVA with Tukey's HSD post-hoc analysis. Table 4.7 provides the descriptive statistics of the root-density data from 2020.

### Root biomass (samples collected in 2020)

A three-way ANOVA was used to evaluate the effect of the three below-ground biomass samples (plant mix types A, B, and C), the two substrates (K and R), and the two soil depths (~4 inches/10 cm and 8 inches/20 cm) on root density, and their interactions. In addition, Tukey's HSD post-hoc test determined a pairwise comparison between two sets of groups, using IBM SPSS Statistics 29 software.

Root density was significantly different among the below-ground biomass of plant mix types A, B, and C ( $F[2, 36] = 18.92, p = 0.000$ ) (Table 4.7). Tukey's HSD post-hoc test indicated that the belowground root density for plant mix types C (mean =  $0.253 \text{ g/cm}^3$ ) and B (mean =  $0.233$ ) were higher than for type A (mean =  $0.075$ ) at  $p = 0.000$ .

**Table 4.7.** Descriptive statistics of the root density data.

Variable		Mean ( $\text{g/cm}^3$ )	Std. error	95% confidence interval	
				Lower bound	Upper bound
Depth	4 in	.206	.018	.169	.243
	8 in	.168	.018	.131	.205
Substrate	K	.193	.018	.156	.230
	R	.181	.018	.144	.218
Plant mix	A	.075	.022	.029	.120
	B	.233	.022	.188	.279
	C	.253	.022	.207	.298

Note: Mix type A—*Sedum* only; mix type B—*Sedum* + native grass; mix type C—native grasses + forbs.

### Root-density interpretations and discussion

The root biomass from the 4-inch-deep and 8-inch-deep beds were examined to better understand soil/substrate C-sequestration potential. From the three-way ANOVA, the below-ground biomass samples containing grasses (i.e., types B and C) had significantly higher root density (Table 4.8) than the *Sedum*-only plots in both the 4-inch-deep and 8-inch-deep beds. In the K and R substrates (Figure 4.13), the below-ground root densities of the three different plant mix types (more evident in types B and C) were relatively higher in the 4-inch-deep bed than the 8-inch-deep bed.

**Table 4.8.** Three-way ANOVA results of the root density data for the 4- and 8-in-deep beds (SPSS).

Variable	Sum of squares	df	Mean square	F	$\rho$ -value
Depth	.018	1	.018	2.210	.146
Substrate	.002	1	.002	.222	.641
Plant	.305	2	.153	18.920	<b>.000***</b>
Depth*Substrate	.002	1	.002	.237	.630
Depth*Plant	.011	2	.006	.701	.503
Substrate*Plant	.010	2	.005	.644	.531
Depth*Substrate*Plant	.017	2	.008	1.043	.363

\*\*\*Significant at the 1% level.

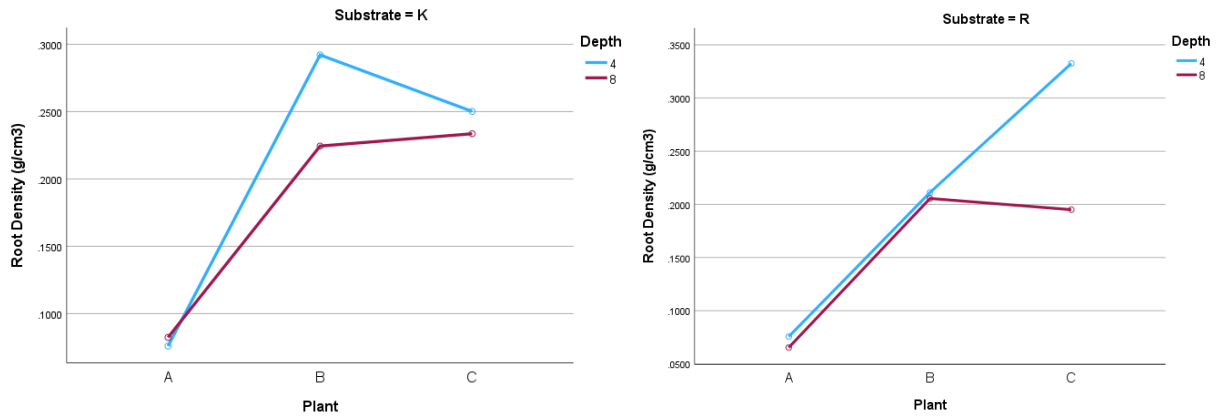


**Figure 4.13.** Average root density at two depths (4-inch and 8 inch) in the belowground biomass of plant mix types A, B, and C and the two substrates (K and R).

### Soil respiration (samples collected in 2020)

A three-way ANOVA was performed to evaluate the effect of the three plant mix types (A, B, and C), two substrates (K and R), and two soil depths (4-inch and 8-inch) on soil respiration, and their interactions. In addition to this, Tukey's HSD post-hoc test was used to determine a pairwise comparison between two sets of groups.

From the three-way ANOVA, soil respiration was found to be significantly different between the substrate types (Table 4.9, Figure 4.14), with higher respiration in R (mean = 954  $\mu\text{g CO}_2\text{-C/ g soil}$ ) than K (mean = 529  $\mu\text{g CO}_2\text{-C/ g soil}$ ) ( $F[1, 36] = 20.317, p = 0.000$ ) (Table 4.10). There was no significant two-way interaction effect between the variables.

**Table 4.9.** Descriptive statistics for soil respiration.

Variable		Mean ( $\mu\text{g CO}_2\text{-C/ g soil}$ )	Std. error	95% Confidence Interval	
				Lower Bound	Upper Bound
Substrate	K	529	66.625	394.285	664.530
	R	954	66.625	818.984	1089.229
Plant mix	A	700	81.599	534.345	865.326
	B	704	81.599	538.910	869.892
	C	821	81.599	655.543	986.525
Depth	4 in	652	66.625	517.270	787.515
	8 in	831	66.625	695.999	966.244

Note: Mix type A—*Sedum* only; mix type B—*Sedum* + native grass; mix type C—native grasses + forbs.

**Table 4.10.** Three-way ANOVA results for soil respiration (SPSS outputs)

Variable	Sum of squares	df	Mean square	F	p-value	Partial eta squared
Substrate	2164433.773	1	2164433.773	20.317	.000***	.361
Plant	151004.459	2	75502.229	.709	.499	.038
Depth	383327.756	1	383327.756	3.598	.066	.091
Substrate*Plant	265962.071	2	132981.035	1.248	.299	.065
Substrate*Depth	3958.692	1	3958.692	.037	.848	.001
Plant*Depth	339192.352	2	169596.176	1.592	.218	.081
Substrate*Plant*Bed	144541.546	2	72270.773	.678	.514	.036

\*\*\*Significant at the 1% level.

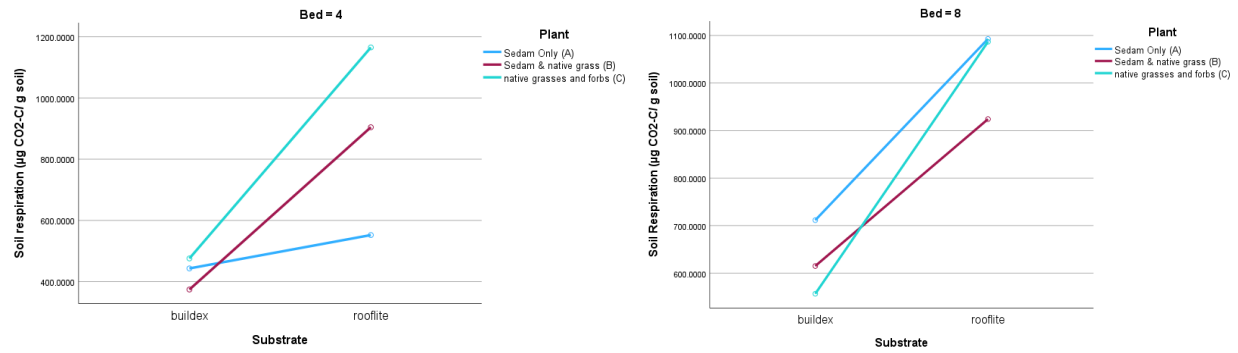


**Figure 4.14.** Soil respiration at two depths (4 and 8 in) in belowground biomass samples from three plant mix types (A, B, and C) and two substrates (K and R).

In this section, two different two-way ANOVAs were conducted in order to better understand the effects of plant mix type, substrate, and depth on soil respiration.

### *Results from the two-way ANOVA*

A two-way ANOVA evaluated the effect of three plant mix types (A, B, and C) and two substrates (K and R) on soil respiration and their interactions. In addition, Tukey’s HSD post-hoc test was used to determine a pairwise comparison between two sets of groups.

From the two-way ANOVA, soil respiration was significantly different between the substrate types, with higher respiration in R (mean = 954.1065) than K (mean = 529.4072) (Table 4. 11, Figure 4.15) ( $F[1, 42] = 19.315, p = 0.000$ ) (Table 4.12). In substrates, K and R (Figure 4.15), the soil respiration of plant mix type C (native grasses + forbs) was relatively higher in the R than in K. There was no significant two-way interaction effect between the variables.

**Table 4.11.** Descriptive statistics of soil respiration from the two-way ANOVA.

Variable		Mean ( $\mu\text{g CO}_2\text{-C/ g soil}$ )	Std. error	95% Confidence Interval	
				Lower Bound	Upper Bound
Substrate	K	529	68.329	391.513	667.302
	R	954	68.329	816.212	1092.001
Plant mix	A	699.835	83.686	530.950	868.721
	B	704.401	83.686	535.515	873.287
	C	821.034	83.686	652.149	989.920

Note: Mix type A—*Sedum* only; mix type B—*Sedum* + native grass; mix type C—native grasses + forbs.

**Table 4.12.** Two-way ANOVA results for soil respiration (SPSS outputs).

Variable	Sum of squares	df	Mean square	F	p-value	Partial eta squared
Substrate	2164433.773	1	2164433.773	19.316	.000***	.315
Plant	151004.459	2	75502.229	.674	.515	.031
Substrate * Plant	265962.071	2	132981.035	1.187	.315	.053

\*\*\* Significant at the 1% level.

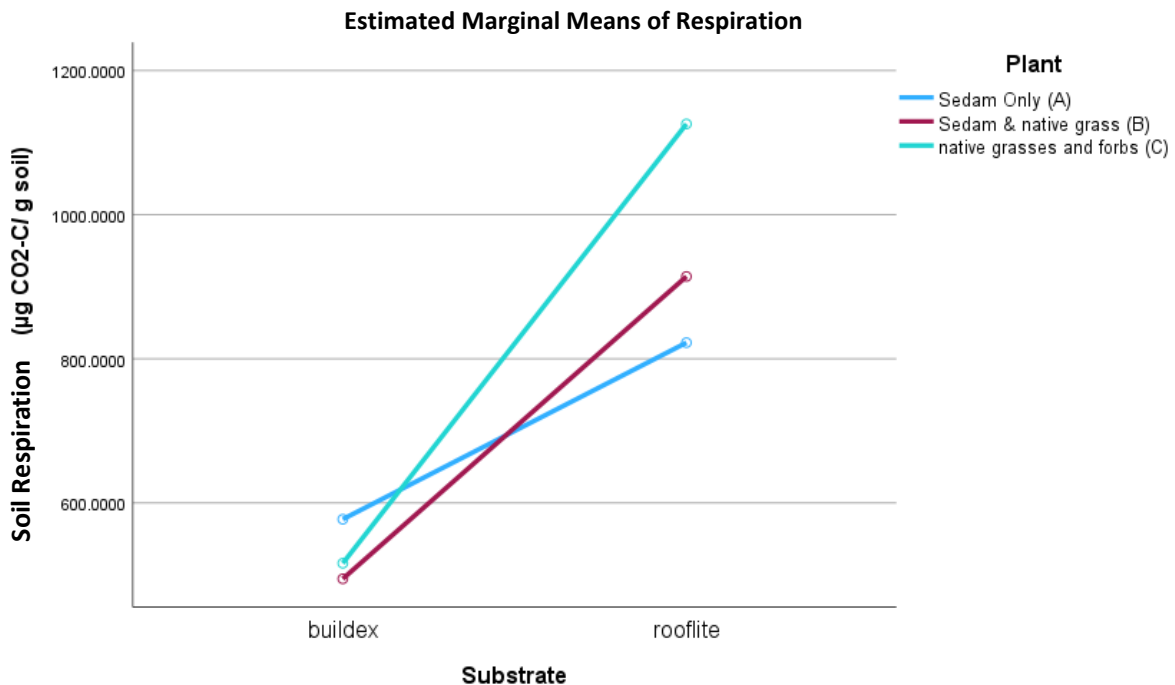


**Figure 4.15.** Soil respiration in belowground biomass samples of three plant mix types (A, B, and C) and two substrates (K and R).

Another two-way ANOVA was performed to evaluate the effect of three plant mixes (A, B, and C) and two soil depths (4-inch and 8-inch) on respiration and their interactions. In addition to this, Tukey’s HSD post-hoc test was used to determine a pairwise comparison between two sets of groups.

From the two-way ANOVA, soil respiration was not significantly different between plant mix types. Also, it was not significantly different between the plant mix types and soil depths. There was no significant two-way interaction effect between the variables (Tables 4.13, 4.14, Figure 4.16).

**Table 4.13.** Descriptive statistics of soil respiration.

Variable		Mean ( $\mu\text{g CO}_2\text{-C/ g soil}$ )	Std. error	95% Confidence Interval	
				Lower Bound	Upper Bound
Plant mix	A	699.835	97.698	502.673	896.998
	B	704.401	97.698	507.239	901.563
	C	821.034	97.698	623.872	1018.196
Depth	4 in	652.392	79.770	491.410	813.375
	8 in	831.121	79.770	670.139	992.103

Note: Mix type A—*Sedum* only; mix type B—*Sedum* + native grass; mix type C—native grasses + forbs.

**Table 4.14.** Two-way ANOVA results of respiration.

Variable	Sum of squares	df	Mean square	F	p-value	Partial eta squared
Plant	151004.459	2	75502.229	.494	.613	.023
Depth	383327.756	1	383327.756	2.510	.121	.056
Plant*Depth	339192.352	2	169596.176	1.111	.339	.050

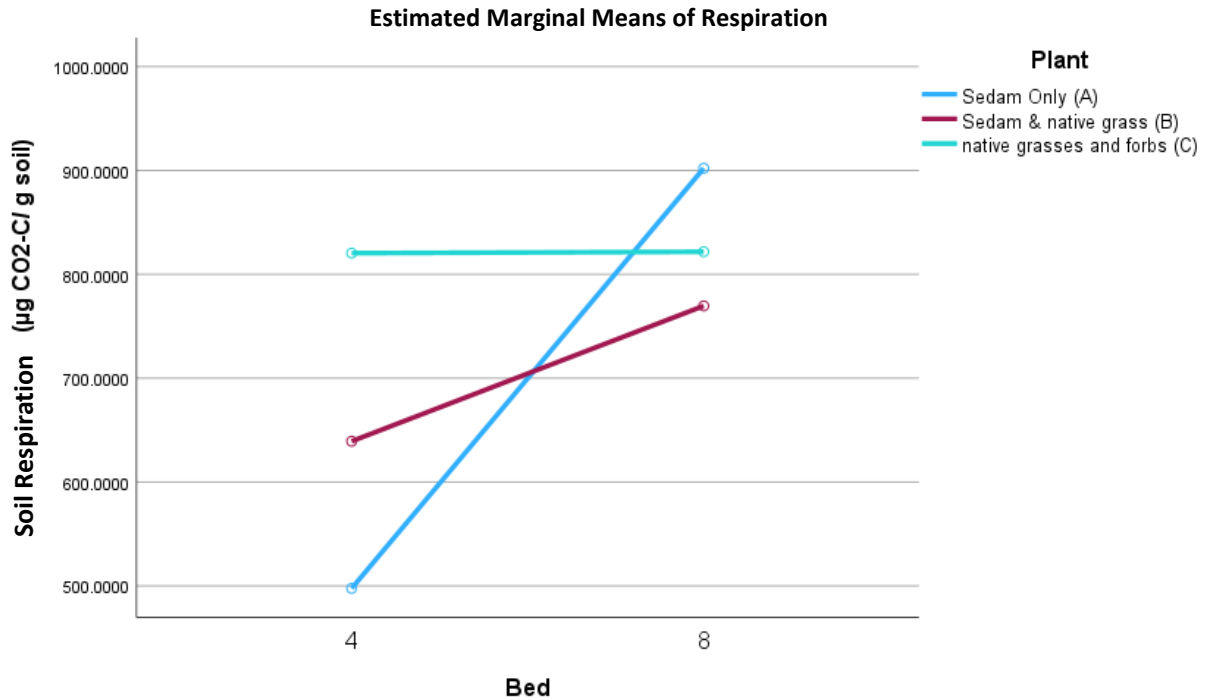


**Figure 4.16.** Soil respiration at two depths (4 and 8 in) and in three belowground biomass samples (A, B, and C).

### *Summary of statistical results from soil-respiration data*

Substrate R had higher soil respiration than K in both beds (4-inch and 8-inch). The ANOVA analyses showed that substrates K and R both had a significant effect on soil respiration, and relatively higher soil respiration was identified for plant mix type C (native grasses + forbs) (Tables 4.12, 4.13). Additional discussion is provided in Chapter 5.

## (b) Thermal analysis of the APD-EGR's Beds

Thermal graphs of two beds (4-inch and 8-inch) from summer months are given below:

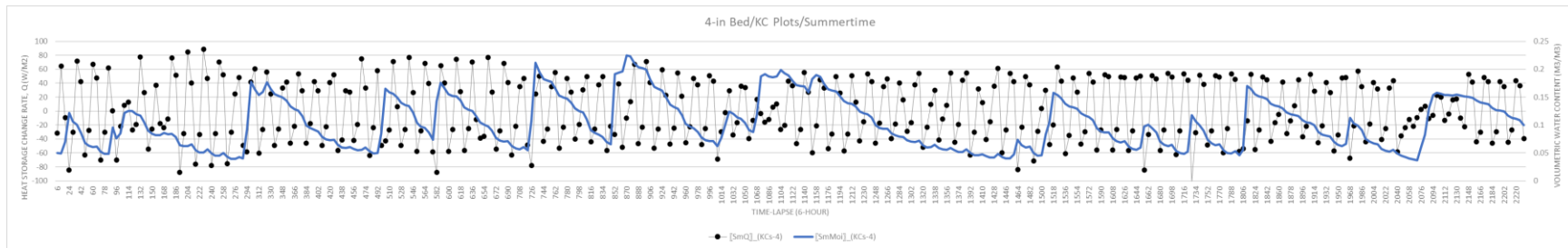


**Figure 4.17.** The rate of change in heat storage within the soil layer ( $Q$ -value) of all KC plots from 4-inch-deep beds at APD-EGR during the summertime.

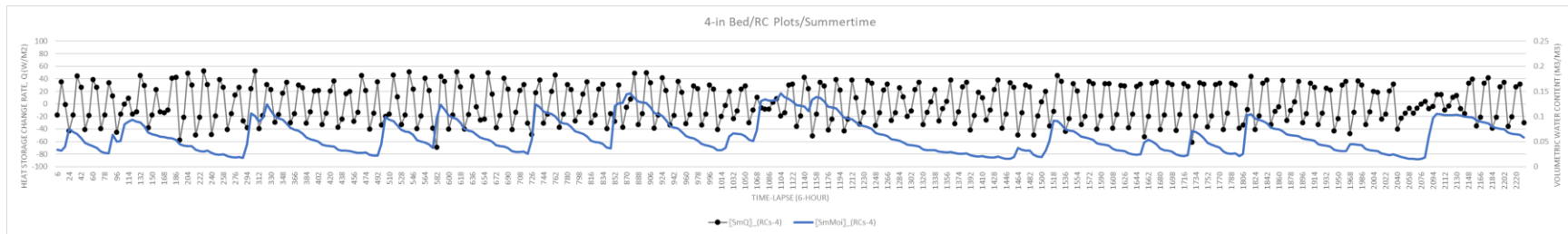


**Figure 4.18.** The rate of change in heat storage within the soil layer ( $Q$ -value) of all RC plots from 4-inch-deep beds at APD-EGR during the summertime.

From Fig 4.17 and 4.18, we can see that  $Q$ -value shows more negative gradients (values) in KC plots (Fig 4.17) than RC plots (Fig 4.18); because of its greater moisture holding capacity than RC plots. So, in the summertime (building cooling season), K substrate type in the 4-inch bed is buffering more heat gain from entering the building than the R substrate at nighttime. Cooling Seasonal Total Load means the total annual amount of heat that is removed from the indoor air when the equipment is operated for cooling in active mode. Active mode means the mode corresponding to the hours with a cooling or heating load of the building and

whereby the cooling or heating function of the unit is activated. In fact, “load” means the amount of heating or cooling a building needs (Bailes, 2015). Inversely, in the daytime, KC is increasing heat gain of the building more than RC because of its high percentage of positive  $Q$ -value in the 4-inch bed. We know that the specific heat of dry soil is 0.2 Cal/g, and water's specific heat is five (5) times higher than that, 1 Cal/g. Moist soils are generally cooler because the heat energy gets spent in the evaporation of soil moisture. The main cause of this situation is that KC is likely working as wetter soil and RC is working as slightly drier (moist) soil given precipitation and supplemental irrigation. Packed/dense bare soils are warmer than loose soils, and wet, dense soils are the warmest of all (Longstroth, 2012). Therefore, relatively moist R substate (more porosity) in the 4-inch bed showed potential to work better especially in the hot summer sun (daytime hours).

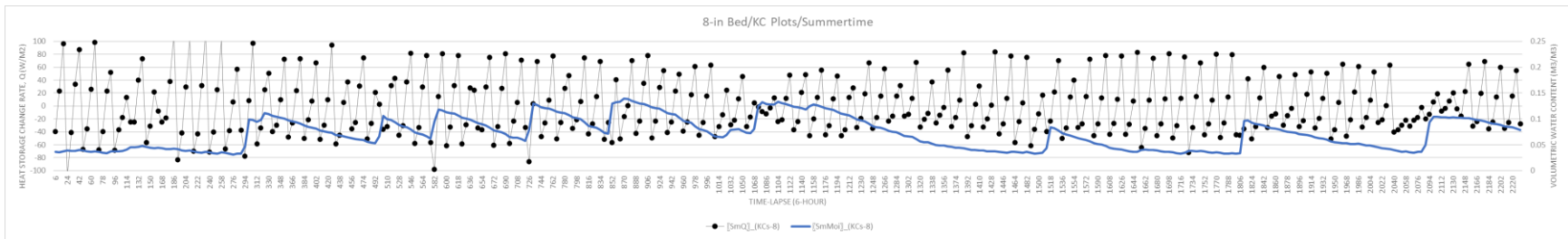


**Figure 4.19.** The rate of change in heat storage within the soil layer ( $Q$ -value) of all KC plots from 8-inch-deep beds at APD-EGR during the summertime.

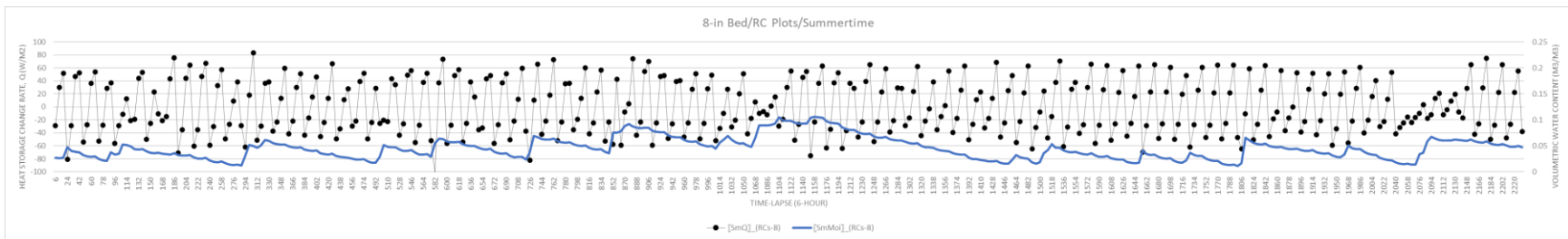


**Figure 4.20.** The rate of change in heat storage within the soil layer ( $Q$ -value) of all RC plots from 8-inch deep beds at APD-EGR during the summertime.

From figures 4.19 and 4.20, we can confirm that soil temperature is intimately linked to soil water and pore space (Howe and Smith, 2021). Water has a greater specific heat (i.e., the energy required to heat a mass by 1°C) than soil minerals (e.g., water is 1 calorie g<sup>-1</sup> and quartz is 0.19 calorie g<sup>-1</sup>). Thus, wet soil requires more energy to heat than dry soil (Howe and Smith, 2021).

Although RC plots contain less moisture, those have relatively high negative (*Q-value*) gradients/values than the KC plots in the 8-inch bed in comparison to the 4-inch bed. I believe this is because of pore space and water vapor (the specific heat of air is approximately 0.24 Btu/lb°F, and for water vapor 0.45 Btu/lb°F.). So, in the summer months (the building cooling season), the R substrate type in the 8-inch bed buffers heat gain entering into the building in the daytime more than for the K substrate. But if we consider all the graphs, the 4-inch bed with R substrate may work more efficiently during the cooling season (summer months) considering both day and night times.

In short, it seems that 4-inch bed with R substrate shows more evidence (see Fig 4.17, 4.18, 4.19 and 4.20) to improve building energy performance by reducing the cooling load. So, depth and moisture have two-way interactions in the context of the APD-EGR. Increasing soil depth in the building physics scenario is not positively correlated with moisture content.

Thermal graphs of two beds (4-inch and 8-inch depths) from the wintertime are given in figures 4.21 and 4.22 below:

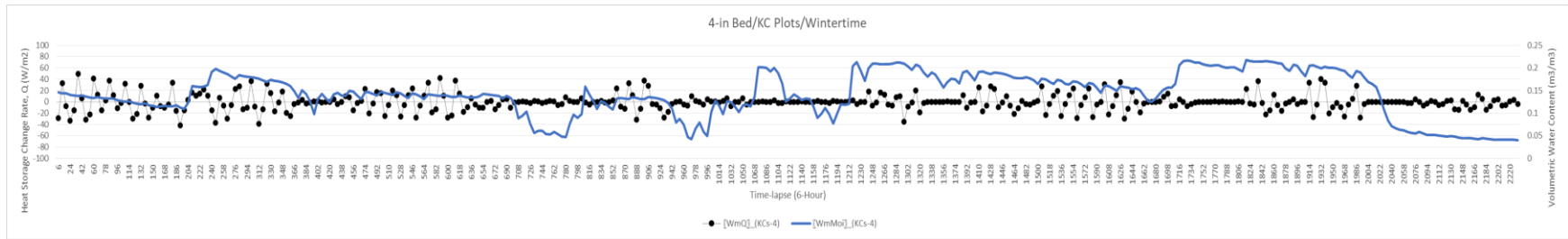


**Figure 4.21.** The rate of change in heat storage within the soil layer ( $Q$ -value) of all KC plots from 4-inch deep beds at APD-EGR during the wintertime.

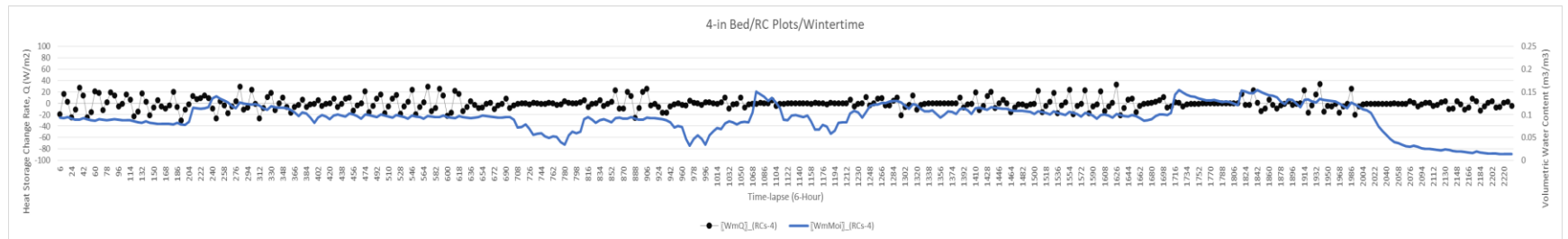


**Figure 4.22.** The rate of change in heat storage within the soil layer ( $Q$ -value) of all RC plots from 4-inch deep beds at APD-EGR during the wintertime.

From figures 4.21 and 4.22, we can see that  $Q$ -value shows slightly more negative gradients (values) in KC plots (Figure 4.21) than in RC plots (Figure 4.22); because of its more moisture holding capacity than in RC plots. So, in the wintertime (the building heating season), the K substrate type in the 4-inch bed helps heat loss of the building more than the R substrate in the nighttime. The daytime performance of both substrate types (K and R) for a 4-inch-deep bed seems quite similar.

The heating load is the amount of heat energy that would need to be added to a space to maintain the temperature in an acceptable range during winter months (Bailes, 2015).

We can also see that the R substrate type in the 4-inch-deep bed shows less fluctuation (positive and negative gradients) in their  $Q$ -values than the K substrates of a 4-inch-deep bed during the day and night. From figures 4.21 and 4.22, we can say that the R substrate types in 4-inch bed should work slightly better during wintertime in the Flint Hills Ecoregion at Manhattan, Kansas. Probably, the leading cause is that KC works as wet soil and RC works as dry soil. One of water's most significant properties is that it takes a lot of energy to heat it. To be precise, water must absorb 4,184 Joules of heat (1 calorie) for the temperature of one kilogram of water to increase 1°C. For comparison's sake, it only takes 385 Joules of heat to raise 1 kilogram of copper 1°C (USGS, 2018). So, the high moisture content of KC plots takes more time to change their state from ice to water during winter months; thus, the ice state of soil moisture helps heat loss of the building. This outcome is totally climate and weather dependent, and the benefits will differ in different places and situations (namely the specific weather conditions).

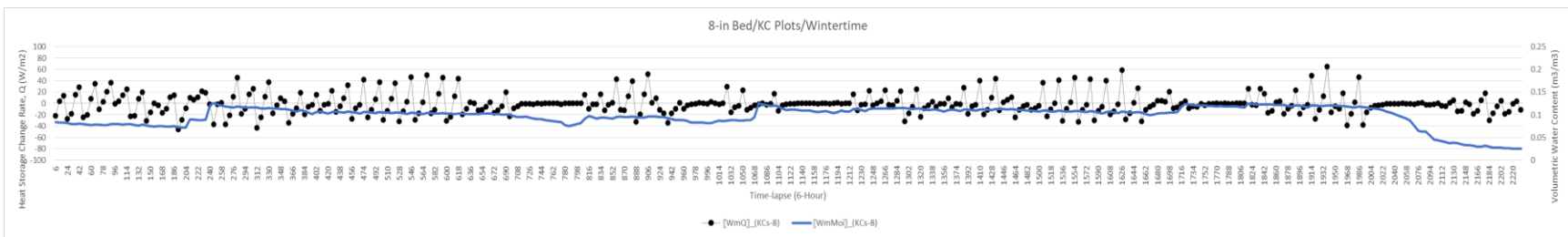


**Figure 4.23** The rate of change in heat storage within the soil layer ( $Q$ -value) of all KC plots from 8-in deep beds at APD-EGR during the wintertime.

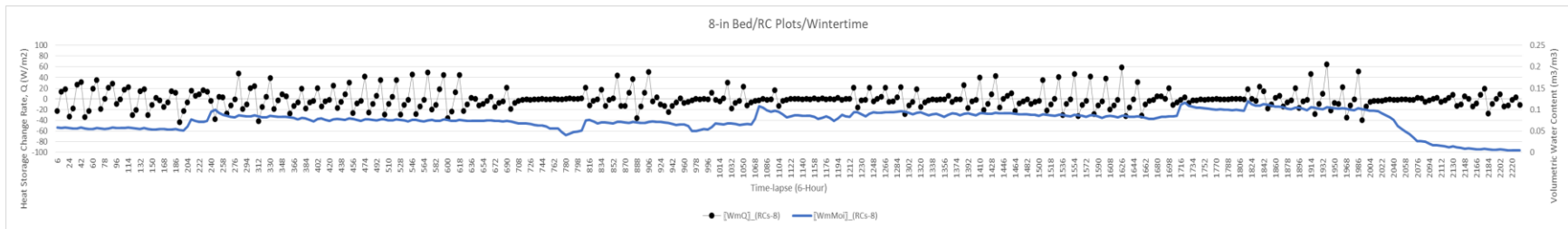


**Figure 4.24** The rate of change in heat storage within the soil layer (*Q-value*) of all RC plots from 8-inch deep beds at APD-EGR during the wintertime.

Interestingly, from figures 4.23 and 4.24, we can see that moisture content is quite similar in both substrates K and R for the 8-inch beds. In the wintertime, because of having greater depth than the 4-inch-deep bed, both substrates (K and R) show a higher percentage of positive *Q*-value in the 8-inch-deep bed, which means the soil is warming and buffering heat loss from the building. But from figures 4.23 and 4.24, it is not very clear which substrate is performing better (having more positive *Q*-values); but it is quite evident that the soil moisture content is playing a significant role in all the graphs from wintertime. So, it can be hypothesized that the extra depth of green roof substrates may be beneficial in the wintertime since the substrate types do not appear to play a significant role in insulating the building below (at least in the context of the Flint Hills Ecoregion at this time of the year).

## **Chapter 5 - Discussion and Conclusions**

### **Soil C Sequestration**

According to Dr. Charles W. Rice, Distinguished Professor in the Department of Agronomy at KSU, “to quantify and explore soil microbes and [their] C sequestration capacity, what we really want to know is root biomass, microbial biomass, and TOC in soils. Aboveground biomass just tells us productivity, which co-relates or translates to how much C is going belowground, in general. If we can get a direct measurement of root biomass, that would be fine for this research. Also, soil moisture is not essential for these analyses” (Zoom communication with Dr. Charles Rice, June 12, 2020). Michigan State University researchers also supported the idea and stated that ecosystem net primary production is estimated by annual maximum plant biomass accumulation with vegetative biomass measured during the growing season (May-October) by quantifying the peak dry mass of plants per unit area in each plot (LTER, 2022).

Total organic carbon (TOC) is the C stored in soil organic matter (SOM). Organic C (OC) enters the soil by decomposing plant and animal residues, root exudates, living and dead microorganisms, and the soil biota (Khatoon et al., 2017). SOM is the organic fraction of soil, excluding non-decomposed plant and animal residues (Khatoon et al., 2017). Nevertheless, most analytical methods do not distinguish between decomposed and non-decomposed residues. SOM is a heterogeneous, dynamic substance that varies in particle size, C content, decomposition rate, and turnover time (Khatoon et al., 2017).

#### ***Role of TOC***

Generally, high TOC levels indicate high rates of organic material decomposition (e.g., plants, algae) (McLatchey and Reddy, 1998). Total OC influences many soil characteristics, including color, nutrient-holding capacity (cation and anion exchange capacity) (Schumacher, 2002), nutrient turnover and stability, which in turn influence water relations, aeration, and workability (Pluske et al., 2022).

In soils with high clay contents, the contribution to cation exchange from the organic fraction is generally small compared to that from the clay (Schumacher, 2002). In sandier soils, the relative contribution of the organic fraction is higher because there is less clay, even though the amount of TOC present may be similar or less to that in the clay (Schumacher, 2002). By providing a food source for microorganisms, OC can help improve soil stability through the microorganisms binding soil particles together into aggregates, or “peds”. Bacterial excretions, root exudates, fungal hyphae, and plant roots can also all contribute to better soil structure (Pluske et al., 2022).

Moist, hot, and well-aerated conditions favor the rapid decay of organic additions to soil. If the rate of OM addition is greater than the rate of decomposition, the organic fraction in a soil will increase (Bot and Benites, 2005; Pluske et al., 2022). Conversely, if the rate at which OM is added to the soil is lower than the decomposition rate, the organic fraction will decrease (Pluske et al., 2022).

At a steady state level, the rate of addition is equal to the rate of decomposition. Large organic additions can temporarily increase the organic fraction in soil, but unless such additions are maintained, the soil will revert to its steady-state equilibrium, which is usually low (Pluske et al., 2022).

Soil OC is a *measurable* component of SOM, and is a very good indicator of soil fertility (Behera, 2012). However, SOC is a component of SOM, and OC makes up approximately 60% of the SOM, with the remaining 40% of the SOM containing N, Ca, hydrogen (H) and oxygen (O) (Kononova, 2013). Soil OM conserves moisture, absorbs and stores nutrients, and acts as a primary food source for soil microorganisms, and thus SOM is the best indicator of soil quality and soil health (Behera, 2012).

Measurements of TOC can quantify the amount of OM contained in sediments (TOC is approximately half the amount of OM contained in a sediment or soil sample) (Ostrowska and Porebska, 2012). Adding organic material to soil accelerates the accumulation of TOC and soil TN (Pan et al., 2015). In soils formed under prairie vegetation, the OM levels are generally relatively high because organic material is supplied from both top growth and the roots

(Funderburg, 2020). Roots are not usually thought of as supplying organic material, but a study on the Upper Great Plains has shown that a mixed prairie can have an aboveground (i.e., shoot) yield of 1.4 tons of organic material per acre, while the root yield can be about 4 tons per acre. These plants were producing roots that were more than twice the weight of the shoots (Funderburg, 2020).

The terms “TOC”, “SOC”, and “OC” generally mean the same thing. There is a direct relationship between SOC and TN content, with an increase in SOC content usually followed by an increase in TN content (Brevik et al., 2018). The correlation between SOC content and TN is positive and has a relatively high correlation coefficient, with a value of 0.80–0.90 (Wibowo and Kasno, 2021). Table 5.1 was adopted from Wibowo and Kasno (2021), and it indicates that there is a strong correlation between SOC and TN in soils.

SOC is strongly correlated with TN, this correlation represents the terrestrial environment cycle of C and N (Iakimenko et al., 1996). Several factors affect the SOC and TN content, including mean annual rainfall and mean annual temperature (Bi et al., 2018). The correlation between SOC and TN among various land uses is positive, with land use playing a major role in the distribution and amount of SOC and TN (Wibowo and Kasno, 2021). Soil OC and TN content are also significantly correlated in seasonally frozen soil (Wibowo and Kasno, 2021).

**Table 5.1.** Average SOC and TN values, and their correlation coefficients (after Wibowo and Kasno, 2021).

Province	Average content (%)		Correlation coefficient
	SOC	TN	
Banten	1.59 ± 0.66	0.15 ± 0.07	0.84
West Java	1.91 ± 0.68	0.17 ± 0.06	0.90
Central Java	1.55 ± 0.86	0.15 ± 0.08	0.89
East Java	1.25 ± 0.50	0.11 ± 0.04	0.80
Yogyakarta	1.54 ± 0.51	0.14 ± 0.04	0.90

Microbes decompose SOM, releasing CO<sub>2</sub> and plant-available nutrients. Soils with more organic (labile) C tend to have a higher MB (Hoyle et al., 2006). Based on other studies,

exudates released by plant roots are the main food source for microorganisms and a driving force behind their population density and activities (Raaijmakers et al., 2009). Processes in the rhizosphere are complex, and the plant–root interface is a hotspot of microbial interactions (Raaijmakers et al., 2009; Korenblum et al., 2020). The rhizosphere is the area around a plant root inhabited by a unique population of microorganisms (McNear, 2013), and living root–soil interfaces are nutrient-rich, acting as a source of energy for microbes (Jones et al., 2004).

Based on data obtained through APD-EGR research, the greater root density on the APD-EGR may be positively correlated with MB measured directly from the two substrates in the 4-inch and 8-inch beds. This means there is a positive relationship between microbial activity and root density.

- TOC and TN were higher in the R substrate than the K substrate in the 4-inch-deep bed, and that MB was higher in the below-ground biomass of plant mix type C (native grasses + forbs) than in A (*Sedum* only) or B (*Sedum* + native grasses) in the 4-inch-deep bed.

Based on the discussion above, we know that the positive correlation between the SOC and TN contents is quite strong. So, an increase in TOC is responsible for the increase in TN in the substrate R plots in the 4-inch-deep bed. Since the addition of organic material accelerated the accumulation of TOC and TN in the substrate R plots, R had a higher organic material content than K in the 4-inch-deep bed. The R substrate plots, with the higher SOM and SOC contents, also had higher MB. Strong evidence was also found for an increase in MB from the high root density in the grass plots (especially plant mix type C—native grasses + forbs).

In soils under prairie vegetation, OM levels are generally relatively high, primarily because of the high percentage of root accumulations in the soil (Funderburg, 2020). Based on data gathered from APD-EGR research, the greater root density on the APD-EGR is positively correlated with MB within the substrate. Also, the root-biomass analysis revealed an overall higher root density in the type C than in the type A and B *Sedum* plant mixes in the 4-inch-deep bed. For the APD-EGR this would need to account for changing protocols in how supplemental irrigation is applied year to year.

For example, in mid-July 2022 after discontinuing irrigation on the APD-EGR, long hot and/or dry periods led to the decision to occasionally irrigate the east side (12 plots in each bed) of the APD-EGR beginning July 20, while the 12 plots on the west side of each bed would not be given any supplemental irrigation. As a result, a majority of prairie species on the unirrigated west side died back or browned out (as of October 2022 most looked dead although a few may be dormant; refer to figures 5.1a and 5.1b). On the east side partial dieback (for an estimated 60% of the native plant species) occurred in the 4-inch bed, while very few plants (less than 5%) died back in the 8-inch bed (Lee Skabelund, personal communication, Nov. 2022). Such green roof management decisions impact root density and total root biomass (living or dead), and very likely microorganisms and carbon sequestration. These management decisions likewise influence substrate moisture levels, substrate temperatures, and heat flows and fluxes.



**Figure 5.1a.** APD-EGR 4-inch bed on Oct 6, 2022. An estimated 60% of prairie grasses and *Dalea purpurea* look to have survived the July 2022 dry spell, when only the east side (shown in the foreground) was irrigated starting July 20, 2022. (Photo taken by Lee Skabelund.)



**Figure 5.1b.** APD-EGR 8-inch bed on Oct 6, 2022. More than 95% of prairie grasses and *Dalea purpurea* look to have survived the July 2022 dry spell, when only the east side (shown in the foreground) was irrigated starting July 20, 2022. Except for a single line of living prairie plants growing along the pathway to the west of the APD-EGR (which has pavers set on a sand base that stays moist for long periods of time), no other prairie plants survived in the 4-inch bed. Prairie plants right along this same north-south walkway and prairie plants within a few other 8-inch-deep plots also survived the four-week July 2022 dry spell when temperatures ranged between 70-103F/21-39.5C with no measurable precipitation during this period per the new 2022 Kansas Mesonet Ekdahl weather station -- <http://secondary.mesonet.ksu.edu/weather/historical/>. This indicates that there must be some sub-surface pockets of moisture some prairie species could tap in the non-irrigated plots. (Photo taken by Lee Skabelund.)

### ***Fundamentals of SOC***

Soil organic matter (SOM) is composed of soil microbes, including bacteria and fungi, decaying material from once-living organisms, such as plant and animal tissues, fecal material, and products formed from their decomposition (Ontl and Schulte, 2012). Soil C is the solid C stored in global soils. This includes both SOM and the inorganic C in carbonate minerals (Jobbágy and Jackson, 2000). Soil C is a carbon sink, within the global C cycle, playing a role in biogeochemistry, climate-change mitigation, and the construction of global climate models (Amelung et al., 2020).

Soil OC levels are directly related to the amount of OM contained in soil (Ontl and Schulte, 2012), and result from the interactions of several ecosystem processes, in which photosynthesis, respiration, and decomposition are key (Ontl and Schulte, 2012). Decomposition of biomass by soil microbes results in C loss from the soil in the form of CO<sub>2</sub> due to microbial respiration (Ontl and Schulte, 2012). It is known that soil respiration is a measure of the CO<sub>2</sub> released from the soil by the decomposition of SOM by soil microbes and the respiration from plant roots and the soil fauna (USDA, n.d.).

- Another research finding was that the two-way substrate-by-year interactions for TOC, TN, and MB in the 8-inch-deep bed were due to decreases in each of these materials in the K substrate plots in 2020 compared to 2019.

The TOC, TN, and MB had decreased in the 8-inch-deep bed of the substrate K plots one year later, in 2020. A loss of SOC content can limit a soil's ability to provide nutrients for sustainable plant production. This can lead to lower yields and affect food security. Less OC also means less food for the living organisms present in the soil, thus reducing soil biodiversity (ESDAC, 2009). The decrease in TOC and TN could also have caused a decrease in the SOM in the substrate K plots of the 8-inch-deep bed. Sources of OM include crop residues, animal and green manures, compost, and other organic materials (ESDAC, 2009), but none of these were added to the APD-EGR during the 2019 and 2020 study period, nor in the years prior to this study (fall 2017 to fall 2018). Some vegetative residue remained on each APD-EGR bed, but residues were not measured. A decline in OM is caused by the reduced presence of decaying organisms, or an increased rate of decay as a result of changes in natural or anthropogenic factors (ESDAC, 2009).

The soil respiration statistical analysis revealed that substrate has a significant effect on soil respiration, with the R substrate having higher respiration than the K substrate in both beds (4 inch and 8-inch).

Soil respiration refers to the production of CO<sub>2</sub> when soil organisms respire. Soil respiration generally increases as soil moisture increases (USDA, n.d.); however, O<sub>2</sub> is limited when soil pores are filled with water because this interferes with the ability of soil organisms to

respire (USDA, n.d.). Soil respiration is a measure of the CO<sub>2</sub> released from the soil from the decomposition of SOM by soil microbes (USDA, n.d.). Ideally, the soil moisture content would be close to field capacity, or when approximately 60% of the pore space is filled with water. Respiration is limited in dry soils because of the lack of moisture for microbial and other biological activities (Figure 5.1).

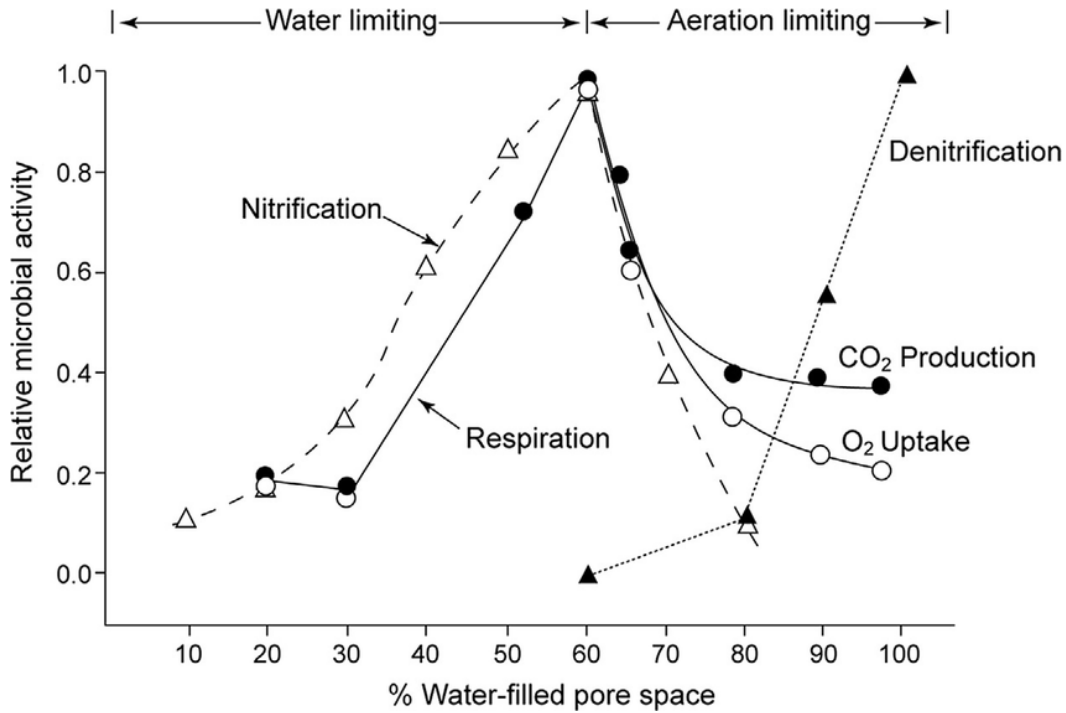


**Figure 5.1.** Relative aerobic (respiration, ammonification, and nitrification) and anaerobic (denitrification) microbial activity related to water-filled pore space in soil (after Linn and Doran, 1984; Parkin et al., 1997).

The decomposition (aerobic respiration) of biomass by soil microbes results in C loss in the form of CO<sub>2</sub> from the soil due to microbial respiration (Ontl and Schulte, 2012). When organic materials decompose in the presence of O<sub>2</sub>, the process is aerobic.

Since substrate K had less respiration than R, we can infer that the decreases in TOC, TN, and MB in the K plots of the 8-inch-deep bed indicate a decline in OM in those plots and that bed in 2020 compared to 2019. The reduction in SOM in the 8-inch-deep K plots was not due to the decomposition of biomass by soil microbes since we got low respiration rates in K plots.

Based on the discussion above, we can also infer that the reduced pore space (porosity) and higher moisture content in the K substrate may have affected the respiration capacity in those plots. Moisture content in K plots is always higher than in R plots. In-situ moisture content data was used to generate graphs to compare the moisture-holding capacity of two substrates (K and R) in Figure 5.3. A comparison of the moisture content of two soil types (K & R) and depths (4-inch versus 8-inch) of the APD-EGR was made between summertime (June 15, 2020- September 15, 2020) and wintertime (November 15, 2020- February 15, 2021) in the Flint Hills Ecoregion at Manhattan, KS, USA. Interestingly, the 4-inch-deep bed did not experience significant SOM loss from the K plots. However, this observation remains to be confirmed with more conclusive evidence from further research, which could potentially be done to explore the effect of time and the observed decrease or increase in SOM in the two substrates (K and R) and both beds (4-inch and 8-inch depths).

As SOM increases, soil porosity also increases (Figure 5.2), in response to the positive effect of OM on soil aggregation, tilth, and biopore development (Kay and VandenBygaart, 2002). Biopores are voids in the soil that are formed by the activities of soil life (Kautz, 2015). Typically, the term “biopore” refers to a tubular-shaped, continuous pore formed by plant roots and burrowing soil animals, such as earthworms (Kautz, 2015). Increased OM contributes indirectly to soil porosity (via increased soil faunal activity). The soil fauna includes earthworms, collembolans, mites, nematodes, and protozoa. Fresh OM also stimulates the activity of the macrofauna such, as earthworms, which create burrows lined with glue-like secretions from their bodies that are intermittently filled with worm-cast material (Bot and Benites, 2005). Increased levels of OM and the associated soil fauna lead to greater pore space with the immediate result that water infiltrates more readily and can be held in the soil (Bot and Benites, 2005). The improved pore space is a consequence of the bioturbating activities of earthworms and other macro-organisms and channels left in the soil by decayed plant roots (Bot and Benites, 2005).

However, many other things can also affect the soil moisture content and porosity, such as soil cover, macroaggregates, raindrop impact, and plant residues (Bot and Benites, 2005). Our findings suggest that further research on the soil fauna and its effect on the different substrates on the APD-EGR would be beneficial.

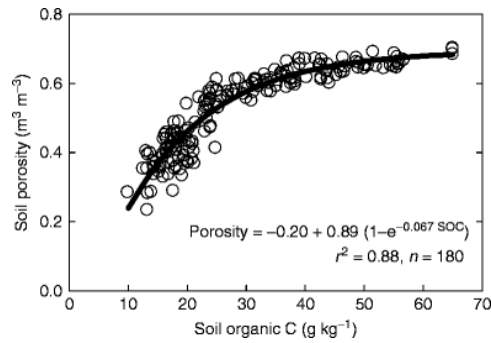


**Figure 5.2.** Relationship between porosity and SOC (after Franzluebbers, 2011).

Preliminarily, we collected 24 soil samples from the APD-EGR 8-inch bed for nematode analysis on the morning of October 3, 2019 (7:45 am- 11:30 am), very near the end of the growing season in north-central Kansas. During the remainder of the growing season, nematode populations decline steadily (Jardine and Todd, 1990) in the Midwestern United States. The Nematode Analysis was performed by the Department of Plant Pathology at Kansas State University. The results showed that the nematode populations were too low to draw meaningful conclusions. The protocols for collecting soil samples for the nematode analysis from the APD-EGR followed soil/substrate analysis *Protocol 1*. Lab work followed the exact procedures from this paper, “*A rapid centrifugal-flotation technique for separating nematodes from soil*” (Jenkins, 1964). My doctoral committee members agreed not to use the nematode analysis data from the year 2019 and encouraged me to take nematode samples in July 2020.

July 28, 2020, we collected 24 soil samples, following the same protocols (outdoor collection and indoor processing and analysis as per 2019), again from the 8-inch bed. Samples were again sent to the Department of Plant Pathology at Kansas State University for processing and statistical analysis, and that year (2020), we observed both nematode abundance and nematode diversity compared with the last year. Working with Tim Todd, we extracted 9801 nematodes from the 24 soil samples collected from each of the APD-EGR’s 8-inch-deep plots. Counts are the numbers of nematodes per 100-gram dry soil weight. So, we saw a significant presence of different nematode communities. We decided not to use nematode data since data was not collected from the 4-inch-deep bed. The research team concluded that the research design for nematode analysis should be appropriately set before formal statistical interpretations be made and published and suggested that the samples should be collected in early July from both beds of APD-EGR after at least five growing seasons to provide a useful nematode analysis.

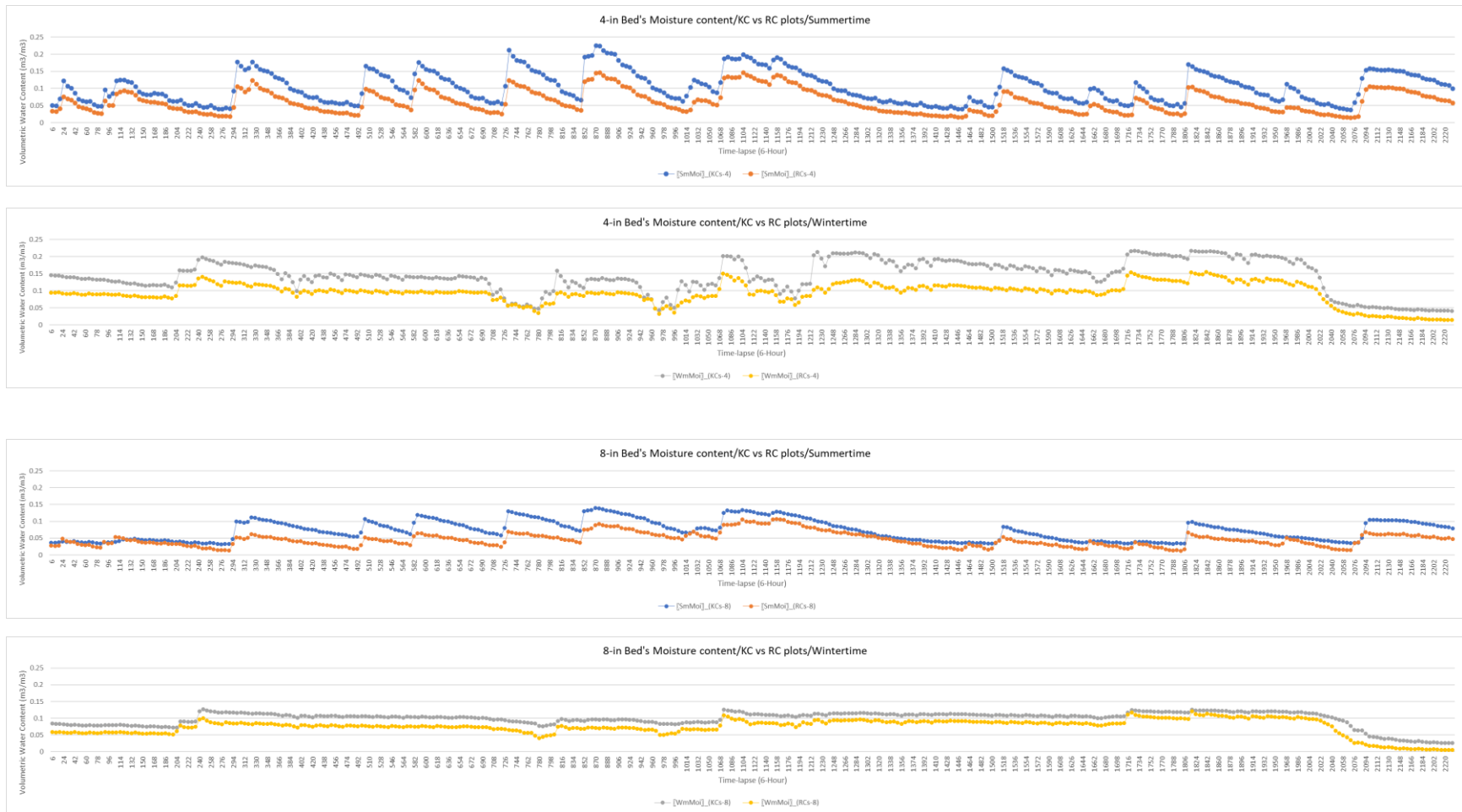


**Figure 5.3** Summertime vs. Wintertime moisture content comparison of K and R.

The overall mean of  $Moi_6$  (Table 3.13) approximated from the data collected from the APD-EGR in the summertime (June 15, 2020- September 15, 2020) was expressed as  $SmMoi_{KCs-4}$ ,  $SmMoi_{RCs-4}$ ,  $SmMoi_{KCs-8}$ , and  $SmMoi_{RCs-8}$ .

The overall mean of  $Moi_6$  (Table 3.13) approximated from the data collected from the APD-EGR in the wintertime (November 15, 2020- February 15, 2021) was expressed as  $WmMoi_{KCs-4}$ ,  $WmMoi_{RCs-4}$ ,  $WmMoi_{KCs-8}$ , and  $WmMoi_{RCs-8}$ .

- The statistical analyses conducted in this study revealed that the two-way plant-mix-type-by-year interaction for MB in the 8-inch-deep bed was due to a decrease in MB in the plant mix type B (*Sedum* + native grasses) plots in 2020 compared to 2019.

In 2020 (compared to 2019), significant decreases in MB were found for the plant mix type B (*Sedum* + native grasses) plots in the 8-inch-deep bed. Based on the discussion above, a reduction in MB in any plot would mean a decrease in TOC and TN. Under prairie vegetation, SOM largely depends on the root biomass and root density in the soil. The statistical analysis of root biomass showed that the biomass from samples containing grasses (types B and C) had overall significantly higher root densities than the *Sedum*-only plots in both the 4-inch and 8-inch beds. Higher amounts of MB were found in the belowground biomass samples of plant mix type C (native grasses + forbs), which suggests that the high root density from the native grass and forbs plots may have helped to increase MB, TOC, and TN in the 4-inch-deep bed. Our research team found a significant decrease in MB in the plant mix type B (*Sedum* + native grass) plots, which suggests that further study of the plant dynamics on the APD-EGR may be appropriate to observe the effect of *Sedum* species and time on MB accumulation in the plant mix type B plots of the 8-inch bed.

In this study, species dynamics were excluded from the research variables. One of the primary independent variables of this study—different plant mixes—focused only on the three different belowground biomass samples for the plant mix types A, B, and C. However, even from this two-year study, a strong relationship between plant species dynamics and soil MB, and thus with TOC and N, was observed.

The separate bed-depth analyses (4-inch and 8-inch) revealed significant differences among the dependent variables, such as TOC, TN, and MB, and between the independent variables, including substrate type, time (age of the APD-EGR), and belowground biomass. Each significant value from the statistical analyses indicates that substrate depth may have some sort of control over these variables. The repeated-measure ANOVA and other statistical analyses from 2019 and 2020 (Figure 5.4) showed that MB, TOC, and TN were consistently higher in substrate R compared to substrate K in the 4-inch bed. In this study, we did not directly obtain or compare the statistical significance between the two depths of the APD-EGR beds (4-inch vs. 8-inch depths) in terms of the dependable variables TOC, TN, and MB.

From Figure 5.4, the 4-inch-deep bed appears to have a two-year-long consistency of higher MB, TOC, and TN values as opposed to the 8-inch-deep bed. This somewhat surprising finding suggests that a longer-term study is needed to more precisely examine the effect of depth on TOC, MB, and TN.

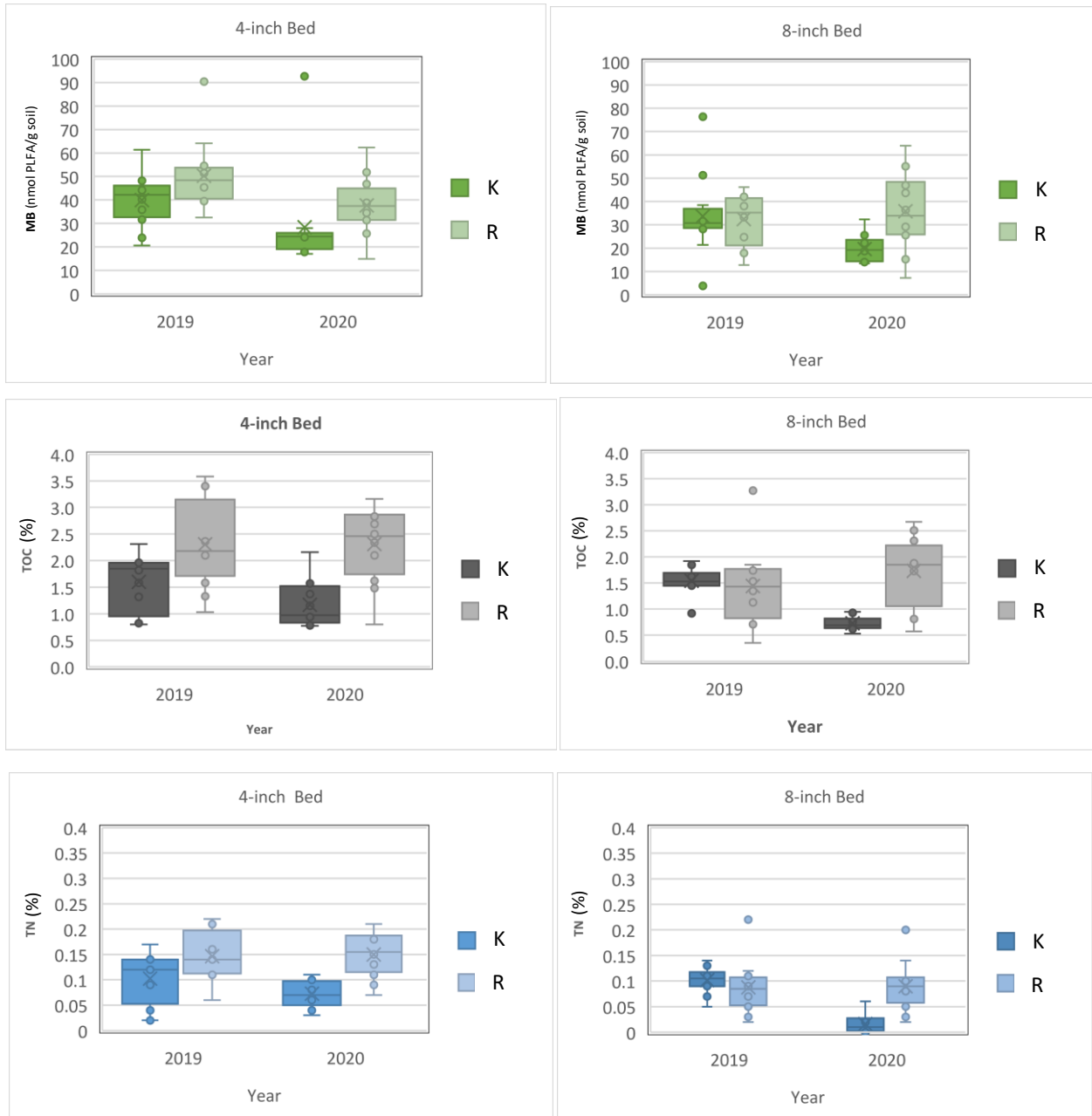


**Figure 5.4.** All the box-and-whisker plots together, showing the data distribution for TOC, TN, and MB from the two substrates (K and R).

The short roots of the native grass used in this study produced significantly more belowground biomass than the *Sedum* spp., and the greater root biomass of these perennial grasses contributed more C to the soil (Sainju et al., 2017). We also explored the potential for a long-term effect of plant mix type C (native grasses + forbs) on MB on the APD-EGR due to the high root density in the grass plots. Note that this study was not concerned with the different root systems of the various plants, rather focusing on the overall root density in the substrates.

### ***Research Findings from C Sequestration Analysis***

As far as I know, an analysis of the MB, TOC, TN, and root biomass on a green roof has not been undertaken before in the context of the Great Plains, USA. This study was not intended to recommend a substrate depth, but rather was aimed at understanding the consequences of shallow and deep green-roof growing media (substrates) and the factors that affected its ability to sequester C in this region. The potential influences of the belowground biomass of three plant mix types (A, B, and C) in two different substrates (R and K) in two growing seasons (2019 and 2020) were investigated, and statistical analyses performed to assess the C-sequestration potential of the APD-EGR. The analyses identified some of the potential causes of the MB, TOC, and TN concentrations in the substrates on the APD-EGR, allowing a hypothesis on the effect of depth to be formed from empirical data.

From the beginning, this study was focused on quantifying soil microbes and their C-sequestration capacity by exploring the root biomass, MB, and TOC produced in two different substrates, and especially on estimating MB, with the understanding that microbes are an early indicator of changes in total SOC. Soils with more organic (labile) C tend to have a higher MB (Hoyle et al., 2006).

It seems that MB may positively correlate with higher root density (especially in plant mix type C), this being more evident in the 4-inch bed than the 8-inch bed. In the shallower rooting depth of the 4-inch-deep bed, roots proliferated throughout the entire profile, more than in the 8-inch-deep bed, because they had the least amount of space. In the 4-inch bed, the belowground biomass for plant mix types A, B, and C would have become root-bound with time, and their

roots would likely reach the bottom of the plot first occupying all the available substrate space. This explains the higher root density in the shallower plot. But it is not clear what the root density situation in the 8-inch-deep bed will be in the next 10 to 20 years, or how vegetation in the 4-inch bed will cope with soil depth constraints in the future. Consequently, more in-depth and long-term research is required to provide evidence for interactions involving varying depths on the APD-EGR.

Although there were many limitations to this study, this two-year (2019 and 2020) analysis found that shallower beds with the R substrate (with its lower bulk density, higher pore space, and lower water-holding capacity than substrate K) would sequester a greater amount of C per substrate volume, which could (at least partially) offset the need for deeper beds and may effectively contribute to climate-change mitigation in similar ways to deeper substrate profiles. Nevertheless, more long-term research is needed to gather conclusive evidence regarding this possibility. It is therefore hoped that MB, root biomass, TOC, TN, and soil respiration studies will continue on the APD-EGR and on other green roofs in the Flint Hills Ecoregion and U.S. Great Plains over future growing seasons to provide an important reference for longer-term studies on C sequestration and green roofs. Such studies would be expected to have great relevance in the U.S. Great Plains and in other parts of the world.

## Green Roof Systems at APD-EGR as Climate Change Mitigation Strategy

The design of the APD-EGR consists of vegetation, the growing medium or substrate, a filter fabric/filtering membrane, a gravel leveling and drainage layer, a drainage panel that holds some water for a longer period, a root barrier, and the waterproofing layer immediately above the structural roof support (Figure 5.5).

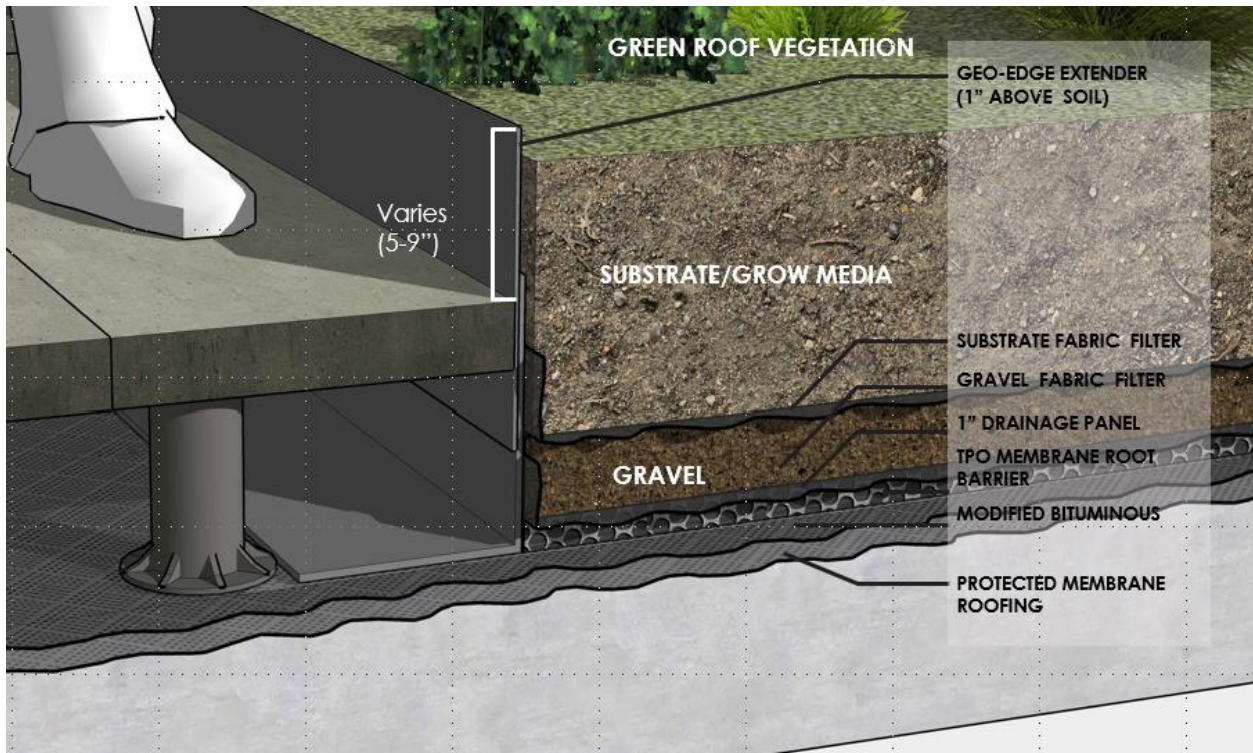


**Figure 5.5.** The research focused only on the substrate layer of the APD-EGR (Confluence, 2019).

The thermal performance of a green roof system (in this research context, APD-EGR) depends on all the layers one can see in Figure 5.5. It is evident that the most dynamic elements of a green roof system are the vegetation and the substrates as these interact with variables such as precipitation; soil moisture, texture, porosity, and bulk density; and temperature (micro-climate) which is strongly influenced by shading from architectural elements. A critical element related to green roof vegetation is total vegetative coverage or the Leaf Area Index (LAI) (Sailor, 2008).

The LAI of a plant canopy is defined as its leaf area per unit of ground area. The leaf area index (LAI) is an important parameter in plant ecology (Sailor, 2008). The LAI value is an essential input (value) for the “Green Roof Energy Calculator” developed by Dr. David Sailor at Portland State University and used to estimate Kansas State University Memorial Stadium green roof energy benefits (Skabelund and Alam, 2020). Researcher Dr. David Sailor also provided the mathematical calculation details to determine LAI value Sailor (2008).

### *Leaf Area Index (LAI) Value Examples*

- According to Yu (2006) and Tabares Velasco (2009), the LAI for a rooftop garden, especially for an intensive green roof, ranges from 1.0 to 6.0 (or up to 7.0) depending on the species of plants.
- LAI values for extensive green roofs (with substrate or soil thickness of less than 6") are typically around 1.0 to 3.0 (Tabares Velasco, 2009).

One can easily understand that green roof systems are very complex. Building energy performance can improve where all layers of a green roof system contribute to being insulators at various times of the day and different seasons. This study was conducted in such a way as to explore the most dynamic layer of the system, the “Substrate or Growth Medium,” and its efficiency as a thermal storage battery for the building. By utilizing stored thermal energy from thermal energy storage units (the substrates), peak load demand could be moved to off-peak hours (Mughees, 2022). Even a small volume of buffer thermal storage (heat storage) could be used effectively for shifting the thermal load from peak to off-peak periods and can improve energy efficiency of the building. This would result in good performance while reducing the energy consumption during peak load period (Lee et al., 2015).

The study compared two different substrates [Kansas BuildEx® (K) and rooflite® (R)] and two different substrate depths (approximately 4 inches and 8 inches). The literature review (background) section discussed the potential for green roofs to improve building energy performance (Henry, 2020). However, designers require an in-depth understanding of local climate and proposed rooftop microclimates to create the conditions that will support living plant biomass and adequately support microbial life in green roof substrates. Thermal storage or the

rate of change in heat storage within the soil layer of green roof substrates depends on solar and wind energy, shading, and precipitation or irrigation patterns, meaning that the green roof insulation potential changes depending on day-to-day and year-round weather patterns, solar radiation, and maintenance practices. Therefore, it is clear that the net change (*Q-value*) of any green roof system (including the APD-EGR) will show different thermal storage (*Q-value*) or change rate capacity in summertime and wintertime. Because each rooftop microclimate is unique depending on orientation in relation to the sun and seasonal changes in shading it is unwise to suggest a specific green roof depth with a substrate type and species composition that will improve building energy performance.

What is clear is that the amount and intensity of solar radiation hitting a green roof in the Flint Hills Ecoregion in combination with adequate substrate moisture will dictate if the selected plant species survive and thus allow for new root growth and coverage of the substrates used. This became very clear after I completed my data collection and our research team reduced irrigation in 2021, and then eliminated irrigation in 2022 for the APD-EGR until July 20, 2022. As shown in figures 5.1a and 5.1b, significant portions of the APD-EGR vegetation could not handle the extended hot, dry period that occurred late June to mid-July (thus extensive dieback occurred in July 2022), and supplemental irrigation was required to keep most of the native prairie species from also dying out on the east half of the APD-EGR.

The research setting for the APD-EGR and the graphical analyses used to explore the primary dependent variable, the rate of change in heat storage within the soil layer or net change (*Q-value*)--to find the best combination of depth and substrate type, for building energy efficiency in the context of the Flint Hills Ecoregion—are a step in the effort to improve both green roof design and building energy efficiency. Improving building energy efficiency can contribute to the resilience and adaptation of cities to the effects of climate change and bring many other additional benefits such as reduced energy bills, healthier homes and workplaces, new jobs, and greater energy security (Project Drawdown, 2020).

### ***Research Findings from Thermal Analysis***

By closely examining all the graphs and thermal analysis, I can say that soil moisture content plays a key role in improving building performance in the context of the APD-EGR. Depth and moisture have two-way interactions in the context of the APD-EGR. Increasing soil depth in the building physics scenario is not always positively correlated with moisture content and influences building performance in different ways at different times of the year (summertime versus wintertime).

The performance of the 4-inch-deep and 8-inch-deep green roof systems at the APD-EGR are not similar for summertime and wintertime months, especially because of the different percentage ratios of water/moisture content. In the summertime, the moisture content plays a significant role in improving building energy performance, whereas in the wintertime, depth appears to have a significant effect on it. We can conclude by saying that the 4-inch bed with R substrate showed the potential to work efficiently in the cooling season (summertime), considering both day and night times. Extra soil depth associated with the 8-inch plots appeared to have more positive Q-values that could improve building performance in Manhattan, Kansas. Interestingly, substrate types do not seem to play a significant role in influencing Q-values in the wintertime. Depth appears to be the key factor in improving wintertime building energy efficiency.

In the end, the study suggests more research on this topic with more instrumentation (such as installing thermal flux sensors at APD-EGR) that could help researchers to derive the R-values of different soil types at different depths.

### ***Conclusion***

The study concludes that in both cases of C sequestration and thermal performance, a shallower bed with R substrate (having lower bulk density, higher pore space, and lower water holding capacity than K) might work better as a climate change mitigation strategy in the context of Flint Hills Ecoregion. There are many other perspectives and variables that are well connected to this conclusion and have been discussed in this dissertation, where different combinations of “substrate + plant mix type + depth” showed significant differences in their climate change

mitigation potential. The study suggests further research and more efficient instrumentation for this combined analysis where a combination of green roof systems will work the most efficiently for a certain climate zone.

By doing all these studies in the last four years at Kansas State University related to the thermal benefits and C-sequestration potential of a green roof system, ***I would like to suggest green roof designers, architects, and landscape architects that substrate depths are not positively working as a climate change mitigation strategy in the Flint Hills Ecoregion.*** This means that an increase in substrate depth in a green roof system may work negatively as a climate change mitigation strategy within the continental climate of Manhattan, Kansas. From both studies (thermal and C sequestration) the moisture-holding capacity of different substrate types at different depths appeared to be the key factor in determining the APD-EGR's climate change mitigation potential. So, a green roof designer should study climate zones first. If the site is in one of the continental climate zones, designers can help create relatively shallower green roof systems (shallow growing medium) with lower moisture-holding capacity in general. From this study, I also hypothesized that a green roof system might improve building energy performance (~70%) more efficiently than sequestering carbon (~30%) from the environment. But this hypothesis can only be proven if you can determine the approximate R-value of green roof substrates (attempting to use the methods provided in Chapter 3).

### **Limitations of the study and future research needs**

The limitations of this study included the substrate depths being known to vary in some plots, although these variations were not investigated for this initial C-sequestration study and thermal analysis as well. Also, the plant residue (aboveground vegetative biomass) data were not interpreted in this study, nor were the plant species dynamics or their interactions in the belowground biomass of different plant mixes. Plant residues are crop materials, such as stems, leaves, and roots, that are left on the field after the harvest, and these have proven effects on soil organic carbon (Ontl and Schulte, 2012). Also, root density and total root biomass may vary in two different beds (4-inch and 8-inch). More root density in the 4-inch bed doesn't necessarily mean the amount of total root biomass was higher than in the 8-inch-deep bed in 2020. Root

density and the amount of root biomass may change and play a different role in the future growing years at the APD-EGR.

Therefore, I recommend that root biomass studies again be done in 2025 and 2030. At least a 10-year-long study may provide conclusive evidence regarding the soil C potential of two depths. For this 2019-2020 APD-EGR carbon sequestration research, it is a limitation that the study can only interpret one year of root biomass data. Including all these topics, an excellent future research agenda for APD-EGR would be to see the effect of moisture content in the belowground biomass samples where the study can compare at least 10 years of root biomass data with TOC, TN, and MB. However, given the changes to the APD-EGR in 2022 the usefulness of such studies (given the extensive dieback of vegetation on the west side of the experimental green roof beds) need to be carefully thought through. Such studies need to recognize the dramatically different plant coverage conditions that now exist, and that are likely to evolve in the coming years on the APD-EGR.

From the beginning, this study excluded the effect of plant mix types from the variables; therefore, researchers decided not to include plant residue data. Indeed, having and analyzing plant residue data in C-sequestration possibilities of different green roof types can be essential for future research agendas.

For thermal studies, building components and green roof components (like drainage layer, waterproofing, filter layer, and so on) were not discussed or explained, assuming that the materials and organization for these components remain constant and provide constant R-value from interiors for both depths (4-inch and 8-inch). Another limitation of this study is that it was not able to determine the R-value for the discussion because of insufficient data. Therefore, this study suggests appropriate instrumentations (detailed in Chapter 3).

## References

- Abdulnabi, R. (2004). Traditional repeated measures analysis versus random coefficients models using PROC MIXED. *Paper SP10. Pfizer Inc.*
- Akbari, H., & Konopacki, S. (2005). Calculating energy-saving potentials of heat-island reduction strategies. *Energy Policy*, 33(6), 721-756.
- Akther, M., He, J., Chu, A., Huang, J., & Van Duin, B. (2018). A review of green roof applications for managing urban stormwater in different climatic zones. *Sustainability*, 10(8), 2864.
- Alam, M. R., Zain, M. F. M., Kaish, A., & Jamil, M. (2015). Underground soil and thermal conductivity materials based heat reduction for energy-efficient building in tropical environment. *Indoor and Built Environment*, 24(2), 185-200.
- Alexandri, E., & Jones, P. (2008). Temperature decreases in an urban canyon due to green walls and green roofs in diverse climates. *Building and environment*, 43(4), 480-493.
- Amelung, W., Bossio, D., de Vries, W., Kögel-Knabner, I., Lehmann, J., Amundson, R., . . . Leifeld, J. (2020). Towards a global-scale soil climate mitigation strategy. *Nature communications*, 11(1), 1-10.
- Anderson, K. L., & Fly, C. I. (1955). Vegetation-soil relationships in Flint Hills bluestem pastures. *Rangeland Ecology & Management/Journal of Range Management Archives*, 8(4), 163-169.
- Avramidis, P., Nikolaou, K., & Bekiari, V. (2015). Total organic carbon and total nitrogen in sediments and soils: a comparison of the wet oxidation–titration method with the combustion-infrared method. *Agriculture and Agricultural Science Procedia*, 4, 425-430.
- Bailes, A. (2015). *The 3 Types of Heating and Cooling Loads*.  
<https://www.energyvanguard.com/blog/the-3-types-of-heating-and-cooling-loads/>
- Bardgett, R. D., Mommer, L., & De Vries, F. T. (2014). Going underground: root traits as drivers of ecosystem processes. *Trends in Ecology & Evolution*, 29(12), 692-699.
- BerkeleyLab. (2021). *Turning Up the Heat: Thermal Energy Storage Could Help Decarbonize Buildings*. Lawrence Berkeley National Laboratory (Berkeley Lab).  
<https://scitechdaily.com/turning-up-the-heat-thermal-energy-storage-could-help-decarbonize-buildings/>
- Barrachina, M., Cristóbal, J., & Tulla, A. F. (2015). Estimating above-ground biomass on mountain meadows and pastures through remote sensing. *International Journal of Applied Earth Observation and Geoinformation*, 38, 184-192.
- Batjes, N. H. (1996). Total carbon and nitrogen in the soils of the world. *European journal of soil science*, 47(2), 151-163.
- Baveye, P. C., Otten, W., Kravchenko, A., Balseiro-Romero, M., Beckers, É., Chalhoub, M., . . . Hapca, S. (2018). Emergent properties of microbial activity in heterogeneous soil microenvironments: different research approaches are slowly converging, yet major challenges remain. *Frontiers in microbiology*, 9, 1929.
- Behera, K. K. (2012). *Green Agriculture: Newer Technologies*. New India Publishing.
- Best, B. B., Swadek, R. K., & Burgess, T. L. (2015). Soil-based green roofs. In *Green Roof Ecosystems* (pp. 139-174). Springer.

- Bi, X., Li, B., Fu, Q., Fan, Y., Ma, L., Yang, Z., . . . Zhang, X. (2018). Effects of grazing exclusion on the grassland ecosystems of mountain meadows and temperate typical steppe in a mountain-basin system in Central Asia's arid regions, China. *Science of the Total Environment*, 630, 254-263.
- Bligh, E. G., & Dyer, W. J. (1959). A rapid method of total lipid extraction and purification. *Canadian journal of biochemistry and physiology*, 37(8), 911-917.
- Blozan, W. (2006). Tree measuring guidelines of the eastern native tree society. *Bulletin of the Eastern Native Tree Society*, 1(1), 3-10.
- Bolinder, M. A., Janzen, H. H., Gregorich, E. G., Angers, D. A., & VandenBygaart, A. J. (2007). An approach for estimating net primary productivity and annual carbon inputs to soil for common agricultural crops in Canada. *Agriculture, Ecosystems & Environment*, 118(1-4), 29-42.
- Bot, A., & Benites, J. (2005). *The importance of soil organic matter: Key to drought-resistant soil and sustained food production*. Food & Agriculture Org.
- Boyle, M., Frankenberger Jr, W. T., & Stolzy, L. H. (1989). The influence of organic matter on soil aggregation and water infiltration. *Journal of production agriculture*, 2(4), 290-299.
- Brevik, E. C., Homburg, J. A., & Sandor, J. A. (2018). Soils, climate, and ancient civilizations. In *Developments in Soil Science* (Vol. 35, pp. 1-28). Elsevier.
- Brutsaert, W. (1982). Evaporation into the atmosphere: Theory. *History, and Applications*, 1.
- Castleton, H. F., Stovin, V., Beck, S. B. M., & Davison, J. B. (2010). Green roofs; building energy savings and the potential for retrofit. *Energy and buildings*, 42(10), 1582-1591.
- Chao, J. (2014). *White, Green or Black Roofs? Berkeley Lab Report Compares Economic Payoffs*. N. C.-B. Lab.
- Chaplin, S., Simms, P., Cook, T., & Dinerstein, E. (2007). *Flint Hills tall grasslands*. <https://www.worldwildlife.org/>. <https://www.worldwildlife.org/ecoregions/na0807>
- Chapman, S. S., Omernik, J. M., Freeouf, J. A., Huggins, D. G., McCauley, J. R., Freeman, C. C., . . . Schleppe, R. L. (2001). Ecoregions of Nebraska and Kansas (color poster with map, descriptive text, summary tables, and photographs). *US Geological Survey, Reston, Virginia*, 1(1,950,000).
- Ciais, P., Sabine, C., Bala, G., Bopp, L., Brovkin, V., Canadell, J., . . . Heimann, M. (2014). Carbon and other biogeochemical cycles. In *Climate change 2013: the physical science basis. Contribution of Working Group I to the Fifth Assessment Report of the Intergovernmental Panel on Climate Change* (pp. 465-570). Cambridge University Press.
- Combs, S. M., & Nathan, M. V. (1998). Soil organic matter. *Recommended chemical soil test procedures for the north central region. North Central Regional Res. Publ*, 221, 53-58.
- Cooper, J. A. G., & Lemckert, C. (2012). Extreme sea-level rise and adaptation options for coastal resort cities: A qualitative assessment from the Gold Coast, Australia. *Ocean & coastal management*, 64, 1-14.
- Cresswell, H., & Hamilton, G. J. (2002). Bulk density and pore space relations. *Soil physical measurement and interpretation for land evaluation*, 35-58.
- Davis, C. (2015, July 13). 4 Reasons Green Roofs Do A Building Good.
- Decker, A. (2021). "An Experimental Design to Assess Soil-Plant-Water-Relations on a Kansas Green Roof." Unpublished Kansas State University Dissertation (September 2021).
- Del Barrio, E. P. (1998). Analysis of the green roofs cooling potential in buildings. *Energy and buildings*, 27(2), 179-193.

- Demuzere, M., Orru, K., Heidrich, O., Olazabal, E., Geneletti, D., Orru, H., . . . Faehnle, M. (2014). Mitigating and adapting to climate change: Multi-functional and multi-scale assessment of green urban infrastructure. *Journal of Environmental Management*, 146, 107-115. <https://doi.org/https://doi.org/10.1016/j.jenvman.2014.07.025>
- Dexter, A. R., Richard, G., Arrouays, D., Czyż, E. A., Jolivet, C., & Duval, O. (2008). Complexed organic matter controls soil physical properties. *Geoderma*, 144(3-4), 620-627.
- Díaz-Zorita, M., & Grosso, G. A. (2000). Effect of soil texture, organic carbon and water retention on the compactability of soils from the Argentinean pampas. *Soil and Tillage Research*, 54(1-2), 121-126.
- ESDAC. (2009). *Organic matter decline*. chrome-extension://efaidnbnmnnibpcajpcglcclfindmkaj/<https://esdac.jrc.ec.europa.eu/projects/SO/CO/FactSheets/ENFactSheet-03.pdf>
- Faaij, A., Jager, D., & Kok, M. (2013). *Global warming and social innovation: the challenge of a climate neutral society*. Routledge.
- Fageria, N. K. (2012). *The role of plant roots in crop production*. CRC Press.
- Feng, C., Meng, Q., & Zhang, Y. (2010). Theoretical and experimental analysis of the energy balance of extensive green roofs. *Energy and buildings*, 42(6), 959-965.
- Fioretti, R., Palla, A., Lanza, L. G., & Principi, P. (2010). Green roof energy and water related performance in the Mediterranean climate. *Building and Environment*, 45(8), 1890-1904. <https://doi.org/https://doi.org/10.1016/j.buildenv.2010.03.001>
- Flanders, S. N. (1992, 1992). The convergence criterion in measuring building R-values.
- Foster, J., Lowe, A., & Winkelman, S. (2011). The value of green infrastructure for urban climate adaptation. *Center for Clean Air Policy*, 750(1), 1-52.
- Frankenstein, S., & Koenig, G. (2004). *FASST vegetation models*.
- Franzluebbers, A. J. (2011). Stratification of soil porosity and organic matter. In (pp. 858-861): Springer: Dordrecht, The Netherlands.
- Frasier, I., Noellemeyer, E., Fernández, R., & Quiroga, A. (2016). Direct field method for root biomass quantification in agroecosystems. *MethodsX*, 3, 513-519.
- Funderburg, E. (2020). The role of organic matter in soil. *Stockfarm*, 10(9), 31-33.
- Gao, Z., Russell, E. S., Missik, J. E. C., Huang, M., Chen, X., Strickland, C. E., . . . Liu, H. (2017). A novel approach to evaluate soil heat flux calculation: An analytical review of nine methods. *Journal of Geophysical Research: Atmospheres*, 122(13), 6934-6949.
- Garratt, J. R. (1994). The atmospheric boundary layer. *Earth-Science Reviews*, 37(1-2), 89-134.
- Garrison, N., Horowitz, C., & Lunghino, C. A. (2012). *Looking Up: How Green Roofs and Cool Roofs Can Reduce Energy Use, Address Climate Change, and Protect Water Resources in Southern California*.
- Getter, K. L., Rowe, D. B., & Cregg, B. M. (2009). Solar radiation intensity influences extensive green roof plant communities. *Urban Forestry & Urban Greening*, 8(4), 269-281.
- Getter, K. L., Rowe, D. B., Robertson, G. P., Cregg, B. M., & Andresen, J. A. (2009). Carbon Sequestration Potential of Extensive Green Roofs. *Environmental Science & Technology*, 43(19), 7564-7570. <https://doi.org/10.1021/es901539x>
- Graceson, A., Hare, M., Hall, N., & Monaghan, J. (2014). Use of inorganic substrates and composted green waste in growing media for green roofs. *biosystems engineering*, 124, 1-7.

- Gregory, P. J. (2006). Roots, rhizosphere and soil: the route to a better understanding of soil science? *European Journal of Soil Science*, 57(1), 2-12.
- Hamin, E. M., & Gurran, N. (2009). Urban form and climate change: Balancing adaptation and mitigation in the US and Australia. *Habitat international*, 33(3), 238-245.
- Haney, R. L., & Haney, E. B. (2010). Simple and rapid laboratory method for rewetting dry soil for incubations. *Communications in Soil Science and Plant Analysis*, 41(12), 1493-1501.
- Heitman, J. L., Horton, R., Sauer, T. J., Ren, T. S., & Xiao, X. (2010). Latent heat in soil heat flux measurements. *Agricultural and Forest Meteorology*, 150(7-8), 1147-1153.
- Henry, A. (2020). *Energy Storage*. C. Portal. <https://climate.mit.edu/explainers/energy-storage>
- Herman, R. (2003). Green roofs in Germany: yesterday, today and tomorrow. *Greening Rooftops for Sustainable Communities*, 41-45.
- Hillel, D. (2003). *Introduction to environmental soil physics*. Elsevier.
- Hiraiwa, Y., & Kasubuchi, T. (2000). Temperature dependence of thermal conductivity of soil over a wide range of temperature (5–75 C). *European Journal of Soil Science*, 51(2), 211-218.
- Hirte, J., Leifeld, J., Abiven, S., Oberholzer, H.-R., Hammelehle, A., & Mayer, J. (2017). Overestimation of crop root biomass in field experiments due to extraneous organic matter. *Frontiers in plant science*, 8, 284.
- Hockstad, L., & Hanel, L. (2018). *Inventory of US greenhouse gas emissions and sinks*.
- Hodge, R., Brasington, J., & Richards, K. (2009). Analysing laser-scanned digital terrain models of gravel bed surfaces: linking morphology to sediment transport processes and hydraulics. *Sedimentology*, 56(7), 2024-2043.
- Hoepfl, M. C. (1997). Choosing qualitative research: A primer for technology education researchers. *Volume 9 Issue 1 (fall 1997)*.
- Howe, J. A., & Smith, A. P. (2021). The soil habitat. In *Principles and Applications of Soil Microbiology* (pp. 23-55). Elsevier.
- Hoyle, F. C., Murphy, D. V., & Fillery, I. R. P. (2006). Temperature and stubble management influence microbial CO<sub>2</sub>–C evolution and gross N transformation rates. *Soil Biology and Biochemistry*, 38(1), 71-80.
- Iakimenko, O., Otabbong, E., Sadovnikova, L., Persson, J., Nilsson, I., Orlov, D., & Ammosova, Y. (1996). Dynamic transformation of sewage sludge and farmyard manure components. 1. Content of humic substances and mineralisation of organic carbon and nitrogen in incubated soils. *Agriculture, ecosystems & environment*, 58(2-3), 121-126.
- Islands, R. U. H. (2008). Compendium of Strategies. Green Roofs. In: US Environmental Protection Agency.
- Ismail, W. Z. W., & Abdullah, M. N. (2016). Mitigating climate change through green roof implementation: a review of significant literature. *Journal of Architecture, Planning and Construction Management*, 6(2).
- Jaffal, I., Ouldboukhite, S.-E., & Belarbi, R. (2012). A comprehensive study of the impact of green roofs on building energy performance. *Renewable Energy*, 43, 157-164. <https://doi.org/https://doi.org/10.1016/j.renene.2011.12.004>
- Jardine, D. J. & Todd, T. C. (1990). The sting nematode. *L-Cooperative Extension Service, Kansas State University (USA)*.
- Jenkins, W. (1964). A rapid centrifugal-flotation technique for separating nematodes from soil. *Plant disease reporter*, 48.
- Jarchow, M. E., & Liebman, M. (2011). Incorporating prairies into multifunctional landscapes.

- Jiang, Y., Zhou, H., Chen, L., Fang, H., Luan, L., Chen, Y., . . . Peng, X. (2018). Nematodes and microorganisms interactively stimulate soil organic carbon turnover in the macroaggregates. *Frontiers in microbiology*, 9, 2803.
- Jim, C. Y. (2017). Green roof evolution through exemplars: Germinal prototypes to modern variants. *Sustainable cities and society*, 35, 69-82.
- Jobbágy, E. G., & Jackson, R. B. (2000). The vertical distribution of soil organic carbon and its relation to climate and vegetation. *Ecological applications*, 10(2), 423-436.
- Jones, D. L., Hodge, A., & Kuzyakov, Y. (2004). Plant and mycorrhizal regulation of rhizodeposition. *New phytologist*, 163(3), 459-480.
- Kautz, T. (2015). Research on subsoil biopores and their functions in organically managed soils: A review. *Renewable Agriculture and Food Systems*, 30(4), 318-327.  
<https://doi.org/10.1017/S1742170513000549>
- Kay, B. D., & VandenBygaart, A. J. (2002). Conservation tillage and depth stratification of porosity and soil organic matter. *Soil and Tillage Research*, 66(2), 107-118.
- Khatoon, H., Solanki, P., Narayan, M., Tewari, L., Rai, J. P. N., & Hina Khatoon, C. (2017). Role of microbes in organic carbon decomposition and maintenance of soil ecosystem. *International Journal of Chemical Studies*, 5(6), 1648-1656.
- King, A. E., Congreves, K. A., Deen, B., Dunfield, K. E., Voroney, R. P., & Wagner-Riddle, C. (2019). Quantifying the relationships between soil fraction mass, fraction carbon, and total soil carbon to assess mechanisms of physical protection. *Soil Biology and Biochemistry*, 135, 95-107.
- Klein, T., Vasl, A., Shalom, H., Kadas, G., & Blaustein, L. (2017). Sedum-dominated green-roofs in a semi-arid region increase CO<sub>2</sub> concentrations during the dry season. *Science of The Total Environment*, 584, 1147-1151.
- Knapp, M. (2017). Weather Reports for Research Field Locations. *Kansas Agricultural Experiment Station Research Reports*, 3(6), 3.
- Knight, C. (2011). *Green roofs, a key step in climate change mitigation*. C. Action.  
<https://www.climateaction.org/news/green-roofs-a-key-step-in-climate-change-mitigation>
- Knowledge, C. (2019). *Reducing climate change impacts on private buildings*.  
[https://www.c40knowledgehub.org/s/article/Reducing-climate-change-impacts-on-private-buildings?language=en\\_US](https://www.c40knowledgehub.org/s/article/Reducing-climate-change-impacts-on-private-buildings?language=en_US)
- Kononova, M. a. M. (2013). *Soil organic matter: its nature, its role in soil formation and in soil fertility*. Elsevier.
- Korenblum, E., Dong, Y., Szymanski, J., Panda, S., Jozwiak, A., Massalha, H., . . . Aharoni, A. (2020). Rhizosphere microbiome mediates systemic root metabolite exudation by root-to-root signaling. *Proceedings of the National Academy of Sciences*, 117(7), 3874-3883.
- KSU. (2012). *Konza Prairie Site Description*. Konza Prairie Biological Station (KPBS).  
<http://www.konza.ksu.edu/general/knzsite.aspx?currMenu=9&depth=1>
- Kumar, R., & Kaushik, S. C. (2005). Performance evaluation of green roof and shading for thermal protection of buildings. *Building and environment*, 40(11), 1505-1511.
- Kuronuma, T., Watanabe, H., Ishihara, T., Kou, D., Touda, K., Ando, M., & Shindo, S. (2018). CO<sub>2</sub> payoff of extensive green roofs with different vegetation species. *Sustainability*, 10(7), 2256.
- Köhler, M. (2006). Long-term vegetation research on two extensive green roofs in Berlin. *Urban Habitats*, 4(1), 3-26.

- Lal, R., & Follett, R. F. (2009). *Soil carbon sequestration and the greenhouse effect* (Vol. 57). ASA-CSSA-SSSA.
- Langemeyer, J., Wedgwood, D., McPhearson, T., Baró, F., Madsen, A. L., & Barton, D. N. (2020). Creating urban green infrastructure where it is needed—A spatial ecosystem service-based decision analysis of green roofs in Barcelona. *Science of the total environment*, 707, 135487.
- Langer, M., Westermann, S., Muster, S., Piel, K., & Boike, J. (2011). The surface energy balance of a polygonal tundra site in northern Siberia—Part 1: Spring to fall. *The Cryosphere*, 5(1), 151-171.
- Lauenroth, W. K., Hunt, H. W., Swift, D. M., & Singh, J. S. (1986). Estimating aboveground net primary production in grasslands: a simulation approach. *Ecological Modelling*, 33(2-4), 297-314.
- Laukkonen, J., Blanco, P. K., Lenhart, J., Keiner, M., Cavric, B., & Kinuthia-Njenga, C. (2009). Combining climate change adaptation and mitigation measures at the local level. *Habitat international*, 33(3), 287-292.
- Lee, K.-H., Joo, M.-C., & Baek, N.-C. (2015). Experimental evaluation of simple thermal storage control strategies in low-energy solar houses to reduce electricity consumption during grid on-peak periods. *Energies*, 8(9), 9344-9364.
- Li, J.-f., Wai, O. W. H., Li, Y. S., Zhan, J.-m., Ho, Y. A., Li, J., & Lam, E. (2010). Effect of green roof on ambient CO<sub>2</sub> concentration. *Building and Environment*, 45(12), 2644-2651. <https://doi.org/https://doi.org/10.1016/j.buildenv.2010.05.025>
- Li, W. C., & Yeung, K. K. A. (2014). A comprehensive study of green roof performance from environmental perspective. *International Journal of Sustainable Built Environment*, 3(1), 127-134. <https://doi.org/https://doi.org/10.1016/j.ijbsbe.2014.05.001>
- Libonati, R., Geirinhas, J. L., Silva, P. S., Russo, A., Rodrigues, J. A., Belém, L. B., ... & Trigo, R. M. (2022). Assessing the role of compound drought and heatwave events on unprecedented 2020 wildfires in the Pantanal. *Environmental Research Letters*, 17(1), 015005.
- Lin, B.-S., Yu, C.-C., Su, A.-T., & Lin, Y.-J. (2013). Impact of climatic conditions on the thermal effectiveness of an extensive green roof. *Building and Environment*, 67, 26-33. <https://doi.org/https://doi.org/10.1016/j.buildenv.2013.04.026>
- Linn, D. M., & Doran, J. W. (1984). Effect of water-filled pore space on carbon dioxide and nitrous oxide production in tilled and nontilled soils. *Soil Science Society of America Journal*, 48(6), 1267-1272.
- Longstroth, M. (2012). *Moist, weed-free soil retains more heat*. [https://www.canr.msu.edu/news/moist\\_weed\\_free\\_soil\\_retains\\_more\\_heat](https://www.canr.msu.edu/news/moist_weed_free_soil_retains_more_heat)
- LTER, K. B. S. (2022). *MCSE: Aboveground Net Primary Productivity*. Kellogg Biological Station. Retrieved September 10, 2022, from <https://lter.kbs.msu.edu/protocols/111>
- Materials, A. S. f. T. (2013). *Standard Practice for Determining Thermal Resistance of Building Envelope Components from the In-situ Data*. ASTM International.
- McCarthy, J. J., Canziani, O. F., Leary, N. A., Dokken, D. J., & White, K. S. (Eds.). (2001). *Climate change 2001: impacts, adaptation, and vulnerability: contribution of Working Group II to the third assessment report of the Intergovernmental Panel on Climate Change* (Vol. 2). Cambridge University Press.
- McLatchey, G. P., & Reddy, K. R. (1998). *Regulation of organic matter decomposition and nutrient release in a wetland soil* (0047-2425).

- McNear Jr, D. H. (2013). The rhizosphere-roots, soil and everything in between. *Nature Education Knowledge*, 4(3), 1.
- McVay, K. A., Budde, J. A., Fabrizzi, K., Mikha, M. M., Rice, C. W., Schlegel, A. J., . . . Thompson, C. (2006). Management effects on soil physical properties in long-term tillage studies in Kansas. *Soil Science Society of America Journal*, 70(2), 434-438.
- METERGROUP. (2020). *ZENTRA Mobile Apps*. <https://www.metergroup.com/zentra-mobile-apps/>
- Moghbel, M., & Erfanian Salim, R. (2017). Environmental benefits of green roofs on microclimate of Tehran with specific focus on air temperature, humidity and CO2 content. *Urban Climate*, 20, 46-58. <https://doi.org/https://doi.org/10.1016/j.uclim.2017.02.012>
- Mughees, N. (2022). *Thermal energy storage solutions for buildings*. <https://insights.globalspec.com/article/18659/thermal-energy-storage-solutions-for-buildings>
- Neher, D. A. (2010). Ecology of Plant and Free-Living Nematodes in Natural and Agricultural Soil. *Annual Review of Phytopathology*, 48(1), 371-394. <https://doi.org/10.1146/annurev-phyto-073009-114439>
- Niachou, A., Papakonstantinou, K., Santamouris, M., Tsangrassoulis, A., & Mihalakakou, G. (2001). Analysis of the green roof thermal properties and investigation of its energy performance. *Energy and buildings*, 33(7), 719-729.
- NPS. (n.d.). *What is a Green Roof?* <https://www.nps.gov/tps/sustainability/new-technology/green-roofs/define.htm>
- Ochsner, T. (2019). *Rain or Shine: An Introduction to Soil Physical Properties and Processes*.
- Oncley, S. P., Foken, T., Vogt, R., Kohsiek, W., DeBruin, H. A. R., Bernhofer, C., . . . Feigenwinter, C. (2007). The energy balance experiment EBEX-2000. Part I: overview and energy balance. *Boundary-Layer Meteorology*, 123(1), 1-28.
- O'Brien, K. L., Sygna, L., Leichenko, R., Adger, W. N., Barnett, J., Mitchell, T., ... & Mortreux, C. (2008). Disaster Risk Reduction, Climate Change Adaptation and Human Security: A Commissioned Report for the Norwegian Ministry of Foreign Affairs by the Global Environmental Change and Human Security (GECHS) Project.
- Ontl, T. A., & Schulte, L. A. (2012). Soil carbon storage. *Nature Education Knowledge*, 3(10).
- Ostrowska, A., & Porebska, G. (2012). Assessment of TOC-SOM and SOM-TOC conversion in forest soil. *Polish Journal of Environmental Studies*, 21(6).
- Pan, L., Peng, S. U. I., Gao, W.-s., Wang, B.-b., Huang, J.-x., Peng, Y. A. N., . . . Chen, Y.-q. (2015). Aggregate stability and associated C and N in a silty loam soil as affected by organic material inputs. *Journal of Integrative Agriculture*, 14(4), 774-787.
- Parkin, T. B., Doran, J. W., & Franco-Vizcaíno, E. (1997). Field and laboratory tests of soil respiration. *Methods for assessing soil quality*, 49, 231-245.
- Paustian, K., Lehmann, J., Ogle, S., Reay, D., Robertson, G. P., & Smith, P. (2016). Climate-smart soils. *Nature*, 532(7597), 49-57.
- Peck, S. W. (2002). Green roofs: infrastructure for the 21st century. *Clean Air Partnership and presented at the 1st Annual Urban Heat Island Summit, May*, 2-3.
- Philip, J. R. (1961). The theory of heat flux meters. *Journal of Geophysical Research*, 66(2), 571-579.

- Philippot, L., Raaijmakers, J. M., Lemanceau, P., & Van Der Putten, W. H. (2013). Going back to the roots: the microbial ecology of the rhizosphere. *Nature Reviews Microbiology*, *11*(11), 789-799.
- Pluske, W., Murphy, D., & Sheppard, J. (2022). *Fact Sheets: Total Organic Carbon*. <https://www.soilquality.org.au/factsheets/organic-carbon>
- Potter, S., & Cabbage, M. (2017). *NASA, NOAA Data Show 2016 Warmest Year on Record Globally*. NASA.
- Price, A., Jones, E. C., & Jefferson, F. (2015). Vertical greenery systems as a strategy in urban heat island mitigation. *Water, Air, & Soil Pollution*, *226*(8), 247.
- Project Drawdown. (2020). Table of Solutions. Project Drawdown. <https://drawdown.org/solutions/table-of-solutions>
- Puget, P., Chenu, C., & Balesdent, J. (2000). Dynamics of soil organic matter associated with particle-size fractions of water-stable aggregates. *European Journal of Soil Science*, *51*(4), 595-605.
- Quideau, S. A., McIntosh, A. C. S., Norris, C. E., Lloret, E., Swallow, M. J. B., & Hannam, K. (2016). Extraction and analysis of microbial phospholipid fatty acids in soils. *JoVE (Journal of Visualized Experiments)*(114), e54360.
- Raaijmakers, J. M., Paulitz, T. C., Steinberg, C., Alabouvette, C., & Moënne-Loccoz, Y. (2009). The rhizosphere: a playground and battlefield for soilborne pathogens and beneficial microorganisms. *Plant and soil*, *321*(1-2), 341-361.
- Refahi, A. H., & Talkhabi, H. (2015). Investigating the effective factors on the reduction of energy consumption in residential buildings with green roofs. *Renewable Energy*, *80*, 595-603. <https://doi.org/https://doi.org/10.1016/j.renene.2015.02.030>
- Rice, C. W., Pires, C. B., Lin, J., & Sarto, M. V. M. (2021). Soil Organic Carbon Assessment Methods. *Soil Health Series: Volume 2 Laboratory Methods for Soil Health Analysis*, 38-51.
- Roxy, M. S., Sumithranand, V. B., & Renuka, G. (2014). Soil heat flux and day time surface energy balance closure at astronomical observatory, Thiruvananthapuram, south Kerala. *Journal of earth system science*, *123*(4), 741-750.
- Sailor, D. (2009). *Cooling Our Cities: An Interview with Dr. David Sailor* [Interview]. Green Infrastructure Digest sustainable site solutions for a sustainable world.
- Sailor, D. J. (2008). A green roof model for building energy simulation programs. *Energy and Buildings*, *40*(8), 1466-1478. <https://doi.org/https://doi.org/10.1016/j.enbuild.2008.02.001>
- Sailor, D. J., Elley, T. B., & Gibson, M. (2011). Exploring the building energy impacts of green roof design decisions – a modeling study of buildings in four distinct climates. *Journal of Building Physics*, *35*(4), 372-391. <https://doi.org/10.1177/1744259111420076>
- Sainju, U. M., Allen, B. L., Lenssen, A. W., & Ghimire, R. P. (2017). Root biomass, root/shoot ratio, and soil water content under perennial grasses with different nitrogen rates. *Field Crops Research*, *210*, 183-191.
- Santamouris, M., Pavlou, C., Doukas, P., Mihalakakou, G., Synnefa, A., Hatzibiros, A., & Patargias, P. (2007). Investigating and analysing the energy and environmental performance of an experimental green roof system installed in a nursery school building in Athens, Greece. *Energy*, *32*(9), 1781-1788.
- Schrader, S., & Böning, M. (2006). Soil formation on green roofs and its contribution to urban biodiversity with emphasis on Collembolans. *Pedobiologia*, *50*(4), 347-356. <https://doi.org/https://doi.org/10.1016/j.pedobi.2006.06.003>

- Schumacher, B. A. (2002). Methods for the determination of total organic carbon (TOC) in soils and sediments.
- Selker, J., & Or, D. (2021). Heat Flow and Thermal Effects in Soils. *Soil Hydrology and Biophysics*.
- Services, T. P. (2018). *Green Roof Benefits*. National Park Service.  
<https://home1.nps.gov/tps/sustainability/new-technology/green-roofs/benefits.htm>
- Sharifi, A. (2020). Trade-offs and conflicts between urban climate change mitigation and adaptation measures: A literature review. *Journal of Cleaner Production*, 276, 122813.
- Shrestha, P. (2019). Assessment of first-year survival, growth, and physiological performance of seven species of graminoids within two substrate types on a green roof in the Flint Hills Ecoregion.
- Sikora, L. J., & Stott, D. E. (1997). Soil organic carbon and nitrogen. *Methods for assessing soil quality*, 49, 157-167.
- Skabelund, L. R., & Alam, M. M. L. (2020). Kansas State University Memorial Stadium Green Roofs Methods. In.
- Skabelund, L. R., Blocksome, C., Hamehkasi, M., Jin Kim, H., Knapp, M., & Brokesh, D. (2014, 2014). Semi-arid green roof research 2009–2014: resilience of native species.
- Skabelund, L. R., Decker, A., Moore, T., Shrestha, P., & Bruce, J. L. (2017, 2017). Monitoring two large-scale prairie-like green roofs in Manhattan, Kansas.
- Skabelund, L. R., DiGiovanni, K., & Starry, O. (2015). Monitoring abiotic inputs and outputs. In *Green Roof Ecosystems* (pp. 27-62). Springer.
- Snyder, R. L., & Paw-U, K. T. (2001). Soil Heat Flow and Temperature. *Soil Heat Flow and Temperature*.
- Sohn, E. (2009). Green Roofs Offset Global Warming, Study Finds. *NBC News*.
- Spala, A., Bagiorgas, H. S., Assimakopoulos, M. N., Kalavrouziotis, J., Matthopoulos, D., & Mihalakakou, G. (2008). On the green roof system. Selection, state of the art and energy potential investigation of a system installed in an office building in Athens, Greece. *Renewable Energy*, 33(1), 173-177.
- Spark, W. (2020-2021). *Weather Data for the Manhattan, KS (zip code 66502)*.  
<https://weatherspark.com/>. <https://weatherspark.com/y/8981/Average-Weather-in-Manhattan-Kansas-United-States-Year-Round>
- Statistics, L. (n.d.). *Repeated Measures ANOVA*. <https://statistics.laerd.com/statistical-guides/repeated-measures-anova-statistical-guide.php>
- Stephens, D. B., Kron, A. J., & Kron, A. (2018). *Vadose zone hydrology*. CRC press.
- Sutton, R. K. (2013). Rethinking extensive green roofs to lessen emphasis on above-ground biomass.
- Sutton, R. K. (2015). Introduction to green roof ecosystems. In *Green Roof Ecosystems* (pp. 1-25). Springer.
- Sutton, R. K., Harrington, J. A., Skabelund, L., MacDonagh, P., Coffman, R. R., & Koch, G. (2012). Prairie-based green roofs: literature, templates, and analogs. *Journal of Green Building*, 7(1), 143-172.
- Tabares Velasco, P. C. (2009). Predictive heat and mass transfer model of plant-based roofing materials for assessment of energy savings.
- Takakura, T., Kitade, S., & Goto, E. (2000). Cooling effect of greenery cover over a building. *Energy and buildings*, 31(1), 1-6.

- Takebayashi, H., & Moriyama, M. (2007). Surface heat budget on green roof and high reflection roof for mitigation of urban heat island. *Building and Environment*, 42(8), 2971-2979.
- Thomas, J. R., Nelson, J. K., & Silverman, S. J. (2015). *Research methods in physical activity*. Human kinetics.
- Tollerud, H., Brown, J., Loveland, T., Mahmood, R., & Bliss, N. (2018). Drought and land-cover conditions in the great plains. *Earth Interactions*, 22(17), 1-25.
- Towell, G. (2020). *Thermal Conductivity: Definition, Units, Equation & Example*. sciencing. <https://sciencing.com/phase-transitions-types-classifications-properties-examples-w-diagram-13722760.html>
- Tubiello, F. N., Salvatore, M., Ferrara, A. F., House, J., Federici, S., Rossi, S., . . . Flammini, A. (2015). The contribution of agriculture, forestry and other land use activities to global warming, 1990–2012. *Global change biology*, 21(7), 2655-2660.
- United Nations Development, P. (2007). *Fighting climate change: Human solidarity in a divided world*. Springer.
- USDA. (n.d.). *Soil Respiration*. [https://www.nrcs.usda.gov/Internet/FSE\\_DOCUMENTS/nrcs142p2\\_053267.pdf](https://www.nrcs.usda.gov/Internet/FSE_DOCUMENTS/nrcs142p2_053267.pdf)
- USGS. (2018). *Specific Heat Capacity and Water*. <https://www.usgs.gov/special-topics/water-science-school/science/specific-heat-capacity-and-water>
- Van Renterghem, T., & Botteldooren, D. (2011). In-situ measurements of sound propagating over extensive green roofs. *Building and environment*, 46(3), 729-738.
- Weatherspark. (2020-2021). *Weather Data for the Manhattan, KS (zip code 66502)*. <https://weatherspark.com/>. <https://weatherspark.com/y/8981/Average-Weather-in-Manhattan-Kansas-United-States-Year-Round>
- Wei, T., Jim, C. Y., Chen, A., & Li, X. (2020). Adjusting soil parameters to improve green roof winter energy performance based on neural-network modeling. *Energy Reports*, 6, 2549-2559.
- White, P. M., & Rice, C. W. (2009). Tillage effects on microbial and carbon dynamics during plant residue decomposition. *Soil Science Society of America Journal*, 73(1), 138-145.
- Whittinghill, L. J., Rowe, D. B., Schutzki, R., & Cregg, B. M. (2014). Quantifying carbon sequestration of various green roof and ornamental landscape systems. *Landscape and Urban Planning*, 123, 41-48. <https://doi.org/https://doi.org/10.1016/j.landurbplan.2013.11.015>
- Wibowo, H., & Kasno, A. (2021, 2021). Soil organic carbon and total nitrogen dynamics in paddy soils on the Java Island, Indonesia.
- Williams, N. S. G., Rayner, J. P., & Raynor, K. J. (2010). Green roofs for a wide brown land: Opportunities and barriers for rooftop greening in Australia. *Urban Forestry & Urban Greening*, 9(3), 245-251.
- Wilsey, B. J., & Polley, H. W. (2006). Aboveground productivity and root–shoot allocation differ between native and introduced grass species. *Oecologia*, 150(2), 300-309.
- Wilson, G. W. T., Rice, C. W., Rillig, M. C., Springer, A., & Hartnett, D. C. (2009). Soil aggregation and carbon sequestration are tightly correlated with the abundance of arbuscular mycorrhizal fungi: results from long-term field experiments. *Ecology letters*, 12(5), 452-461.
- Wollum, A. G., & Gomez, J. E. (1970). A conductivity method for measuring microbially evolved carbon dioxide. *Ecology*, 51(1), 155-156.

- Wong, N. H., Chen, Y., Ong, C. L., & Sia, A. (2003). Investigation of thermal benefits of rooftop garden in the tropical environment. *Building and environment*, 38(2), 261-270.
- Yang, J., Yu, Q., & Gong, P. (2008). Quantifying air pollution removal by green roofs in Chicago. *Atmospheric Environment*, 42(31), 7266-7273.  
<https://doi.org/https://doi.org/10.1016/j.atmosenv.2008.07.003>
- Zibilske, L. M. (1994). Carbon mineralization. *Methods of Soil Analysis: Part 2 Microbiological and Biochemical Properties*, 5, 835-863.

## Appendix A - Climate of Manhattan Kansas

**Table A-1: Monthly mean maximum temperatures (°F) for Manhattan, Kansas 2000-2019**

(Source: NOAA, <https://w2.weather.gov/climate/xmacis.php?wfo=top>)

### Monthly Highest Max Temperature for MANHATTAN, KS

Click column heading to sort ascending, click again to sort descending.

Year	Jan	Feb	Mar	Apr	May	Jun	Jul	Aug	Sep	Oct	Nov	Dec	Annual
2000	64	77	80	92	99	95	102	109	111	97	72	61	111
2001	61	64	70	90	95	95	107	103	94	87	82	72	107
2002	70	70	74	93	95	99	108	101	100	94	73	69	108
2003	72	68	85	91	93	94	105	106	90	90	71	62	106
2004	60	66	83	90	96	96	102	100	95	86	76	69	102
2005	68	69	78	89	95	100	103	102	97	90	81	66	103
2006	70	84	80	92	98	100	108	109	95	97	84	63	109
2007	61	71	86	89	90	92	98	105	96	94	79	63	105
2008	65	57	75	84	90	97	100	107	94	82	80	69	107
2009	64	73	83	87	93	100	97	100	87	78	77	62	100
2010	57	58	81	88	89	98	100	107	98	91	77	66	107
2011	56	72	85	92	100	98	110	107	107	91	75	62	110
2012	70	65	85	93	96	105	107	102	100	87	80	69	107
2013	75	66	83	88	94	97	105	101	102	89	74	67	105
2014	62	71	79	87	93	94	103	102	95	89	70	59	103
2015	70	72	85	84	87	99	101	95	99	89	80	67	101
2016	67	78	81	87	88	103	102	98	95	89	83	66	103
2017	64	78	90	83	91	97	104	95	95	88	79	70	104
2018	66	71	78	87	99	105	102	98	95	91	65	57	105
2019	62	69	73	86	91	97	100	95	95	90	73	65	100
<b>Mean</b>	65	70	81	89	94	98	103	102	97	89	77	65	105
<b>Max</b>	75 2013	84 2006	90 2017	93 2012	100 2011	105 2018	110 2011	109 2006	111 2000	97 2006	84 2006	72 2001	111 2000
<b>Min</b>	56 2011	57 2008	70 2001	83 2017	87 2015	92 2007	97 2009	95 2019	87 2009	78 2009	65 2018	57 2018	100 2019

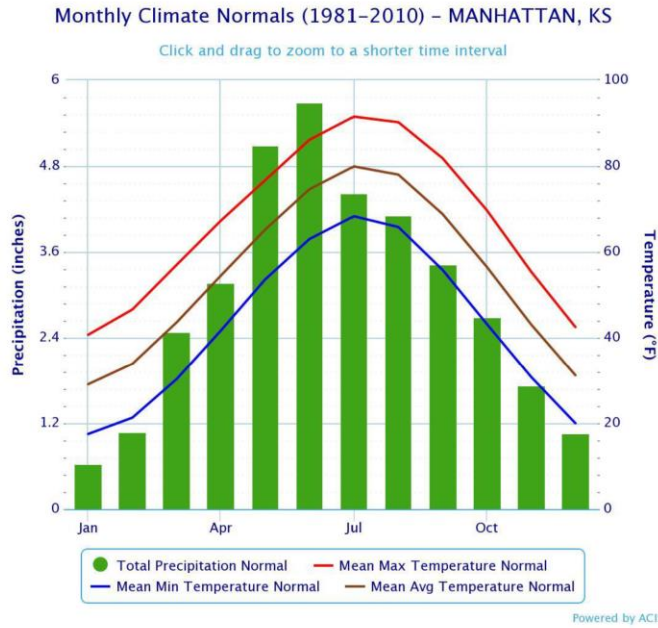


**Figure A-1: 1981-2010 monthly climate normal temperatures and precipitation in Manhattan, Kansas**

(Source: NOAA, <https://w2.weather.gov/climate/xmacis.php?wfo=top>)

**Monthly Lowest Min Temperature for MANHATTAN, KS**  
 Click column heading to sort ascending, click again to sort descending.

Year	Jan	Feb	Mar	Apr	May	Jun	Jul	Aug	Sep	Oct	Nov	Dec	Annual
2000	7	11	20	25	41	46	57	59	34	19	12	-9	-9
2001	-10	-9	13	25	39	44	59	50	35	24	18	2	-10
2002	-1	1	0	20	35	50	58	54	41	28	14	10	-1
2003	-8	-3	6	19	37	45	56	58	35	25	11	9	-8
2004	-5	-5	19	25	30	48	48	47	47	29	21	-4	-5
2005	-2	1	12	25	28	53	51	50	35	24	12	-9	-9
2006	20	0	22	32	41	50	56	51	41	26	19	8	0
2007	-1	0	18	14	44	50	54	57	44	29	9	5	-1
2008	-8	2	8	27	32	52	53	55	39	21	13	-6	-8
2009	0	8	9	22	40	52	50	45	35	27	22	-8	-8
2010	-10	5	15	30	37	54	57	48	42	31	17	7	-10
2011	-2	-6	17	32	36	52	69	62	43	27	19	13	-6
2012	8	7	23	35	44	45	64	52	40	26	14	6	6
2013	8	2	16	26	34	51	55	55	45	28	12	0	0
2014	-10	-5	-4	26	34	53	51	56	37	33	9	3	-10
2015	1	2	9	33	40	53	60	52	51	30	25	16	1
2016	0	17	24	30	42	56	63	55	44	33	25	-10	-10
2017	-1	14	22	32	37	55	59	54	46	24	18	-3	-3
2018	-8	1	16	16	52	56	59	58	44	29	11	12	-8
2019	-2	3	-2	29	41	48	58	57	55	18	7	11	-2
<b>Mean</b>	-1	2	13	26	38	51	57	54	42	27	15	3	-5
<b>Max</b>	20	17	24	35	52	56	69	62	55	33	25	16	6
	2006	2016	2016	2012	2018	2018	2011	2011	2019	2016	2016	2015	2012
<b>Min</b>	-10	-9	-4	14	28	44	48	45	34	18	7	-10	-10
	2014	2001	2014	2007	2005	2001	2004	2009	2000	2019	2019	2016	2016

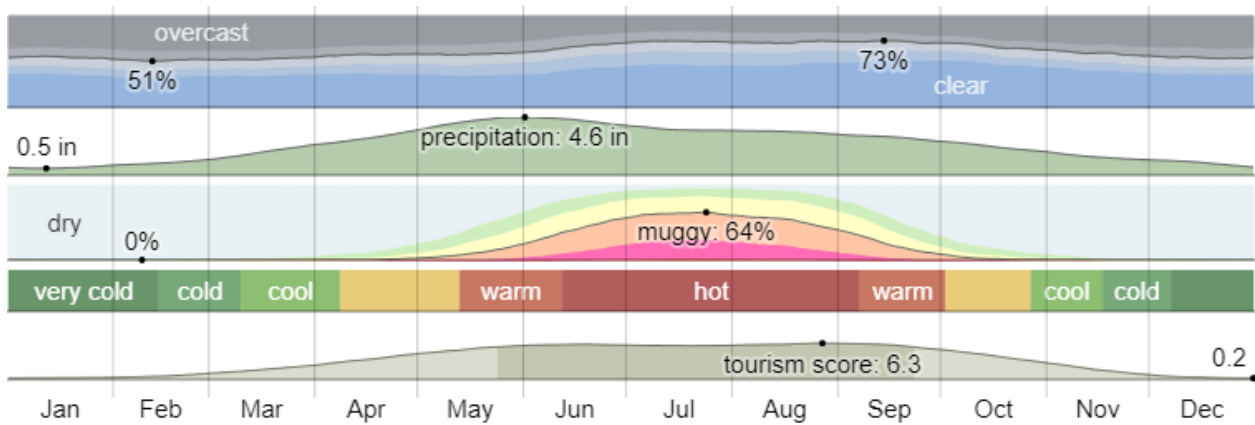
**Table A-2: Monthly mean minimum temperatures (°F) for Manhattan, Kansas 2000-2019**

(Source: NOAA, <https://w2.weather.gov/climate/xmacis.php?wfo=top>)

In Manhattan, the summers are hot, humid, wet, and mostly clear and the winters are very cold, snowy, windy, and partly cloudy. Over the course of the year, the temperature typically varies from 20°F to 92°F and is rarely below 3°F or above 101°F.

**Figure A-2 Manhattan weather by month. Click on each chart for more information**

(Source: <https://weatherspark.com/y/8981/Average-Weather-in-Manhattan-Kansas-United-States-Year-Round>)



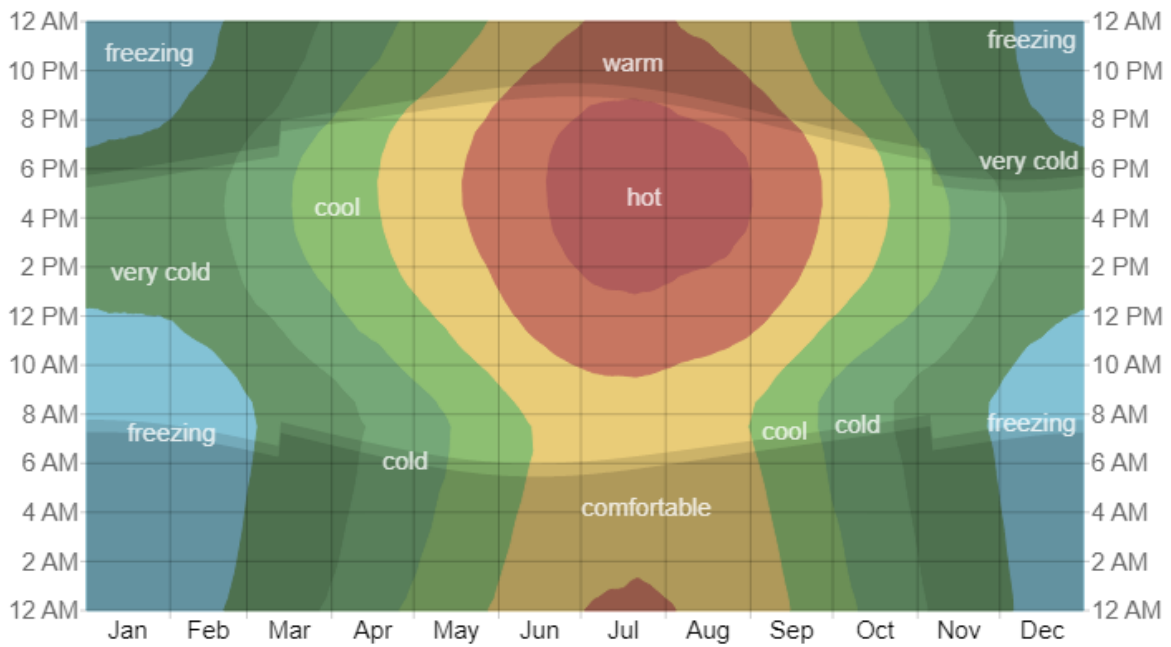


**Figure A-3 The average hourly temperature, color coded into bands. The shaded overlays indicate night and civil twilight.**

(Source: <https://weatherspark.com/y/8981/Average-Weather-in-Manhattan-Kansas-United-States-Year-Round>)

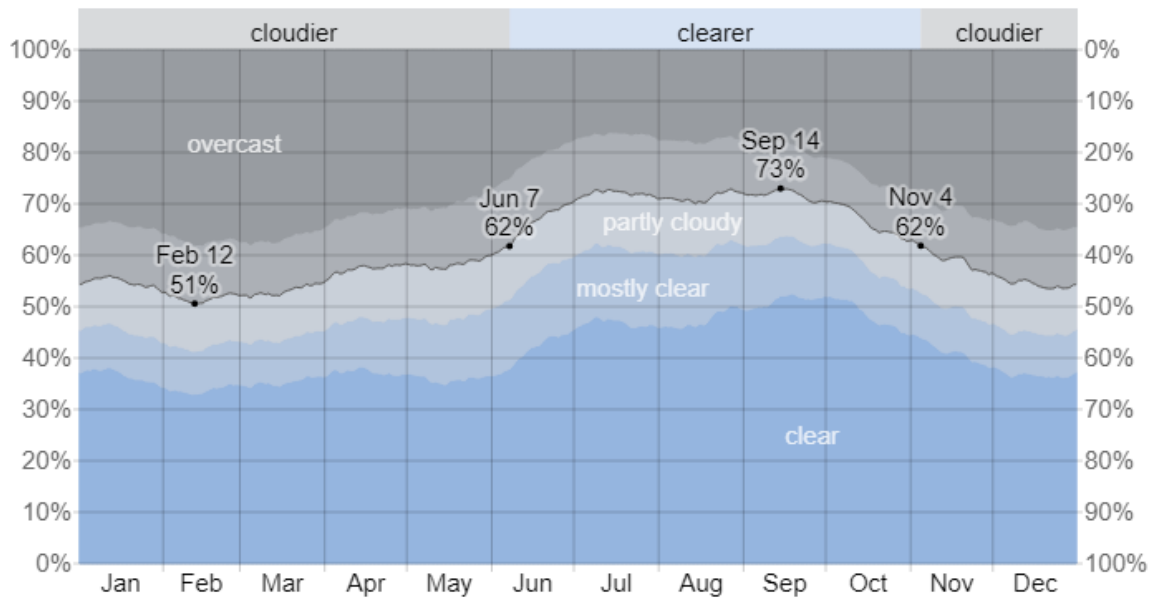


**Figure A-4 The percentage of time spent in each cloud cover band, categorized by the percentage of the sky covered by clouds.**

(Source: <https://weatherspark.com/y/8981/Average-Weather-in-Manhattan-Kansas-United-States-Year-Round>)

## **Appendix B - Substrate Analysis and Testing Procedures by the KSU Soil Testing Lab and Turf and Soil Diagnostics**

**Substrate Analysis:** Per personal communications between Bryan Rutter (Manager, KSU Soil Testing Lab) and Jialin Liu (2018-2019), the following procedures were used to obtain soil test results:

**“Total N and P analysis:** 1 to 10 ml sample is digested with Potassium Persulfate Reagent in an autoclave and then analyzed using an Alpkem RFA for nitrate nitrogen (cadmium reduction method) and phosphorus according to:

1. Hosomi, M. and Sudu, R. 1986. Simultaneous determination of total nitrogen and total phosphorus in freshwater samples using persulfate digestion. *International Journal of Environmental Studies*. 27; 267-275.
2. Nelson N.S. 1987. An Acid-persulfate digestion procedure for determination of phosphorus in sediments. *Communications in Soil Science Plant Analysis*, 18(4); 359-369.
3. Alpkem Corporation. 1986. RFA Methodology no. A303-S170. Nitrate-Nitrite Nitrogen. Clackamas, OR 97015.

**Ammonia and Nitrate Nitrogen:** Alpkem RFA autoanalyzer according to:

1. Alpkem Corporation. 1986. RFA Methodology no. A303-S021. Ammonia Nitrogen. Clackamas, OR 97015.
2. Alpkem Corporation. 1986. RFA Methodology no. A303-S170. Nitrate+Nitrite Nitrogen. Clackamas, OR 97015.

**Analysis of Ca, Mg, Na, Zn, Cu** is done by an Inductively Coupled Plasma (ICP) Spectrometer, Model 720-ES ICP Optical Emission Spectrometer, manufactured by Varian Australia Pty Ltd, Mulgrave, Vic Australia.

**Chloride analysis** uses the calcium nitrate extraction and colorimetric analysis in the Mercury Thiocyanate method listed in “Recommended Chemical Soil Test Procedures for the North Central Region” on pp. 49-50 (Gelderman, R.H., Denning, J.L., and Goos, R.J.). The colorimetric assay is performed using an Alpkem RFA Methodology No. A303-S090. Water samples are not extracted in calcium nitrate but are diluted in calcium nitrate prior to analysis.”

**Exchangeable Cations** Calcium - Magnesium - Potassium - Sodium

1. Scoop 2 g of soil for public samples. Weigh or scoop, according to submitted info sheet, 2 g of soil for research samples.
2. Dump soil into appropriate flask in K rack, tapping the scoop on the funnel to remove all of the soil from the scoop. Put LOW K CK in #12 and CK14 in #24 spot. After the samples, scoop or weigh Quality Control Samples, T-1 #1 and #13, T-2 #1 and #13, etc. End with LOW, HI, and Blank.
3. Dispense 20 mL of ammonium acetate (NH<sub>4</sub>OAC) extracting solution into each flask. Shake at 200 rpm (high) for 5 minutes at room temperature; 24 to 27°C.
4. Filter immediately through Ahlstrom 642 filter paper for calcium (Ca), potassium (K), and magnesium (Mg). Use Ahlstrom 74 filter paper if sodium (Na) was requested on samples.
5. If analyzing for potassium (K), read filtrates on atomic absorption spectrometer (AA), using appropriate K standards as listed in Table 2.5.
6. If analyzing for calcium (Ca<sup>2+</sup>), magnesium (Mg<sup>2+</sup>), and sodium (Na<sup>+</sup>), read filtrates on ICP. Pour samples from filtering racks into glass autosampler tubes and place in white ICP rack. Use appropriate cations standards as listed in Table 2.6.

## References

- Jones, J.B. 2001. Soil Analysis. p. 79-93. In Laboratory Guide for Conduction Soil Tests and Plant Analysis. CRC Press Boca Raton, FL.
- Schollenberger, C.J. and R.H. Simon. 1945. Determination of exchange capacity and exchangeable basis in soil-ammonium acetate method. Soil Sci. 59:13-24.
- Warncke D. and J.R. Brown. 1998. Potassium and Other Basic Cations. P. 31-33. In J.R. Brown (ed.) Recommended Chemical Soil Test Procedures for the North Central Region. North Central Regional Publication Number 221 (revised). Missouri Ag. Exp. Station SB 1001. Univ. of Missouri, Columbia, MO.

## Cation Exchange Capacity Estimation

### Summation - pH 7.0

1. Refer to Exchangeable Cation Procedure Steps (1-4). Use Ahlstrom 74 filter paper.
2. When analyzing for calcium ( $\text{Ca}^{2+}$ ), magnesium ( $\text{Mg}^{2+}$ ), and sodium ( $\text{Na}^+$ ), read filtrates on ICP. Pour samples from filtering racks into glass autosampler tubes and place in white ICP rack. Use appropriate cations standards as listed in Table 2.6.
3. Open ICP cation Excel file. Multiply data by 10 (dilution factor) and subtract the blank. Verify check soils are in correct range.
4. Open CEC Calculation template. Input ICP cation values into the appropriate columns. If the SMP buffer pH is less than 7, enter the SMP buffer pH value into the H column. If the buffer pH is 7 or greater, enter 7.
5. Report values as meq/100g.

## References

- Chapman, H. D., "Cation Exchange Capacity," Methods of Soil Analysis, C. A. Black, ed. Agronomy Monograph No. 9, American Society of Agronomy: Inc., 1965, pp. 891-901.
- "Diagnosis and improvement of saline and alkali soils," L. A. Richards, ed., United States Department of Agriculture Handbook, No. 60, February 1954, 160 pp. Jackson, M. L., Soil Chemical Analysis--Advanced Course, 2nd ed, 11th printing. Published by author, Madison, WI, 1979, pp. 256-285.
- Rich, C. I., "Removal of excess salt in cation exchange capacity determinations," Soil Science, Vol. 93, 1969, pp. 87-93.

## Exchangeable Cations Calcium - Magnesium - Potassium - Sodium

1. Scoop 2 g of soil for public samples. Weigh or scoop, according to submitted information sheet, 2 g of soil for research samples.
2. Dump soil into appropriate flask in K rack, tapping the scoop on the funnel to remove all of the soil from the scoop. Put LOW K CK in #12 and CK14 in #24 spot. After the samples, scoop or weigh Quality Control Samples, T-1 #1 and #13, T-2 #1 and #13 etc.. End with LOW, HI, and Blank.
3. Dispense 20 mL of ammonium acetate ( $\text{NH}_4\text{OAC}$ ) extracting solution into each flask. Shake at 200 rpm (high) for 5 minutes at room temperature; 24 to 27°C.
4. Filter immediately through Ahlstrom 642 filter paper for calcium (Ca), potassium (K), and magnesium (Mg). Important: Use Ahlstrom 74 filter paper if sodium (Na) was requested on samples.
5. If analyzing for potassium (K), read filtrates on atomic absorption spectrometer (AA), using appropriate K standards as listed in Table 2.5.
6. If analyzing for calcium ( $\text{Ca}^{2+}$ ), magnesium ( $\text{Mg}^{2+}$ ), and sodium ( $\text{Na}^+$ ), read filtrates on ICP. Pour samples from filtering racks into glass autosampler tubes and place in white ICP rack. Use appropriate cations standards as listed in Table 2.6.

## References

- Jones, J.B. 2001. Soil Analysis. p. 79-93. In Laboratory Guide for Conduction Soil Tests and Plant Analysis. CRC Press Boca Raton, FL.
- Schollenberger, C.J. and R.H. Simon. 1945. Determination of exchange capacity and exchangeable basis in soil-ammonium acetate method. *Soil Sci.* 59:13-24.
- Warncke D. and J.R. Brown. 1998. Potassium and Other Basic Cations. P. 31-33. In J.R. Brown (ed.) Recommended Chemical Soil Test Procedures for the North Central Region. North Central Regional Publication Number 221 (revised). Missouri Ag. Exp. Station SB 1001. Univ. of Missouri, Columbia, MO.

### **DTPA Extractable Micronutrients: Zinc – Iron – Copper – Manganese**

1. Scoop 10 g of soil for public samples. Weigh or scoop, according to submitted information sheet, 10 g of soil for research samples.
2. Dump soil into appropriate flask in DTPA rack using 50 mL polypropylene Erlenmeyer flasks, tapping the scoop on the funnel to remove all of the soil from the scoop. Put Blank in #12 and NAPT 2001-120 in #24 spot. After the samples, scoop or weigh Quality Control Samples, T-1 #1 and #13, T-2 #1 and #13 etc. End with NAPT CK and Blank.
3. Dispense 20 mL of DTPA extracting solution in each flask.
4. Shake for 2 hours and filter immediately through Ahlstrom 74 filter paper into filtering tubes. Refilter if extract is cloudy. Note: Samples high in Fe will have a yellow color.
5. Pour samples from filtering racks into glass autosampler tubes and place in white ICP rack. Read samples ICP unit using appropriate standards as listed in Table 2.9.

## References

- Khan, A. and P. N. Soltanpour, "Effect of Wetting and Drying on DTPA-extractable Fe, Zn, Mn, and Cu in Soil" *Comm. Soil Sci. Plant Anal.*, Vol. 9, p 193-202, 1978.
- Lindsay, W. L. and W. A. Norvell, "Development of a DTPA Soil Test for Zinc, Iron, Manganese, and Copper" *Soil Science Amer. J.*, Vol. 42, p 421-428, 1978.
- Soltanpour, P.N., A. Kahn, and W. L. Lindsay, "Factors Affecting DTPA-extractable Zn, Fe, Mn, and Cu from Soils" *Comm. Soil Sci. Plant Anal.*, Vol. 17 p 797-820, 1976.
- Whitney, D.A. 1998. Micronutrients: Zinc, Iron, Manganese and Copper. p. 41-44. In Ellis et al. (ed.) Recommended chemical soil test procedures for the North Central Region. North Central Regional Research Publication No. 221 (Revised). Missouri Agricultural Experiment Station SB 1001, Columbia, MO, USA."

**Substrate water release testing and other green roof media testing:** Per the personal communication between Duane Otto (Turf and Soil Diagnostics) and Jialin Liu (2019), the following procedures were used to obtain the substrate water release test results and other green roof media test results:

"Our water release testing follows our lab SOP which follows ASTM D6836. We used Method C (using a pressure chamber similar to Figure 4) for tension points up to 4 bars and Method D (a Decagon DewPoint Potentiometer – see Fig. 7 in the ASTM method) for the 15 bar testing. Samples used in ASTM D6836 Method C were saturated from bottom up.

For the data on the first report sent labeled "Maximum Media Density for Dead Load Analysis", testing methods include ASTM F1632 (particle size), ASTM D4972 (pH in CaCl<sub>2</sub>), ASTM D5550 (particle density), and ASTM E2399 (saturated hydraulic conductivity and all weights and porosity data). Organic matter content was determined at 550°C per FLL Guidelines. Other than the temperature, the method is the same as ASTM D2974 Method C (which uses 440°C). Electrical conductivity is determined using a 1:5 solution following our Lab SOP, which is based on standard electrical conductivity methods."

## Appendix C - Protocols of the PLFA Analysis in the Lab (Indoor Portion)

Getting PLFA results from soil labs:

### Protocols of PLFA are given below:

Microbial Fatty Acid Analysis

Revision July 2007

By: Paul White and Cody Burton: Original version by Vicki Allison and Mike Miller

Transcribed June 2015

By: Tiffany Carter and Abbie Lasater

Edited August 2015 by Noortje Notenbaert

### **Extraction of lipids (Phase 1)**

#### **Preparation**

Calibrate the repipettors to dispense 5 mL of chloroform and methanol.

#### **Items needed:**

- Two sets of muffled large test tubes (50 mL size) pre-acid-washed, 400° for minimum 4 h, remove and place in aluminum foil
- One set of small (10 mL) test tubes.
- Two small muffled beakers to hold phosphate buffer and nanopure water.
- One muffled Pasteur pipette/sample.

#### ***Procedure***

##### **Day 1**

1. Label centrifuge tubes and beakers before putting on gloves. Each sample gets two 50 mL and one 10 mL test tubes.
2. Weigh out pre-determined amount of ground material (plant ~ 30-100 mg) (soil ~ 0.5 to 5 g, depending on soil type) into one of the 50 mL tubes. For soil, 5 g is typically used.
3. Using the Eppendorf pipet, add 4 mL of phosphate buffer to each sample.
4. Using the repipettors, add 10 mL of methanol and 5 mL of chloroform to each sample and swirl between additions.
5. Vortex for 30 seconds and vent. Closely examine the fluid in the tube for one phase solution. If there is more than one phase start over.

6. Leave tubes with caps for 3 hours in vent hood, re-vortexing briefly and vent every hour.
7. Centrifuge (in Dr. Hettarachchi Lab TH 2201) samples for 10 minutes at 1500 -2000 rpm.
8. Decant supernatant into the second 50 mL test tube.
9. Using repipetter, add 5 mL of chloroform to the second tube.
10. Using eppendorf, add 5 mL of nanopure water to the second tube.
11. Vortex briefly, vent tubes, and store in the dark at 25°C overnight.

## Day 2

1. Use a Pasteur pipette to transfer the bottom organic phase from each sample into the 10 mL test tubes. To prevent uptake of aqueous and inter-phases, blow bubbles through tip of the pipette while pushing down into the organic phase.
2. Evaporate the solvent in the N-EVAP at 50°C. Fill the water bath completely to maximize the evaporation rate and clean needles with acetone. Samples can either be stored in the freezer (-20°C) or moved directly to the next step which is the silicic acid chromatography.

### Notes on N\_EVAP:

1. Clean each needle with acetone on a Kimwipe prior to use. For phase 1, the needles should be kept as close to the evaporating solvent as possible.
2. N<sub>2</sub> gas source: Matheson (785-537-0395) Thursday delivery. Ask for industrial nitrogen.
3. Use de-ionized water for the N-EVAP bath.

### *Silicic Acid Chromatography (Phase 2)*

#### Preparation

1. If frozen, remove samples from freezer and allow to thaw to room temperature.
2. **Glassware needed**
3. Two small muffled tubes per sample (10-mL) to collect the polar and neutral lipid fraction. Strongly advise a color scheme, e.g. green labels for 'total fraction' from day 1, red tape for 'neutral lipids,' and blue tape for 'polar lipids'.
4. Extra test tubes for waste.
5. Muffled Pasteur pipettes.

## Procedure

1. **Note:** It is important that the silicic acid columns are not allowed to dry once the samples have been introduced. For this reason, it is best to run samples in groups of 4-6. Always close the port valves on individual columns when not pulling the solvent through the column. In addition, separation is most efficient if each aliquot of solvent is in contact with the sample for 30 seconds to 1 minute. **Resist the temptation to pull solvents through fast!** This can vary based on experience.
2. Label tubes before putting on gloves.
3. Place waste tubes into the vacuum manifold and condition each column with 5 mL of methanol, 5 mL of acetone, and then 5 mL of chloroform. Pull all solvents through (dry column). When conditioning columns with methanol, acetone, and chloroform make sure to squirt liquids to the side of the column, not directly onto the silica gel bed.
4. Put tubes labeled for neutral lipids into vacuum manifold.
5. Add ~200  $\mu$ L of chloroform (1-2 drops or **smallest** possible with repipetter) to dried sample and swirl to dissolve lipids. Remember that smaller solvent amounts are better than larger ones.
6. Load the suspended sample on the column with a Pasteur pipette, being careful to drip the liquid directly into the center of the column. Use a new muffled pipette for each sample.
7. Repeat steps 4 and 5 two more times for each sample. If needed, do more. But be consistent.
8. Elute columns with 10 mL of chloroform to remove the neutral lipid fraction. Use 5 mL with acidic soils. If only collecting PLFAs, use waste tubes at this point.
9. Put in waste tubes. Elute with 10 mL of acetone to remove glycolipid fraction unless plant samples. With acidic soils use 5 mL acetone
10. Put in tubes for polar lipids (phospholipids). Elute with 10 mL of methanol to remove the phospholipids. Use 5 mL in acidic soils.
11. Evaporate the solvents in the N-EVAP at 50°C. You can lower the needles as they evaporate but keep them out of solvents. Watch samples closely at all times while evaporating and take off evaporator as soon as they are dry (~0.5hr) cap with acetone cleaned caps.
12. Store sample in the freezer (-20°).

## Lipid Methylation (Step 3)

### Preparation

Reset methanol and chloroform repipettors to 0.5 mL. Calibrate using a graduated cylinder. Measuring volume is easiest by pipetting 6 times to get 3 mL.

### Glassware needed

- One Pasteur pipette/sample
- One small (10 mL) muffled test tube/sample
- Two 50 mL or 100mL Erlenmeyer flasks
- A 50 mL volumetric flask
- Muffled beakers

### Procedure

1. Label a set of small test tubes before putting on gloves. Turn on N-EVAP heat unit and set temperature to 60°C. Remove samples from freezer. Allow these to thaw while engaged in the next step.
2. Prepare 0.2 M methanolic KOH (make fresh!). Start with ~10 mL methanol in the volumetric flask. Using acetone-wiped tweezers, quickly weigh ~0.56g of KOH, rinse with a few drops of chloroform and drop them immediately into the methanol. KOH is hygroscopic and water will interfere with the methylation, hence the need for speed. Add enough methanol to bring volume to 50mL. Dissolve KOH (use a stir plate if necessary). Pour methanol/KOH mixture into 100mL Erlenmeyer flask. Do Calculation:
3.  $50/0.56 * X =$  total volume needed
4. X= g of KOH weighed into flask
5. For example: Your four pellets of KOH weighed 0.61 g. Using the equation, total volume needed is going to be 54.5 mL. So add 4.5 mL of methanol to your methanolic KOH. Now it is ready to use. Note: New methanolic KOH must be made every day because KOH absorbs CO<sub>2</sub>, neutralizing the alkali.
6. Use repipettors to place 0.5 mL chloroform and 0.5mL methanol into each sample tube (no need to be specific, several drops from Pasteur pipet or using Eppendorf pipette is fine).

7. Using 1.0 mL Eppendorf pipette, place 1.0 mL methanolic KOH into each tube.  
Swirl to mix. Note: For high clay content soils use 2mL.
8. Cap sample tubes and place on N-EVAP (set to 60°C). DO NOT EVAPORATE. A white precipitate will form when this step is completed. Usually 0.5 to 1 hour. (this will be more than 1 h in high clay soils). Turn down the N-EVAP to 37°C.
9. Using the repipetter, add 2.0 mL of hexane to each sample and swirl to mix.
10. Using pipette, add 200µL of 1 N acetic acid to each sample. Swirl to mix. You will start to see phase separation taking place.
11. Using the 5.0mL Eppendorf pipette, add 2.0 mL of nanopure water to each sample to break phase.
12. Vortex for 30s (10s \*3 is fine).
13. Centrifuge samples for 5 minutes at 1000 rpm. (Ask for help from someone with experience the first time you do this in the high-speed centrifuge.
14. Using a separate Pasteur pipette for each sample, transfer the top phase into a clean, 10-mL test tube.
15. Re-extract the samples with 2.0 mL of hexane (twice for samples with high organic matter content), following the same procedure laid out in steps 9-11.
16. Evaporate the solvent in the N-EVAP at 37°C. To prevent FAMES from being volatilized by N<sub>2</sub>, keep gas flow rates low, and place needles near the top of the tubes. DO NOT MOVE needles down tubes as done during Phase 2. Watch samples carefully and take them off as soon as evaporation is completed (~20 min). Cap (acetone-cleaned) and store samples in freezer. **Failure to remove samples will result in the loss of FAMES, which =’s no sample to analyze.**
17. Make internal standard and add 1.0 mL to dried samples.
18. Transfer sample to labeled GC vial using a new Pasteur pipette. Crimp cap. Cross fingers and hold breath. Hope that everything works properly.

### **\*Standards for GC/MS**

**-Stock Solution** - measure 20 mg Methyl nonadecanoate (C19:0) into 100 mL of Hexane.

**-Internal Standard** - measure 10 mL of stock solution and add 90 mL of Hexane.

### **Preparation of Phosphate Buffer**

- Muffled glassware needed: 1000-mL volumetric flask, 1000-mL beaker, 1000-mL vacuum flask and filter apparatus, two brown storage bottles
- Sonicated in acetone: filter tweezers, stir bar

### **Procedure**

1. Weigh out 8.7 g of Potassium Phosphate Dibasic into a 1000 mL muffled volumetric flask.
2. Add in enough nanopure water to fill the bulb of the flask and swirl until all the powder dissolves. Top up with nanopure water to the mark. Pour into a large beaker for the titration and add a clean (sonicated in acetone) stir bar.
3. Standardize the pH meter then titrate the buffer with 3M HCl to a pH of 7.4. Be careful not to overshoot (a pH of 7.39 is acceptable).
4. Assemble the microfilter apparatus: using acetone washed tweezers, insert the Millipore filter paper between the reservoir and the funnel and clamp together into the flask. Connect the flask to the vacuum pump and turn it on. Check for leaks first by filtering a small amount of buffer, and then filter the buffer.
5. Add ~50 mL of chloroform into a muffled brown storage bottle, and then pour in the buffer. Add the stir bar from the beaker. Stir the buffer vigorously to thoroughly mix in the chloroform, then let sit overnight before using. Excess buffer can be stored in the second brown bottle until needed. Be sure that after adding this excess buffer to the original bottle to chloroform extract again by placing on a stir plate.

## Solution Recipes

- **3 M HCl**

For 50 mL: Put 35.25 g of nanopure water in bottle. Add 14.75 g of concentrated (12.1 M) HCl.

- **1 N Acetic Acid**

To 50 mL of nanopure water, add 3 g of glacial acetic acid (99.8% assay, density 1.0492).

- **N-evap needle washing solution**

Mix together 50% chloroform and 50% methanol by volume

## Fatty Acid Standard Mixes

1. **19:0** (using 19:0 FAME, Matreya catalogue number 1029)

- A. **Stock Solution**

To make 200 ng/ $\mu$ L, weigh out 20 mg in a 100 mL volumetric flask

- B. **Quantitative Standard**

Take 10 mL stock, add 90 mL hexane to give a concentration of 20 ng/ $\mu$ L

Note: will not weigh out exactly 20 mg. Calculate concentration from the amount weighed out (e.g. 20.2 mg gives a stock concentration of 202 ng/ $\mu$ L), and record on stock solution bottle. Also record exact concentration on the quantitative standard bottle (e.g. stock concentration of 202 ng/ $\mu$ L gives a quantitative standard with a concentration of 20.2 ng/ $\mu$ L).

2. **Qualitative Standards (to identify peak position)**

- A. **Individual**

Weigh out ~4 mg of each FAME into each small vial. Add 10 mL hexane, to give an approximate concentration of 400 ng/ $\mu$ L.

- B. **Combined**

Take 1mL of each FAME solution, combine to give a single qualitative standard, with a concentration of each FAME of approximately 20 ng/ $\mu$ L (VERY approximately).

## **Appendix D - Protocols of the Total Organic Carbon & Nitrogen as well as Organic Matter Analysis in the Lab (Indoor Portion)**

SOIL (APD-EGR SUBSTRATE) METHOD REFERENCES AND PROCEDURAL NOTES  
(Provided by\_\_\_)

PRIMARY REFERENCE: (cited by individual chapter authors and page numbers).

1998. "Recommended Chemical Soil Test Procedures for the North Central Region." North Central Regional Publication No. 221 (Revised). University of Missouri Agricultural Experiment Station, Columbia, MO.

Soil (substrate) was ground using a Dynacrush grinder with flailers and a 2mm sieve.

For **pH**, a 1:1 slurry method with a 10 g scoop of soil and 10 ml of DI water is used. This is described in principle on pp. 13-14 of "Recommended Chemical Soil Test Procedures for the North Central Region" (Wateson, M.E. and Brown, J.R.), except that calcium chloride is not used. For lime requirement, the SMP buffer method is used (20 ml buffer). After stirring and a 45-minute incubation, the buffer pH is measured, as described on p.14 in the same chapter of that same reference. All pH measurements are made with a Skalar SP50 Robotic Analyzer. Skalar Inc. Buford, GA 30518.

For **Mehlich 3 Phosphorus**, soil is extracted with a solution of glacial acetic acid, ammonium nitrate, ammonium fluoride and nitric acid. The extraction and colorimetric assay are described on pp 23-25 of "Recommended Chemical Soil Test Procedures for the North Central Region." The colorimetric assay is performed using a Lachat Quickchem 8500 Series 2. Method Orthophosphate 12-115-01-1-A.

For **Bray-1 Phosphorus**, HCl-ammonium fluoride extraction is used. This extraction and the colorimetric assay are described on pp. 21-22 and pp. 24-25, respectively, of "Recommended Chemical Soil Test Procedures for the North Central Region" (Frank, K., Beegle, D., and Denning, J.). The colorimetric assay is performed using a Lachat Quickchem 8500 Series 2. Method Orthophosphate 12-115-01-1-A.

For **Olsen Phosphorus** (soil pH >7.5), sodium bicarbonate extraction is used. This extraction and colorimetric assay are described on pp. 25-26 in the Beegle and Denning chapter of "Recommended Chemical Soil Test Procedures for the North Central Region." The colorimetric assay is performed using a Model PC910 Fiber Optic Spectrophotometer from Brinkmann Instruments, Inc., Westbury, NY.

DTPA extraction for Fe, Zn, Cu, and Mn uses the method described on pp. 41-42 (Whitney, D.A.) in “Recommended Chemical Soil Test Procedures for the North Central Region”. Analysis is done by an Inductively Coupled Plasma (ICP) Spectrometer, Model 720-ES ICP Optical Emission Spectrometer, manufactured by Varian Australia Pty Ltd, Mulgrave, Vic Australia or a Model 3110 Flame Atomic Absorption (AA) Spectrometer from Perkin Elmer Corp., Norwalk, CT.

**Nitric Digest for Heavy Metals (Fe, Zn, Cu, Mn, Cd, Cr, Ni, Pb).** Adapted from Sposito, et.al., 1982. Soil Sci. Soc. Am. J. 46, 260-264. Analysis is done by an Inductively Coupled Plasma (ICP) Spectrometer, Model 720-ES ICP Optical Emission Spectrometer, manufactured by Varian Australia Pty Ltd, Mulgrave, Vic Australia or a Model 3110 Flame Atomic Absorption (AA) Spectrometer from Perkin Elmer Corp., Norwalk, CT.

Chloride analysis uses the calcium nitrate extraction and colorimetric analysis in the Mercury Thiocyanate method listed in “Recommended Chemical Soil Test Procedures for the North Central Region” on pp. 49-50 (Gelderman, R.H., Denning, J.L., and Goos, R.J.). The colorimetric assay is performed using an Alpkem RFA Methodology No. A303-S090.

For **Extractable (plant available) Potassium** Ammonium Acetate extraction is used as described on pp 31-32 of “Recommended Chemical Soil Test Procedures for the North Central Region” (Warncke, D., and Brown, J.R.). Analysis is done by an Inductively Coupled Plasma (ICP) Spectrometer, Accuris Model, manufactured by ARL/Fisons of Eclublens, Switzerland, or a Model 3110 Flame Atomic Absorption (AA) Spectrometer from Perkin Elmer Corp., Norwalk, CT.

**Extractable cations (Ca, K, Mg, & Na)** are determined by the ammonium acetate (1M, pH 7.0) method as described by Warncke, D.M. and Brown, J.R. on pp. 31-32 in “Recommended Chemical Soil Test Procedures for the North Central Region.” A low-sodium filter paper was used. Analysis is done by an Inductively Coupled Plasma (ICP) Spectrometer, Model 720-ES ICP Optical Emission Spectrometer, manufactured by Varian Australia Pty Ltd, Mulgrave, Vic Australia or prior to June 2010: a Model 3110 Flame Atomic Absorption (AA) Spectrometer from Perkin Elmer Corp., Norwalk, CT. and after June 2010: a Model A Anylyst 200 (AA) Spectrometer from Perkin Elmer Life and Analytical Sciences, Shelton, CT.

**Cation Exchange Capacity (CEC)** displacement is determined by the ammonium ion replacement method as described by Chapman, H.D., Cation Exchange Capacity *In Black*, et al., (ed.) Methods of Soil Analysis. Agronomy, 9: 891-901. Am. Soc. of Agron., Inc. Madison, WI. The ammonia extract representing the CEC of the sample is analyzed by an indophenol colorimetric reaction, as described in: Alpkem Corporation. 1986. RFA Methodology No. A303-S021. Ammonia Nitrogen. Clackamas, OR. Analyses of the ammonia is performed on a Rapid

Flow Analyzer (Model RFA-300) from Alpkem Corporation, Clackamas, OR.

For **soil-extractable Nitrate**, a 1M KCl extraction (2 g in 20 ml, 15 min.) and cadmium reduction/colorimetry for analysis are used. These are found in Ch. 5, (Gelderman, R.H., and Beegle, D.) pp. 18-19, 1998. "Recommended Chemical Soil Test Procedures for the North Central Region" North Central Regional Publication No. 221 (Revised). University of Missouri Agricultural Experiment Station, Columbia, MO. The cadmium reduction and colorimetric reaction are also described in: Alpkem Corporation. 1986. RFA Methodology No. A303-S170. Nitrate/Nitrite Nitrogen Clackamas, OR 97015.

Ammonia is extracted from soil by 1 M KCl (2 g in 20 ml, 30 min.) in a modification of the method described in Keeney, D.R., and D.W. Nelson. 1982 Nitrogen - Inorganic Forms In A.L. Page et al. (ed.) Methods of Soil Analysis, Part 2. Agronomy 9: 648-649. ASA and SSSA., Madison, WI.

**Ammonia** in soil extracts was analyzed by an indophenol colorimetric reaction, as described in: Alpkem Corporation. 1986. RFA Methodology No. A303-S021. Ammonia Nitrogen. Clackamas, OR. Analyses of both nitrate and ammonia are performed on a Rapid Flow Analyzer (Model RFA-300) from Alpkem Corporation, Clackamas, OR.

### **Loss on Ignition for Organic Matter content**

The organic matter soil/substrate test is based on a modified version of: Combs, S.M and M.V. Nathan. 1998. Soil organic matter. In: recommended chemical soil test procedures for the north central region. Missouri Ag. Exp. Stn. SB 1001. Colombia, MO. P. 53 – 58. The modifications being 1 g of soil were used, drying at 150 for 2 hours, and igniting at 400 for 3 hours.

For substrate **Organic Matter**, the Walkley-Black method is used, found on pp. 55-57 of "Recommended Chemical Soil Test Procedures for the North Central Region" (Combs, S.M., and Nathan, M.V.), with the "heat of dilution" modification. Colorimetric analysis of the solution is done by a Model PC910 Fiber Optic Spectrophotometer from Brinkmann Instruments, Inc., Westbury, NY.

**Soluble Salts (Conductivity)** is determined by the saturated paste method as described on pp. 59-60 of "Recommended Chemical Soil Test Procedures for the North Central Region" (Whitney, D.A.), using a Corning Model 441 Conductivity Meter from Corning, Inc., Corning, NY.

**Particle Size (Texture)** is estimated by a modification of the Bouyoucos Hydrometer Method. That method is presented in "Bouyoucos, G.J. 1962. Hydrometer Method Improved for Making

Particle Size Analysis of Soils.” *Agro. J.* 54:464-465.

### **Total Carbon & Nitrogen**

A LECO TruSpec CN Carbon/Nitrogen combustion analyzer reports total levels (inorganic and organic) of C and N on a weight percent basis, according to the TruSpec CN instrument method "Carbon and Nitrogen in Soil and Sediment", LECO Corporation, St. Joseph, MI, 2005.

LECO reports (in the above LECO method) the standard deviation (precision) for this instrument and the above method as 0.06 with 2.18% Rel. Std. Dev. for soil carbon and 0.006 with 3.35% Rel. Std. Dev. for soil nitrogen.

### **Calcium Carbonate Percentage**

By pretreatment of a second LECO combustion sample with dilute Phosphoric Acid, CO<sub>2</sub> is released from calcium and magnesium carbonates in calcareous soils, leaving only the total organic carbon present. The total inorganic carbon is calculated as the difference in the treated and untreated values. The percentage of carbonates is expressed as a percentage of CaCO<sub>3</sub> by dividing the inorganic carbon by a factor of 0.12.

## **PLANT METHOD REFERENCES**

(Provided by\_\_\_)

**Total Nitrogen and Total Phosphorus on soil and plant tissue** are analyzed by the salicylic-sulfuric acid digestion method. This method is found in the article Bremner, J.M., and Mulvaney, C.S.. 1982. “Salicylic acid thiosulfate modification of the Kjeldhal method to include nitrate and nitrite.” p. 621. *In* Miller, R.H. Miller, and Keeney, D.R., (eds.) *Methods of Soil Analysis. Part 2.* Am. Soc. Agron., Inc., Madison, WI. The digest is analyzed for nitrogen by colorimetric procedure using the Rapid Flow Analyzer (Model RFA-300) from Alpkem Corporation, Clackamas, OR 97015. RFA Methodology No. A303-S072. Phosphorus is analyzed by an Inductively Coupled Plasma (ICP) Spectrometer, Model 720-ES ICP Optical Emission Spectrometer, manufactured by Varian Australia Pty Ltd, Mulgrave, Victoria Australia.

**Nitrogen, Phosphorus and Potassium in plant tissue** is analyzed by the Sulfuric Peroxide digest, as described by Linder, R.C., and C.P. Harley. 1942. “A Rapid Method for the Determination of Nitrogen in Plant Tissue.” in *Science*, 96:565-566, and Thomas, R.L., R.W. Sheard, and J.R. Moyer. 1967. Comparison of Conventional and Automated Procedures for Nitrogen, Phosphorus, and Potassium Analysis of Plant Material Using a Single Digest. *Agron. J.* 59:240-243.

The digest containing ammonia is analyzed by an indophenol blue colorimetric procedure using

the Rapid Flow Analyzer (Model RFA-300) from Alpkem Corporation, Clackamas, OR 97015. RFA Methodology No. A303-S072. Phosphorus and Potassium are determined using an Inductively Coupled Plasma (ICP) Spectrometer, Model 720-ES ICP Optical Emission Spectrometer, manufactured by Varian Australia Pty Ltd, Mulgrave, Vic Australia

For Perchloric digest for Ca, Mg, Zn, Fe, Cu, Mn, SO<sub>4</sub>:

Gieseking, J.E., Snider, H.J., and Getz, C.A. 1935. Destruction of organic matter in plant material by the use of nitric and perchloric acids. *Ind. and Eng. Chem., Anal. Ed.*, V.7, p185-186.

Analysis of Ca, Mg, Zn, Fe, Cu Mn and SO<sub>4</sub> from Perchloric digest is done by an Inductively Coupled Plasma (ICP) Spectrometer, Model 720-ES ICP Optical Emission Spectrometer, manufactured by Varian Australia Pty Ltd, Mulgrave, Vic Australia

Total Carbon & Nitrogen

A LECO TruSpec CN Carbon/Nitrogen combustion analyzer reports total levels (inorganic and organic) of C and N on a weight percent basis, according to the TruSpec CN instrument method "Carbon, Hydrogen, and Nitrogen in Flour and Plant Tissue", LECO Corporation, St. Joseph, MI, 2005.

## WATER METHOD REFERENCES

(Provided by\_\_\_)

### **Total Suspended Solids:**

50-100 ml of the samples are filtered through 0.45 micron filters using a vacuum. The dry weight of the filter membrane is measured before and after filtration. TSS is calculated based on mg/L according to:

Csuros, M. *Environmental Sampling and Analysis Lab Manual*. Lewis Publishers, CRC Press LLC, Boca Raton, FL 1997. Traceable to EPA Method 160.2

### **Total N and P analysis:**

1 to 10 ml sample is digested with Potassium Persulfate Reagent in an autoclave and then analyzed using an Alpkem RFA for nitrate nitrogen (cadmium reduction method) and phosphorus according to:

Hosomi, M. and Sudu, R. 1986. "Simultaneous determination of total nitrogen and total phosphorus in freshwater samples using persulfate digestion." *International Journal of Environmental Studies*. 27;267-275.

Nelson N.S. 1987. An acid-persulfate digestion procedure for determination of phosphorus in sediments. *Communications in Soil Science and Plant Analysis*, 18(4);359-369.

Alpkem Corporation. 1986. RFA Methodology no. A303-S170. Nitrate-Nitrite Nitrogen. Clackamas, OR.

Alpkem Corporation. 1986. RFA Methodology no. A303-S200-13. Ortho-Phosphate. Clackamas, OR.

### **Total Dissolved Solids:**

Filtrate from the TSS procedure is measured for conductivity. This value is multiplied by 700 to convert mS/cm to TDS in mg/L.

### **Ortho Phosphorus:**

Filtrate from the TSS procedure is measured for P using an Alpkem RFA autoanalyzer using the ammonium molybdate blue colorometric procedure. RFA Methodology no. A303-S200-13. Ortho-Phosphate. Clackamas, OR.

### **Ammonia and Nitrate Nitrogen:**

Filtrate from the TSS procedure is measured for NH<sub>4</sub>-N and NO<sub>3</sub>-N using an Alpkem RFA autoanalyzer according to:

1. Alpkem Corporation. 1986. RFA Methodology no. A303-S021. Ammonia Nitrogen. Clackamas, OR.
2. Alpkem Corporation. 1986. RFA Methodology no. A303-S170. Nitrate+Nitrite Nitrogen. Clackamas, OR.

## **Appendix E - Protocols of the Soil Respiration Analysis in the Lab (Indoor Portion)**

### **Procedure for Respiration Measurement (Haney and Haney, 2010, Wollum and Gomez, 1970, Zibilske, 1994)**

#### Materials

##### *Pre-Setup:*

- Soil Samples (sieved to 8mm, air dried to constant mass)
- Jars with Lids (wide mouth, 1 pint, Ball brand mason jars, with standard 2-part lids)
- Mason Jars (980mL)
- Flat lids are modified with a rubber septa for gas extraction
- Labeling tape and Sharpie marker
- Filter papers (55mm)
- Weighing paper (3" x 3" or 4" x 4")
- Pre-perforated aluminum weigh boats (with 9 holes in bottom)

##### *Incubation:*

- distilled, deionized H<sub>2</sub>O (ddH<sub>2</sub>O)
- 10 ml pipettor
- 10 ml pipette tips
- Marker
- Gloves
- 10 ml syringe
- 1 ml syringe
- 20 ml sealed glass vial
- Gas chromatography (Shimadzu GC-8A, Shimadzu Scientific Instruments, and Columbia, MD)

#### Method

Start with sieved, air-dried soil. Gather clean, dry mason jars with lids, filter papers, labeling tape and sharpie, pre-perforated aluminum weigh boats, and weighing papers.

Have an area ready to place jars with soil samples in after weighing.

- Label a set of jars for the range of samples you will be weighing out.
- Use labeling tape with sharpie rather than writing on jar, to facilitate jar cleanup.

To a set of empty jars:

- Add 2 filter papers to the bottom of each jar, offset from each other.
  - Use long forceps if necessary for adjusting placement of filter papers.
- Weigh 20.00 g dry soil into a pre-perforated aluminum weigh boat.
  - Use a weigh paper below the weigh boat on the balance pan to catch soil that falls through the perforations in the bottom of the boat.
  - Be sure to reset the balance when placing a new weighing paper on it.
- Place the weigh boat into the jar.
  - Use long large forceps to pick up the weigh boat by the back tab, holding with the tips far enough down to pick up the boat without it flexing.

- o Gently place the weigh boat onto the weighing papers in the jar.
- o Tap soil remaining on the weighing paper on the balance pan into pile of soil in the weigh boat while transferring the weigh boat to the jar.
- Jars can be stored with soil pre-weighed a few days ahead of time, covered with individual lids.

Set up incubations.

- Draw distilled deionized water (ddH<sub>2</sub>O from the deionization column tap) into clean, dry beaker.
- To all jars and 2 blanks with no soil.
  - o Secure pipettor for H<sub>2</sub>O
  - o Set volume to 7.50 ml
  - o Draw and dispense 7.5 ml ddH<sub>2</sub>O into each jar.
    - Dispense the water gently onto the inside wall of the jar, holding the tip just a small distance away from the wall of the jar, as far down as you can safely and effectively hold the pipette tip without it contacting anything else in the jar.
    - Avoid dripping or dispensing onto the soil directly
  - o Place a lid flat onto each jar, minimizing the amount of time that the jar is open and the trap dispensed, to prevent unnecessary CO<sub>2</sub> absorption from the room air. Minimize the difference in amount of time that different jars are open, and keep blanks in sequence with sample jars.
  - o Close the jars securely with the screw top rings and grease applied to lids. Screw on tight enough to make an airtight seal. Keep in mind that opening the jars at the end of the incubation without jarring them enough that the traps spill will be necessary.
- Carefully move closed jars to the room temperature incubation area avoiding tipping the trap assemblies inside.
- Set a note (tape sticks around better than a post-it) indicating sample number range, date and time set up (note beginning time for batch, when traps began to be dispensed) and date and time to take down (4 days incubation time, start reading at the same time of day as the batch incubations were started – timing from when traps are dispensed).

Measure after incubation every 24 hours for 4 days.

- Gather a clean 10 ml syringe.
- Insert syringe into mason jar septa lid.
- Extract and purge syringe 5 times to mix mason jar air head space.
- Extract 10 ml of gas and store in a 20 ml sealed glass vial.
- Repeat for all jars.

Cleanup:

- Remove lid assembly and store separately. No cleaning necessary for lids.
- Empty the trap waste with soil and filter paper.
- Place jars and weight boats in wash.

After the 4-day incubation use a gas chromatograph (GC) with a thermal conductivity detector to measure the amount of CO<sub>2</sub> produced at the end of the incubation using the following steps:

1. Inject 0.2, 0.4, 0.6, 0.8, and 1.0 ml volumes of a 1% CO<sub>2</sub> standard into the GC. This will serve as a standard curve to calculate the concentration of CO<sub>2</sub> in the samples.

2. Make standard curve by graphing mass CO<sub>2</sub>-C/injections against GC peak area using regression. Below is an example of a general regression equation. The y-intercept and slope come from the standard curve. The peak area is the peak area from the GC.

$$\mu\text{g C} = y \text{ intercept} + (\text{slope} \times \text{peak area of sample})$$

3. Sample headspace gas in 20 ml sealed glass vial or directly from Mason jars and inject 0.5 mL into GC. Insert the resulting peak areas for your samples into the regression equation you determined in the previous step to calculate  $\mu\text{g C}$  content of samples.

Volume of CO <sub>2</sub> - C injected (ml)	Concentration of CO <sub>2</sub> ( $\mu\text{g C}$ )	Peak Area
0.2	0.981	
0.4	1.963	
0.6	2.944	
0.8	3.926	
1	4.907	

**Appendix F - The SAS output for the TOC analyses by different bed (both 4-inch and 8-inch-deep bed) and year (year as repeated measure)**

**4-inch-deep bed**

<b>Type 3 Tests of Fixed Effects</b>				
<b>Effect</b>	<b>Num DF</b>	<b>Den DF</b>	<b>F Value</b>	<b>Pr &gt; F</b>
<b>SUBSTRATE</b>	1	3	25.04	0.0154
<b>MIX</b>	2	6	1.12	0.3861
<b>SUBSTRATE*MIX</b>	2	6	2.28	0.1833
<b>YR</b>	1	18	2.37	0.1408
<b>SUBSTRATE*YR</b>	1	18	2.43	0.1365
<b>MIX*YR</b>	2	18	0.67	0.5248
<b>SUBSTRATE*MIX*YR</b>	2	18	1.51	0.2474

<b>Least Squares Means</b>								
<b>Effect</b>	<b>SUBSTRATE</b>	<b>MIX</b>	<b>YR</b>	<b>Estimate</b>	<b>Standard Error</b>	<b>DF</b>	<b>t Value</b>	<b>Pr &gt;  t </b>
<b>SUBSTRATE</b>	buildex			1.3833	0.1471	3	9.41	0.0025
<b>SUBSTRATE</b>	rooflite			2.3079	0.1471	3	15.69	0.0006
<b>MIX</b>		0		1.6738	0.1982	6	8.44	0.0002
<b>MIX</b>		1		1.7838	0.1982	6	9	0.0001
<b>MIX</b>		2		2.0794	0.1982	6	10.49	<.0001
<b>SUBSTRATE*MIX</b>	buildex	0		1.22	0.2548	6	4.79	0.003
<b>SUBSTRATE*MIX</b>	buildex	1		1.5587	0.2548	6	6.12	0.0009
<b>SUBSTRATE*MIX</b>	buildex	2		1.3713	0.2548	6	5.38	0.0017
<b>SUBSTRATE*MIX</b>	rooflite	0		2.1275	0.2548	6	8.35	0.0002
<b>SUBSTRATE*MIX</b>	rooflite	1		2.0088	0.2548	6	7.88	0.0002
<b>SUBSTRATE*MIX</b>	rooflite	2		2.7875	0.2548	6	10.94	<.0001
<b>SUBSTRATE</b>	buildex			1.3833	0.1471	3	9.41	0.0025
<b>SUBSTRATE</b>	rooflite			2.3079	0.1471	3	15.69	0.0006
<b>YR</b>			2019	1.9521	0.1337	18	14.6	<.0001
<b>YR</b>			2020	1.7392	0.1337	18	13.01	<.0001
<b>SUBSTRATE*YR</b>	buildex		2019	1.5975	0.1766	18	9.05	<.0001
<b>SUBSTRATE*YR</b>	buildex		2020	1.1692	0.1766	18	6.62	<.0001
<b>SUBSTRATE*YR</b>	rooflite		2019	2.3067	0.1766	18	13.06	<.0001
<b>SUBSTRATE*YR</b>	rooflite		2020	2.3092	0.1766	18	13.08	<.0001
<b>SUBSTRATE*MIX*YR</b>	buildex	0	2019	1.5075	0.3059	18	4.93	0.0001
<b>SUBSTRATE*MIX*YR</b>	buildex	0	2020	0.9325	0.3059	18	3.05	0.0069

SUBSTRATE*MIX*YR	builddex	1	2019	1.5625	0.3059	18	5.11	<.0001
SUBSTRATE*MIX*YR	builddex	1	2020	1.555	0.3059	18	5.08	<.0001
SUBSTRATE*MIX*YR	builddex	2	2019	1.7225	0.3059	18	5.63	<.0001
SUBSTRATE*MIX*YR	builddex	2	2020	1.02	0.3059	18	3.33	0.0037
SUBSTRATE*MIX*YR	rooflite	0	2019	1.9325	0.3059	18	6.32	<.0001
SUBSTRATE*MIX*YR	rooflite	0	2020	2.3225	0.3059	18	7.59	<.0001
SUBSTRATE*MIX*YR	rooflite	1	2019	2.1125	0.3059	18	6.91	<.0001
SUBSTRATE*MIX*YR	rooflite	1	2020	1.905	0.3059	18	6.23	<.0001
SUBSTRATE*MIX*YR	rooflite	2	2019	2.875	0.3059	18	9.4	<.0001
SUBSTRATE*MIX*YR	rooflite	2	2020	2.7	0.3059	18	8.83	<.0001

Differences of Least Squares Means													
Effect	SUBSTRAT	MIX	YR	_SUBSTRA	_MIX	_YR	Estimate	Standard Error	DF	t Value	Pr >  t	Adjustmer	Adj P
SUBSTRATE	builddex			rooflite			-0.9246	0.1848	3	-5	0.0154	Tukey-Krai	0.0154
MIX		0				1	-0.11	0.2803	6	-0.39	0.7083	Tukey	0.9197
MIX		0				2	-0.4056	0.2803	6	-1.45	0.1981	Tukey	0.3779
MIX		1				2	-0.2956	0.2803	6	-1.05	0.3323	Tukey	0.5732
SUBSTRATE*MIX	builddex	0		builddex		1	-0.3387	0.3603	6	-0.94	0.3834	Tukey-Krai	0.9215
SUBSTRATE*MIX	builddex	0		builddex		2	-0.1513	0.3603	6	-0.42	0.6892	Tukey-Krai	0.9974
SUBSTRATE*MIX	builddex	0		rooflite		0	-0.9075	0.32	6	-2.84	0.0297	Tukey-Krai	0.1762
SUBSTRATE*MIX	builddex	0		rooflite		1	-0.7888	0.3603	6	-2.19	0.0711	Tukey-Krai	0.3579
SUBSTRATE*MIX	builddex	0		rooflite		2	-1.5675	0.3603	6	-4.35	0.0048	Tukey-Krai	0.034
SUBSTRATE*MIX	builddex	1		builddex		2	0.1875	0.3603	6	0.52	0.6214	Tukey-Krai	0.9931
SUBSTRATE*MIX	builddex	1		rooflite		0	-0.5688	0.3603	6	-1.58	0.1655	Tukey-Krai	0.637
SUBSTRATE*MIX	builddex	1		rooflite		1	-0.45	0.32	6	-1.41	0.2093	Tukey-Krai	0.725
SUBSTRATE*MIX	builddex	1		rooflite		2	-1.2287	0.3603	6	-3.41	0.0143	Tukey-Krai	0.0927
SUBSTRATE*MIX	builddex	2		rooflite		0	-0.7562	0.3603	6	-2.1	0.0806	Tukey-Krai	0.3929
SUBSTRATE*MIX	builddex	2		rooflite		1	-0.6375	0.3603	6	-1.77	0.1272	Tukey-Krai	0.5409
SUBSTRATE*MIX	builddex	2		rooflite		2	-1.4162	0.32	6	-4.43	0.0044	Tukey-Krai	0.0315
SUBSTRATE*MIX	rooflite	0		rooflite		1	0.1188	0.3603	6	0.33	0.7529	Tukey-Krai	0.9992
SUBSTRATE*MIX	rooflite	0		rooflite		2	-0.66	0.3603	6	-1.83	0.1167	Tukey-Krai	0.5108
SUBSTRATE*MIX	rooflite	1		rooflite		2	-0.7787	0.3603	6	-2.16	0.0739	Tukey-Krai	0.3684
SUBSTRATE	builddex			rooflite			-0.9246	0.1848	3	-5	0.0154	Tukey-Krai	0.0154
YR			2019			2020	0.2129	0.1382	18	1.54	0.1408	Tukey-Krai	0.1408
SUBSTRATE*YR	builddex		2019	builddex		2020	0.4283	0.1955	18	2.19	0.0418	Tukey-Krai	0.1634
SUBSTRATE*YR	builddex		2019	rooflite		2019	-0.7092	0.2307	18	-3.07	0.0065	Tukey-Krai	0.0303
SUBSTRATE*YR	builddex		2019	rooflite		2020	-0.7117	0.2307	18	-3.08	0.0064	Tukey-Krai	0.0297
SUBSTRATE*YR	builddex		2020	rooflite		2019	-1.1375	0.2307	18	-4.93	0.0001	Tukey-Krai	0.0006
SUBSTRATE*YR	builddex		2020	rooflite		2020	-1.14	0.2307	18	-4.94	0.0001	Tukey-Krai	0.0006
SUBSTRATE*YR	rooflite		2019	rooflite		2020	-0.0025	0.1955	18	-0.01	0.9899	Tukey-Krai	1
SUBSTRATE*MIX*YR	builddex	0	2019	builddex	0	2020	0.575	0.3385	18	1.7	0.1066	Tukey-Krai	0.8476
SUBSTRATE*MIX*YR	builddex	0	2019	builddex	1	2019	-0.055	0.4326	18	-0.13	0.9002	Tukey-Krai	1
SUBSTRATE*MIX*YR	builddex	0	2019	builddex	1	2020	-0.0475	0.4326	18	-0.11	0.9138	Tukey-Krai	1
SUBSTRATE*MIX*YR	builddex	0	2019	builddex	2	2019	-0.215	0.4326	18	-0.5	0.6252	Tukey-Krai	1
SUBSTRATE*MIX*YR	builddex	0	2019	builddex	2	2020	0.4875	0.4326	18	1.13	0.2745	Tukey-Krai	0.9888
SUBSTRATE*MIX*YR	builddex	0	2019	rooflite	0	2019	-0.425	0.3996	18	-1.06	0.3016	Tukey-Krai	0.9928
SUBSTRATE*MIX*YR	builddex	0	2019	rooflite	0	2020	-0.815	0.3996	18	-2.04	0.0564	Tukey-Krai	0.6653
SUBSTRATE*MIX*YR	builddex	0	2019	rooflite	1	2019	-0.605	0.4326	18	-1.4	0.1789	Tukey-Krai	0.9492
SUBSTRATE*MIX*YR	builddex	0	2019	rooflite	1	2020	-0.3975	0.4326	18	-0.92	0.3703	Tukey-Krai	0.9978
SUBSTRATE*MIX*YR	builddex	0	2019	rooflite	2	2019	-1.3675	0.4326	18	-3.16	0.0054	Tukey-Krai	0.1415
SUBSTRATE*MIX*YR	builddex	0	2019	rooflite	2	2020	-1.1925	0.4326	18	-2.76	0.013	Tukey-Krai	0.2748
SUBSTRATE*MIX*YR	builddex	0	2020	builddex	1	2019	-0.63	0.4326	18	-1.46	0.1625	Tukey-Krai	0.9348
SUBSTRATE*MIX*YR	builddex	0	2020	builddex	1	2020	-0.6225	0.4326	18	-1.44	0.1673	Tukey-Krai	0.9394
SUBSTRATE*MIX*YR	builddex	0	2020	builddex	2	2019	-0.79	0.4326	18	-1.83	0.0844	Tukey-Krai	0.7855

SUBSTRATE*MIX*YI buildex	0	2020	buildex	2	2020	-0.0875	0.4326	18	-0.2	0.842	Tukey-Kr	-
SUBSTRATE*MIX*YI buildex	0	2020	rooflite	0	2019	-1	0.3996	18	-2.5	0.0222	Tukey-Kr	0.395E
SUBSTRATE*MIX*YI buildex	0	2020	rooflite	0	2020	-1.39	0.3996	18	-3.48	0.0027	Tukey-Kr	0.079E
SUBSTRATE*MIX*YI buildex	0	2020	rooflite	1	2019	-1.18	0.4326	18	-2.73	0.0138	Tukey-Kr	0.287
SUBSTRATE*MIX*YI buildex	0	2020	rooflite	1	2020	-0.9725	0.4326	18	-2.25	0.0373	Tukey-Kr	0.539E
SUBSTRATE*MIX*YI buildex	0	2020	rooflite	2	2019	-1.9425	0.4326	18	-4.49	0.0003	Tukey-Kr	0.010E
SUBSTRATE*MIX*YI buildex	0	2020	rooflite	2	2020	-1.7675	0.4326	18	-4.09	0.0007	Tukey-Kr	0.024E
SUBSTRATE*MIX*YI buildex	1	2019	buildex	1	2020	0.0075	0.3385	18	0.02	0.9826	Tukey-Kr	-
SUBSTRATE*MIX*YI buildex	1	2019	buildex	2	2019	-0.16	0.4326	18	-0.37	0.7158	Tukey-Kr	-
SUBSTRATE*MIX*YI buildex	1	2019	buildex	2	2020	0.5425	0.4326	18	1.25	0.2258	Tukey-Kr	0.975E
SUBSTRATE*MIX*YI buildex	1	2019	rooflite	0	2019	-0.37	0.4326	18	-0.86	0.4036	Tukey-Kr	0.998E
SUBSTRATE*MIX*YI buildex	1	2019	rooflite	0	2020	-0.76	0.4326	18	-1.76	0.0959	Tukey-Kr	0.8204
SUBSTRATE*MIX*YI buildex	1	2019	rooflite	1	2019	-0.55	0.3996	18	-1.38	0.1856	Tukey-Kr	0.9542
SUBSTRATE*MIX*YI buildex	1	2019	rooflite	1	2020	-0.3425	0.3996	18	-0.86	0.4027	Tukey-Kr	0.998E
SUBSTRATE*MIX*YI buildex	1	2019	rooflite	2	2019	-1.3125	0.4326	18	-3.03	0.0071	Tukey-Kr	0.17E
SUBSTRATE*MIX*YI buildex	1	2019	rooflite	2	2020	-1.1375	0.4326	18	-2.63	0.017	Tukey-Kr	0.331E
SUBSTRATE*MIX*YI buildex	1	2020	buildex	2	2019	-0.1675	0.4326	18	-0.39	0.7031	Tukey-Kr	-
SUBSTRATE*MIX*YI buildex	1	2020	buildex	2	2020	0.535	0.4326	18	1.24	0.232	Tukey-Kr	0.9777
SUBSTRATE*MIX*YI buildex	1	2020	rooflite	0	2019	-0.3775	0.4326	18	-0.87	0.3943	Tukey-Kr	0.998E
SUBSTRATE*MIX*YI buildex	1	2020	rooflite	0	2020	-0.7675	0.4326	18	-1.77	0.0929	Tukey-Kr	0.811E
SUBSTRATE*MIX*YI buildex	1	2020	rooflite	1	2019	-0.5575	0.3996	18	-1.39	0.18	Tukey-Kr	0.950
SUBSTRATE*MIX*YI buildex	1	2020	rooflite	1	2020	-0.35	0.3996	18	-0.88	0.3927	Tukey-Kr	0.998E
SUBSTRATE*MIX*YI buildex	1	2020	rooflite	2	2019	-1.32	0.4326	18	-3.05	0.0069	Tukey-Kr	0.170E
SUBSTRATE*MIX*YI buildex	1	2020	rooflite	2	2020	-1.145	0.4326	18	-2.65	0.0164	Tukey-Kr	0.3234
SUBSTRATE*MIX*YI buildex	2	2019	buildex	2	2020	0.7025	0.3385	18	2.08	0.0526	Tukey-Kr	0.643E
SUBSTRATE*MIX*YI buildex	2	2019	rooflite	0	2019	-0.21	0.4326	18	-0.49	0.6332	Tukey-Kr	-
SUBSTRATE*MIX*YI buildex	2	2019	rooflite	0	2020	-0.6	0.4326	18	-1.39	0.1823	Tukey-Kr	0.951E
SUBSTRATE*MIX*YI buildex	2	2019	rooflite	1	2019	-0.39	0.4326	18	-0.9	0.3792	Tukey-Kr	0.998E
SUBSTRATE*MIX*YI buildex	2	2019	rooflite	1	2020	-0.1825	0.4326	18	-0.42	0.6781	Tukey-Kr	-
SUBSTRATE*MIX*YI buildex	2	2019	rooflite	2	2019	-1.1525	0.3996	18	-2.88	0.0099	Tukey-Kr	0.2254
SUBSTRATE*MIX*YI buildex	2	2019	rooflite	2	2020	-0.9775	0.3996	18	-2.45	0.025	Tukey-Kr	0.425E
SUBSTRATE*MIX*YI buildex	2	2020	rooflite	0	2019	-0.9125	0.4326	18	-2.11	0.0492	Tukey-Kr	0.623E
SUBSTRATE*MIX*YI buildex	2	2020	rooflite	0	2020	-1.3025	0.4326	18	-3.01	0.0075	Tukey-Kr	0.182E
SUBSTRATE*MIX*YI buildex	2	2020	rooflite	1	2019	-1.0925	0.4326	18	-2.53	0.0211	Tukey-Kr	0.383E
SUBSTRATE*MIX*YI buildex	2	2020	rooflite	1	2020	-0.885	0.4326	18	-2.05	0.0557	Tukey-Kr	0.661E
SUBSTRATE*MIX*YI buildex	2	2020	rooflite	2	2019	-1.855	0.3996	18	-4.64	0.0002	Tukey-Kr	0.00E
SUBSTRATE*MIX*YI buildex	2	2020	rooflite	2	2020	-1.68	0.3996	18	-4.2	0.0005	Tukey-Kr	0.0194
SUBSTRATE*MIX*YI rooflite	0	2019	rooflite	0	2020	-0.39	0.3385	18	-1.15	0.2644	Tukey-Kr	0.9867
SUBSTRATE*MIX*YI rooflite	0	2019	rooflite	1	2019	-0.18	0.4326	18	-0.42	0.6822	Tukey-Kr	-
SUBSTRATE*MIX*YI rooflite	0	2019	rooflite	1	2020	0.0275	0.4326	18	0.06	0.95	Tukey-Kr	-
SUBSTRATE*MIX*YI rooflite	0	2019	rooflite	2	2019	-0.9425	0.4326	18	-2.18	0.0429	Tukey-Kr	0.581E
SUBSTRATE*MIX*YI rooflite	0	2019	rooflite	2	2020	-0.7675	0.4326	18	-1.77	0.0929	Tukey-Kr	0.811E
SUBSTRATE*MIX*YI rooflite	0	2020	rooflite	1	2019	0.21	0.4326	18	0.49	0.6332	Tukey-Kr	-
SUBSTRATE*MIX*YI rooflite	0	2020	rooflite	1	2020	0.4175	0.4326	18	0.97	0.3472	Tukey-Kr	0.9967
SUBSTRATE*MIX*YI rooflite	0	2020	rooflite	2	2019	-0.5525	0.4326	18	-1.28	0.2177	Tukey-Kr	0.972
SUBSTRATE*MIX*YI rooflite	0	2020	rooflite	2	2020	-0.3775	0.4326	18	-0.87	0.3943	Tukey-Kr	0.998E
SUBSTRATE*MIX*YI rooflite	1	2019	rooflite	1	2020	0.2075	0.3385	18	0.61	0.5476	Tukey-Kr	0.999E
SUBSTRATE*MIX*YI rooflite	1	2019	rooflite	2	2019	-0.7625	0.4326	18	-1.76	0.0949	Tukey-Kr	0.817E
SUBSTRATE*MIX*YI rooflite	1	2019	rooflite	2	2020	-0.5875	0.4326	18	-1.36	0.1912	Tukey-Kr	0.95E
SUBSTRATE*MIX*YI rooflite	1	2020	rooflite	2	2019	-0.97	0.4326	18	-2.24	0.0378	Tukey-Kr	0.543
SUBSTRATE*MIX*YI rooflite	1	2020	rooflite	2	2020	-0.795	0.4326	18	-1.84	0.0826	Tukey-Kr	0.7794
SUBSTRATE*MIX*YI rooflite	2	2019	rooflite	2	2020	0.175	0.3385	18	0.52	0.6115	Tukey-Kr	-

# 8-inch-deep bed

## The SAS System

### The Mixed Procedure

BED=8

Model Information	
Data Set	WORK.A3
Dependent Variable	TOC
Covariance Structure	Variance Components
Subject Effect	BLK(SUBSTRATE*MIX)
Estimation Method	REML
Residual Variance Method	Parameter
Fixed Effects SE Method	Model-Based
Degrees of Freedom Method	Containment

Class Level Information		
Class	Levels	Values
BLK	4	1 2 3 4
SUBSTRATE	2	buildex rooflite
MIX	3	0 1 2
YR	2	2019 2020

Dimensions	
Covariance Parameters	5
Columns in X	36
Columns in Z	48
Subjects	1
Max Obs per Subject	48

Number of Observations	
Number of Observations Read	48
Number of Observations Used	48
Number of Observations Not Used	0

Iteration History			
Iteration	Evaluations	-2 Res Log Like	Criterion
0	1	76.29026275	
1	4	66.89238015	2.27106797
2	4	66.36081950	0.06392333
3	1	66.35475408	0.00019470
4	1	66.35473543	0.00000000

Convergence criteria met.

Covariance Parameter Estimates					
Cov Parm	Subject	Estimate	Standard Error	Z Value	Pr > Z
BLK		0	.	.	.
BLK*SUBSTRATE		0	.	.	.
BLK*MIX		0	.	.	.
BLK*SUBSTRATE*MIX		0.2000	0.08636	2.32	0.0103

YR	BLK(SUBSTRATE*MIX)	0.1071	0.03569	3.00	0.0013
----	--------------------	--------	---------	------	--------

Fit Statistics	
-2 Res Log Likelihood	66.4
AIC (Smaller is Better)	70.4
AICC (Smaller is Better)	70.7
BIC (Smaller is Better)	69.1

Type 3 Tests of Fixed Effects				
Effect	Num DF	Den DF	F Value	Pr > F
SUBSTRATE	1	3	4.82	0.1157
MIX	2	6	0.31	0.7458
SUBSTRATE*MIX	2	6	0.36	0.7142
YR	1	18	7.60	0.0130
SUBSTRATE*YR	1	18	34.37	<.0001
MIX*YR	2	18	0.75	0.4858
SUBSTRATE*MIX*YR	2	18	0.13	0.8759

Least Squares Means								
Effect	SUBSTRATE	MIX	YR	Estimate	Standard Error	DF	t Value	Pr >  t
SUBSTRATE	builddex			1.1362	0.1453	3	7.82	0.0044
SUBSTRATE	rooflite			1.5875	0.1453	3	10.92	0.0016
MIX		0		1.3656	0.1780	6	7.67	0.0003
MIX		1		1.4588	0.1780	6	8.19	0.0002
MIX		2		1.2612	0.1780	6	7.09	0.0004
SUBSTRATE*MIX	builddex	0		1.1213	0.2517	6	4.45	0.0043
SUBSTRATE*MIX	builddex	1		1.1375	0.2517	6	4.52	0.0040
SUBSTRATE*MIX	builddex	2		1.1500	0.2517	6	4.57	0.0038
SUBSTRATE*MIX	rooflite	0		1.6100	0.2517	6	6.40	0.0007
SUBSTRATE*MIX	rooflite	1		1.7800	0.2517	6	7.07	0.0004
SUBSTRATE*MIX	rooflite	2		1.3725	0.2517	6	5.45	0.0016
SUBSTRATE	builddex			1.1362	0.1453	3	7.82	0.0044
SUBSTRATE	rooflite			1.5875	0.1453	3	10.92	0.0016
YR			2019	1.4921	0.1131	18	13.19	<.0001
YR			2020	1.2317	0.1131	18	10.89	<.0001
SUBSTRATE*YR	builddex		2019	1.5433	0.1600	18	9.65	<.0001
SUBSTRATE*YR	builddex		2020	0.7292	0.1600	18	4.56	0.0002
SUBSTRATE*YR	rooflite		2019	1.4408	0.1600	18	9.01	<.0001
SUBSTRATE*YR	rooflite		2020	1.7342	0.1600	18	10.84	<.0001
SUBSTRATE*MIX*YR	builddex	0	2019	1.4325	0.2771	18	5.17	<.0001
SUBSTRATE*MIX*YR	builddex	0	2020	0.8100	0.2771	18	2.92	0.0091
SUBSTRATE*MIX*YR	builddex	1	2019	1.6325	0.2771	18	5.89	<.0001
SUBSTRATE*MIX*YR	builddex	1	2020	0.6425	0.2771	18	2.32	0.0324
SUBSTRATE*MIX*YR	builddex	2	2019	1.5650	0.2771	18	5.65	<.0001
SUBSTRATE*MIX*YR	builddex	2	2020	0.7350	0.2771	18	2.65	0.0162
SUBSTRATE*MIX*YR	rooflite	0	2019	1.4350	0.2771	18	5.18	<.0001
SUBSTRATE*MIX*YR	rooflite	0	2020	1.7850	0.2771	18	6.44	<.0001
SUBSTRATE*MIX*YR	rooflite	1	2019	1.7000	0.2771	18	6.14	<.0001

SUBSTRATE*MIX*YR	rooflite	1	2020	1.8600	0.2771	18	6.71	<.0001
SUBSTRATE*MIX*YR	rooflite	2	2019	1.1875	0.2771	18	4.29	0.0004
SUBSTRATE*MIX*YR	rooflite	2	2020	1.5575	0.2771	18	5.62	<.0001

Differences of Least Squares Means													
Effect	SUBSTRATE	MIX	YR	_SUBSTRATE	_MIX	_YR	Estimate	Standard Error	DF	t Value	Pr >  t	Adjustment	Adj P
SUBSTRATE	builddex			rooflite			-0.4512	0.2055	3	-2.20	0.1157	Tukey	0.1157
MIX		0			1		-0.09312	0.2517	6	-0.37	0.7241	Tukey	0.9282
MIX		0			2		0.1044	0.2517	6	0.41	0.6928	Tukey	0.9110
MIX		1			2		0.1975	0.2517	6	0.78	0.4626	Tukey	0.7254
SUBSTRATE*MIX	builddex	0		builddex	1		-0.01625	0.3560	6	-0.05	0.9651	Tukey	1.0000
SUBSTRATE*MIX	builddex	0		builddex	2		-0.02875	0.3560	6	-0.08	0.9383	Tukey	1.0000
SUBSTRATE*MIX	builddex	0		rooflite	0		-0.4888	0.3560	6	-1.37	0.2189	Tukey	0.7417
SUBSTRATE*MIX	builddex	0		rooflite	1		-0.6588	0.3560	6	-1.85	0.1137	Tukey	0.5021
SUBSTRATE*MIX	builddex	0		rooflite	2		-0.2512	0.3560	6	-0.71	0.5068	Tukey	0.9743
SUBSTRATE*MIX	builddex	1		builddex	2		-0.01250	0.3560	6	-0.04	0.9731	Tukey	1.0000
SUBSTRATE*MIX	builddex	1		rooflite	0		-0.4725	0.3560	6	-1.33	0.2327	Tukey	0.7641
SUBSTRATE*MIX	builddex	1		rooflite	1		-0.6425	0.3560	6	-1.80	0.1212	Tukey	0.5238
SUBSTRATE*MIX	builddex	1		rooflite	2		-0.2350	0.3560	6	-0.66	0.5337	Tukey	0.9805
SUBSTRATE*MIX	builddex	2		rooflite	0		-0.4600	0.3560	6	-1.29	0.2439	Tukey	0.7810
SUBSTRATE*MIX	builddex	2		rooflite	1		-0.6300	0.3560	6	-1.77	0.1272	Tukey	0.5409
SUBSTRATE*MIX	builddex	2		rooflite	2		-0.2225	0.3560	6	-0.62	0.5550	Tukey	0.9846
SUBSTRATE*MIX	rooflite	0		rooflite	1		-0.1700	0.3560	6	-0.48	0.6499	Tukey	0.9953
SUBSTRATE*MIX	rooflite	0		rooflite	2		0.2375	0.3560	6	0.67	0.5295	Tukey	0.9796
SUBSTRATE*MIX	rooflite	1		rooflite	2		0.4075	0.3560	6	1.14	0.2960	Tukey	0.8474
SUBSTRATE	builddex			rooflite			-0.4512	0.2055	3	-2.20	0.1157	Tukey	0.1157
YR			2019			2020	0.2604	0.09446	18	2.76	0.0130	Tukey-Kramer	0.0130
SUBSTRATE*YR	builddex		2019	builddex		2020	0.8142	0.1336	18	6.09	<.0001	Tukey-Kramer	<.0001
SUBSTRATE*YR	builddex		2019	rooflite		2019	0.1025	0.2262	18	0.45	0.6559	Tukey-Kramer	0.9682
SUBSTRATE*YR	builddex		2019	rooflite		2020	-0.1908	0.2262	18	-0.84	0.4100	Tukey-Kramer	0.8330
SUBSTRATE*YR	builddex		2020	rooflite		2019	-0.7117	0.2262	18	-3.15	0.0056	Tukey-Kramer	0.0261
SUBSTRATE*YR	builddex		2020	rooflite		2020	-1.0050	0.2262	18	-4.44	0.0003	Tukey-Kramer	0.0016
SUBSTRATE*YR	rooflite		2019	rooflite		2020	-0.2933	0.1336	18	-2.20	0.0414	Tukey-Kramer	0.1621
SUBSTRATE*MIX*YR	builddex	0	2019	builddex	0	2020	0.6225	0.2314	18	2.69	0.0149	Tukey-Kramer	0.3035
SUBSTRATE*MIX*YR	builddex	0	2019	builddex	1	2019	-0.2000	0.3918	18	-0.51	0.6159	Tukey-Kramer	1.0000
SUBSTRATE*MIX*YR	builddex	0	2019	builddex	1	2020	0.7900	0.3918	18	2.02	0.0589	Tukey-Kramer	0.6789
SUBSTRATE*MIX*YR	builddex	0	2019	builddex	2	2019	-0.1325	0.3918	18	-0.34	0.7391	Tukey-Kramer	1.0000
SUBSTRATE*MIX*YR	builddex	0	2019	builddex	2	2020	0.6975	0.3918	18	1.78	0.0919	Tukey-Kramer	0.8090
SUBSTRATE*MIX*YR	builddex	0	2019	rooflite	0	2019	-0.00250	0.3918	18	-0.01	0.9950	Tukey-Kramer	1.0000
SUBSTRATE*MIX*YR	builddex	0	2019	rooflite	0	2020	-0.3525	0.3918	18	-0.90	0.3802	Tukey-	0.9982

												Kramer	
SUBSTRATE*MIX*YR	builddex	0	2019	rooflite	1	2019	-0.2675	0.3918	18	-0.68	0.5035	Tukey-Kramer	0.9999
SUBSTRATE*MIX*YR	builddex	0	2019	rooflite	1	2020	-0.4275	0.3918	18	-1.09	0.2896	Tukey-Kramer	0.9912
SUBSTRATE*MIX*YR	builddex	0	2019	rooflite	2	2019	0.2450	0.3918	18	0.63	0.5396	Tukey-Kramer	0.9999
SUBSTRATE*MIX*YR	builddex	0	2019	rooflite	2	2020	-0.1250	0.3918	18	-0.32	0.7534	Tukey-Kramer	1.0000
SUBSTRATE*MIX*YR	builddex	0	2020	builddex	1	2019	-0.8225	0.3918	18	-2.10	0.0502	Tukey-Kramer	0.6294
SUBSTRATE*MIX*YR	builddex	0	2020	builddex	1	2020	0.1675	0.3918	18	0.43	0.6741	Tukey-Kramer	1.0000
SUBSTRATE*MIX*YR	builddex	0	2020	builddex	2	2019	-0.7550	0.3918	18	-1.93	0.0699	Tukey-Kramer	0.7307
SUBSTRATE*MIX*YR	builddex	0	2020	builddex	2	2020	0.07500	0.3918	18	0.19	0.8503	Tukey-Kramer	1.0000
SUBSTRATE*MIX*YR	builddex	0	2020	rooflite	0	2019	-0.6250	0.3918	18	-1.60	0.1281	Tukey-Kramer	0.8901
SUBSTRATE*MIX*YR	builddex	0	2020	rooflite	0	2020	-0.9750	0.3918	18	-2.49	0.0228	Tukey-Kramer	0.4029
SUBSTRATE*MIX*YR	builddex	0	2020	rooflite	1	2019	-0.8900	0.3918	18	-2.27	0.0356	Tukey-Kramer	0.5258
SUBSTRATE*MIX*YR	builddex	0	2020	rooflite	1	2020	-1.0500	0.3918	18	-2.68	0.0153	Tukey-Kramer	0.3083
SUBSTRATE*MIX*YR	builddex	0	2020	rooflite	2	2019	-0.3775	0.3918	18	-0.96	0.3481	Tukey-Kramer	0.9968
SUBSTRATE*MIX*YR	builddex	0	2020	rooflite	2	2020	-0.7475	0.3918	18	-1.91	0.0725	Tukey-Kramer	0.7414
SUBSTRATE*MIX*YR	builddex	1	2019	builddex	1	2020	0.9900	0.2314	18	4.28	0.0005	Tukey-Kramer	0.0167
SUBSTRATE*MIX*YR	builddex	1	2019	builddex	2	2019	0.06750	0.3918	18	0.17	0.8651	Tukey-Kramer	1.0000
SUBSTRATE*MIX*YR	builddex	1	2019	builddex	2	2020	0.8975	0.3918	18	2.29	0.0343	Tukey-Kramer	0.5145
SUBSTRATE*MIX*YR	builddex	1	2019	rooflite	0	2019	0.1975	0.3918	18	0.50	0.6203	Tukey-Kramer	1.0000
SUBSTRATE*MIX*YR	builddex	1	2019	rooflite	0	2020	-0.1525	0.3918	18	-0.39	0.7017	Tukey-Kramer	1.0000
SUBSTRATE*MIX*YR	builddex	1	2019	rooflite	1	2019	-0.06750	0.3918	18	-0.17	0.8651	Tukey-Kramer	1.0000
SUBSTRATE*MIX*YR	builddex	1	2019	rooflite	1	2020	-0.2275	0.3918	18	-0.58	0.5687	Tukey-Kramer	1.0000
SUBSTRATE*MIX*YR	builddex	1	2019	rooflite	2	2019	0.4450	0.3918	18	1.14	0.2710	Tukey-Kramer	0.9881
SUBSTRATE*MIX*YR	builddex	1	2019	rooflite	2	2020	0.07500	0.3918	18	0.19	0.8503	Tukey-Kramer	1.0000
SUBSTRATE*MIX*YR	builddex	1	2020	builddex	2	2019	-0.9225	0.3918	18	-2.35	0.0301	Tukey-Kramer	0.4773
SUBSTRATE*MIX*YR	builddex	1	2020	builddex	2	2020	-0.09250	0.3918	18	-0.24	0.8160	Tukey-Kramer	1.0000
SUBSTRATE*MIX*YR	builddex	1	2020	rooflite	0	2019	-0.7925	0.3918	18	-2.02	0.0582	Tukey-Kramer	0.6752
SUBSTRATE*MIX*YR	builddex	1	2020	rooflite	0	2020	-1.1425	0.3918	18	-2.92	0.0092	Tukey-Kramer	0.2140
SUBSTRATE*MIX*YR	builddex	1	2020	rooflite	1	2019	-1.0575	0.3918	18	-2.70	0.0147	Tukey-Kramer	0.2997
SUBSTRATE*MIX*YR	builddex	1	2020	rooflite	1	2020	-1.2175	0.3918	18	-3.11	0.0061	Tukey-Kramer	0.1554
SUBSTRATE*MIX*YR	builddex	1	2020	rooflite	2	2019	-0.5450	0.3918	18	-1.39	0.1812	Tukey-	0.9510

												Kramer	
SUBSTRATE*MIX*YR	builddex	1	2020	rooflite	2	2020	-0.9150	0.3918	18	-2.34	0.0313	Tukey-Kramer	0.4883
SUBSTRATE*MIX*YR	builddex	2	2019	builddex	2	2020	0.8300	0.2314	18	3.59	0.0021	Tukey-Kramer	0.0650
SUBSTRATE*MIX*YR	builddex	2	2019	rooflite	0	2019	0.1300	0.3918	18	0.33	0.7439	Tukey-Kramer	1.0000
SUBSTRATE*MIX*YR	builddex	2	2019	rooflite	0	2020	-0.2200	0.3918	18	-0.56	0.5814	Tukey-Kramer	1.0000
SUBSTRATE*MIX*YR	builddex	2	2019	rooflite	1	2019	-0.1350	0.3918	18	-0.34	0.7344	Tukey-Kramer	1.0000
SUBSTRATE*MIX*YR	builddex	2	2019	rooflite	1	2020	-0.2950	0.3918	18	-0.75	0.4612	Tukey-Kramer	0.9996
SUBSTRATE*MIX*YR	builddex	2	2019	rooflite	2	2019	0.3775	0.3918	18	0.96	0.3481	Tukey-Kramer	0.9968
SUBSTRATE*MIX*YR	builddex	2	2019	rooflite	2	2020	0.007500	0.3918	18	0.02	0.9849	Tukey-Kramer	1.0000
SUBSTRATE*MIX*YR	builddex	2	2020	rooflite	0	2019	-0.7000	0.3918	18	-1.79	0.0909	Tukey-Kramer	0.8058
SUBSTRATE*MIX*YR	builddex	2	2020	rooflite	0	2020	-1.0500	0.3918	18	-2.68	0.0153	Tukey-Kramer	0.3083
SUBSTRATE*MIX*YR	builddex	2	2020	rooflite	1	2019	-0.9650	0.3918	18	-2.46	0.0241	Tukey-Kramer	0.4166
SUBSTRATE*MIX*YR	builddex	2	2020	rooflite	1	2020	-1.1250	0.3918	18	-2.87	0.0102	Tukey-Kramer	0.2299
SUBSTRATE*MIX*YR	builddex	2	2020	rooflite	2	2019	-0.4525	0.3918	18	-1.15	0.2632	Tukey-Kramer	0.9865
SUBSTRATE*MIX*YR	builddex	2	2020	rooflite	2	2020	-0.8225	0.3918	18	-2.10	0.0502	Tukey-Kramer	0.6294
SUBSTRATE*MIX*YR	rooflite	0	2019	rooflite	0	2020	-0.3500	0.2314	18	-1.51	0.1477	Tukey-Kramer	0.9184
SUBSTRATE*MIX*YR	rooflite	0	2019	rooflite	1	2019	-0.2650	0.3918	18	-0.68	0.5074	Tukey-Kramer	0.9999
SUBSTRATE*MIX*YR	rooflite	0	2019	rooflite	1	2020	-0.4250	0.3918	18	-1.08	0.2924	Tukey-Kramer	0.9916
SUBSTRATE*MIX*YR	rooflite	0	2019	rooflite	2	2019	0.2475	0.3918	18	0.63	0.5355	Tukey-Kramer	0.9999
SUBSTRATE*MIX*YR	rooflite	0	2019	rooflite	2	2020	-0.1225	0.3918	18	-0.31	0.7581	Tukey-Kramer	1.0000
SUBSTRATE*MIX*YR	rooflite	0	2020	rooflite	1	2019	0.08500	0.3918	18	0.22	0.8307	Tukey-Kramer	1.0000
SUBSTRATE*MIX*YR	rooflite	0	2020	rooflite	1	2020	-0.07500	0.3918	18	-0.19	0.8503	Tukey-Kramer	1.0000
SUBSTRATE*MIX*YR	rooflite	0	2020	rooflite	2	2019	0.5975	0.3918	18	1.52	0.1446	Tukey-Kramer	0.9145
SUBSTRATE*MIX*YR	rooflite	0	2020	rooflite	2	2020	0.2275	0.3918	18	0.58	0.5687	Tukey-Kramer	1.0000
SUBSTRATE*MIX*YR	rooflite	1	2019	rooflite	1	2020	-0.1600	0.2314	18	-0.69	0.4981	Tukey-Kramer	0.9998
SUBSTRATE*MIX*YR	rooflite	1	2019	rooflite	2	2019	0.5125	0.3918	18	1.31	0.2073	Tukey-Kramer	0.9672
SUBSTRATE*MIX*YR	rooflite	1	2019	rooflite	2	2020	0.1425	0.3918	18	0.36	0.7203	Tukey-Kramer	1.0000
SUBSTRATE*MIX*YR	rooflite	1	2020	rooflite	2	2019	0.6725	0.3918	18	1.72	0.1033	Tukey-Kramer	0.8395
SUBSTRATE*MIX*YR	rooflite	1	2020	rooflite	2	2020	0.3025	0.3918	18	0.77	0.4501	Tukey-Kramer	0.9995
SUBSTRATE*MIX*YR	rooflite	2	2019	rooflite	2	2020	-0.3700	0.2314	18	-1.60	0.1272	Tukey-Kramer	0.8885

**Appendix G - The SAS output for the TN analyses by different bed (both 4-inch and 8-inch-deep bed) and year (year as repeated measure)**

**4-inch-deep bed at APD-EGR**

<b>Type 3 Tests of Fixed Effects</b>				
<b>Effect</b>	<b>Num DF</b>	<b>Den DF</b>	<b>F Value</b>	<b>Pr &gt; F</b>
<b>SUBSTRATE</b>	1	3	21.19	0.0193
<b>MIX</b>	2	6	1.07	0.4008
<b>SUBSTRATE*MIX</b>	2	6	1.33	0.3323
<b>YR</b>	1	18	1.58	0.2252
<b>SUBSTRATE*YR</b>	1	18	2.46	0.1339
<b>MIX*YR</b>	2	18	0.15	0.8623
<b>SUBSTRATE*MIX*YR</b>	2	18	1.58	0.2329

Least Squares Means								
Effect	SUBSTRATE	MIX	YR	Estimate	Standard Error	DF	t Value	Pr >  t
SUBSTRATE	buillex			0.0875	0.01001	3	8.74	0.0032
SUBSTRATE	rooflite			0.1483	0.01001	3	14.82	0.0007
MIX		0		0.1075	0.01303	6	8.25	0.0002
MIX		1		0.1131	0.01303	6	8.68	0.0001
MIX		2		0.1331	0.01303	6	10.22	<.0001
SUBSTRATE*MIX	buillex	0		0.07875	0.01734	6	4.54	0.0039
SUBSTRATE*MIX	buillex	1		0.095	0.01734	6	5.48	0.0015
SUBSTRATE*MIX	buillex	2		0.08875	0.01734	6	5.12	0.0022
SUBSTRATE*MIX	rooflite	0		0.1363	0.01734	6	7.86	0.0002
SUBSTRATE*MIX	rooflite	1		0.1312	0.01734	6	7.57	0.0003
SUBSTRATE*MIX	rooflite	2		0.1775	0.01734	6	10.24	<.0001
SUBSTRATE	buillex			0.0875	0.01001	3	8.74	0.0032
SUBSTRATE	rooflite			0.1483	0.01001	3	14.82	0.0007
YR			2019	0.1246	0.009206	18	13.53	<.0001
YR			2020	0.1113	0.009206	18	12.08	<.0001
SUBSTRATE*YR	buillex		2019	0.1025	0.01251	18	8.19	<.0001
SUBSTRATE*YR	buillex		2020	0.0725	0.01251	18	5.79	<.0001
SUBSTRATE*YR	rooflite		2019	0.1467	0.01251	18	11.72	<.0001
SUBSTRATE*YR	rooflite		2020	0.15	0.01251	18	11.99	<.0001
SUBSTRATE*MIX*YR	buillex	0	2019	0.1025	0.02167	18	4.73	0.0002
SUBSTRATE*MIX*YR	buillex	0	2020	0.055	0.02167	18	2.54	0.0206
SUBSTRATE*MIX*YR	buillex	1	2019	0.0975	0.02167	18	4.5	0.0003

SUBSTRATE*MIX*YR	builddex	1	2020	0.0925	0.02167	18	4.27	0.0005
SUBSTRATE*MIX*YR	builddex	2	2019	0.1075	0.02167	18	4.96	0.0001
SUBSTRATE*MIX*YR	builddex	2	2020	0.07	0.02167	18	3.23	0.0046
SUBSTRATE*MIX*YR	rooflite	0	2019	0.12	0.02167	18	5.54	<.0001
SUBSTRATE*MIX*YR	rooflite	0	2020	0.1525	0.02167	18	7.04	<.0001
SUBSTRATE*MIX*YR	rooflite	1	2019	0.14	0.02167	18	6.46	<.0001
SUBSTRATE*MIX*YR	rooflite	1	2020	0.1225	0.02167	18	5.65	<.0001
SUBSTRATE*MIX*YR	rooflite	2	2019	0.18	0.02167	18	8.3	<.0001
SUBSTRATE*MIX*YR	rooflite	2	2020	0.175	0.02167	18	8.07	<.0001

Differences of Least Squares Means

Effect	SUBSTRATE	MIX	YR	_SUBSTRAT	_MIX	_YR	Estimate	Standard Error	DF	t Value	Pr >  t	Adjustmen	Adj P
<b>SUBSTRATE</b>	<b>builddex</b>			<b>rooflite</b>			<b>-0.06083</b>	<b>0.01322</b>	<b>3</b>	<b>-4.6</b>	<b>0.0193</b>	<b>Tukey-Krarr</b>	<b>0.0193</b>
MIX		0			1		-0.00562	0.01842	6	-0.31	0.7704	Tukey	0.9503
MIX		0			2		-0.02563	0.01842	6	-1.39	0.2136	Tukey	0.4027
MIX		1			2		-0.02	0.01842	6	-1.09	0.3193	Tukey	0.5561
SUBSTRATE*MIX	builddex	0		builddex	1		-0.01625	0.02452	6	-0.66	0.5322	Tukey-Krarr	0.9802
SUBSTRATE*MIX	builddex	0		builddex	2		-0.01	0.02452	6	-0.41	0.6976	Tukey-Krarr	0.9978
SUBSTRATE*MIX	builddex	0		rooflite	0		-0.0575	0.02289	6	-2.51	0.0458	Tukey-Krarr	0.2527
SUBSTRATE*MIX	builddex	0		rooflite	1		-0.0525	0.02452	6	-2.14	0.0761	Tukey-Krarr	0.3764
SUBSTRATE*MIX	builddex	0		rooflite	2		-0.09875	0.02452	6	-4.03	0.0069	Tukey-Krarr	0.0476
SUBSTRATE*MIX	builddex	1		builddex	2		0.00625	0.02452	6	0.25	0.8073	Tukey-Krarr	0.9998
SUBSTRATE*MIX	builddex	1		rooflite	0		-0.04125	0.02452	6	-1.68	0.1435	Tukey-Krarr	0.5843
SUBSTRATE*MIX	builddex	1		rooflite	1		-0.03625	0.02289	6	-1.58	0.1644	Tukey-Krarr	0.6344
SUBSTRATE*MIX	builddex	1		rooflite	2		-0.0825	0.02452	6	-3.36	0.0152	Tukey-Krarr	0.0976
SUBSTRATE*MIX	builddex	2		rooflite	0		-0.0475	0.02452	6	-1.94	0.1009	Tukey-Krarr	0.4621
SUBSTRATE*MIX	builddex	2		rooflite	1		-0.0425	0.02452	6	-1.73	0.1338	Tukey-Krarr	0.5589
SUBSTRATE*MIX	builddex	2		rooflite	2		-0.08875	0.02289	6	-3.88	0.0082	Tukey-Krarr	0.0558
SUBSTRATE*MIX	rooflite	0		rooflite	1		0.005	0.02452	6	0.2	0.8452	Tukey-Krarr	0.9999
SUBSTRATE*MIX	rooflite	0		rooflite	2		-0.04125	0.02452	6	-1.68	0.1435	Tukey-Krarr	0.5843
SUBSTRATE*MIX	rooflite	1		rooflite	2		-0.04625	0.02452	6	-1.89	0.1083	Tukey-Krarr	0.4854
SUBSTRATE	builddex			rooflite			-0.06083	0.01322	3	-4.6	0.0193	Tukey-Krarr	0.0193
YR			2019			2020	0.01333	0.01062	18	1.26	0.2252	Tukey-Krarr	0.2252
SUBSTRATE*YR	builddex		2019	builddex		2020	0.03	0.01502	18	2	0.0611	Tukey-Krarr	0.2253
SUBSTRATE*YR	builddex		2019	rooflite		2019	-0.04417	0.01695	18	-2.61	0.0179	Tukey-Krarr	0.0769
SUBSTRATE*YR	builddex		2019	rooflite		2020	-0.0475	0.01695	18	-2.8	0.0118	Tukey-Krarr	0.0525
SUBSTRATE*YR	builddex		2020	rooflite		2019	-0.07417	0.01695	18	-4.37	0.0004	Tukey-Krarr	0.0019
SUBSTRATE*YR	builddex		2020	rooflite		2020	-0.0775	0.01695	18	-4.57	0.0002	Tukey-Krarr	0.0012
SUBSTRATE*YR	rooflite		2019	rooflite		2020	-0.00333	0.01502	18	-0.22	0.8268	Tukey-Krarr	0.996
SUBSTRATE*MIX*YR	builddex	0	2019	builddex	0	2020	0.0475	0.02601	18	1.83	0.0844	Tukey-Krarr	0.7855
SUBSTRATE*MIX*YR	builddex	0	2019	builddex	1	2019	0.005	0.03065	18	0.16	0.8722	Tukey-Krarr	1
SUBSTRATE*MIX*YR	builddex	0	2019	builddex	1	2020	0.01	0.03065	18	0.33	0.748	Tukey-Krarr	1
SUBSTRATE*MIX*YR	builddex	0	2019	builddex	2	2019	-0.005	0.03065	18	-0.16	0.8722	Tukey-Krarr	1
SUBSTRATE*MIX*YR	builddex	0	2019	builddex	2	2020	0.0325	0.03065	18	1.06	0.303	Tukey-Krarr	0.993
SUBSTRATE*MIX*YR	builddex	0	2019	rooflite	0	2019	-0.0175	0.02936	18	-0.6	0.5586	Tukey-Krarr	1
SUBSTRATE*MIX*YR	builddex	0	2019	rooflite	0	2020	-0.05	0.02936	18	-1.7	0.1058	Tukey-Krarr	0.8456
SUBSTRATE*MIX*YR	builddex	0	2019	rooflite	1	2019	-0.0375	0.03065	18	-1.22	0.237	Tukey-Krarr	0.9794
SUBSTRATE*MIX*YR	builddex	0	2019	rooflite	1	2020	-0.02	0.03065	18	-0.65	0.5223	Tukey-Krarr	0.9999
SUBSTRATE*MIX*YR	builddex	0	2019	rooflite	2	2019	-0.0775	0.03065	18	-2.53	0.021	Tukey-Krarr	0.3819

SUBSTRATE*MIX*YI buildex	0	2019	rooflite	2	2019	-0.0775	0.03065	18	-2.53	0.021	Tukey-Kr	0.3819
SUBSTRATE*MIX*YI buildex	0	2019	rooflite	2	2020	-0.0725	0.03065	18	-2.37	0.0295	Tukey-Kr	0.4711
SUBSTRATE*MIX*YI buildex	0	2020	buildex	1	2019	-0.0425	0.03065	18	-1.39	0.1825	Tukey-Kr	0.952
SUBSTRATE*MIX*YI buildex	0	2020	buildex	1	2020	-0.0375	0.03065	18	-1.22	0.237	Tukey-Kr	0.9794
SUBSTRATE*MIX*YI buildex	0	2020	buildex	2	2019	-0.0525	0.03065	18	-1.71	0.1039	Tukey-Kr	0.8412
SUBSTRATE*MIX*YI buildex	0	2020	buildex	2	2020	-0.015	0.03065	18	-0.49	0.6305	Tukey-Kr	1
SUBSTRATE*MIX*YI buildex	0	2020	rooflite	0	2019	-0.065	0.02936	18	-2.21	0.04	Tukey-Kr	0.5603
SUBSTRATE*MIX*YI buildex	0	2020	rooflite	0	2020	-0.0975	0.02936	18	-3.32	0.0038	Tukey-Kr	0.1066
SUBSTRATE*MIX*YI buildex	0	2020	rooflite	1	2019	-0.085	0.03065	18	-2.77	0.0125	Tukey-Kr	0.2681
SUBSTRATE*MIX*YI buildex	0	2020	rooflite	1	2020	-0.0675	0.03065	18	-2.2	0.0409	Tukey-Kr	0.5673
SUBSTRATE*MIX*YI buildex	0	2020	rooflite	2	2019	-0.125	0.03065	18	-4.08	0.0007	Tukey-Kr	0.0249
SUBSTRATE*MIX*YI buildex	0	2020	rooflite	2	2020	-0.12	0.03065	18	-3.91	0.001	Tukey-Kr	0.0344
SUBSTRATE*MIX*YI buildex	1	2019	buildex	1	2020	0.005	0.02601	18	0.19	0.8497	Tukey-Kr	1
SUBSTRATE*MIX*YI buildex	1	2019	buildex	2	2019	-0.01	0.03065	18	-0.33	0.748	Tukey-Kr	1
SUBSTRATE*MIX*YI buildex	1	2019	buildex	2	2020	0.0275	0.03065	18	0.9	0.3815	Tukey-Kr	0.9982
SUBSTRATE*MIX*YI buildex	1	2019	rooflite	0	2019	-0.0225	0.03065	18	-0.73	0.4724	Tukey-Kr	0.9997
SUBSTRATE*MIX*YI buildex	1	2019	rooflite	0	2020	-0.055	0.03065	18	-1.79	0.0896	Tukey-Kr	0.8019
SUBSTRATE*MIX*YI buildex	1	2019	rooflite	1	2019	-0.0425	0.02936	18	-1.45	0.165	Tukey-Kr	0.9372
SUBSTRATE*MIX*YI buildex	1	2019	rooflite	1	2020	-0.025	0.02936	18	-0.85	0.4057	Tukey-Kr	0.9989
SUBSTRATE*MIX*YI buildex	1	2019	rooflite	2	2019	-0.0825	0.03065	18	-2.69	0.0149	Tukey-Kr	0.3031
SUBSTRATE*MIX*YI buildex	1	2019	rooflite	2	2020	-0.0775	0.03065	18	-2.53	0.021	Tukey-Kr	0.3819
SUBSTRATE*MIX*YI buildex	1	2020	buildex	2	2019	-0.015	0.03065	18	-0.49	0.6305	Tukey-Kr	1
SUBSTRATE*MIX*YI buildex	1	2020	buildex	2	2020	0.0225	0.03065	18	0.73	0.4724	Tukey-Kr	0.9997
SUBSTRATE*MIX*YI buildex	1	2020	rooflite	0	2019	-0.0275	0.03065	18	-0.9	0.3815	Tukey-Kr	0.9982
SUBSTRATE*MIX*YI buildex	1	2020	rooflite	0	2020	-0.06	0.03065	18	-1.96	0.066	Tukey-Kr	0.7133
SUBSTRATE*MIX*YI buildex	1	2020	rooflite	1	2019	-0.0475	0.02936	18	-1.62	0.1231	Tukey-Kr	0.8814
SUBSTRATE*MIX*YI buildex	1	2020	rooflite	1	2020	-0.03	0.02936	18	-1.02	0.3205	Tukey-Kr	0.9948
SUBSTRATE*MIX*YI buildex	1	2020	rooflite	2	2019	-0.0875	0.03065	18	-2.85	0.0105	Tukey-Kr	0.2361
SUBSTRATE*MIX*YI buildex	1	2020	rooflite	2	2020	-0.0825	0.03065	18	-2.69	0.0149	Tukey-Kr	0.3031
SUBSTRATE*MIX*YI buildex	2	2019	buildex	2	2020	0.0375	0.02601	18	1.44	0.1665	Tukey-Kr	0.9387
SUBSTRATE*MIX*YI buildex	2	2019	rooflite	0	2019	-0.0125	0.03065	18	-0.41	0.6882	Tukey-Kr	1
SUBSTRATE*MIX*YI buildex	2	2019	rooflite	0	2020	-0.045	0.03065	18	-1.47	0.1593	Tukey-Kr	0.9316
SUBSTRATE*MIX*YI buildex	2	2019	rooflite	1	2019	-0.0325	0.03065	18	-1.06	0.303	Tukey-Kr	0.993
SUBSTRATE*MIX*YI buildex	2	2019	rooflite	1	2020	-0.015	0.03065	18	-0.49	0.6305	Tukey-Kr	1
SUBSTRATE*MIX*YI buildex	2	2019	rooflite	2	2019	-0.0725	0.02936	18	-2.47	0.0238	Tukey-Kr	0.4132
SUBSTRATE*MIX*YI buildex	2	2019	rooflite	2	2020	-0.0675	0.02936	18	-2.3	0.0337	Tukey-Kr	0.5096
SUBSTRATE*MIX*YI buildex	2	2020	rooflite	0	2019	-0.05	0.03065	18	-1.63	0.1202	Tukey-Kr	0.8761
SUBSTRATE*MIX*YI buildex	2	2020	rooflite	0	2020	-0.0825	0.03065	18	-2.69	0.0149	Tukey-Kr	0.3031
SUBSTRATE*MIX*YI buildex	2	2020	rooflite	1	2019	-0.07	0.03065	18	-2.28	0.0348	Tukey-Kr	0.5186
SUBSTRATE*MIX*YI buildex	2	2020	rooflite	1	2020	-0.0525	0.03065	18	-1.71	0.1039	Tukey-Kr	0.8412
SUBSTRATE*MIX*YI buildex	2	2020	rooflite	2	2019	-0.11	0.02936	18	-3.75	0.0015	Tukey-Kr	0.0479
SUBSTRATE*MIX*YI buildex	2	2020	rooflite	2	2020	-0.105	0.02936	18	-3.58	0.0022	Tukey-Kr	0.0664
SUBSTRATE*MIX*YI rooflite	0	2019	rooflite	0	2020	-0.0325	0.02601	18	-1.25	0.2274	Tukey-Kr	0.9761
SUBSTRATE*MIX*YI rooflite	0	2019	rooflite	1	2019	-0.02	0.03065	18	-0.65	0.5223	Tukey-Kr	0.9999
SUBSTRATE*MIX*YI rooflite	0	2019	rooflite	1	2020	-0.0025	0.03065	18	-0.08	0.9359	Tukey-Kr	1
SUBSTRATE*MIX*YI rooflite	0	2019	rooflite	2	2019	-0.06	0.03065	18	-1.96	0.066	Tukey-Kr	0.7133
SUBSTRATE*MIX*YI rooflite	0	2019	rooflite	2	2020	-0.055	0.03065	18	-1.79	0.0896	Tukey-Kr	0.8019
SUBSTRATE*MIX*YI rooflite	0	2020	rooflite	1	2019	0.0125	0.03065	18	0.41	0.6882	Tukey-Kr	1
SUBSTRATE*MIX*YI rooflite	0	2020	rooflite	1	2020	0.03	0.03065	18	0.98	0.3407	Tukey-Kr	0.9963
SUBSTRATE*MIX*YI rooflite	0	2020	rooflite	2	2019	-0.0275	0.03065	18	-0.9	0.3815	Tukey-Kr	0.9982
SUBSTRATE*MIX*YI rooflite	0	2020	rooflite	2	2020	-0.0225	0.03065	18	-0.73	0.4724	Tukey-Kr	0.9997
SUBSTRATE*MIX*YI rooflite	1	2019	rooflite	1	2020	0.0175	0.02601	18	0.67	0.5096	Tukey-Kr	0.9999
SUBSTRATE*MIX*YI rooflite	1	2019	rooflite	2	2019	-0.04	0.03065	18	-1.3	0.2083	Tukey-Kr	0.9678
SUBSTRATE*MIX*YI rooflite	1	2019	rooflite	2	2020	-0.035	0.03065	18	-1.14	0.2685	Tukey-Kr	0.9876
SUBSTRATE*MIX*YI rooflite	1	2020	rooflite	2	2019	-0.0575	0.03065	18	-1.88	0.077	Tukey-Kr	0.7591
SUBSTRATE*MIX*YI rooflite	1	2020	rooflite	2	2020	-0.0525	0.03065	18	-1.71	0.1039	Tukey-Kr	0.8412
SUBSTRATE*MIX*YI rooflite	2	2019	rooflite	2	2020	0.005	0.02601	18	0.19	0.8497	Tukey-Kr	1

### 4-inch-deep bed at APD-EGR

Type 3 Tests of Fixed Effects					
Effect	Num DF	Den DF	F Value	Pr > F	
<b>SUBSTRATE</b>	1	3	4.23	0.1321	
<b>MIX</b>	2	6	0.09	0.9147	
<b>SUBSTRATE*MIX</b>	2	6	0.46	0.6506	
<b>YR</b>	1	18	33.78	<.0001	***
<b>SUBSTRATE*YR</b>	1	18	37.96	<.0001	***
<b>MIX*YR</b>	2	18	1.16	0.3362	
<b>SUBSTRATE*MIX*YR</b>	2	18	0.35	0.7108	

Least Squares Means								
Effect	SUBSTRATE	MIX	YR	Estimate	Standard Error	DF	t Value	Pr >  t
SUBSTRATE	buildex			0.05875	0.01143	3	5.14	0.0143
SUBSTRATE	rooflite			0.08875	0.01143	3	7.76	0.0044
MIX		0		0.07625	0.01356	6	5.62	0.0014
MIX		1		0.07563	0.01356	6	5.58	0.0014
MIX		2		0.06937	0.01356	6	5.11	0.0022
SUBSTRATE*MIX	buildex	0		0.05375	0.01854	6	2.9	0.0274
SUBSTRATE*MIX	buildex	1		0.05875	0.01854	6	3.17	0.0193
SUBSTRATE*MIX	buildex	2		0.06375	0.01854	6	3.44	0.0138
SUBSTRATE*MIX	rooflite	0		0.09875	0.01854	6	5.33	0.0018
SUBSTRATE*MIX	rooflite	1		0.0925	0.01854	6	4.99	0.0025
SUBSTRATE*MIX	rooflite	2		0.075	0.01854	6	4.05	0.0068
SUBSTRATE	buildex			0.05875	0.01143	3	5.14	0.0143
SUBSTRATE	rooflite			0.08875	0.01143	3	7.76	0.0044
YR			2019	0.09458	0.009503	18	9.95	<.0001
YR			2020	0.05292	0.009503	18	5.57	<.0001
SUBSTRATE*YR	Buildex		2019	0.1017	0.01251	18	8.13	<.0001
SUBSTRATE*YR	Buildex		2020	0.01583	0.01251	18	1.27	0.2216
SUBSTRATE*YR	Rooflite		2019	0.0875	0.01251	18	7	<.0001
SUBSTRATE*YR	Rooflite		2020	0.09	0.01251	18	7.2	<.0001
SUBSTRATE*MIX*YR	buildex	0	2019	0.095	0.02051	18	4.63	0.0002
SUBSTRATE*MIX*YR	buildex	0	2020	0.0125	0.02051	18	0.61	0.5499
SUBSTRATE*MIX*YR	buildex	1	2019	0.1075	0.02051	18	5.24	<.0001
SUBSTRATE*MIX*YR	buildex	1	2020	0.01	0.02051	18	0.49	0.6318

SUBSTRATE*MIX*YR	builddex	2	2019	0.1025	0.02051	18	5	<.0001
SUBSTRATE*MIX*YR	builddex	2	2020	0.025	0.02051	18	1.22	0.2387
SUBSTRATE*MIX*YR	rooflite	0	2019	0.0875	0.02051	18	4.27	0.0005
SUBSTRATE*MIX*YR	rooflite	0	2020	0.11	0.02051	18	5.36	<.0001
SUBSTRATE*MIX*YR	rooflite	1	2019	0.1	0.02051	18	4.87	0.0001
SUBSTRATE*MIX*YR	rooflite	1	2020	0.085	0.02051	18	4.14	0.0006
SUBSTRATE*MIX*YR	rooflite	2	2019	0.075	0.02051	18	3.66	0.0018
SUBSTRATE*MIX*YR	rooflite	2	2020	0.075	0.02051	18	3.66	0.0018

Differences of Least Squares Means													
Effect	SUBSTRAT	MIX	YR	_SUBSTRA	_MIX	_YR	Estimate	Standard Error	DF	t Value	Pr >  t	Adjustment	Adj P
SUBSTRATE	builddex			rooflite			-0.03	0.01459	3	-2.06	0.1321	Tukey-Kramer	0.1321
MIX		0				1	0.00625	0.01787	6	0.38	0.7138	Tukey-Kramer	0.9993
MIX		0				2	0.006875	0.01787	6	0.38	0.7138	Tukey-Kramer	0.9227
MIX		1				2	0.00625	0.01787	6	0.35	0.7385	Tukey-Kramer	0.9355
SUBSTRATE*MIX	builddex	0		builddex		1	-0.005	0.02528	6	-0.2	0.8497	Tukey-Kramer	0.9999
SUBSTRATE*MIX	builddex	0		builddex		2	-0.01	0.02528	6	-0.4	0.7061	Tukey-Kramer	0.9981
SUBSTRATE*MIX	builddex	0		rooflite		0	-0.045	0.02528	6	-1.78	0.1254	Tukey-Kramer	0.5357
SUBSTRATE*MIX	builddex	0		rooflite		1	-0.03875	0.02528	6	-1.53	0.1762	Tukey-Kramer	0.6604
SUBSTRATE*MIX	builddex	0		rooflite		2	-0.02125	0.02528	6	-0.84	0.4328	Tukey-Kramer	0.9483
SUBSTRATE*MIX	builddex	1		builddex		2	-0.005	0.02528	6	-0.2	0.8497	Tukey-Kramer	0.9999
SUBSTRATE*MIX	builddex	1		rooflite		0	-0.04	0.02528	6	-1.58	0.1647	Tukey-Kramer	0.6351
SUBSTRATE*MIX	builddex	1		rooflite		1	-0.03375	0.02528	6	-1.34	0.2303	Tukey-Kramer	0.7602
SUBSTRATE*MIX	builddex	1		rooflite		2	-0.01625	0.02528	6	-0.64	0.5441	Tukey-Kramer	0.9826
SUBSTRATE*MIX	builddex	2		rooflite		0	-0.035	0.02528	6	-1.38	0.2155	Tukey-Kramer	0.7358
SUBSTRATE*MIX	builddex	2		rooflite		1	-0.02875	0.02528	6	-1.14	0.2988	Tukey-Kramer	0.8504
SUBSTRATE*MIX	builddex	2		rooflite		2	-0.01125	0.02528	6	-0.45	0.6719	Tukey-Kramer	0.9966
SUBSTRATE*MIX	rooflite	0		rooflite		1	0.00625	0.02528	6	0.25	0.813	Tukey-Kramer	0.9998
SUBSTRATE*MIX	rooflite	0		rooflite		2	0.02375	0.02528	6	0.94	0.3837	Tukey-Kramer	0.9217
SUBSTRATE*MIX	rooflite	1		rooflite		2	0.0175	0.02528	6	0.69	0.5146	Tukey-Kramer	0.9762
SUBSTRATE	builddex			rooflite			-0.03	0.01459	3	-2.06	0.1321	Tukey-Kramer	0.1321
YR			2019			2020	0.04167	0.007169	18	5.81	<.0001	Tukey-Kramer	<.0001
SUBSTRATE*YR	builddex		2019	builddex		2020	0.08583	0.01014	18	8.47	<.0001	Tukey-Kramer	<.0001
SUBSTRATE*YR	builddex		2019	rooflite		2019	0.01417	0.01626	18	0.87	0.3951	Tukey-Kramer	0.8195
SUBSTRATE*YR	builddex		2019	rooflite		2020	0.01167	0.01626	18	0.72	0.4823	Tukey-Kramer	0.8888
SUBSTRATE*YR	builddex		2020	rooflite		2019	-0.07167	0.01626	18	-4.41	0.0003	Tukey-Kramer	0.0018
SUBSTRATE*YR	builddex		2020	rooflite		2020	-0.07417	0.01626	18	-4.56	0.0002	Tukey-Kramer	0.0013
SUBSTRATE*YR	rooflite		2019	rooflite		2020	-0.0025	0.01014	18	-0.25	0.808	Tukey-Kramer	0.9945
SUBSTRATE*MIX*YR	builddex	0	2019	builddex	0	2020	0.0825	0.01756	18	4.7	0.0002	Tukey-Kramer	0.0071
SUBSTRATE*MIX*YR	builddex	0	2019	builddex	1	2019	-0.0125	0.02816	18	-0.44	0.6625	Tukey-Kramer	1
SUBSTRATE*MIX*YR	builddex	0	2019	builddex	1	2020	0.085	0.02816	18	3.02	0.0074	Tukey-Kramer	0.1808
SUBSTRATE*MIX*YR	builddex	0	2019	builddex	2	2019	-0.0075	0.02816	18	-0.27	0.793	Tukey-Kramer	1
SUBSTRATE*MIX*YR	builddex	0	2019	builddex	2	2020	0.07	0.02816	18	2.49	0.023	Tukey-Kramer	0.4045
SUBSTRATE*MIX*YR	builddex	0	2019	rooflite	0	2019	0.0075	0.02816	18	0.27	0.793	Tukey-Kramer	1
SUBSTRATE*MIX*YR	builddex	0	2019	rooflite	0	2020	-0.015	0.02816	18	-0.53	0.6008	Tukey-Kramer	1
SUBSTRATE*MIX*YR	builddex	0	2019	rooflite	1	2019	-0.005	0.02816	18	-0.18	0.8611	Tukey-Kramer	1
SUBSTRATE*MIX*YR	builddex	0	2019	rooflite	1	2020	0.01	0.02816	18	0.36	0.7267	Tukey-Kramer	1
SUBSTRATE*MIX*YR	builddex	0	2019	rooflite	2	2019	0.02	0.02816	18	0.71	0.4867	Tukey-Kramer	0.9998
SUBSTRATE*MIX*YR	builddex	0	2019	rooflite	2	2020	0.02	0.02816	18	0.71	0.4867	Tukey-Kramer	0.9998
SUBSTRATE*MIX*YR	builddex	0	2020	builddex	1	2019	-0.095	0.02816	18	-3.37	0.0034	Tukey-Kramer	0.0969
SUBSTRATE*MIX*YR	builddex	0	2020	builddex	1	2020	0.0025	0.02816	18	0.09	0.9302	Tukey-Kramer	1
SUBSTRATE*MIX*YR	builddex	0	2020	builddex	2	2019	-0.09	0.02816	18	-3.2	0.005	Tukey-Kramer	0.1333
SUBSTRATE*MIX*YR	builddex	0	2020	builddex	2	2020	-0.0125	0.02816	18	-0.44	0.6625	Tukey-Kramer	1
SUBSTRATE*MIX*YR	builddex	0	2020	rooflite	0	2019	-0.075	0.02816	18	-2.66	0.0158	Tukey-Kramer	0.316
SUBSTRATE*MIX*YR	builddex	0	2020	rooflite	0	2020	-0.0975	0.02816	18	-3.46	0.0028	Tukey-Kramer	0.0822
SUBSTRATE*MIX*YR	builddex	0	2020	rooflite	1	2019	-0.0875	0.02816	18	-3.11	0.0061	Tukey-Kramer	0.1555
SUBSTRATE*MIX*YR	builddex	0	2020	rooflite	1	2020	-0.0725	0.02816	18	-2.57	0.0191	Tukey-Kramer	0.3586
SUBSTRATE*MIX*YR	builddex	0	2020	rooflite	2	2019	-0.0625	0.02816	18	-2.22	0.0396	Tukey-Kramer	0.557

SUBSTRATE*MIX*YR	builddex	0	2020	rooflite	2	2020	-0.0625	0.02816	18	-2.22	0.0396	Tukey-Kramer	0.557
SUBSTRATE*MIX*YR	builddex	1	2019	builddex	1	2020	0.0975	0.01756	18	5.55	<.0001	Tukey-Kramer	0.0013
SUBSTRATE*MIX*YR	builddex	1	2019	builddex	2	2019	0.005	0.02816	18	0.18	0.8611	Tukey-Kramer	1
SUBSTRATE*MIX*YR	builddex	1	2019	builddex	2	2020	0.0825	0.02816	18	2.93	0.009	Tukey-Kramer	0.2094
SUBSTRATE*MIX*YR	builddex	1	2019	rooflite	0	2019	0.02	0.02816	18	0.71	0.4867	Tukey-Kramer	0.9998
SUBSTRATE*MIX*YR	builddex	1	2019	rooflite	0	2020	-0.0025	0.02816	18	-0.09	0.9302	Tukey-Kramer	1
SUBSTRATE*MIX*YR	builddex	1	2019	rooflite	1	2019	0.0075	0.02816	18	0.27	0.793	Tukey-Kramer	1
SUBSTRATE*MIX*YR	builddex	1	2019	rooflite	1	2020	0.0225	0.02816	18	0.8	0.4348	Tukey-Kramer	0.9994
SUBSTRATE*MIX*YR	builddex	1	2019	rooflite	2	2019	0.0325	0.02816	18	1.15	0.2636	Tukey-Kramer	0.9866
SUBSTRATE*MIX*YR	builddex	1	2019	rooflite	2	2020	0.0325	0.02816	18	1.15	0.2636	Tukey-Kramer	0.9866
SUBSTRATE*MIX*YR	builddex	1	2020	builddex	2	2019	-0.0925	0.02816	18	-3.28	0.0041	Tukey-Kramer	0.1138
SUBSTRATE*MIX*YR	builddex	1	2020	builddex	2	2020	-0.015	0.02816	18	-0.53	0.6008	Tukey-Kramer	1
SUBSTRATE*MIX*YR	builddex	1	2020	rooflite	0	2019	-0.0775	0.02816	18	-2.75	0.0131	Tukey-Kramer	0.2769
SUBSTRATE*MIX*YR	builddex	1	2020	rooflite	0	2020	-0.1	0.02816	18	-3.55	0.0023	Tukey-Kramer	0.0696
SUBSTRATE*MIX*YR	builddex	1	2020	rooflite	1	2019	-0.09	0.02816	18	-3.2	0.005	Tukey-Kramer	0.1333
SUBSTRATE*MIX*YR	builddex	1	2020	rooflite	1	2020	-0.075	0.02816	18	-2.66	0.0158	Tukey-Kramer	0.316
SUBSTRATE*MIX*YR	builddex	1	2020	rooflite	2	2019	-0.065	0.02816	18	-2.31	0.0331	Tukey-Kramer	0.5043
SUBSTRATE*MIX*YR	builddex	1	2020	rooflite	2	2020	-0.065	0.02816	18	-2.31	0.0331	Tukey-Kramer	0.5043
SUBSTRATE*MIX*YR	builddex	2	2019	builddex	2	2020	0.0775	0.01756	18	4.41	0.0003	Tukey-Kramer	0.0127
SUBSTRATE*MIX*YR	builddex	2	2019	rooflite	0	2019	0.015	0.02816	18	0.53	0.6008	Tukey-Kramer	1
SUBSTRATE*MIX*YR	builddex	2	2019	rooflite	0	2020	-0.0075	0.02816	18	-0.27	0.793	Tukey-Kramer	1
SUBSTRATE*MIX*YR	builddex	2	2019	rooflite	1	2019	0.0025	0.02816	18	0.09	0.9302	Tukey-Kramer	1
SUBSTRATE*MIX*YR	builddex	2	2019	rooflite	1	2020	0.0175	0.02816	18	0.62	0.5421	Tukey-Kramer	0.9999
SUBSTRATE*MIX*YR	builddex	2	2019	rooflite	2	2019	0.0275	0.02816	18	0.98	0.3418	Tukey-Kramer	0.9964
SUBSTRATE*MIX*YR	builddex	2	2019	rooflite	2	2020	0.0275	0.02816	18	0.98	0.3418	Tukey-Kramer	0.9964
SUBSTRATE*MIX*YR	builddex	2	2020	rooflite	0	2019	-0.0625	0.02816	18	-2.22	0.0396	Tukey-Kramer	0.557
SUBSTRATE*MIX*YR	builddex	2	2020	rooflite	0	2020	-0.085	0.02816	18	-3.02	0.0074	Tukey-Kramer	0.1808
SUBSTRATE*MIX*YR	builddex	2	2020	rooflite	1	2019	-0.075	0.02816	18	-2.66	0.0158	Tukey-Kramer	0.316
SUBSTRATE*MIX*YR	builddex	2	2020	rooflite	1	2020	-0.06	0.02816	18	-2.13	0.0472	Tukey-Kramer	0.6106
SUBSTRATE*MIX*YR	builddex	2	2020	rooflite	2	2019	-0.05	0.02816	18	-1.78	0.0928	Tukey-Kramer	0.8114
SUBSTRATE*MIX*YR	builddex	2	2020	rooflite	2	2020	-0.05	0.02816	18	-1.78	0.0928	Tukey-Kramer	0.8114
SUBSTRATE*MIX*YR	rooflite	0	2019	rooflite	0	2020	-0.0225	0.01756	18	-1.28	0.2163	Tukey-Kramer	0.9715
SUBSTRATE*MIX*YR	rooflite	0	2019	rooflite	1	2019	-0.0125	0.02816	18	-0.44	0.6625	Tukey-Kramer	1
SUBSTRATE*MIX*YR	rooflite	0	2019	rooflite	1	2020	0.0025	0.02816	18	0.09	0.9302	Tukey-Kramer	1
SUBSTRATE*MIX*YR	rooflite	0	2019	rooflite	2	2019	0.0125	0.02816	18	0.44	0.6625	Tukey-Kramer	1
SUBSTRATE*MIX*YR	rooflite	0	2019	rooflite	2	2020	0.0125	0.02816	18	0.44	0.6625	Tukey-Kramer	1
SUBSTRATE*MIX*YR	rooflite	0	2020	rooflite	1	2019	0.01	0.02816	18	0.36	0.7267	Tukey-Kramer	1
SUBSTRATE*MIX*YR	rooflite	0	2020	rooflite	1	2020	0.025	0.02816	18	0.89	0.3864	Tukey-Kramer	0.9984
SUBSTRATE*MIX*YR	rooflite	0	2020	rooflite	2	2019	0.035	0.02816	18	1.24	0.2299	Tukey-Kramer	0.977
SUBSTRATE*MIX*YR	rooflite	0	2020	rooflite	2	2020	0.035	0.02816	18	1.24	0.2299	Tukey-Kramer	0.977
SUBSTRATE*MIX*YR	rooflite	1	2019	rooflite	1	2020	0.015	0.01756	18	0.85	0.4042	Tukey-Kramer	0.9989
SUBSTRATE*MIX*YR	rooflite	1	2019	rooflite	2	2019	0.025	0.02816	18	0.89	0.3864	Tukey-Kramer	0.9984
SUBSTRATE*MIX*YR	rooflite	1	2019	rooflite	2	2020	0.025	0.02816	18	0.89	0.3864	Tukey-Kramer	0.9984
SUBSTRATE*MIX*YR	rooflite	1	2020	rooflite	2	2019	0.01	0.02816	18	0.36	0.7267	Tukey-Kramer	1
SUBSTRATE*MIX*YR	rooflite	1	2020	rooflite	2	2020	0.01	0.02816	18	0.36	0.7267	Tukey-Kramer	1
SUBSTRATE*MIX*YR	rooflite	2	2019	rooflite	2	2020	1.22E-15	0.01756	18	0	1	Tukey-Kramer	1

**Appendix H - The SAS output for the MB analyses by different bed (both 4-inch and 8-inch-deep bed) and year (year as repeated measure)**

4-inch-deep Bed

Type 3 Tests of Fixed Effects					
Effect	Num DF	Den DF	F Value	Pr > F	
SUBSTRATE	1	3	5.6	0.0988	
MIX	2	6	8.64	0.0171	*
SUBSTRATE*MIX	2	6	0.41	0.6837	
YR	1	18	9.88	0.0056	**
SUBSTRATE*YR	1	18	0.02	0.8902	
MIX*YR	2	18	0.41	0.672	
SUBSTRATE*MIX*YR	2	18	0.77	0.4773	

Least Squares Means								
Effect	SUBSTRATE	MIX	YR	Estimate	Standard Error	DF	t Value	Pr >  t
SUBSTRATE	buildex			34.1097	2.958	3	11.53	0.0014
SUBSTRATE	rooflite			44.0107	2.958	3	14.88	0.0007
MIX		0		32.0385	3.4297	6	9.34	<.0001
MIX		1		34.9018	3.4297	6	10.18	<.0001
MIX		2		50.2403	3.4297	6	14.65	<.0001
SUBSTRATE*MIX	buildex		0	26.7673	4.8503	6	5.52	0.0015
SUBSTRATE*MIX	buildex		1	32.2127	4.8503	6	6.64	0.0006
SUBSTRATE*MIX	buildex		2	43.349	4.8503	6	8.94	0.0001
SUBSTRATE*MIX	rooflite		0	37.3097	4.8503	6	7.69	0.0003
SUBSTRATE*MIX	rooflite		1	37.5909	4.8503	6	7.75	0.0002
SUBSTRATE*MIX	rooflite		2	57.1315	4.8503	6	11.78	<.0001
SUBSTRATE	buildex			34.1097	2.958	3	11.53	0.0014
SUBSTRATE	rooflite			44.0107	2.958	3	14.88	0.0007
YR			2019	45.1	2.8406	18	15.88	<.0001
YR			2020	33.0203	2.8406	18	11.62	<.0001
SUBSTRATE*YR	buildex		2019	39.8804	4.0171	18	9.93	<.0001
SUBSTRATE*YR	buildex		2020	28.3389	4.0171	18	7.05	<.0001
SUBSTRATE*YR	rooflite		2019	50.3197	4.0171	18	12.53	<.0001
SUBSTRATE*YR	rooflite		2020	37.7018	4.0171	18	9.39	<.0001
SUBSTRATE*MIX*YR	buildex	0	2019	33.4462	6.7593	18	4.95	0.0001
SUBSTRATE*MIX*YR	buildex	0	2020	20.0883	6.7593	18	2.97	0.0082
SUBSTRATE*MIX*YR	buildex	1	2019	42.5118	6.7593	18	6.29	<.0001
SUBSTRATE*MIX*YR	buildex	1	2020	21.9137	6.7593	18	3.24	0.0045
SUBSTRATE*MIX*YR	buildex	2	2019	43.6832	6.7593	18	6.46	<.0001
SUBSTRATE*MIX*YR	buildex	2	2020	43.0148	6.7593	18	6.36	<.0001
SUBSTRATE*MIX*YR	rooflite	0	2019	43.3757	6.7593	18	6.42	<.0001
SUBSTRATE*MIX*YR	rooflite	0	2020	31.2436	6.7593	18	4.62	0.0002
SUBSTRATE*MIX*YR	rooflite	1	2019	43.2443	6.7593	18	6.4	<.0001
SUBSTRATE*MIX*YR	rooflite	1	2020	31.9376	6.7593	18	4.72	0.0002
SUBSTRATE*MIX*YR	rooflite	2	2019	64.339	6.7593	18	9.52	<.0001
SUBSTRATE*MIX*YR	rooflite	2	2020	49.9241	6.7593	18	7.39	<.0001

Differences of Least Squares Means															
Effect	SUBSTRAT	MIX	YR	_SUBSTRAT	_MIX	_YR	Estimate	Standard Error	DF	t Value	Pr >  t	Adjustment	Adj P		
SUBSTRATE	buil	dex		roof	lite		-9.901	4.1832	3	-2.37	0.0988	Tukey	0.0988		
MIX		0				1	-2.8634	4.7078	6	-0.61	0.5653	Tukey-Kramer	0.8211		
MIX		0				2	-18.2018	4.7078	6	-3.87	0.0083	Tukey-Kramer	0.0194		
MIX		1				2	-15.3384	4.7078	6	-3.26	0.0173	Tukey-Kramer	0.0397		
SUBSTRATE*MIX	buil	dex	0	buil	dex	1	-5.4455	6.6578	6	-0.82	0.4447	Tukey-Kramer	0.9535		
SUBSTRATE*MIX	buil	dex	0	buil	dex	2	-16.5817	6.6578	6	-2.49	0.0471	Tukey-Kramer	0.2587		
SUBSTRATE*MIX	buil	dex	0	roof	lite	0	-10.5424	6.8593	6	-1.54	0.1752	Tukey-Kramer	0.6584		
SUBSTRATE*MIX	buil	dex	0	roof	lite	1	-10.8237	6.8593	6	-1.58	0.1657	Tukey-Kramer	0.6373		
SUBSTRATE*MIX	buil	dex	0	roof	lite	2	-30.3642	6.8593	6	-4.43	0.0044	Tukey-Kramer	0.0315		
SUBSTRATE*MIX	buil	dex	1	buil	dex	2	-11.1363	6.6578	6	-1.67	0.1454	Tukey-Kramer	0.5891		
SUBSTRATE*MIX	buil	dex	1	roof	lite	0	-5.0969	6.8593	6	-0.74	0.4855	Tukey-Kramer	0.9682		
SUBSTRATE*MIX	buil	dex	1	roof	lite	1	-5.3782	6.8593	6	-0.78	0.4628	Tukey-Kramer	0.9606		
SUBSTRATE*MIX	buil	dex	1	roof	lite	2	-24.9188	6.8593	6	-3.63	0.0109	Tukey-Kramer	0.0726		
SUBSTRATE*MIX	buil	dex	2	roof	lite	0	6.0393	6.8593	6	0.88	0.4125	Tukey-Kramer	0.9384		
SUBSTRATE*MIX	buil	dex	2	roof	lite	1	5.7581	6.8593	6	0.84	0.4334	Tukey-Kramer	0.9486		
SUBSTRATE*MIX	buil	dex	2	roof	lite	2	-13.7825	6.8593	6	-2.01	0.0912	Tukey-Kramer	0.4303		
SUBSTRATE*MIX	roof	lite	0	roof	lite	1	-0.2813	6.6578	6	-0.04	0.9677	Tukey-Kramer	1		
SUBSTRATE*MIX	roof	lite	0	roof	lite	2	-19.8219	6.6578	6	-2.98	0.0247	Tukey-Kramer	0.1503		
SUBSTRATE*MIX	roof	lite	1	roof	lite	2	-19.5406	6.6578	6	-2.93	0.0261	Tukey-Kramer	0.1576		
SUBSTRATE	buil	dex		roof	lite		-9.901	4.1832	3	-2.37	0.0988	Tukey	0.0988		
YR			2019			2020	12.0797	3.8439	18	3.14	0.0056	Tukey-Kramer	0.0056		
SUBSTRATE*YR	buil	dex	2019	buil	dex	2020	11.5415	5.4361	18	2.12	0.0479	Tukey-Kramer	0.1835		
SUBSTRATE*YR	buil	dex	2019	roof	lite	2019	-10.4392	5.6811	18	-1.84	0.0827	Tukey-Kramer	0.2889		
SUBSTRATE*YR	buil	dex	2019	roof	lite	2020	2.1787	5.6811	18	0.38	0.7058	Tukey-Kramer	0.9802		
SUBSTRATE*YR	buil	dex	2020	roof	lite	2019	-21.9807	5.6811	18	-3.87	0.0011	Tukey-Kramer	0.0056		
SUBSTRATE*YR	buil	dex	2020	roof	lite	2020	-9.3628	5.6811	18	-1.65	0.1167	Tukey-Kramer	0.3784		
SUBSTRATE*YR	roof	lite	2019	roof	lite	2020	12.6179	5.4361	18	2.32	0.0322	Tukey-Kramer	0.1302		
SUBSTRATE*MIX*YR	buil	dex	0	2019	buil	dex	0	2020	13.3579	9.4156	18	1.42	0.1731	Tukey-Kramer	0.9445
SUBSTRATE*MIX*YR	buil	dex	0	2019	buil	dex	1	2019	-9.0656	9.4156	18	-0.96	0.3484	Tukey-Kramer	0.9968
SUBSTRATE*MIX*YR	buil	dex	0	2019	buil	dex	1	2020	11.5326	9.4156	18	1.22	0.2364	Tukey-Kramer	0.9792
SUBSTRATE*MIX*YR	buil	dex	0	2019	buil	dex	2	2019	-10.237	9.4156	18	-1.09	0.2913	Tukey-Kramer	0.9915
SUBSTRATE*MIX*YR	buil	dex	0	2019	buil	dex	2	2020	-9.5685	9.4156	18	-1.02	0.323	Tukey-Kramer	0.995
SUBSTRATE*MIX*YR	buil	dex	0	2019	roof	lite	0	2019	-9.9295	9.5591	18	-1.04	0.3127	Tukey-Kramer	0.9941
SUBSTRATE*MIX*YR	buil	dex	0	2019	roof	lite	0	2020	2.2026	9.5591	18	0.23	0.8204	Tukey-Kramer	1
SUBSTRATE*MIX*YR	buil	dex	0	2019	roof	lite	1	2019	-9.7981	9.5591	18	-1.02	0.3189	Tukey-Kramer	0.9947
SUBSTRATE*MIX*YR	buil	dex	0	2019	roof	lite	1	2020	1.5087	9.5591	18	0.16	0.8764	Tukey-Kramer	1
SUBSTRATE*MIX*YR	buil	dex	0	2019	roof	lite	2	2019	-30.8927	9.5591	18	-3.23	0.0046	Tukey-Kramer	0.125
SUBSTRATE*MIX*YR	buil	dex	0	2019	roof	lite	2	2020	-16.4778	9.5591	18	-1.72	0.1019	Tukey-Kramer	0.8361
SUBSTRATE*MIX*YR	buil	dex	0	2020	buil	dex	1	2019	-22.4235	9.4156	18	-2.38	0.0285	Tukey-Kramer	0.4618
SUBSTRATE*MIX*YR	buil	dex	0	2020	buil	dex	1	2020	-1.8254	9.4156	18	-0.19	0.8485	Tukey-Kramer	1
SUBSTRATE*MIX*YR	buil	dex	0	2020	buil	dex	2	2019	-23.5949	9.4156	18	-2.51	0.022	Tukey-Kramer	0.3936
SUBSTRATE*MIX*YR	buil	dex	0	2020	buil	dex	2	2020	-22.9265	9.4156	18	-2.43	0.0255	Tukey-Kramer	0.4319
SUBSTRATE*MIX*YR	buil	dex	0	2020	roof	lite	0	2019	-23.2874	9.5591	18	-2.44	0.0255	Tukey-Kramer	0.4312
SUBSTRATE*MIX*YR	buil	dex	0	2020	roof	lite	0	2020	-11.1553	9.5591	18	-1.17	0.2584	Tukey-Kramer	0.9854
SUBSTRATE*MIX*YR	buil	dex	0	2020	roof	lite	1	2019	-23.156	9.5591	18	-2.42	0.0262	Tukey-Kramer	0.4388
SUBSTRATE*MIX*YR	buil	dex	0	2020	roof	lite	1	2020	-11.8492	9.5591	18	-1.24	0.2311	Tukey-Kramer	0.9774
SUBSTRATE*MIX*YR	buil	dex	0	2020	roof	lite	2	2019	-44.2507	9.5591	18	-4.63	0.0002	Tukey-Kramer	0.0082
SUBSTRATE*MIX*YR	buil	dex	0	2020	roof	lite	2	2020	-29.8358	9.5591	18	-3.12	0.0059	Tukey-Kramer	0.1517
SUBSTRATE*MIX*YR	buil	dex	1	2019	buil	dex	1	2020	20.5981	9.4156	18	2.19	0.0421	Tukey-Kramer	0.576
SUBSTRATE*MIX*YR	buil	dex	1	2019	buil	dex	2	2019	-1.1714	9.4156	18	-0.12	0.9024	Tukey-Kramer	1
SUBSTRATE*MIX*YR	buil	dex	1	2019	buil	dex	2	2020	-0.503	9.4156	18	-0.05	0.958	Tukey-Kramer	1
SUBSTRATE*MIX*YR	buil	dex	1	2019	roof	lite	0	2019	-0.8639	9.5591	18	-0.09	0.929	Tukey-Kramer	1
SUBSTRATE*MIX*YR	buil	dex	1	2019	roof	lite	0	2020	11.2682	9.5591	18	1.18	0.2538	Tukey-Kramer	0.9843
SUBSTRATE*MIX*YR	buil	dex	1	2019	roof	lite	1	2019	-0.7325	9.5591	18	-0.08	0.9398	Tukey-Kramer	1
SUBSTRATE*MIX*YR	buil	dex	1	2019	roof	lite	1	2020	10.5743	9.5591	18	1.11	0.2832	Tukey-Kramer	0.9903
SUBSTRATE*MIX*YR	buil	dex	1	2019	roof	lite	2	2019	-21.8272	9.5591	18	-2.28	0.0348	Tukey-Kramer	0.5188
SUBSTRATE*MIX*YR	buil	dex	1	2019	roof	lite	2	2020	-7.4123	9.5591	18	-0.78	0.4482	Tukey-Kramer	0.9995
SUBSTRATE*MIX*YR	buil	dex	1	2020	buil	dex	2	2019	-21.7696	9.4156	18	-2.31	0.0328	Tukey-Kramer	0.5019
SUBSTRATE*MIX*YR	buil	dex	1	2020	buil	dex	2	2020	-21.1011	9.4156	18	-2.24	0.0379	Tukey-Kramer	0.5439
SUBSTRATE*MIX*YR	buil	dex	1	2020	roof	lite	0	2019	-21.462	9.5591	18	-2.25	0.0376	Tukey-Kramer	0.5415
SUBSTRATE*MIX*YR	buil	dex	1	2020	roof	lite	0	2020	-9.33	9.5591	18	-0.98	0.342	Tukey-Kramer	0.9964
SUBSTRATE*MIX*YR	buil	dex	1	2020	roof	lite	1	2019	-21.3307	9.5591	18	-2.23	0.0386	Tukey-Kramer	0.5497
SUBSTRATE*MIX*YR	buil	dex	1	2020	roof	lite	1	2020	-10.0239	9.5591	18	-1.05	0.3082	Tukey-Kramer	0.9936
SUBSTRATE*MIX*YR	buil	dex	1	2020	roof	lite	2	2019	-42.4253	9.5591	18	-4.44	0.0003	Tukey-Kramer	0.0121
SUBSTRATE*MIX*YR	buil	dex	1	2020	roof	lite	2	2020	-28.0104	9.5591	18	-2.93	0.0089	Tukey-Kramer	0.2091
SUBSTRATE*MIX*YR	buil	dex	2	2019	buil	dex	2	2020	0.6685	9.4156	18	0.07	0.9442	Tukey-Kramer	1
SUBSTRATE*MIX*YR	buil	dex	2	2019	roof	lite	0	2019	0.3075	9.5591	18	0.03	0.9747	Tukey-Kramer	1

SUBSTRATE*MIX*YR	builddex	2	2019	rooflite	0	2019	0.3075	9.5591	18	0.03	0.9747	Tukey-Kramer	1
SUBSTRATE*MIX*YR	builddex	2	2019	rooflite	0	2020	12.4396	9.5591	18	1.3	0.2096	Tukey-Kramer	0.9684
SUBSTRATE*MIX*YR	builddex	2	2019	rooflite	1	2019	0.4389	9.5591	18	0.05	0.9639	Tukey-Kramer	1
SUBSTRATE*MIX*YR	builddex	2	2019	rooflite	1	2020	11.7457	9.5591	18	1.23	0.235	Tukey-Kramer	0.9788
SUBSTRATE*MIX*YR	builddex	2	2019	rooflite	2	2019	-20.6558	9.5591	18	-2.16	0.0444	Tukey-Kramer	0.5922
SUBSTRATE*MIX*YR	builddex	2	2019	rooflite	2	2020	-6.2409	9.5591	18	-0.65	0.5221	Tukey-Kramer	0.9999
SUBSTRATE*MIX*YR	builddex	2	2020	rooflite	0	2019	-0.3609	9.5591	18	-0.04	0.9703	Tukey-Kramer	1
SUBSTRATE*MIX*YR	builddex	2	2020	rooflite	0	2020	11.7711	9.5591	18	1.23	0.234	Tukey-Kramer	0.9784
SUBSTRATE*MIX*YR	builddex	2	2020	rooflite	1	2019	-0.2296	9.5591	18	-0.02	0.9811	Tukey-Kramer	1
SUBSTRATE*MIX*YR	builddex	2	2020	rooflite	1	2020	11.0772	9.5591	18	1.16	0.2617	Tukey-Kramer	0.9861
SUBSTRATE*MIX*YR	builddex	2	2020	rooflite	2	2019	-21.3242	9.5591	18	-2.23	0.0387	Tukey-Kramer	0.5501
SUBSTRATE*MIX*YR	builddex	2	2020	rooflite	2	2020	-6.9093	9.5591	18	-0.72	0.4791	Tukey-Kramer	0.9998
SUBSTRATE*MIX*YR	rooflite	0	2019	rooflite	0	2020	12.1321	9.4156	18	1.29	0.2139	Tukey-Kramer	0.9704
SUBSTRATE*MIX*YR	rooflite	0	2019	rooflite	1	2019	0.1314	9.4156	18	0.01	0.989	Tukey-Kramer	1
SUBSTRATE*MIX*YR	rooflite	0	2019	rooflite	1	2020	11.4381	9.4156	18	1.21	0.2401	Tukey-Kramer	0.9804
SUBSTRATE*MIX*YR	rooflite	0	2019	rooflite	2	2019	-20.9633	9.4156	18	-2.23	0.039	Tukey-Kramer	0.5527
SUBSTRATE*MIX*YR	rooflite	0	2019	rooflite	2	2020	-6.5484	9.4156	18	-0.7	0.4956	Tukey-Kramer	0.9998
SUBSTRATE*MIX*YR	rooflite	0	2020	rooflite	1	2019	-12.0007	9.4156	18	-1.27	0.2187	Tukey-Kramer	0.9725
SUBSTRATE*MIX*YR	rooflite	0	2020	rooflite	1	2020	-0.6939	9.4156	18	-0.07	0.9421	Tukey-Kramer	1
SUBSTRATE*MIX*YR	rooflite	0	2020	rooflite	2	2019	-33.0953	9.4156	18	-3.51	0.0025	Tukey-Kramer	0.0745
SUBSTRATE*MIX*YR	rooflite	0	2020	rooflite	2	2020	-18.6805	9.4156	18	-1.98	0.0627	Tukey-Kramer	0.6979
SUBSTRATE*MIX*YR	rooflite	1	2019	rooflite	1	2020	11.3068	9.4156	18	1.2	0.2454	Tukey-Kramer	0.982
SUBSTRATE*MIX*YR	rooflite	1	2019	rooflite	2	2019	-21.0946	9.4156	18	-2.24	0.0379	Tukey-Kramer	0.5443
SUBSTRATE*MIX*YR	rooflite	1	2019	rooflite	2	2020	-6.6798	9.4156	18	-0.71	0.4871	Tukey-Kramer	0.9998
SUBSTRATE*MIX*YR	rooflite	1	2020	rooflite	2	2019	-32.4014	9.4156	18	-3.44	0.0029	Tukey-Kramer	0.0854
SUBSTRATE*MIX*YR	rooflite	1	2020	rooflite	2	2020	-17.9865	9.4156	18	-1.91	0.0722	Tukey-Kramer	0.74
SUBSTRATE*MIX*YR	rooflite	2	2019	rooflite	2	2020	14.4149	9.4156	18	1.53	0.1432	Tukey-Kramer	0.9125

## 8-inch-deep Bed

Type 3 Tests of Fixed Effects					
Effect	Num DF	Den DF	F Value	Pr > F	
<b>SUBSTRATE</b>	1	3	2.96	0.1837	
<b>MIX</b>	2	6	0.62	0.5668	
<b>SUBSTRATE*MIX</b>	2	6	0.85	0.4728	
<b>YR</b>	1	18	4.35	0.0516	*
<b>SUBSTRATE*YR</b>	1	18	11.73	0.003	**
<b>MIX*YR</b>	2	18	9.37	0.0016	**
<b>SUBSTRATE*MIX*YR</b>	2	18	1.69	0.2129	

Least Squares Means								
Effect	SUBSTRATE	MIX	YR	Estimate	Standard Error	DF	t Value	Pr >  t
SUBSTRATE	builddex			26.6007	3.0962	3	8.59	0.0033
SUBSTRATE	rooflite			34.1377	3.0962	3	11.03	0.0016
MIX		0		26.9703	3.7921	6	7.11	0.0004
MIX		1		32.6366	3.7921	6	8.61	0.0001
MIX		2		31.5007	3.7921	6	8.31	0.0002
SUBSTRATE*MIX	builddex	0		22.5843	5.3628	6	4.21	0.0056
SUBSTRATE*MIX	builddex	1		32.6335	5.3628	6	6.09	0.0009
SUBSTRATE*MIX	builddex	2		24.5843	5.3628	6	4.58	0.0038
SUBSTRATE*MIX	rooflite	0		31.3562	5.3628	6	5.85	0.0011
SUBSTRATE*MIX	rooflite	1		32.6397	5.3628	6	6.09	0.0009
SUBSTRATE*MIX	rooflite	2		38.4171	5.3628	6	7.16	0.0004
SUBSTRATE	builddex			26.6007	3.0962	3	8.59	0.0033
SUBSTRATE	rooflite			34.1377	3.0962	3	11.03	0.0016
YR			2019	33.0443	2.5378	18	13.02	<.0001
YR			2020	27.694	2.5378	18	10.91	<.0001
SUBSTRATE*YR	Builddex		2019	33.6708	3.589	18	9.38	<.0001
SUBSTRATE*YR	builddex		2020	19.5305	3.589	18	5.44	<.0001
SUBSTRATE*YR	Rooflite		2019	32.4179	3.589	18	9.03	<.0001
SUBSTRATE*YR	rooflite		2020	35.8574	3.589	18	9.99	<.0001
MIX*YR		Plant Mix A	2019	30.2173	4.3956	18	6.87	<.0001
MIX*YR		Plant Mix A	2020	23.7232	4.3956	18	5.4	<.0001
MIX*YR		Plant Mix B	2019	41.8105	4.3956	18	9.51	<.0001
MIX*YR		Plant Mix B	2020	23.4626	4.3956	18	5.34	<.0001
MIX*YR		Plant Mix C	2019	27.1052	4.3956	18	6.17	<.0001
MIX*YR		Plant Mix C	2020	35.8962	4.3956	18	8.17	<.0001
SUBSTRATE*MIX*YR	builddex	0	2019	28.3094	6.2163	18	4.55	0.0002
SUBSTRATE*MIX*YR	builddex	0	2020	16.8592	6.2163	18	2.71	0.0143
SUBSTRATE*MIX*YR	builddex	1	2019	49.5241	6.2163	18	7.97	<.0001
SUBSTRATE*MIX*YR	builddex	1	2020	15.7429	6.2163	18	2.53	0.0208
SUBSTRATE*MIX*YR	builddex	2	2019	23.179	6.2163	18	3.73	0.0015
SUBSTRATE*MIX*YR	builddex	2	2020	25.9896	6.2163	18	4.18	0.0006
SUBSTRATE*MIX*YR	rooflite	0	2019	32.1252	6.2163	18	5.17	<.0001
SUBSTRATE*MIX*YR	rooflite	0	2020	30.5872	6.2163	18	4.92	0.0001
SUBSTRATE*MIX*YR	rooflite	1	2019	34.097	6.2163	18	5.49	<.0001
SUBSTRATE*MIX*YR	rooflite	1	2020	31.1824	6.2163	18	5.02	<.0001
SUBSTRATE*MIX*YR	rooflite	2	2019	31.0314	6.2163	18	4.99	<.0001
SUBSTRATE*MIX*YR	rooflite	2	2020	45.8028	6.2163	18	7.37	<.0001

Differences of Least Squares Means													
Effect	SUBSTRATE MIX	YR	_SUBSTRAT	_MIX	_YR	Estimate	Standard Error	DF	t Value	Pr >  t	Adjustmen	Adj P	
SUBSTRATE	builddex		rooflite			-7.537	4.3787	3	-1.72	0.1837	Tukey	0.1837	
MIX		0			1	-5.6663	5.3628	6	-1.06	0.3314	Tukey	0.572	
MIX		0			2	-4.5304	5.3628	6	-0.84	0.4306	Tukey	0.6914	
MIX		1			2	1.1359	5.3628	6	0.21	0.8393	Tukey	0.9757	
SUBSTRATE*MIX	builddex	0	builddex		1	-10.0492	7.5841	6	-1.33	0.2334	Tukey	0.7652	
SUBSTRATE*MIX	builddex	0	builddex		2	-2	7.5841	6	-0.26	0.8008	Tukey	0.9997	
SUBSTRATE*MIX	builddex	0	rooflite		0	-8.7719	7.5841	6	-1.16	0.2914	Tukey	0.8423	
SUBSTRATE*MIX	builddex	0	rooflite		1	-10.0554	7.5841	6	-1.33	0.2331	Tukey	0.7648	
SUBSTRATE*MIX	builddex	0	rooflite		2	-15.8328	7.5841	6	-2.09	0.0819	Tukey	0.3976	
SUBSTRATE*MIX	builddex	1	builddex		2	8.0492	7.5841	6	1.06	0.3294	Tukey	0.8805	
SUBSTRATE*MIX	builddex	1	rooflite		0	1.2773	7.5841	6	0.17	0.8718	Tukey	1	
SUBSTRATE*MIX	builddex	1	rooflite		1	-0.00619	7.5841	6	0	0.9994	Tukey	1	
SUBSTRATE*MIX	builddex	1	rooflite		2	-5.7836	7.5841	6	-0.76	0.4746	Tukey	0.9647	
SUBSTRATE*MIX	builddex	2	rooflite		0	-6.772	7.5841	6	-0.89	0.4063	Tukey	0.9351	
SUBSTRATE*MIX	builddex	2	rooflite		1	-8.0554	7.5841	6	-1.06	0.329	Tukey	0.8802	
SUBSTRATE*MIX	builddex	2	rooflite		2	-13.8328	7.5841	6	-1.82	0.118	Tukey	0.5146	
SUBSTRATE*MIX	rooflite	0	rooflite		1	-1.2834	7.5841	6	-0.17	0.8712	Tukey	1	
SUBSTRATE*MIX	rooflite	0	rooflite		2	-7.0608	7.5841	6	-0.93	0.3878	Tukey	0.9243	
SUBSTRATE*MIX	rooflite	1	rooflite		2	-5.7774	7.5841	6	-0.76	0.4751	Tukey	0.9649	
SUBSTRATE	builddex		rooflite			-7.537	4.3787	3	-1.72	0.1837	Tukey	0.1837	
YR		2019			2020	5.3503	2.5667	18	2.08	0.0516	Tukey-Kran	0.0516	
SUBSTRATE*YR	builddex	2019	builddex		2020	14.1403	3.6299	18	3.9	0.0011	Tukey-Kran	0.0053	
SUBSTRATE*YR	builddex	2019	rooflite		2019	1.253	5.0755	18	0.25	0.8078	Tukey-Kran	0.9945	
SUBSTRATE*YR	builddex	2019	rooflite		2020	-2.1866	5.0755	18	-0.43	0.6717	Tukey-Kran	0.9724	
SUBSTRATE*YR	builddex	2020	rooflite		2019	-12.8873	5.0755	18	-2.54	0.0206	Tukey-Kran	0.0872	
SUBSTRATE*YR	builddex	2020	rooflite		2020	-16.3269	5.0755	18	-3.22	0.0048	Tukey-Kran	0.0226	
SUBSTRATE*YR	rooflite	2019	rooflite		2020	-3.4396	3.6299	18	-0.95	0.3559	Tukey-Kran	0.78	
MIX*YR		0	2019		0	2020	6.4941	4.4457	18	1.46	0.1613	Tukey-Kran	0.6917
MIX*YR		0	2019		1	2019	-11.5932	6.2163	18	-1.86	0.0786	Tukey-Kran	0.4527
MIX*YR		0	2019		1	2020	6.7547	6.2163	18	1.09	0.2915	Tukey-Kran	0.8804
MIX*YR		0	2019		2	2019	3.1122	6.2163	18	0.5	0.6227	Tukey-Kran	0.9955
MIX*YR		0	2019		2	2020	-5.6788	6.2163	18	-0.91	0.373	Tukey-Kran	0.9379
MIX*YR		0	2020		1	2019	-18.0873	6.2163	18	-2.91	0.0093	Tukey-Kran	0.084
MIX*YR		0	2020		1	2020	0.2606	6.2163	18	0.04	0.967	Tukey-Kran	1
MIX*YR		0	2020		2	2019	-3.382	6.2163	18	-0.54	0.5931	Tukey-Kran	0.9934
MIX*YR		0	2020		2	2020	-12.173	6.2163	18	-1.96	0.0659	Tukey-Kran	0.4017
MIX*YR		1	2019		1	2020	18.3479	4.4457	18	4.13	0.0006	Tukey-Kran	0.0071
MIX*YR		1	2019		2	2019	14.7053	6.2163	18	2.37	0.0294	Tukey-Kran	0.2198
MIX*YR		1	2019		2	2020	5.9144	6.2163	18	0.95	0.354	Tukey-Kran	0.9272
MIX*YR		1	2020		2	2019	-3.6425	6.2163	18	-0.59	0.5652	Tukey-Kran	0.9907
MIX*YR		1	2020		2	2020	-12.4335	6.2163	18	-2	0.0608	Tukey-Kran	0.3797
MIX*YR		2	2019		2	2020	-8.791	4.4457	18	-1.98	0.0635	Tukey-Kran	0.3916
SUBSTRATE*MIX*YR	builddex	0	2019	builddex	1	2019	-21.2146	8.7911	18	-2.41	0.0267	Tukey-Kran	0.4439
SUBSTRATE*MIX*YR	builddex	0	2019	builddex	1	2020	12.5666	8.7911	18	1.43	0.17	Tukey-Kran	0.9418
SUBSTRATE*MIX*YR	builddex	0	2019	builddex	2	2019	5.1305	8.7911	18	0.58	0.5667	Tukey-Kran	1
SUBSTRATE*MIX*YR	builddex	0	2019	builddex	2	2020	2.3199	8.7911	18	0.26	0.7949	Tukey-Kran	1
SUBSTRATE*MIX*YR	builddex	0	2019	rooflite	0	2019	-3.8158	8.7911	18	-0.43	0.6694	Tukey-Kran	1
SUBSTRATE*MIX*YR	builddex	0	2019	rooflite	0	2020	-2.2778	8.7911	18	-0.26	0.7985	Tukey-Kran	1
SUBSTRATE*MIX*YR	builddex	0	2019	rooflite	1	2019	-5.7875	8.7911	18	-0.66	0.5187	Tukey-Kran	0.9999
SUBSTRATE*MIX*YR	builddex	0	2019	rooflite	1	2020	-2.8729	8.7911	18	-0.33	0.7476	Tukey-Kran	1
SUBSTRATE*MIX*YR	builddex	0	2019	rooflite	2	2019	-2.7219	8.7911	18	-0.31	0.7604	Tukey-Kran	1
SUBSTRATE*MIX*YR	builddex	0	2019	rooflite	2	2020	-17.4933	8.7911	18	-1.99	0.062	Tukey-Kran	0.6945
SUBSTRATE*MIX*YR	builddex	0	2020	builddex	1	2019	-32.6649	8.7911	18	-3.72	0.0016	Tukey-Kran	0.0508
SUBSTRATE*MIX*YR	builddex	0	2020	builddex	1	2020	1.1163	8.7911	18	0.13	0.9004	Tukey-Kran	1
SUBSTRATE*MIX*YR	builddex	0	2020	builddex	2	2019	-6.3198	8.7911	18	-0.72	0.4814	Tukey-Kran	0.9998
SUBSTRATE*MIX*YR	builddex	0	2020	builddex	2	2020	-9.1304	8.7911	18	-1.04	0.3127	Tukey-Kran	0.9941
SUBSTRATE*MIX*YR	builddex	0	2020	rooflite	0	2019	-15.2661	8.7911	18	-1.74	0.0996	Tukey-Kran	0.8301
SUBSTRATE*MIX*YR	builddex	0	2020	rooflite	0	2020	-13.7281	8.7911	18	-1.56	0.1358	Tukey-Kran	0.9022
SUBSTRATE*MIX*YR	builddex	0	2020	rooflite	1	2019	-17.2378	8.7911	18	-1.96	0.0656	Tukey-Kran	0.7113
SUBSTRATE*MIX*YR	builddex	0	2020	rooflite	1	2020	-14.3232	8.7911	18	-1.63	0.1206	Tukey-Kran	0.8769
SUBSTRATE*MIX*YR	builddex	0	2020	rooflite	2	2019	-14.1722	8.7911	18	-1.61	0.1243	Tukey-Kran	0.8836
SUBSTRATE*MIX*YR	builddex	0	2020	rooflite	2	2020	-28.9436	8.7911	18	-3.29	0.004	Tukey-Kran	0.1122
SUBSTRATE*MIX*YR	builddex	1	2019	builddex	1	2020	33.7812	6.2872	18	5.37	<.0001	Tukey-Kran	0.0018
SUBSTRATE*MIX*YR	builddex	1	2019	builddex	2	2019	26.3451	8.7911	18	3	0.0077	Tukey-Kran	0.1874
SUBSTRATE*MIX*YR	builddex	1	2019	builddex	2	2020	23.5345	8.7911	18	2.68	0.0154	Tukey-Kran	0.3096
SUBSTRATE*MIX*YR	builddex	1	2019	rooflite	0	2019	17.3988	8.7911	18	1.98	0.0633	Tukey-Kran	0.7007

SUBSTRATE*MIX*YR	builindex	1	2019	rooflite	0	2019	17.3988	8.7911	18	1.98	0.0633	Tukey-Kran	0.7007
SUBSTRATE*MIX*YR	builindex	1	2019	rooflite	0	2020	18.9368	8.7911	18	2.15	0.045	Tukey-Kran	0.5963
SUBSTRATE*MIX*YR	builindex	1	2019	rooflite	1	2019	15.4271	8.7911	18	1.75	0.0963	Tukey-Kran	0.8214
SUBSTRATE*MIX*YR	builindex	1	2019	rooflite	1	2020	18.3417	8.7911	18	2.09	0.0514	Tukey-Kran	0.6371
SUBSTRATE*MIX*YR	builindex	1	2019	rooflite	2	2019	18.4927	8.7911	18	2.1	0.0497	Tukey-Kran	0.6268
SUBSTRATE*MIX*YR	builindex	1	2019	rooflite	2	2020	3.7213	8.7911	18	0.42	0.6771	Tukey-Kran	1
SUBSTRATE*MIX*YR	builindex	1	2020	builindex	2	2019	-7.4361	8.7911	18	-0.85	0.4087	Tukey-Kran	0.999
SUBSTRATE*MIX*YR	builindex	1	2020	builindex	2	2020	-10.2467	8.7911	18	-1.17	0.259	Tukey-Kran	0.9855
SUBSTRATE*MIX*YR	builindex	1	2020	rooflite	0	2019	-16.3823	8.7911	18	-1.86	0.0788	Tukey-Kran	0.7658
SUBSTRATE*MIX*YR	builindex	1	2020	rooflite	0	2020	-14.8443	8.7911	18	-1.69	0.1086	Tukey-Kran	0.852
SUBSTRATE*MIX*YR	builindex	1	2020	rooflite	1	2019	-18.3541	8.7911	18	-2.09	0.0513	Tukey-Kran	0.6363
SUBSTRATE*MIX*YR	builindex	1	2020	rooflite	1	2020	-15.4395	8.7911	18	-1.76	0.096	Tukey-Kran	0.8207
SUBSTRATE*MIX*YR	builindex	1	2020	rooflite	2	2019	-15.2885	8.7911	18	-1.74	0.0991	Tukey-Kran	0.8289
SUBSTRATE*MIX*YR	builindex	1	2020	rooflite	2	2020	-30.0599	8.7911	18	-3.42	0.0031	Tukey-Kran	0.089
SUBSTRATE*MIX*YR	builindex	2	2019	builindex	2	2020	-2.8106	6.2872	18	-0.45	0.6602	Tukey-Kran	1
SUBSTRATE*MIX*YR	builindex	2	2019	rooflite	0	2019	-8.9463	8.7911	18	-1.02	0.3223	Tukey-Kran	0.995
SUBSTRATE*MIX*YR	builindex	2	2019	rooflite	0	2020	-7.4083	8.7911	18	-0.84	0.4105	Tukey-Kran	0.999
SUBSTRATE*MIX*YR	builindex	2	2019	rooflite	1	2019	-10.918	8.7911	18	-1.24	0.2302	Tukey-Kran	0.9771
SUBSTRATE*MIX*YR	builindex	2	2019	rooflite	1	2020	-8.0034	8.7911	18	-0.91	0.3746	Tukey-Kran	0.998
SUBSTRATE*MIX*YR	builindex	2	2019	rooflite	2	2019	-7.8524	8.7911	18	-0.89	0.3835	Tukey-Kran	0.9983
SUBSTRATE*MIX*YR	builindex	2	2019	rooflite	2	2020	-22.6238	8.7911	18	-2.57	0.0191	Tukey-Kran	0.359
SUBSTRATE*MIX*YR	builindex	2	2020	rooflite	0	2019	-6.1357	8.7911	18	-0.7	0.4941	Tukey-Kran	0.9998
SUBSTRATE*MIX*YR	builindex	2	2020	rooflite	0	2020	-4.5977	8.7911	18	-0.52	0.6074	Tukey-Kran	1
SUBSTRATE*MIX*YR	builindex	2	2020	rooflite	1	2019	-8.1074	8.7911	18	-0.92	0.3686	Tukey-Kran	0.9978
SUBSTRATE*MIX*YR	builindex	2	2020	rooflite	1	2020	-5.1928	8.7911	18	-0.59	0.5621	Tukey-Kran	1
SUBSTRATE*MIX*YR	builindex	2	2020	rooflite	2	2019	-5.0418	8.7911	18	-0.57	0.5734	Tukey-Kran	1
SUBSTRATE*MIX*YR	builindex	2	2020	rooflite	2	2020	-19.8132	8.7911	18	-2.25	0.0369	Tukey-Kran	0.5363
SUBSTRATE*MIX*YR	rooflite	0	2019	rooflite	0	2020	1.538	6.2872	18	0.24	0.8095	Tukey-Kran	1
SUBSTRATE*MIX*YR	rooflite	0	2019	rooflite	1	2019	-1.9718	8.7911	18	-0.22	0.8251	Tukey-Kran	1
SUBSTRATE*MIX*YR	rooflite	0	2019	rooflite	1	2020	0.9429	8.7911	18	0.11	0.9158	Tukey-Kran	1
SUBSTRATE*MIX*YR	rooflite	0	2019	rooflite	2	2019	1.0938	8.7911	18	0.12	0.9024	Tukey-Kran	1
SUBSTRATE*MIX*YR	rooflite	0	2019	rooflite	2	2020	-13.6775	8.7911	18	-1.56	0.1372	Tukey-Kran	0.9042
SUBSTRATE*MIX*YR	rooflite	0	2020	rooflite	1	2019	-3.5097	8.7911	18	-0.4	0.6944	Tukey-Kran	1
SUBSTRATE*MIX*YR	rooflite	0	2020	rooflite	1	2020	-0.5951	8.7911	18	-0.07	0.9468	Tukey-Kran	1
SUBSTRATE*MIX*YR	rooflite	0	2020	rooflite	2	2019	-0.4441	8.7911	18	-0.05	0.9603	Tukey-Kran	1
SUBSTRATE*MIX*YR	rooflite	0	2020	rooflite	2	2020	-15.2155	8.7911	18	-1.73	0.1006	Tukey-Kran	0.8328
SUBSTRATE*MIX*YR	rooflite	1	2019	rooflite	1	2020	2.9146	6.2872	18	0.46	0.6485	Tukey-Kran	1
SUBSTRATE*MIX*YR	rooflite	1	2019	rooflite	2	2019	3.0656	8.7911	18	0.35	0.7313	Tukey-Kran	1
SUBSTRATE*MIX*YR	rooflite	1	2019	rooflite	2	2020	-11.7058	8.7911	18	-1.33	0.1996	Tukey-Kran	0.9631
SUBSTRATE*MIX*YR	rooflite	1	2020	rooflite	2	2019	0.151	8.7911	18	0.02	0.9865	Tukey-Kran	1
SUBSTRATE*MIX*YR	rooflite	1	2020	rooflite	2	2020	-14.6204	8.7911	18	-1.66	0.1136	Tukey-Kran	0.863
SUBSTRATE*MIX*YR	rooflite	2	2019	rooflite	2	2020	-14.7714	6.2872	18	-2.35	0.0304	Tukey-Kran	0.4802